Functional organic materials: singlet oxygen responsive acenes and stiffness-tunable polymeric films

A dissertation submitted by

Yu Yan

in partial fulfillment for the degree of

Doctor of Philosophy

In

Chemistry

TUFTS UNIVERSITY

August 2023

Adviser: Professor Samuel W. Thomas III

Abstract

Organic materials, including organic small molecules and polymers, are advantaged in their unlimited potential for functionalization due to the ease of chemical modifications. Pristine organic materials can be rendered to have desired functions with proper structural engineering. For example, in this work, acenes are subjected to various substitutions to achieve favored properties. Besides, the stiffness of polymeric layer-by-layer assembled thin films was tuned by coordination chemistry and photo-chemistry.

Chapter One gives a general introduction to acene-based materials. The synthesis, spectroscopic properties, and application of acene-based materials are described. The cycloaddition reaction between singlet oxygen and acene is emphasized. The chapter summarizes the historical development of acene-based singlet oxygen probes and points out other important singlet oxygen related applications of acenes, such as photo-cleavable drug delivery systems. Finally, this chapter summarizes some current challenges of acene-based materials and provides an outlook in this field from the author's perspective.

Chapter Two describes work on developing singlet oxygen responsive acene derivatives using extended aromatic pendants. Installation of aromatic substitutions groups, namely phenyl, naphthyl, and anthryl groups, to ethylated tetracene and anthradithiophene cores does not impact the kinetics of the cycloaddition with singlet oxygen but significantly impacts the photo-physical properties. For instance, the anthracene-substituted molecules have quenched fluorescence but still react with singlet oxygen at a similar rate to phenyl or naphthyl substituted tetracenes. Moreover, these non-emissive molecules display unusual resistance to unwanted photooxidation, which can

be attributed to the poor photo-sensitizing capability resulting from fast internal conversion relaxation of their excited states.

Chapter Three describes work on using electron-donating/ withdrawing groups to tune the kinetics and photo-physical properties of ethynylated tetracenes. The emission maxima of modified tetracenes are red-shifted, including the one with benzothiadiazole pendants that reaches the NIR window. The reaction rates with singlet oxygen are either accelerated with electron donors or decelerated with electron acceptors. We believe this understanding could help develop a new singlet oxygen sensor with favorable emission and reaction rate.

Chapter Four describes work on directing the crystallization of acene-based materials by non-covalent interactions. While the structure-property relationship in solution states is well-studied, there is still a gap in understanding the influence of structure on solid-state packing and properties. In this chapter, we intentionally introduce a non-covalent interaction, ArF-ArH interaction, into the system by installing non-conjugated fluorinated side chains onto acenes. With the help of single-crystal XRD tests, we identify the impact of ArF-ArH interactions and explain the different photo-physical properties of these materials in the solid state.

Chapter Five describes work on using metal coordination to tune the stiffness of layer-by-layer polymer thin films. LbL polymeric films that rely on H-bonding suffer from unwanted environmental sensitivity, especially relative humidity. With higher RH, the moisture can interrupt the H-bonds in the films and significantly decrease their stiffness. To address this problem, we develop a simple, synthesis-free, and all-aqueous method to enhance the stiffness of such films. Moreover, the crosslinking can be partially removed via irradiation-triggered photo-reduction of iron ions.

Acknowledgments

First and foremost, I would like to extend my deepest appreciation to my supervisor, Dr. Sam Thomas. Not only as an advisor for my research, but Sam also provides me enormous valuable suggestions in the development of my professional career, in facing challenges, and in living a positive life. It is Sam's kindness, patience, and encouragement that support me to finish this long journey. Also, I would like to express my gratefulness to my research committee members, Dr. Krishna Kumar and Dr. Charlie Sykes. Their cross-disciplinary expertise inspired my research and broadened my horizon in chemistry. I appreciate my guest committee member, Prof. Yang Qin, and our collaborators, Prof. Luke Davis, Prof. Ioannis Kymissis, Prof. David Kaplan, and Prof. Atistide Gumyusenge, for their help and guidance in my graduate studies. Besides, I thank all the staff and faculties in the Chemistry Department at Tufts for their helpful and supportive efforts.

Secondly, I would like to thank my colleagues in Thomas lab: Dr. Fanny Frausto, Dr. Valentina Brega, Dr. Matt Feeney, Dr. Seth Sharber, Dr. Will Mullin, Sare Kanari, Elisa Guzman, Georges Pichard, Manny Pina, and all the young researchers from undergraduate or high school program (Zach, Sharfeena, Kay, et al.) Thank you all for building up a family-feel atmosphere and accommodating my shortcomings in the past six years.

I want to thank my friends and my family. Thank them very much for always standing by me and watching my back. May the force be with you!

Especially, I want to thank my wife, Jing Wang. Marrying Jing is the greatest achievement I have ever made in my life, and her accompanying truly brightened my time in graduate school. I will continue our lifelong "collaboration" and extend it to eternity.

Table of contents

Chapter 1: Introduction to acenes and their responsiveness toward singlet oxygen

Chapter 2: Multi-acene structures and their resistance to unwanted photo-oxidation

Chapter 3: Tuning the fluorescence and singlet oxygen responsiveness of ethynylated tetracenes by electron-donating or withdrawing effect

Chapter 4: Directing the crystallization of acene-based materials

Chapter 5: Tuning stiffness of free-standing hydrogen-bonded LBL films with Fe^{3+} coordination

List of tables

List of figures

List of schemes

Functional organic materials: singlet oxygen responsive acenes and stiffness-tunable polymeric films

Chapter 1:

Introduction to acenes and their responsiveness toward singlet oxygen

Reproduced in part with permission from:
Brega, V.; Yan, Y.; Thomas, S. W., 3rd. Acenes beyond organic electronics: sensing of singlet oxygen and stimuli-responsive materials. *Org Biomol Chem* **2020**, *18* (45), 9191-9209. DOI: 10.1039/d0ob01744b

1.1 Introduction to acenes

Acenes comprise linearly fused benzene rings that can be considered as 1-dimensional fragments of graphene. The resulting extended conjugated structure and possibility for favorable packing motifs in the solid-state have rendered acenes as one of the most promising classes of compounds for organic field-effect transistors (OFETs).[1, 2] Increasing the length of acenes can improve the performance of the materials so the development of longer acenes is critical in this field. However, due to their high HOMO levels and lower per-ring resonance energies, longer acenes can suffer from poor stability, especially during photoirradiation. This challenge around stability has resulted in a wide variety of strategies that harness substituent effects to suppress undesirable reactivity.[3] On the other hand, the generally increased reactivity of longer acenes could open possibilities for applications beyond organic electronics,[4] as shown in **Figure 1.1**.

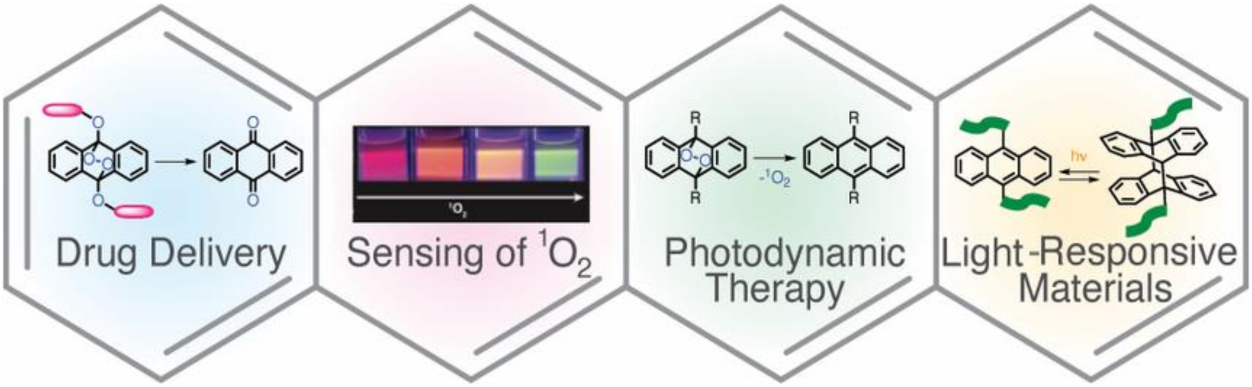

Figure 1.1: Illustration of acene's applications embedded in the chemical structure of a tetracene molecule. Figure reproduced from Ref. 4. Copyright 2020 Royal Society of Chemistry.

1.2 Synthesis of pristine acenes

Overall, regardless of the intended application space, the instability and lack of solubility of longer acenes are problematic in terms of large-scale synthesis. However, various novel strategies and sophisticated synthetic technologies for their synthesis have emerged in recent years[5-7].

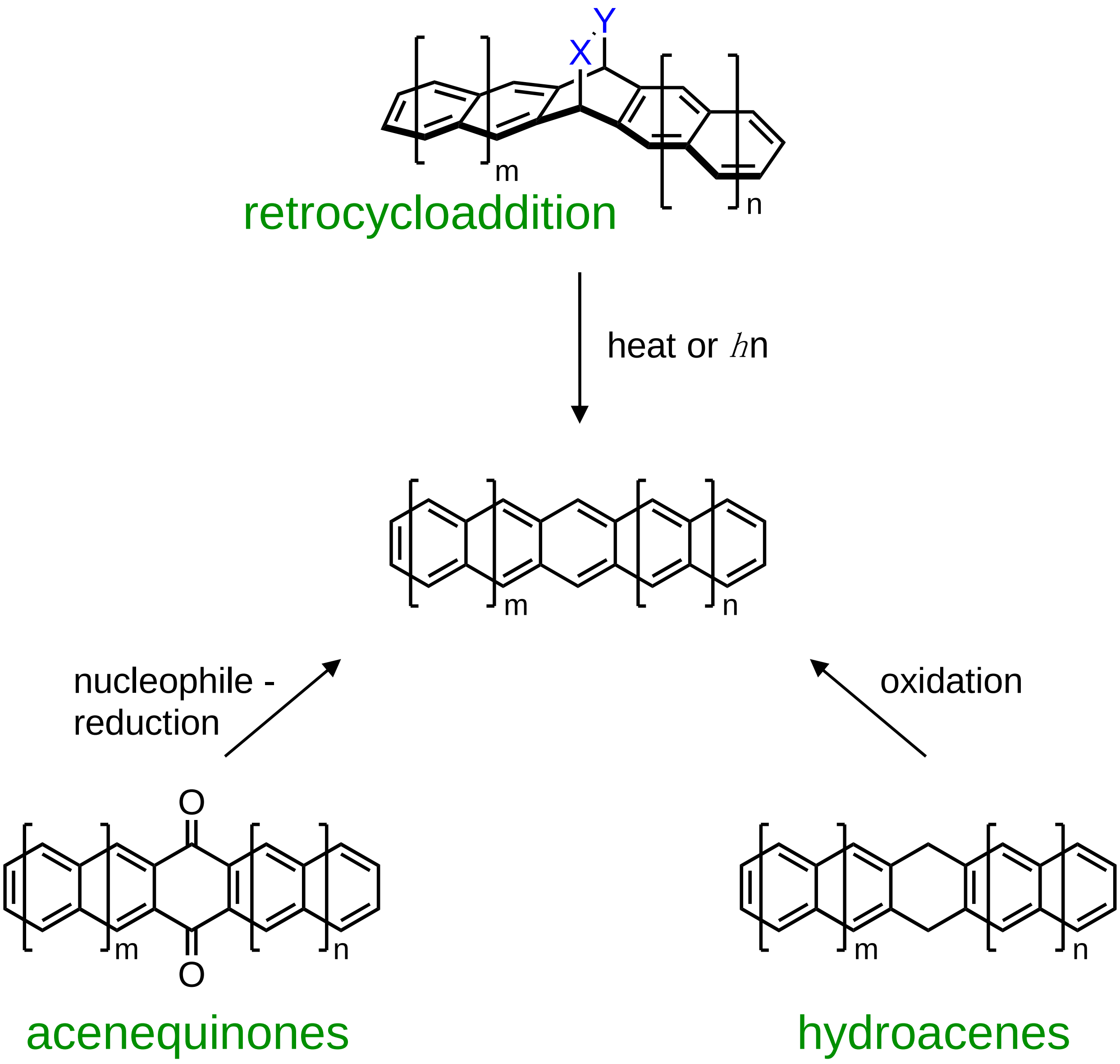

Figure 1.2: Common strategies of longer acene synthesis. Figure reproduced from Ref. 4. Copyright 2020 Royal Society of Chemistry.

As shown in Figure 1.2, the synthesis of longer pristine long acenes commonly follows three strategies, reduction of pentacenedione,[8] oxidation of hydroacenes,[9] and thermal- or photo-induced elimination reactions[10, 11] Importantly, these works enabled thorough characterization of the optical and electronic properties of hexacene, and the authors also demonstrated the high photosensitivity of hexacene—photo-oxidation of the hexane thin-film occurred in minutes under UV light while the film showed no degradation in the dark for more than a month.[11] Longer acenes, such as heptacene, have also been successfully synthesized by fragmenting heptacene dimers[12], thermal decarbonylation[13], and on-surface chemistry[14, 15].

1.3 Development of substituted acenes and beyond

Although numerous methodologies for synthesizing unsubstituted longer acenes have emerged, their limited solubility and stability can limit their applications. Thus, the ability to prepare functionalized longer acenes, especially those with better solubility, is crucial. As a result of these breakthroughs, the applications of longer acenes are no longer limited to the solid-state. The development of stable and soluble longer acenes allows organic chemists and materials scientists to explore other potential applications that both include and reach beyond organic electronics.

One of the most common strategies is to introduce silyl-ethynylene substituents or other carbon-based substituents onto the conjugated acene core by addition-elimination sequences between the corresponding quinone and suitable organometallic reagents, which for ethynyl groups could be traced back to 1969,[16] and to 1942 for aryl substituents on pentacene.[17] Methodologies for acene synthesis was then developed, with the improved lab equipment and better control over the reaction conditions. Around 20 years ago, a milestone material for organic electronics, bis(triisopropylsilylethynyl)-pentacene (**TIPS-pentacene**), was developed using a similar approach.[18] **Tips-pentacene** displayed unusual photo-stability and favored electronic properties comparable with single-crystal silicone devices.[19] Stimulated by this outstanding achievement, diversely functionalized longer acenes have been discovered.[5, 20-22]

Overall, silyl-ethyne substituents can improve both the solubility and stability of longer acenes significantly, both of which enable many of the spectroscopic analyses for acenes longer than pentacene that is commonly performed in the solution phase (**Figure 1.3**).[23] The further tuning of side groups can also optimize the crystal packing of the materials, thereby improving their performance in organic electronic devices.[24, 25] Supporting these discoveries, Linker and coworkers reported a mechanistic rationale for how triple bonds can protect the longer acenes against photo-oxidation.[3] In addition, terminal alkyne substituents, which can be obtained by simple and rapid desilylation, are desirable intermediates for the Sonogashira cross-coupling reaction and click chemistry. Using this approach, subsequent functionalization of the ethynyl substituent on the acene could be achieved.[26-28]

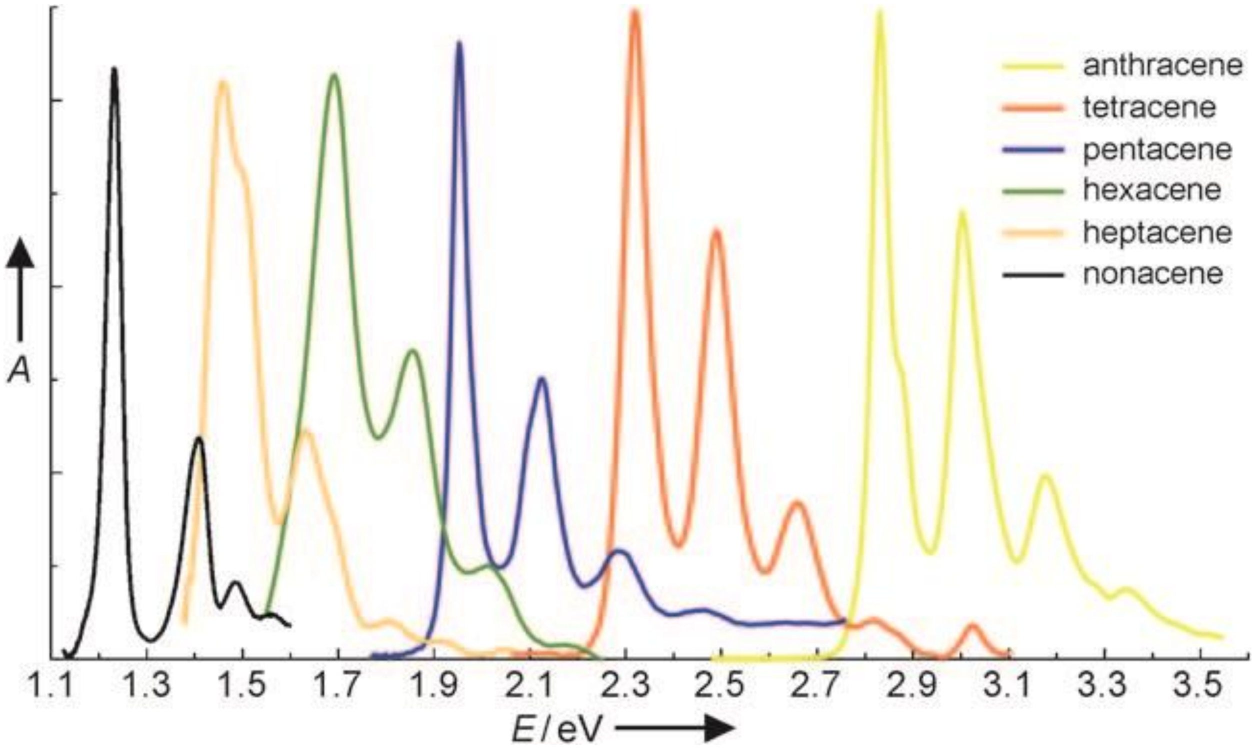

Figure 1.3: Absorbance spectra of silyl-ethyne-substituted acenes. Copyright © 2011 WILEY-VCH

Besides silyl-enthylation, other substituents have been introduced to achieve various functions. For example, fused five-member rings have been used for the stabilization of longer acenes by kinetically blocking two possible sites for photo-oxidation.[29-32] Fluorination, which can improve the crystallization of acenes and tune the frontier orbitals, is another common modification for acene materials.[33, 34] Besides, water-soluble acenes have also been developed by introducing strong solubility groups.[35]

Heteroatom acenes also play a big role in this field. Azaacene, in which aromatic carbon atoms are substituted by nitrogen atoms, is one of hetero-acenes that have been studied the most. In 2003, the Nuckolls group synthesized a pentacene analog, dihydrodiazapentacene, by simply condensing a diol and a diamine.[36] The reported molecule displayed good electronic properties like pentacene but better environmental stability. Following this work, the development of azaacenes thrived in recent years.[37-40] Notably, with efficient condensation reactions and coupling reactions of aromatic amines, pyrene-fused azaacenes[41, 42] and long azaacenes with 15 fused rings[43] have been developed and characterized by XRDs and electrochemistry. However, the research on azaacenes in cycloaddition reactions and singlet oxygen sensing is surprisingly limited.[44] The application of azaacenes is still highly focused on organic electronics.[38, 39]

Acenes containing boron-nitrogen (B ← N) Lewis pairs are another kind of important hetero-atom acenes. Although reported in the 1960s,[45] this kind of molecule did not receive much attention until recent years. The synthesis of BN acenes typically relied on the electrophilic aromatic borylation that directly annulated the nitrogen-containing group with a double bond,[46-49], and the resulting BN acene could then be further functionalized.[50, 51] Switching the carbon-carbon double bond with B ← N bond could significantly change the electronical properties of acenes, and so that change the reactivity and photo-physical properties.[46] For instance, Liu's group has reported that the BN-substituted anthracene displayed similar photo-physical properties as tetracene.[52] Also, it has been reported that BN substitution could decrease the chemical reactivity of acenes in cycloaddition and oxidation.[46, 49]

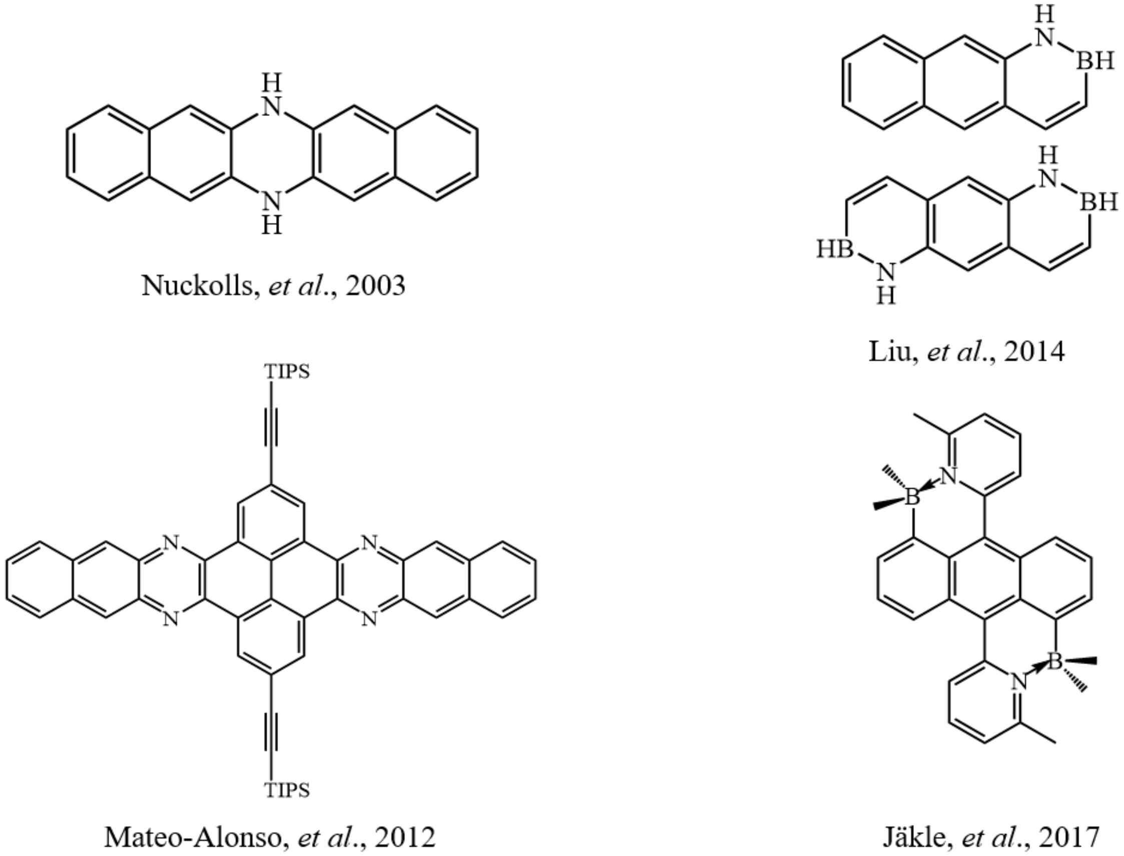

Nuckolls, *et al*., 2003

Liu, *et al*., 2014

Mateo-Alonso, *et al*., 2012

Jäkle, *et al*., 2017

Figure 1.4: Chemical structure of reported azaacenes and BN acenes. Structures adapted form ref.36, 42, 46, and 49.

1.4 Cycloaddition of acenes

Cycloaddition is one of the key reactions of acenes that enabled this kind of molecule in photo-/thermal responsive materials. The basic reaction schemes are displayed in **Figure 1.5**. In general, cycloaddition reactions present numerous advantages for both organic synthesis and materials science: i) they form multiple covalent bonds in one reaction, often with excellent regio- and stereoselectivity, ii) they proceed without byproduct formation, and iii) the low degree of charge separation during these reactions reduces the dependence of their rates on the polarity of the environment. Acenes can react with various dienophiles due to their electron-rich nature and their diene reaction sites. In addition, acenes can also undergo photochemically allowed [4+4] "butterfly" dimerization reactions upon irradiation.[53]

Generally, the reactivity of cycloadditions follows several trends: i) the longer the acene is, the higher reactivity; ii) the interior rings, such as the 5,12 positions of tetracene and 6,13 position of pentacene, are more reactive; iii) steric hindrance can significantly slow down the reaction. These trends have been rationalized by both theoretical simulation[54] and experimental results[55].

Despite the higher reactivity of longer acenes, anthracene is a much more common intentional partner for cycloaddition reactions due to higher stability and accessibility. Such methodology has been heated studied in organic synthesis of complicated structures, [56] post modification of polymer materials[57, 58], and fabrication of nanoparticles[59]. More importantly, both [4+2] and [4+4] cycloadditions exhibit good reversibility, which provides a nature of dynamic covalent bonding. The cycloreversion can be triggered by multiple stimuli, including light, heat, and mechanical

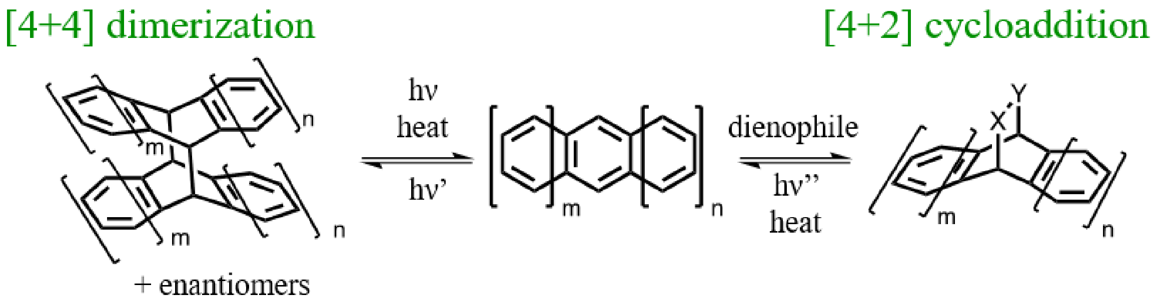

Figure 1.5: The [4+2] and [4+4] cycloaddition reaction of longer acenes. Figure reproduced from Ref. 4. Copyright 2020 Royal Society of Chemistry.

forces[60]. Grounded on these mechanisms, novel applications, such as reversible writing/erasing platform[61], nanoscale patterning[62], and reversible surface modification[63, 64], have been developed.

The study on cycloadditions of longer acenes is relatively scarce, which may be due to the vulnerability towards photo-oxidation of longer acenes. However, Ciszek's group has reported several studies involving cycloaddition chemistry on the surface of long acene crystals.[65-67] The Liao group has also highlighted a series of fundamental studies about the reaction between long acenes and a strong dienophile tetracyanoethylene (**TCNE**).[68, 69] Nevertheless, unlike anthracenes, examples of using longer acenes in applied materials are still lacking.

1.5 Introduction of singlet oxygen

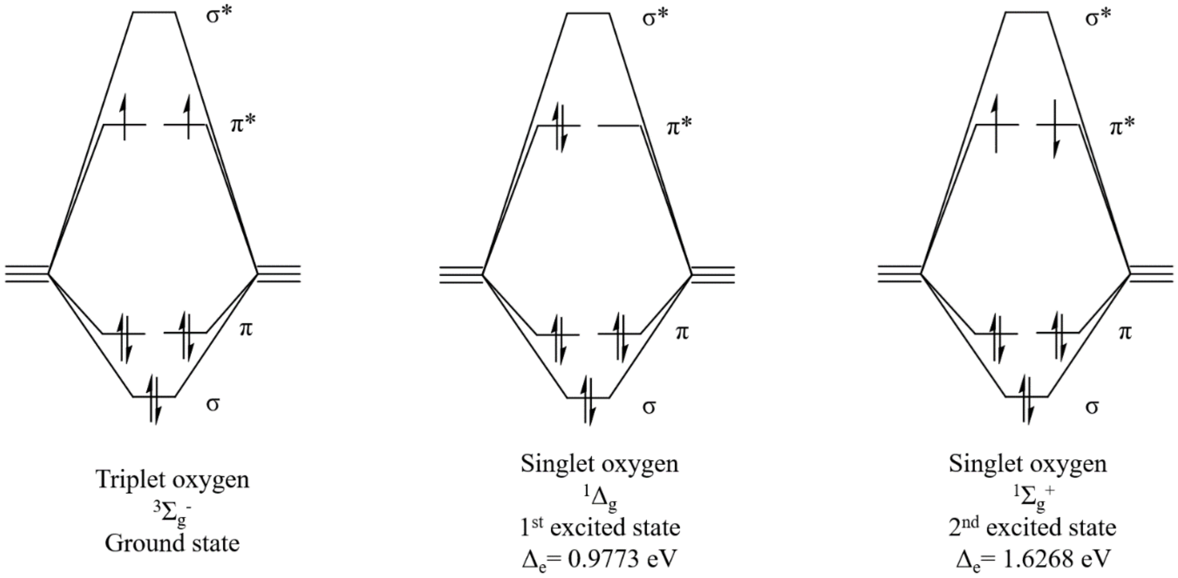

Figure 1.6: Molecular orbitals of molecular oxygen in ground state (triplet), 1st and 2nd excited states (singlet). Δ_e is the energy difference between excited state and ground state in eV.

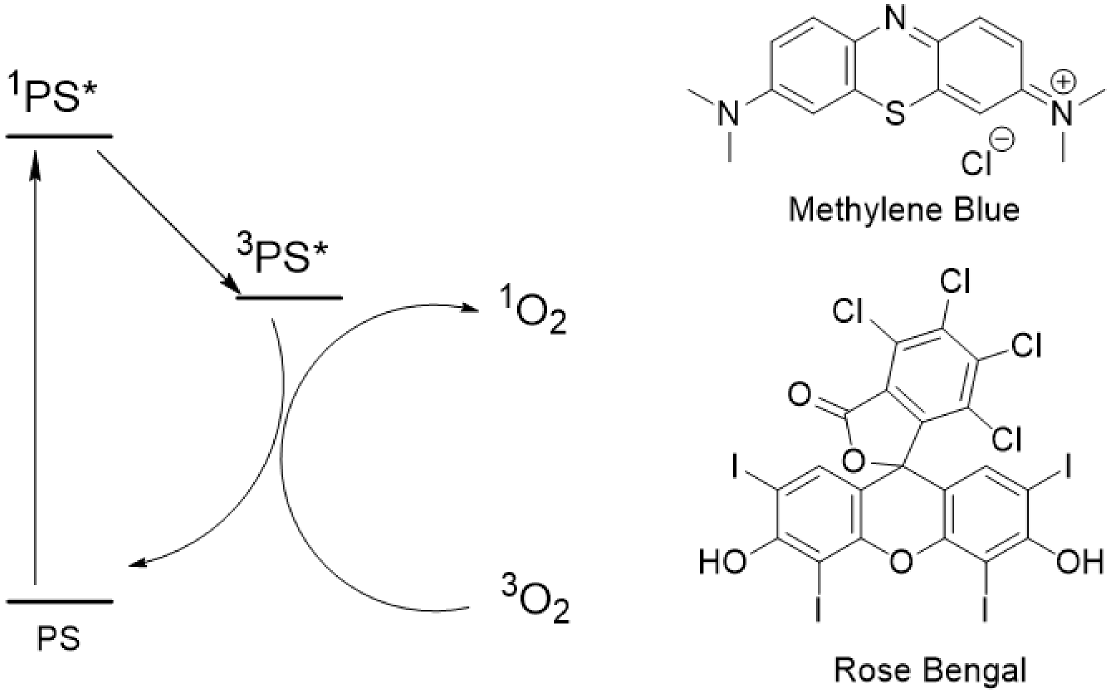

Figure 1.7: Diagrammatic representation of photo-sensitizing process and the chemical structures of two commonly used photosensitizers.

Among the dienophiles being studied with acenes, one of them displays unique properties and attracted frequent attention, singlet oxygen (**$^1O_2$**).[70, 71] Singlet oxygen is the lowest energy electronically excited state of molecular oxygen. Unlike the oxygen in ground states ($^3\Sigma_g^-$), the electron configuration of singlet oxygen is different. Two electrons are paired and only occupy one π^* orbital, resulting in an overall higher energy of the molecule ($^1\Delta_g$) as shown in **Figure 1.6**. The two electrons in π^* may also occupy two different π^* orbitals but have opposite spin, which is the electron configuration of the 2nd excited state of molecular oxygen ($^1\Sigma_g^+$). Such excited state ($^1\Sigma_g^+$) is less stable and rapidly converts to the first excited state ($^1\Delta_g$).[72] In the rest of this dissertation, the term "singlet oxygen" and "$^1O_2$" specifically represent the first excited state of molecular oxygen ($^1\Delta_g$).

To generate singlet oxygen, a process called photo-sensitizing is normally applied.[73] As shown in **Figure 1.7,** a photo-sensitizer (PS) was excited to singlet excited states, followed by an intersystem crossing to triplet states. Such triplet state PS donates its energy to triplet state oxygen (ground state) via a spin-allowed energy transfer resulting in the relaxation of PS and the generation of $^1O_2$. The PS is normally an organic dye,[73] such as Methylene Blue (**MB**) and Rose Bengal. However, a lot of biological molecules or conjugated materials have been found to be capable of serving as PS. As the $\mathbf{O_2}$ is very abundant in the atmosphere, such abundance makes $\mathbf{^1O_2}$ easy to access but, on the other hand, hard to avoid. Thus, the generation of singlet oxygen has been blamed as one of the key steps in plant photodamaging[74], DNA photodegradation[75], and materials photooxidation[76, 77].

1.6 Cycloaddition of singlet oxygen

The study of singlet oxygen cycloaddition on acenes divides into two different objectives: avoiding the reaction or harnessing the reaction.[4, 78] The former is usually proposed by scientists who develop organic materials containing acenes as functional groups, and by slowing or stopping the reaction, the stability of materials can be enhanced.[79-81] The latter, on the other hand, is frequently mentioned in the fluorescent detection of singlet oxygen because this reaction would significantly alter the π conjugation of acenes, which results in absorbance or fluorescence signal.[82-84]

As mentioned earlier in **1.3**, one of the most commonly used substituents on long acenes is silyl acetylenes. Interestingly, installing these substituents significantly slows down the cycloaddition of singlet oxygen. Linker group has carefully studied this phenomenon and proposed rationales in different aspects: i) the triple bonds render the molecule to quenchers for singlet oxygen; ii) the triple bonds accelerated the reverse reaction by lowering the activated energy; iii) the mechanism of cycloaddition changed from a zwitterion intermediated pathway to a slower concerted addition (**Figure 1.8**).[3]

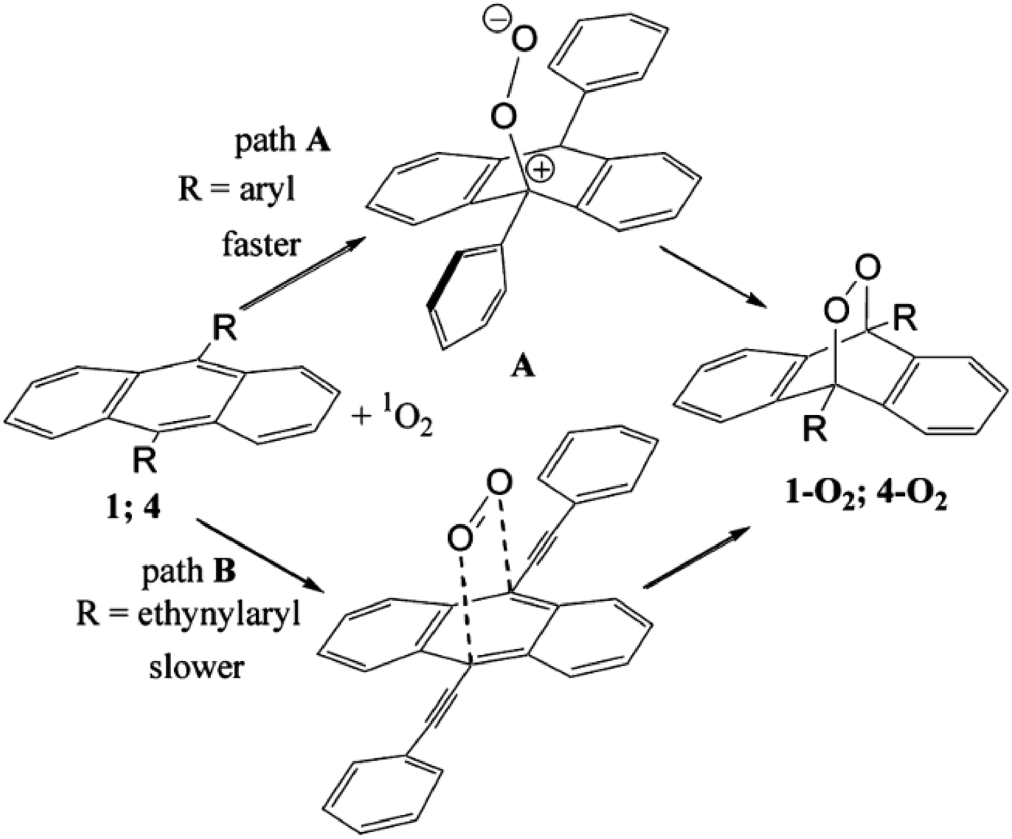

Figure 1.8 Two different reaction mechanisms proposed by Linker group. Anthracene was used for simplification. Copyright © 2012, American Chemical Society

In recent years, our group has made an effort to understand the cycloaddition of singlet oxygen. With a series of works[79-81, 85-88], our group has established a small library of substituted acenes and discovered some trends in the kinetics of this reaction. The results are summarized and adapted in **Figure 1.9**. Generally, the reaction happens faster when a longer acene core is participating.[79, 88] When a thiophene ring is fused to the acene, it provides about two-thirds of the impact of a benzene ring. For instance, the rate constant for cycloaddition of diphenyl-tetracene is higher than it for diphenyl-anthrathiophene and lower than that for diphenyl anthradithiophene.

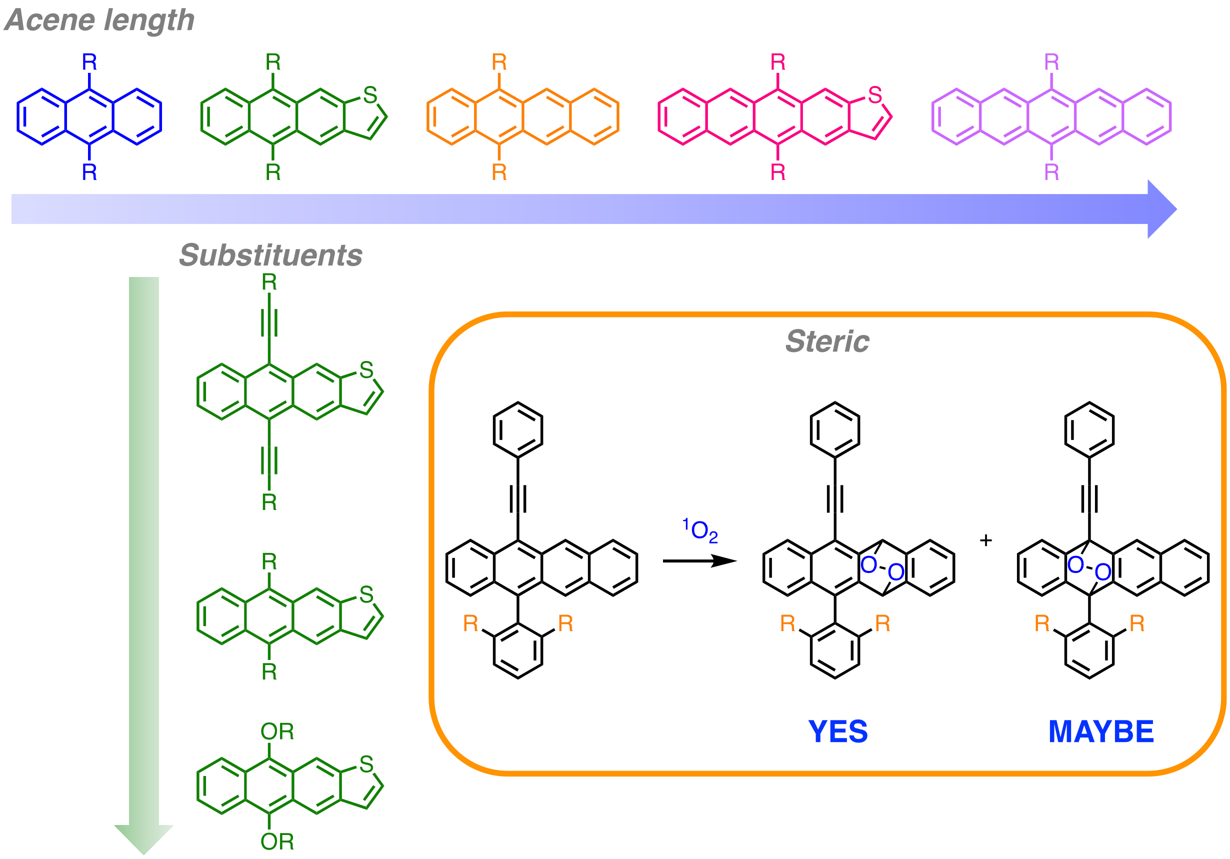

Figure 1.9: The reactivity of acenes toward singlet oxygen increases with the number of aromatic rings in their core. Alkynyl derivatives are the least reactive, while alkoxy derivatives react the fastest. Steric hindrance also plays a role in acene reactivity. Figure reproduced form Ref. 4. Copyright 2020 Royal Society of Chemistry.

Besides, the type of substituents also plays a key role in the kinetics of the reaction. Introducing triple bonds slows down the reaction significantly, which has been discussed in the last section. Moreover, our group found an unsymmetrically mono-substitution of triple bond results in half the consequences of binary substitution.[79] We have also reported that the reaction was accelerated when switching the substituents to electron-donating alkoxy groups.[88]

Steric hindrance is another factor affecting the reaction rate and the regioselectivities of the reaction. Our group installed a phenyl, with alkyl groups on the two ortho-positions, onto a tetracene core. When the alkyl group is less bulky methyl groups, the reaction can happen both on the substituted (5,12) site and the unsubstituted (6,11) site. Nevertheless, when using sterically larger ethyl groups, one of the possible products, endoperoxide at 5,12 positions, could not be found. We believe that is the steric effect that blocks the attack of singlet oxygen towards the acene.[81] Based on a similar design, we have also published a pentacene that is both stabilized by steric hindrance and electronic effect. Such molecules showed great photo-stability and resistance to cycloaddition of singlet oxygen in the solution state.[80]

Efforts have also been made by other groups in this field. Jäkle's lab reported a thorough analysis of the singlet oxygen cycloaddition reaction with a set of BN anthracenes. They found that steric hindrance induced by methyl substituent accelerated the cycloaddition of singlet oxygen. They attribute this phenomenon to the lack of carbocation stabilization of the reaction intermediate resulting from the hindering of planarization.[48] The Anthony group carefully evaluated the impact of atomic substitutions on TES-ADT. The silicon atom was switched by carbon or germanium atoms, and the optoelectronic properties and photo-stabilities were studied. Compared with carbon or germanium, silicon-substituted acene displayed better photo-stability, which was explained by a lower reaction enthalpy determined by theoretical calculations.[89] The same group has also studied the impact of substitutions on the thiophene rings of TES-ADT. They found that all the substituents installed in that work could stabilize the acene to some degree, with fluorine atoms displaying the strongest stabilization effect.[90] Other examples of stabilizing acenes include blocking the reactive sites by annulation reactions[29, 30], protecting the acene by supramolecular encapsulation,[91] and shortening the lifetime of excited states by thiophene substitutions.[92]

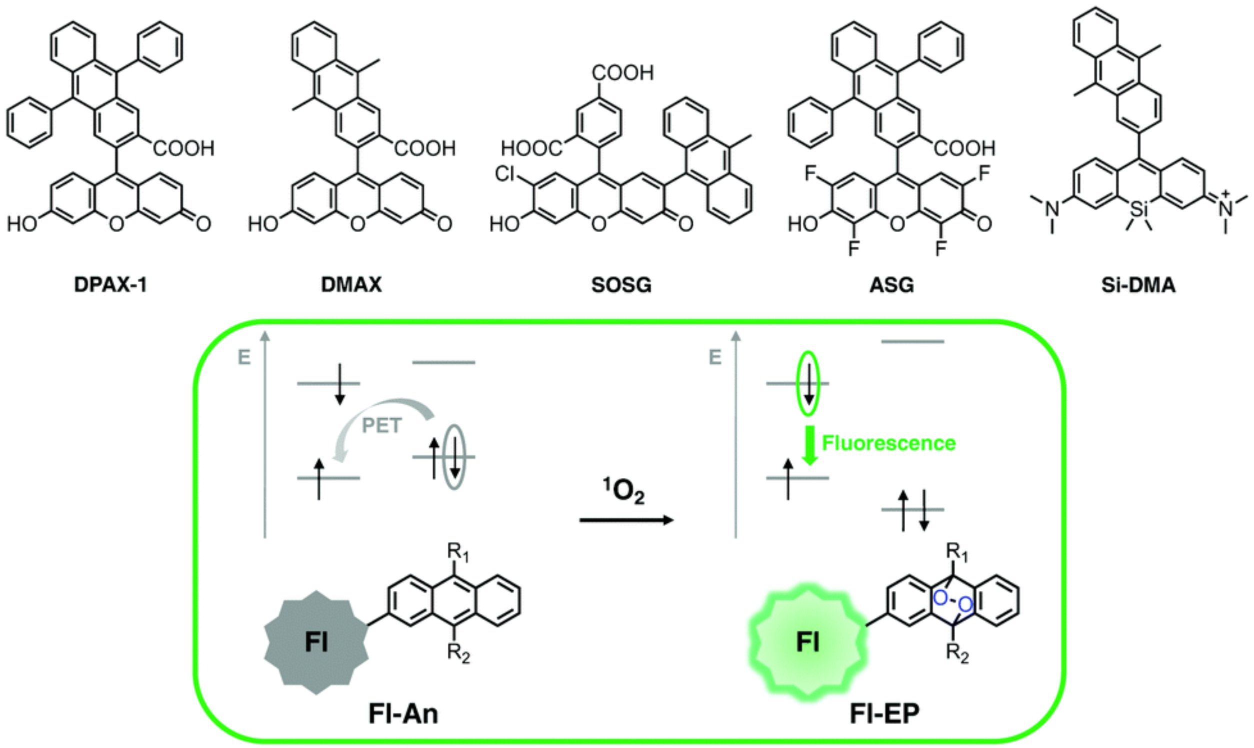

Figure 1.10: *Top:* Chemical Structure of **DPAX-1**, **DMAX**, Singlet Oxygen Sensor Green® (**SOSG**), Aarhus Sensor Green (**ASG**), **Si-DMA**. *Bottom:* Reaction of the anthracene moiety with singlet oxygen and the depression of photoinduced electron transfer (PET) after oxidation. Figure reproduced form Ref. 4. Copyright 2020 Royal Society of Chemistry.

1.7 Fluorescent probing of singlet oxygen

Due to their rich spectroscopic properties and the rapid responsiveness towards singlet oxygen, acenes are great candidates for singlet oxygen spectroscopic probing. For instance, 9,10-diphenyl anthracene (**DPA**) is a well-studied colorimetric probe for singlet oxygen. The absorbance of **DPA** at around 355 nm decreases upon reacting with singlet oxygen with a rate constant of ~10^6 M^{-1} s^{-1}.[93] Thus, the generation of singlet oxygen can be probed by UV-vis spectroscopy. Also, the reliability and stability of **DPA** make it a kinetic standard for the future development of singlet oxygen responsive materials.[27, 79, 94]

Luminescent probing, on the other hand, provides higher sensitivity and possibilities in biological analysis. Thus, the development of fluorescent probes of singlet oxygen is also heatedly discussed in this field. One of the most frequently used designs is to covalently link the responsive part, usually acenes, with a fluorescent organic dye. Due to the photoinduced electron transfer (PET) between the two components, the probe is less or non-emissive before exposure to singlet oxygen. Once the cycloaddition happens, the endoperoxides produced are no longer able to accept electrons from the dye, so a "turn-on" fluorescent signal from the fluorescent dye can be observed.[95] **Figure 1.10** displays some "milestone" probes with similar designs and a generalized scheme of sensing mechanisms.[82, 95-98]

Despite the good sensitivity and quality of signals provided by these probes, they are still suffering from deficiencies such as limited effective pH range[82], self-sensitizing, and slow responsiveness[96]. One major reason for these drawbacks is the reliance on the existing organic dyes, which usually incorporate charged groups to achieve a push-and-pull structure. To address this problem, a solution is to use intrinsically fluorescent acenes. Compared with anthracenes, longer acenes, such as tetracene and tetracenothiophene, have comparable fluorescent quantum yields while the emissions are in a favored, red-shifted range.[79] Meanwhile, the responsiveness can be accelerated due to the higher reaction rates described in the last section.

In contrast to the fluorescent signals that are "turned on," sensors utilizing longer acenes commonly exhibit ratiometric signals. Specifically, these acenes are integrated into the system either through covalent[27, 84] or non-covalent bonding[83, 86, 99] with a conjugated polymer (CP), which functions as both an energy donor and a light harvester.[100] Within this setup, the acenes serve as energy "traps" of Förster resonance energy transfer (FRET) or through-bond energy transfer and emitters prior to undergoing cycloaddition. Upon exposure to singlet oxygen, the endoperoxide's increased HOMO-LUMO gap prevents it from accepting energy from the CP.[83] As a result, the CP takes the role of the new emitter, emitting at a different wavelength that is typically hypochromic. This type of design is advantageous in multiple ways: (i) a ratiometric response of fluorescence that is resistant to the error inherent in simple fluorescence intensity measurements; (ii) the efficient CP-acene energy transfer and the strong light-harvesting capabilities of CP enable the use of a small amount of energy acceptor, the functional acenes.

Figure 1.11 displays an example of a CP/acene probing platform developed by our group. The polymer's maximum emission switched from 510 nm (the same as small molecule diphenyl tetracene) to 410 nm (the same as a non-acene polymer) upon exposure to singlet oxygen while maintaining high fluorescence quantum yield above 50%.[84] Following this work, our group developed a singlet-oxygen-mediated protein sensing platform using acene-doped CP thin films in the next year.[86] This work showed the possibility of interaction between CP and acenes without

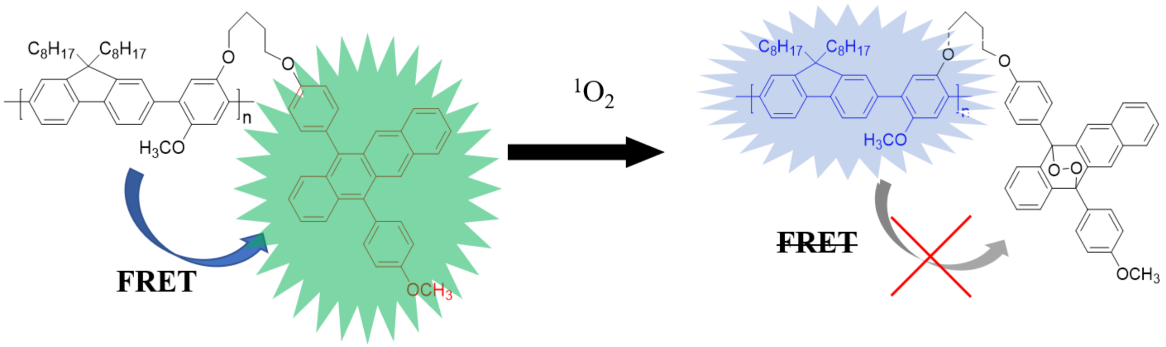

Figure 1.11: The reaction of singlet oxygen cycloaddition in a CP/acene system and the Förster resonance energy transfer (FRET) between the CP and acenes. Figure reproduced from Ref. 4. Copyright 2020 Royal Society of Chemistry.

being covalently connected. Then, we also attempted to use through-bond energy transfer and synthesis of a poly(phenylene ethynylene) (**PPE**) based polymer with tetracene pendants linked to the backbone through all conjugated linkers.[27]

In 2017, inspired by the studies in conjugated polymer nanoparticles (CPNs)[101-103], our group developed an acene-doped, water-dispersible, and nanoscale ratiometric fluorescent singlet oxygen probe.[83] This probe has outcompeted the performance of commercially available **SOSG**, and pushed the signaling window above 500 nm. This was further improved by using a different CP[104] and blending two CPs.[99]

Besides the works of our group, novel singlet oxygen sensors/ sensing platforms have been developed by researchers frequently. Wang and coworkers developed a pentacene derivative that responds to NIR light as a molecule or as supramolecular assemblies. In this work, singlet oxygen

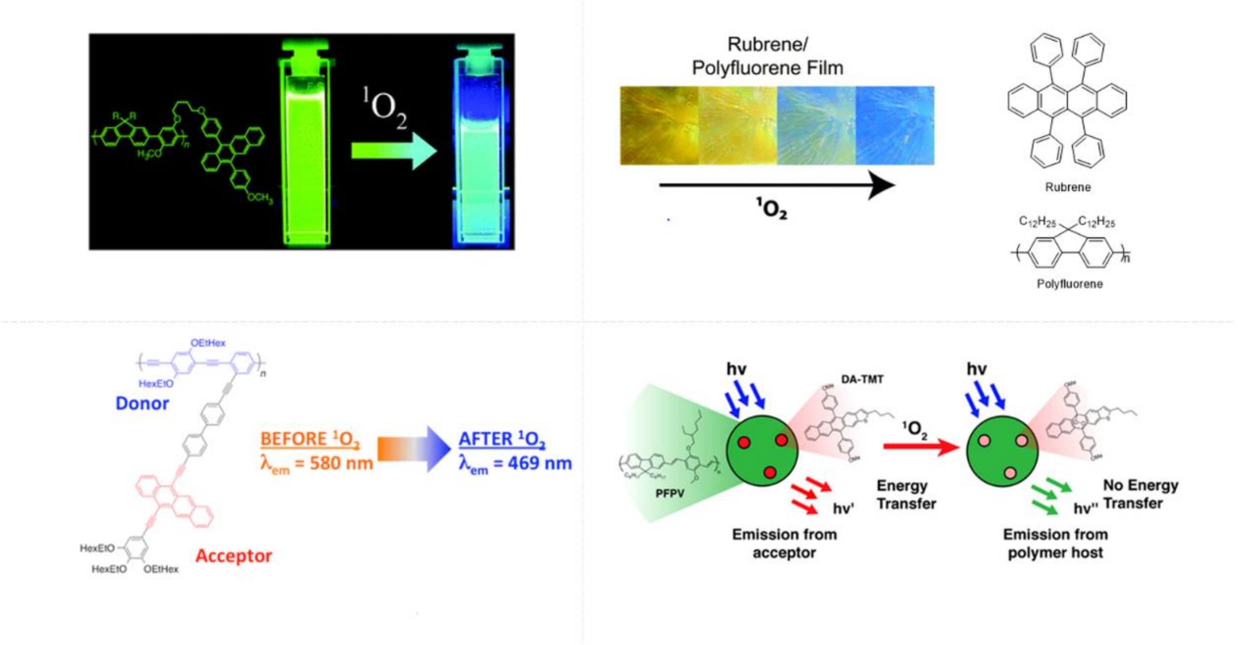

Figure 1.12: CP/acene singlet oxygen sensing platforms developed by Thomas group. Figure reproduced from Ref. 4. Copyright 2020 Royal Society of Chemistry.

was generated by self-sensitizing the pentacene derivative using NIR light and then reacted with the acene.[105] Chen's group developed a colorimetric singlet oxygen sensor using azaacenes doped polymer film.[44] Li and coworkers reported a PET-based, two-photon fluorescence singlet oxygen probe that can be excited by light at a wavelength of 800 nm. In that work, singlet sensing was performed in cell and brain tissues.[106]

Although there are already numerous accomplishments in this field, efforts are still needed in a couple of aspects.

(1) Avoiding self-sensitizing in the sensing process. As the probes are always a fluorescent dye at the same time, singlet oxygen can be generated by photo-sensitization of the probe itself, which can result in fake positive signals.[107] Thus, it is reasonable to develop probes that are not good photosensitizers but are still responsive.

(2) Biocompatibility. Many of these probes are cytotoxic small molecules, which is not good for biological systems. Although there are some successes in using SOSG-doped CPNs to achieve bio-imaging[108], the size of CPNs is not good for cellular penetration, and the staining mechanism is still under determination.

(3) Quantitative analysis. Most of the developed probes can only provide qualitative results. However, knowing the concentration of singlet oxygen is rather important, especially in the medical process, such as photo-dynamic therapy.[109] Step-wise responsiveness could be a promising solution[110]. However, monitoring the concentration in real-time is still desired. Taking advantage of the reversible nature of singlet oxygen cycloaddition may provide another possibility for dynamic analysis.[111]

1.8 Other important $^1O_2$-related applications of acenes

Probing singlet oxygen is only a small proportion of $^1O_2$-related applications of acenes.[4] Other important applications include but are not limited to cancer therapy and drug delivery.

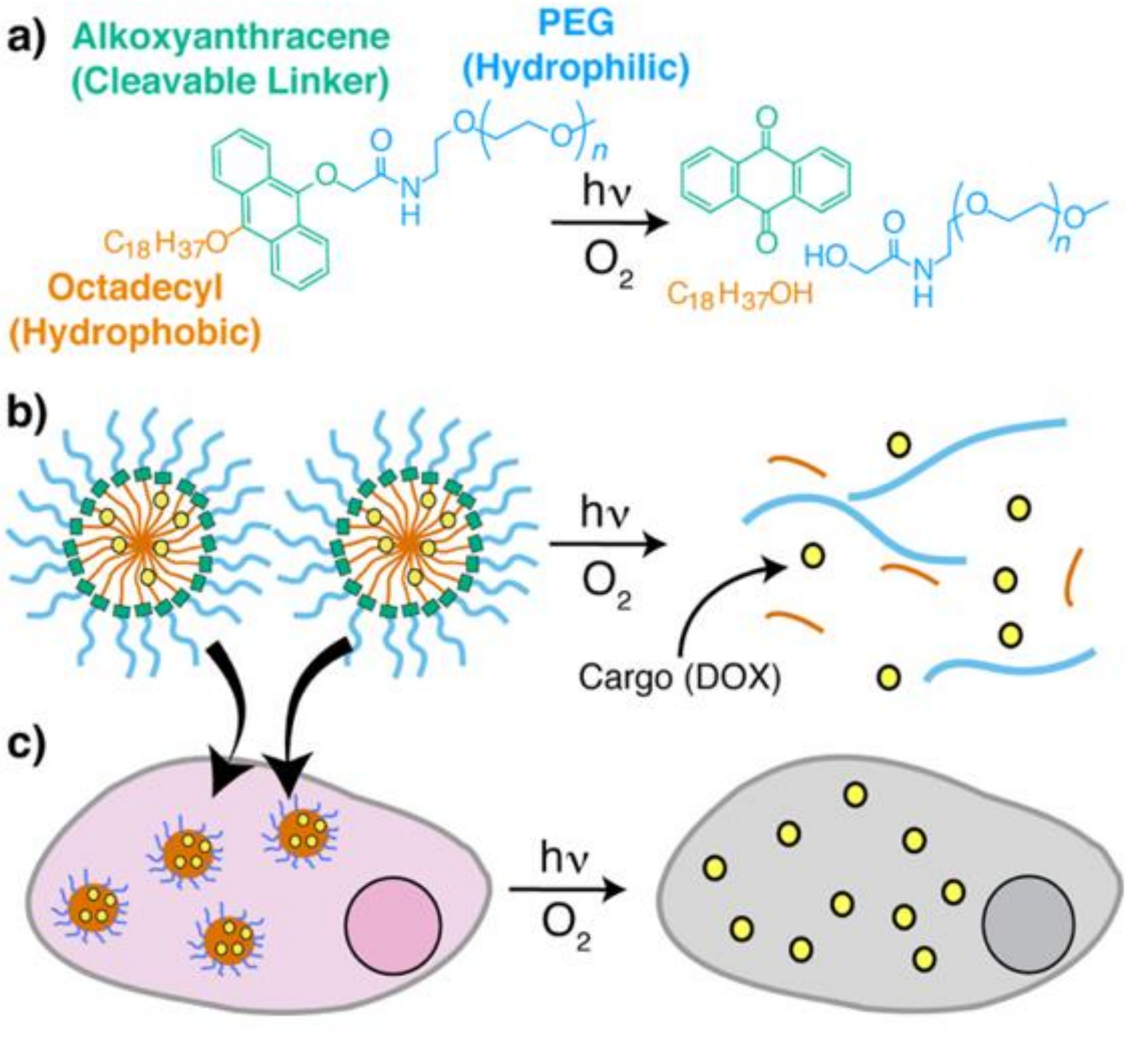

Figure 1.13: Self-assembly of amphiphilic polymers into micelles and intracellular delivery triggered by the cleavage reaction of the dialkoxyanthracene linker. Figure reproduced from Ref. 4. Copyright 2020 Royal Society of Chemistry.

Acenes have been used as photo-sensitizers for photodynamic therapy and photothermal therapy due to their strong absorbance and photo-sensitizing abilities.[4, 112] For instance, Hu and coworkers reported an organic small molecule based photosensitizer with two anthracenes installed on a donor-acceptor chromophore.[113] Jäkle's group reported acenes modified with BN Lewis pairs.[48, 114] The BN bonding enlarged the conjugation and planarized the molecules, red-shifting the absorbance of the materials, allowing the application in photodynamic and photothermal cancer therapies. Recently, the Liu group reported a method encapsulating acenes into nanoparticles. The resulting nanoparticles were then applied as a self-degradable singlet oxygen resource for photodynamic therapy. This work rationalized the advantage of low photo-stability of acenes and broadened the prospect of applications of acene-based materials.

Similar to other dienophiles, the cycloaddition of singlet oxygen is reversible.[111] Thus, it is possible to use acenes to perform singlet oxygen "catch and release" for therapeutic purposes as a mutated version of photodynamic therapy[109]. Generally, the acene derivatives are tethered to nanomaterials[115, 116] or incorporated in supramolecular systems[117, 118]. Then, the material is exposed to photogenerated singlet oxygen and form endoperoxide. Each acene structure can hold one molecule of singlet oxygen so that the material becomes a carrier for singlet oxygen. Then, the material can be introduced to the desired biosystem, and the release is triggered by external stimuli, normally heat. Consequently, the cytotoxicity of singlet oxygen can induce the death of cancer cell around the area.

Another significant application is utilizing the singlet-oxygen-assisted photocleavage to develop drug delivery platforms.[119] Our group reported an amphiphile containing cleavable linkers and fabricated nanoscale micelles based on such amphiphiles.[120] When singlet oxygen is generated, the micelle breaks and releases the cargo, anti-cancer chemotherapeutics, due to the cleavage between the hydrophobic and hydrophilic chains. This kind of design enabled the performance of photo-dynamic and chemical cancer therapy at the same time and has excellent potential to improve their efficiency of them.

Acenes have also been applied in complicated bio-imaging systems. For instance, the Smith group developed a host-guest complex for thermally activated chemiluminescence.[121] In that work, a squaraine fluorophore was encapsulated inside a macrocycle containing two anthracene moieties. The anthracene reacted with singlet oxygen in the air under irradiation to form endoperoxides. When the cycloreversion was triggered by thermal energy, the generated excited-state anthracene transferred energy to the encapsulated squaraine and released a photo in NIR that can penetrate the body tissue of mice. With different chemical modifications, the wavelength of chemiluminescence can be tuned. [122]

Thanks to the rapid development of organic electronics, research on has regained significant attention, with renewed interest sparking innovative studies.[4, 39, 40, 51, 60, 123] We believe this field still holds unlimited possibilities, promising exciting advancements in the future.

References

(1) Sirringhaus, H. 25th Anniversary Article: Organic Field-Effect Transistors: The Path Beyond Amorphous Silicon. *Advanced Materials* **2014**, *26* (9), 1319-1335. DOI: 10.1002/adma.201304346.

(2) Anthony, J. E. Functionalized acenes and heteroacenes for organic electronics. *Chemical Reviews* **2006**, *106* (12), 5028-5048. DOI: 10.1021/cr050966z.

(3) Fudickar, W.; Linker, T. Why Triple Bonds Protect Acenes from Oxidation and Decomposition. *Journal of the American Chemical Society* **2012**, *134* (36), 15071-15082. DOI: 10.1021/ja306056x.

(4) Brega, V.; Yan, Y.; Thomas, S. W., 3rd. Acenes beyond organic electronics: sensing of singlet oxygen and stimuli-responsive materials. *Org Biomol Chem* **2020**, *18* (45), 9191-9209. DOI: 10.1039/d0ob01744b From NLM PubMed-not-MEDLINE.

(5) Dorel, R.; Echavarren, A. M. Strategies for the Synthesis of Higher Acenes. *European Journal of Organic Chemistry* **2017**, *2017* (1), 14-24. DOI: 10.1002/ejoc.201601129.

(6) Watanabe, M.; Chen, K. Y.; Chang, Y. J.; Chow, T. J. Acenes Generated from Precursors and Their Semiconducting Properties. *Accounts of Chemical Research* **2013**, *46* (7), 1606-1615. DOI: 10.1021/ar400002y.

(7) Anthony, J. E. The larger acenes: Versatile organic semiconductors. *Angewandte Chemie-International Edition* **2008**, *47* (3), 452-483. DOI: 10.1002/anie.200604045.

(8) Pramanik, C.; Miller, G. P. An Improved Synthesis of Pentacene: Rapid Access to a Benchmark Organic Semiconductor. *Molecules* **2012**, *17* (4), 4625-4633. DOI: 10.3390/molecules17044625.

(9) Bailey, W. J.; Liao, C.-W. Cyclic Dienes. XI. New Syntheses of Hexacene and Heptacene1, 2. *Journal of the American Chemical Society* **1955**, *77* (4), 992-993.

(10) Chen, K. Y.; Hsieh, H. H.; Wu, C. C.; Hwang, J. J.; Chow, T. J. A new type of soluble pentacene precursor for organic thin-film transistors. *Chemical Communications* **2007**, (10), 1065-1067. DOI: 10.1039/b616511g.

(11) Watanabe, M.; Chang, Y. J.; Liu, S. W.; Chao, T. H.; Goto, K.; Islam, M. M.; Yuan, C. H.; Tao, Y. T.; Shinmyozu, T.; Chow, T. J. The synthesis, crystal structure and charge-transport properties of hexacene. *Nature Chemistry* **2012**, *4* (7), 574-578. DOI: 10.1038/nchem.1381.

(12) Einholz, R.; Fang, T.; Berger, R.; Griininger, P.; Fruh, A.; Chasse, T.; Fink, R. F.; Bettinger, H. F. Heptacene: Characterization in Solution, in the Solid State, and in Films. *Journal of the American Chemical Society* **2017**, *139* (12), 4435-4442. DOI: 10.1021/jacs.6b13212.

(13) Jancarik, A.; Levet, G.; Gourdon, A. A Practical General Method for the Preparation of Long Acenes. *Chemistry-a European Journal* **2019**, *25* (9), 2366-2374. DOI: 10.1002/chem.201805975.

(14) Zuzak, R.; Dorel, R.; Kolmer, M.; Szymonski, M.; Godlewski, S.; Echavarren, A. M. Higher Acenes by On-Surface Dehydrogenation: From Heptacene to Undecacene. *Angewandte Chemie-International Edition* **2018**, *57* (33), 10500-10505. DOI: 10.1002/anie.201802040.

(15) Urgel, J. I.; Mishra, S.; Hayashi, H.; Wilhelm, J.; Pignedoli, C. A.; Di Giovannantonio, M.; Widmer, R.; Yamashita, M.; Hieda, N.; Ruffieux, P.; et al. On-surface light-induced generation of higher acenes and elucidation of their open-shell character. *Nature Communications* **2019**, *10* (1). DOI: 10.1038/s41467-019-08650-y (acccessed 2023-05-30T18:44:38).

(16) Maulding, D. R.; Roberts, B. G. ELECTRONIC ABSORPTION AND FLUORESCENCE OF PHENYLETHYNYL-SUBSTITUTED ACENES. *Journal of Organic Chemistry* **1969**, *34* (6), 1734-&. DOI: 10.1021/jo01258a045.

(17) Allen, C. F. H.; Bell, A. Action of Grignard reagents on certain pentacenequinones, 6,13-diphenylpentacene. *Journal of the American Chemical Society* **1942**, *64*, 1253-1260. DOI: 10.1021/ja01258a005.

(18) Anthony, J. E.; Brooks, J. S.; Eaton, D. L.; Parkin, S. R. Functionalized pentacene: Improved electronic properties from control of solid-state order. *Journal of the American Chemical Society* **2001**, *123* (38), 9482-9483. DOI: 10.1021/ja0162459.

(19) Chen, J. H.; Martin, D. C.; Anthony, J. E. Morphology and molecular orientation of thin-film bis(triisopropylsilylethynyl) pentacene. *Journal of Materials Research* **2007**, *22* (6), 1701-1709. DOI: 10.1557/jmr.2007.0220.

(20) Lehnherr, D.; Tykwinski, R. R. Pentacene oligomers and polymers: Functionalization of pentacene to afford mono-, Di-, Tri-, and polymeric materials. *Organic Letters* **2007**, *9* (22), 4583-4586. DOI: 10.1021/ol702094d.

(21) Marshall, J. L.; Lehnherr, D.; Lindner, B. D.; Tykwinski, R. R. Reductive Aromatization/Dearomatization and Elimination Reactions to Access Conjugated Polycyclic Hydrocarbons, Heteroacenes, and Cumulenes. *Chempluschem* **2017**, *82* (7), 967-1001. DOI: 10.1002/cplu.201700168.

(22) Tykwinski, R. R. Synthesis of Unsymmetrical Derivatives of Pentacene for Materials Applications. *Accounts of Chemical Research* **2019**, *52* (8), 2056-2069. DOI: 10.1021/acs.accounts.9b00216.

(23) Purushothaman, B.; Bruzek, M.; Parkin, S. R.; Miller, A. F.; Anthony, J. E. Synthesis and Structural Characterization of Crystalline Nonacenes. *Angewandte Chemie-International Edition* **2011**, *50* (31), 7013-7017. DOI: 10.1002/anie.201102671.

(24) Sorli, J. C.; Ai, Q. X.; Granger, D. B.; Gu, K. C.; Parkin, S.; Jarolimek, K.; Telesz, N.; Anthony, J. E.; Risko, C.; Loo, Y. L. Impact of Atomistic Substitution on Thin-Film Structure and Charge Transport in a Germanyl-ethynyl Functionalized Pentacene. *Chemistry of Materials* **2019**, *31* (17), 6615-6623. DOI: 10.1021/acs.chemmater.9b00546.

(25) Purushothaman, B.; Parkin, S. R.; Kendrick, M. J.; David, D.; Ward, J. W.; Yu, L. Y.; Stingelin, N.; Jurchescu, O. D.; Ostroverkhova, O.; Anthony, J. E. Synthesis and charge transport studies of stable, soluble hexacenes. *Chemical Communications* **2012**, *48* (66), 8261-8263. DOI: 10.1039/c2cc33919f.

(26) Waterloo, A. R.; Kunakom, S.; Hampel, F.; Tykwinski, R. R. Acenes With a Click. *Macromolecular Chemistry and Physics* **2012**, *213* (10-11), 1020-1032. DOI: 10.1002/macp.201100622 (acccessed 2023-05-30T20:09:04).

(27) Altinok, E.; Smith, Z. C.; Thomas, S. W. Two-Dimensional, Acene-Containing Conjugated Polymers That Show Ratiometric Fluorescent Response to Singlet Oxygen. *Macromolecules* **2015**, *48* (19), 6825-6831. DOI: 10.1021/acs.macromol.5b01076.

(28) Yan, Y.; Lamport, Z. A.; Kymissis, I.; Thomas, S. W., 3rd. Resistance to Unwanted Photo-Oxidation of Multi-Acene Molecules. *J Org Chem* **2020**, *85* (19), 12731-12739. DOI: 10.1021/acs.joc.0c01890 From NLM PubMed-not-MEDLINE.

(29) Dai, G. L.; Chang, J. J.; Luo, J.; Dong, S. Q.; Aratani, N.; Zheng, B.; Huang, K. W.; Yamada, H.; Chi, C. Y. Z-Shaped Pentaleno-Acene Dimers with High Stability and Small Band Gap. *Angewandte Chemie-International Edition* **2016**, *55* (8), 2693-2696. DOI: 10.1002/anie.201508919.

(30) Lakshminarayana, A. N.; Chang, J. J.; Luo, J.; Zheng, B.; Huang, K. W.; Chi, C. Y. Bisindeno-annulated pentacenes with exceptionally high photo-stability and ordered molecular packing: simple synthesis by a regio-selective Scholl reaction. *Chemical Communications* **2015**, *51* (17), 3604-3607. DOI: 10.1039/c4cc09812a.

(31) Shi, X. L.; Chi, C. Y. Different Strategies for the Stabilization of Acenes and Acene Analogues. *Chemical Record* **2016**, *16* (3), 1690-1700. DOI: 10.1002/tcr.201600031.

(32) Murata, M.; Togo, M.; Mishima, D.; Harada, A.; Muraoka, M. Benzo- and Thieno-Annulated Tetracenes: A One-Pot Synthesis via Cross-Dehydrogenative Annulation. *Organic Letters* **2020**, *22* (11), 4160-4163. DOI: 10.1021/acs.orglett.0c01244.
(33) Shen, B.; Geiger, T.; Einholz, R.; Reicherter, F.; Schundelmeier, S.; Maichle-Mossmer, C.; Speiser, B.; Bettinger, H. F. Bridging the Gap between Pentacene and Perfluoropentacene: Synthesis and Characterization of 2,3,9,10-Tetrafluoropentacene in the Neutral, Cationic, and Dicationic States. *Journal of Organic Chemistry* **2018**, *83* (6), 3149-3158. DOI: 10.1021/acs.joc.7b03241.
(34) Agou, T.; Suzuki, S.; Kanno, Y.; Hosoya, T.; Fukumoto, H.; Mizuhata, Y.; Tokitoh, N.; Suda, Y.; Furukawa, S.; Saito, M.; et al. Synthesis and properties of perfluoroalkylated TIPS-pentacenes. *Tetrahedron* **2019**, *75* (47). DOI: 10.1016/j.tet.2019.130678.
(35) Pramanik, C.; Li, Y. S.; Singh, A.; Lin, W. M.; Hodgson, J. L.; Briggs, J. B.; Ellis, S.; Muller, P.; McGruer, N. E.; Miller, G. P. Water soluble pentacene. *Journal of Materials Chemistry C* **2013**, *1* (11), 2193-2201. DOI: 10.1039/c3tc00278k.
(36) Miao, Q.; Nguyen, T. Q.; Someya, T.; Blanchet, G. B.; Nuckolls, C. Synthesis, assembly, and thin film transistors of dihydrodiazapentacene: an isostructural motif for pentacene. *J Am Chem Soc* **2003**, *125* (34), 10284-10287. DOI: 10.1021/ja036466+ From NLM PubMed-not-MEDLINE.
(37) Bunz, U. H.; Engelhart, J. U.; Lindner, B. D.; Schaffroth, M. Large N-heteroacenes: new tricks for very old dogs? *Angew Chem Int Ed Engl* **2013**, *52* (14), 3810-3821. DOI: 10.1002/anie.201209479 From NLM PubMed-not-MEDLINE.
(38) Li, J. B.; Zhang, Q. C. Linearly Fused Azaacenes: Novel Approaches and New Applications Beyond Field-Effect Transistors (FETs). *Acs Applied Materials & Interfaces* **2015**, *7* (51), 28049-28062. DOI: 10.1021/acsami.5b00113.
(39) Gu, P. Y.; Wang, Z. L.; Zhang, Q. C. Azaacenes as active elements for sensing and bio applications. *Journal of Materials Chemistry B* **2016**, *4* (44), 7060-7074. DOI: 10.1039/c6tb02052f.
(40) Zhang, Z. B.; Zhang, Q. C. Recent progress in well-defined higher azaacenes (n >= 6): synthesis, molecular packing, and applications. *Materials Chemistry Frontiers* **2020**, *4* (12), 3419-3432. DOI: 10.1039/c9qm00656g.
(41) Wex, B.; El-Ballouli, A. O.; Vanvooren, A.; Zschieschang, U.; Klauk, H.; Krause, J. A.; Cornil, J.; Kaafarani, B. R. Crystalline TQPP as p-type semiconductor: X-ray crystallographic investigation, OTFT device, and computational analysis of transport properties. *J Mol Struct* **2015**, *1093*, 144-149. DOI: 10.1016/j.molstruc.2015.03.057.
(42) More, S.; Bhosale, R.; Choudhary, S.; Mateo-Alonso, A. Versatile 2,7-substituted pyrene synthons for the synthesis of pyrene-fused azaacenes. *Org Lett* **2012**, *14* (16), 4170-4173. DOI: 10.1021/ol301841h From NLM PubMed-not-MEDLINE.
(43) Wang, Z.; Gu, P.; Liu, G.; Yao, H.; Wu, Y.; Li, Y.; Rakesh, G.; Zhu, J.; Fu, H.; Zhang, Q. A large pyrene-fused N-heteroacene: fifteen aromatic six-membered rings annulated in one row. *Chem Commun (Camb)* **2017**, *53* (55), 7772-7775. DOI: 10.1039/c7cc03898d From NLM PubMed-not-MEDLINE.
(44) Imran, M.; Chen, M. S. Self-Sensitized and Reversible O(2) Reactivity with Bisphenalenyls for Simple, Tunable, and Multicycle Colorimetric Oxygen-Sensing Films. *ACS Appl Mater Interfaces* **2022**, *14* (1), 1817-1825. DOI: 10.1021/acsami.1c16033 From NLM PubMed-not-MEDLINE.

(45) Dewar, M. J.; Poesche, W. H. New Heteroaromatic Compounds. XVIII. 1 Boron-Containing Analogs of Benz [a] anthracene 2. *Journal of the American Chemical Society* **1963**, *85* (15), 2253-2256.

(46) Ishibashi, J. S.; Marshall, J. L.; Maziere, A.; Lovinger, G. J.; Li, B.; Zakharov, L. N.; Dargelos, A.; Graciaa, A.; Chrostowska, A.; Liu, S. Y. Two BN isosteres of anthracene: synthesis and characterization. *J Am Chem Soc* **2014**, *136* (43), 15414-15421. DOI: 10.1021/ja508813v From NLM PubMed-not-MEDLINE.

(47) Ishibashi, J. S. A.; Dargelos, A.; Darrigan, C.; Chrostowska, A.; Liu, S.-Y. BN Tetracene: Extending the Reach of BN/CC Isosterism in Acenes. *Organometallics* **2017**, *36* (14), 2494-2497. DOI: 10.1021/acs.organomet.7b00296.

(48) Liu, K. L.; Lalancette, R. A.; Jakle, F. Tuning the Structure and Electronic Properties of B-N Fused Dipyridylanthracene and Implications on the Self-Sensitized Reactivity with Singlet Oxygen. *Journal of the American Chemical Society* **2019**, *141* (18), 7453-7462. DOI: 10.1021/jacs.9b01958.

(49) Liu, K. L.; Lalancette, R. A.; Jakle, F. B-N Lewis Pair Functionalization of Anthracene: Structural Dynamics, Optoelectronic Properties, and O-2 Sensitization. *Journal of the American Chemical Society* **2017**, *139* (50), 18170-18173. DOI: 10.1021/jacs.7b11062.

(50) Tian, D.; Shi, G.; Fan, M.; Guo, X.; Yuan, Y.; Wu, S.; Liu, J.; Zhang, J.; Xing, S.; Zhu, B. Synthesis, Properties, and Regioselective Functionalization of 9,9a-BN Anthracene. *Org Lett* **2021**, *23* (21), 8163-8168. DOI: 10.1021/acs.orglett.1c02843 From NLM PubMed-not-MEDLINE.

(51) Guo, Y.; Chen, C.; Wang, X. Y. Recent Advances in Boron-Containing Acenes: Synthesis, Properties, and Optoelectronic Applications†. *Chinese Journal of Chemistry* **2023**, *41* (11), 1355-1373. DOI: 10.1002/cjoc.202200700.

(52) Ishibashi, J. S. A.; Darrigan, C.; Chrostowska, A.; Li, B.; Liu, S. Y. A BN anthracene mimics the electronic structure of more highly conjugated systems. *Dalton Trans* **2019**, *48* (8), 2807-2812. DOI: 10.1039/c9dt00481e From NLM PubMed-not-MEDLINE.

(53) Bouas-Laurent, H.; Castellan, A.; Desvergne, J. P.; Lapouyade, R. Photodimerization of anthracenes in fluid solution: structural aspects. *Chemical Society Reviews* **2000**, *29* (1), 43-55. DOI: 10.1039/a801821i.

(54) Zade, S. S.; Bendikov, M. Reactivity of acenes: mechanisms and dependence on acene length. *Journal of Physical Organic Chemistry* **2012**, *25* (6), 452-461. DOI: 10.1002/poc.1941.

(55) Qualizza, B. A.; Ciszek, J. W. Experimental survey of the kinetics of acene Diels-Alder reactions. *Journal of Physical Organic Chemistry* **2015**, *28* (10), 629-634. DOI: 10.1002/poc.3463.

(56) Zhao, Y. C.; Rocha, S. V.; Swager, T. M. Mechanochemical Synthesis of Extended Iptycenes. *Journal of the American Chemical Society* **2016**, *138* (42), 13834-13837. DOI: 10.1021/jacs.6b09011.

(57) Sun, H.; Kabb, C. P.; Dai, Y. Q.; Hill, M. R.; Ghiviriga, I.; Bapat, A. P.; Sumerlin, B. S. Macromolecular metamorphosis via stimulus-induced transformations of polymer architecture. *Nature Chemistry* **2017**, *9* (8), 817-823. DOI: 10.1038/nchem.2730.

(58) Gunay, K. A.; Ceccato, T. L.; Silver, J. S.; Bannister, K. L.; Bednarski, O. J.; Leinwand, L. A.; Anseth, K. S. PEG-Anthracene Hydrogels as an On- Demand Stiffening Matrix To Study Mechanobiology. *Angewandte Chemie-International Edition* **2019**, *58* (29), 9912-9916. DOI: 10.1002/anie.201901989.

(59) Frank, P. G.; Tuten, B. T.; Prasher, A.; Chao, D. M.; Berda, E. B. Intra- Chain Photodimerization of Pendant Anthracene Units as an Efficient Route to Single- Chain

Nanoparticle Fabrication. *Macromolecular Rapid Communications* **2014**, *35* (2), 249-253. DOI: 10.1002/marc.201300677.

(60) Van Damme, J.; Du Prez, F. Anthracene-containing polymers toward high-end applications. *Progress in Polymer Science* **2018**, *82*, 92-119. DOI: 10.1016/j.progpolymsci.2018.02.002.

(61) Claus, T. K.; Telitel, S.; Welle, A.; Bastmeyer, M.; Vogt, A. P.; Delaittre, G.; Barner-Kowollik, C. Light-driven reversible surface functionalization with anthracenes: visible light writing and mild UV erasing. *Chemical Communications* **2017**, *53* (10), 1599-1602. DOI: 10.1039/c6cc09897e.

(62) Sulkanen, A. R.; Sung, J.; Robb, M. J.; Moore, J. S.; Sottos, N. R.; Liu, G. Y. Spatially Selective and Density-Controlled Activation of Interfacial Mechanophores. *Journal of the American Chemical Society* **2019**, *141* (9), 4080-4085. DOI: 10.1021/jacs.8b10257.

(63) Church, D. C.; Peterson, G. I.; Boydston, A. J. Comparison of Mechanochemical Chain Scission Rates for Linear versus Three-Arm Star Polymers in Strong Acoustic Fields. *Acs Macro Letters* **2014**, *3* (7), 648-651. DOI: 10.1021/mz5003068.

(64) Li, J.; Shiraki, T.; Hu, B.; Wright, R. A. E.; Zhao, B.; Moore, J. S. Mechanophore Activation at Heterointerfaces. *Journal of the American Chemical Society* **2014**, *136* (45), 15925-15928. DOI: 10.1021/ja509949d.

(65) Li, F. F.; Ciszek, J. W. Reaction induced morphology changes of tetracene and pentacene surfaces. *Rsc Advances* **2019**, *9* (46), 26942-26948. DOI: 10.1039/c9ra05682c.

(66) Li, F. F.; Hopwood, J. P.; Galey, M. M.; Sanchez, L. M.; Ciszek, J. W. Chemically transformed monolayers on acene thin films for improved metal/organic interfaces. *Chemical Communications* **2019**, *55* (93), 13975-13978. DOI: 10.1039/c9cc07234a.

(67) Qualizza, B. A.; Prasad, S.; Chiarelli, M. P.; Ciszek, J. W. Functionalization of organic semiconductor crystals via the Diels-Alder reaction. *Chemical Communications* **2013**, *49* (40), 4495-4497. DOI: 10.1039/c3cc40866c.

(68) Johns, V. K.; Shi, Z.; Dang, W.; McInnis, M. D.; Weng, Y. X.; Liao, Y. Photo Retro-Diels-Alder Reactions. *Journal of Physical Chemistry A* **2011**, *115* (28), 8093-8099. DOI: 10.1021/jp202063m.

(69) Johns, V. K.; Shi, Z.; Hu, W. F.; Johns, J. B.; Zou, S. L.; Liao, Y. Photo- and Thermal-Induced Isomerization of Diels-Alder Adducts of Pentacene and TCNE. *European Journal of Organic Chemistry* **2012**, *2012* (14), 2707-2710. DOI: 10.1002/ejoc.201200195.

(70) Greer, A. Christopher Foote's discovery of the role of singlet oxygen [1O2 (1Delta g)] in photosensitized oxidation reactions. *Acc Chem Res* **2006**, *39* (11), 797-804. DOI: 10.1021/ar050191g From NLM Medline.

(71) Adam, W.; Prein, M. π-Facial Diastereoselectivity in the [4+2] Cycloaddition of Singlet Oxygen as a Mechanistic Probe. *Accounts of Chemical Research* **1996**, *29* (6), 275-283. DOI: 10.1021/ar950164y (acccessed 2023-06-01T01:00:31).

(72) Schweitzer, C.; Schmidt, R. Physical mechanisms of generation and deactivation of singlet oxygen. *Chem Rev* **2003**, *103* (5), 1685-1757. DOI: 10.1021/cr010371d (acccessed 2023-08-02T11:35:16). From NLM PubMed-not-MEDLINE.

(73) DeRosa, M. Photosensitized singlet oxygen and its applications. *Coordin Chem Rev* **2002**, *233-234*, 351-371. DOI: 10.1016/s0010-8545(02)00034-6.

(74) Weishaupt, K. R.; Gomer, C. J.; Dougherty, T. J. Identification of singlet oxygen as the cytotoxic agent in photo-inactivation of a murine tumor. *Cancer research* **1976**, *36* (7_Part_1), 2326-2329.

(75) Sies, H.; Menck, C. F. Singlet oxygen induced DNA damage. *Mutation Research/DNAging* **1992**, *275* (3-6), 367-375.

(76) Enko, B.; Borisov, S. M.; Regensburger, J.; Bäumler, W.; Gescheidt, G.; Klimant, I. Singlet Oxygen-Induced Photodegradation of the Polymers and Dyes in Optical Sensing Materials and the Effect of Stabilizers on These Processes. *The Journal of Physical Chemistry A* **2013**, *117* (36), 8873-8882. DOI: 10.1021/jp4046462 (acccessed 2023-06-01T01:02:10).

(77) Scurlock, R. D.; Wang, B.; Ogilby, P. R.; Sheats, J. R.; Clough, R. L. Singlet Oxygen as a Reactive Intermediate in the Photodegradation of an Electroluminescent Polymer. *Journal of the American Chemical Society* **1995**, *117* (41), 10194-10202. DOI: 10.1021/ja00146a004 (acccessed 2023-06-01T01:03:12).

(78) Thomas, S.; Altinok, E.; Zhang, J. Cycloadditions of Singlet Oxygen for Responsive Fluorescent Polymers. *Synlett* **2015**, *27* (03), 355-368. DOI: 10.1055/s-0035-1560725.

(79) Zhang, J.; Smith, Z. C.; Thomas, S. W., 3rd. Electronic effects of ring fusion and alkyne substitution on acene properties and reactivity. *J Org Chem* **2014**, *79* (21), 10081-10093. DOI: 10.1021/jo501696d From NLM PubMed-not-MEDLINE.

(80) Zhang, J. J.; Pawle, R. H.; Haas, T. E.; Thomas, S. W. Combining Electronic and Steric Effects for Highly Stable Unsymmetric Pentacenes. *Chemistry-a European Journal* **2014**, *20* (20), 5880-5884. DOI: 10.1002/chem.201402003.

(81) Baral, R. N.; Thomas, S. W. Steric and Electronic Substituent Effects Influencing Regioselectivity of Tetracene Endoperoxidation. *Journal of Organic Chemistry* **2015**, *80* (21), 11086-11091. DOI: 10.1021/acs.joc.5b01692.

(82) Tanaka, K.; Miura, T.; Umezawa, N.; Urano, Y.; Kikuchi, K.; Higuchi, T.; Nagano, T. Rational design of fluorescein-based fluorescence probes, mechanism-based design of a maximum fluorescence probe for singlet oxygen. *Journal of the American Chemical Society* **2001**, *123* (11), 2530-2536. DOI: 10.1021/ja0035708.

(83) Frausto, F.; Thomas, S. W., 3rd. Ratiometric Singlet Oxygen Detection in Water Using Acene-Doped Conjugated Polymer Nanoparticles. *ACS Appl Mater Interfaces* **2017**, *9* (18), 15768-15775. DOI: 10.1021/acsami.7b02034 From NLM PubMed-not-MEDLINE.

(84) Zhang, J. J.; Sarrafpour, S.; Pawle, R. H.; Thomas, S. W. Acene-linked conjugated polymers with ratiometric fluorescent response to O-1(2). *Chemical Communications* **2011**, *47* (12), 3445-3447. DOI: 10.1039/c0cc05770c.

(85) Brega, V.; Kanari, S. N.; Doherty, C. T.; Che, D.; Sharber, S. A.; Thomas, S. W., 3rd. Spectroscopy and Reactivity of Dialkoxy Acenes. *Chemistry* **2019**, *25* (44), 10400-10407. DOI: 10.1002/chem.201901258 From NLM PubMed-not-MEDLINE.

(86) Koylu, D.; Sarrafpour, S.; Zhang, J. J.; Ramjattan, S.; Panzer, M. J.; Thomas, S. W. Acene-doped polymer films: singlet oxygen dosimetry and protein sensing. *Chemical Communications* **2012**, *48* (76), 9489-9491. DOI: 10.1039/c2cc34640k.

(87) Zhang, J.; Sarrafpour, S.; Haas, T. E.; Müller, P.; Thomas, S. W. Structure, photophysics, and photooxidation of crowded diethynyltetracenes. *Journal of Materials Chemistry* **2012**, *22* (13), 6182. DOI: 10.1039/c2jm16173g (acccessed 2023-06-01T01:51:58).

(88) Brega, V.; Kanari, S. N.; Doherty, C. T.; Che, D.; Sharber, S. A.; Thomas, S. W. Spectroscopy and Reactivity of Dialkoxy Acenes. *Chemistry-a European Journal* **2019**, *25* (44), 10400-10407. DOI: 10.1002/chem.201901258.

(89) Thorley, K. J.; Benford, M.; Song, Y.; Parkin, S. R.; Risko, C.; Anthony, J. E. What is special about silicon in functionalised organic semiconductors? *Materials Advances* **2021**, *2* (16), 5415-5421. DOI: 10.1039/d1ma00447f.

(90) Thorley, K. J.; Le, H.; Song, Y.; Anthony, J. E. Unravelling the major factors in photo-oxidative stability of anthradithiophene derivatives. *Journal of Materials Chemistry C* **2022**, *10* (42), 15861-15871. DOI: 10.1039/d2tc02922g (acccessed 2023-03-24T18:04:40).

(91) Stone, M. T.; Anderson, H. L. A cyclodextrin-insulated anthracene rotaxane with enhanced fluorescence and photostability. *Chem Commun (Camb)* **2007**, (23), 2387-2389. DOI: 10.1039/b700868f From NLM PubMed-not-MEDLINE.

(92) Ly, J.; Martin, K.; Thomas, S.; Yamashita, M.; Yu, B. H.; Pointer, C. A.; Yamada, H.; Carter, K. R.; Parkin, S.; Zhang, L.; et al. Short Excited-State Lifetimes Enable Photo-Oxidatively Stable Rubrene Derivatives. *Journal of Physical Chemistry A* **2019**, *123* (35), 7558-7566. DOI: 10.1021/acs.jpca.9b04203.

(93) Wilkinson, F.; Helman, W. P.; Ross, A. B. Rate Constants for the Decay and Reactions of the Lowest Electronically Excited Singlet-State of Molecular-Oxygen in Solution - an Expanded and Revised Compilation. *Journal of Physical and Chemical Reference Data* **1995**, *24* (2), 663-1021. DOI: Doi 10.1063/1.555965.

(94) Altinok, E.; Frausto, F.; Thomas, S. W. Water-Soluble Fluorescent Polymers that Respond to Singlet Oxygen. *Journal of Polymer Science Part a-Polymer Chemistry* **2016**, *54* (16), 2526-2535. DOI: 10.1002/pola.28130.

(95) Kim, S.; Fujitsuka, M.; Majima, T. Photochemistry of Singlet Oxygen Sensor Green. *Journal of Physical Chemistry B* **2013**, *117* (45), 13985-13992. DOI: 10.1021/jp406638g.

(96) Pedersen, S. K.; Holmehave, J.; Blaikie, F. H.; Gollmer, A.; Breitenbach, T.; Jensen, H. H.; Ogilby, P. R. Aarhus Sensor Green: A Fluorescent Probe for Singlet Oxygen. *Journal of Organic Chemistry* **2014**, *79* (7), 3079-3087. DOI: 10.1021/jo500219y.

(97) Umezawa, N.; Tanaka, K.; Urano, Y.; Kikuchi, K.; Higuchi, T.; Nagano, T. Novel fluorescent probes for singlet oxygen. *Angewandte Chemie-International Edition* **1999**, *38* (19), 2899-2901. DOI: 10.1002/(sici)1521-3773(19991004)38:19<2899::Aid-anie2899>3.0.Co;2-m.

(98) Kim, S.; Tachikawa, T.; Fujitsuka, M.; Majima, T. Far-Red Fluorescence Probe for Monitoring Singlet Oxygen during Photodynamic Therapy. *Journal of the American Chemical Society* **2014**, *136* (33), 11707-11715. DOI: 10.1021/ja504279r.

(99) Brega, V.; Thomas, S. W., 3rd. Red-Emitting, Acene-Doped Conjugated Polymer Nanoparticles that Respond Ratiometrically to Photogenerated (1)O(2). *ACS Appl Mater Interfaces* **2021**, *13* (11), 13658-13665. DOI: 10.1021/acsami.0c22313 From NLM PubMed-not-MEDLINE.

(100) Thomas, S. W.; Joly, G. D.; Swager, T. M. Chemical Sensors Based on Amplifying Fluorescent Conjugated Polymers. *Chemical Reviews* **2007**, *107* (4), 1339-1386. DOI: 10.1021/cr0501339 (acccessed 2023-06-01T15:32:15).

(101) Wu, C.; Szymanski, C.; Mcneill, J. Preparation and Encapsulation of Highly Fluorescent Conjugated Polymer Nanoparticles. *Langmuir* **2006**, *22* (7), 2956-2960. DOI: 10.1021/la060188l (acccessed 2023-06-01T17:04:55).

(102) Tuncel, D.; Demir, H. V. Conjugated polymer nanoparticles. *Nanoscale* **2010**, *2* (4), 484. DOI: 10.1039/b9nr00374f (acccessed 2023-06-01T17:03:05).

(103) Feng, L. H.; Zhu, C. L.; Yuan, H. X.; Liu, L. B.; Lv, F. T.; Wang, S. Conjugated polymer nanoparticles: preparation, properties, functionalization and biological applications. *Chemical Society Reviews* **2013**, *42* (16), 6620-6633. DOI: 10.1039/c3cs60036j.

(104) Frausto, F.; Thomas, S. W. Tuning the Key Properties of Singlet Oxygen-Responsive Acene-Doped Conjugated Polymer Nanoparticles. *ChemPhotoChem* **2018**, *2* (7), 632-639. DOI: 10.1002/cptc.201800039.

(105) Han, Y.; Yin, Y.; Wang, F.; Wang, F. Single-Photon Near-Infrared-Responsiveness from the Molecular to the Supramolecular Level via Platination of Pentacenes. *Angew Chem Int Ed Engl* **2021**, *60* (25), 14076-14082. DOI: 10.1002/anie.202103125 From NLM PubMed-not-MEDLINE.
(106) Huang, H.; Chen, B.; Li, L.; Wang, Y.; Shen, Z.; Wang, Y.; Li, X. A two-photon fluorescence probe with endoplasmic reticulum targeting ability for turn-on sensing photosensitized singlet oxygen in living cells and brain tissues. *Talanta* **2022**, *237*, 122963. DOI: 10.1016/j.talanta.2021.122963 From NLM Medline.
(107) Ragas, X.; Jimenez-Banzo, A.; Sanchez-Garcia, D.; Batllori, X.; Nonell, S. Singlet oxygen photosensitisation by the fluorescent probe Singlet Oxygen Sensor Green (R). *Chemical Communications* **2009**, (20), 2920-2922. DOI: 10.1039/b822776d.
(108) Ruiz-Gonzalez, R.; Bresoli-Obach, R.; Gulias, O.; Agut, M.; Savoie, H.; Boyle, R. W.; Nonell, S.; Giuntini, F. NanoSOSG: A Nanostructured Fluorescent Probe for the Detection of Intracellular Singlet Oxygen. *Angewandte Chemie-International Edition* **2017**, *56* (11), 2885-2888. DOI: 10.1002/anie.201609050.
(109) Dolmans, D.; Fukumura, D.; Jain, R. K. Photodynamic therapy for cancer. *Nature Reviews Cancer* **2003**, *3* (5), 380-387. DOI: 10.1038/nrc1071.
(110) Long, L. L.; Yuan, X. Q.; Cao, S. Y.; Han, Y. Y.; Liu, W. G.; Chen, Q.; Gong, A. H.; Wang, K. Construction of a fluorescent probe for selectively detecting singlet oxygen with a high sensitivity and large concentration range based on a two-step cascade sensing reaction. *Chemical Communications* **2019**, *55* (58), 8462-8465. DOI: 10.1039/c9cc04300d.
(111) Fudickar, W.; Linker, T. Release of Singlet Oxygen from Organic Peroxides under Mild Conditions. *Chemphotochem* **2018**, *2* (7), 548-558. DOI: 10.1002/cptc.201700235.
(112) You, Y. Chemical tools for the generation and detection of singlet oxygen. *Organic & Biomolecular Chemistry* **2018**, *16* (22), 4044-4060. DOI: 10.1039/c8ob00504d.
(113) Wang, Q.; Li, C.; Song, Y.; Shi, Q.; Li, H.; Zhong, H.; Wang, J.; Hu, F. Acene enlargement for absorption red-shifting and photosensitization enhancement of photosensitizers with aggregation-induced emission. *Chem Sci* **2023**, *14* (3), 684-690. DOI: 10.1039/d2sc05454j From NLM PubMed-not-MEDLINE.
(114) Liu, K.; Jiang, Z.; Lalancette, R. A.; Tang, X.; Jakle, F. Near-Infrared-Absorbing B-N Lewis Pair-Functionalized Anthracenes: Electronic Structure Tuning, Conformational Isomerism, and Applications in Photothermal Cancer Therapy. *J Am Chem Soc* **2022**, *144* (41), 18908-18917. DOI: 10.1021/jacs.2c06538 From NLM Medline.
(115) Asadirad, A. M.; Erno, Z.; Branda, N. R. Photothermal release of singlet oxygen from gold nanoparticles. *Chemical Communications* **2013**, *49* (50), 5639-5641. DOI: 10.1039/c3cc42217h.
(116) Kolemen, S.; Ozdemir, T.; Lee, D.; Kim, G. M.; Karatas, T.; Yoon, J.; Akkaya, E. U. Remote-Controlled Release of Singlet Oxygen by the Plasmonic Heating of Endoperoxide-Modified Gold Nanorods: Towards a Paradigm Change in Photodynamic Therapy. *Angewandte Chemie-International Edition* **2016**, *55* (11), 3606-3610. DOI: 10.1002/anie.201510064.
(117) Martins, S.; Farinha, J. P. S.; Baleizao, C.; Berberan-Santos, M. N. Controlled release of singlet oxygen using diphenylanthracene functionalized polymer nanoparticles. *Chemical Communications* **2014**, *50* (25), 3317-3320. DOI: 10.1039/c3cc48293f.
(118) Lai, H. W.; Yan, J. Y.; Liu, S.; Yang, Q. Z.; Xing, F. Y.; Xiao, P. Peripheral RAFT Polymerization on a Covalent Organic Polymer with Enhanced Aqueous Compatibility for Controlled Generation of Singlet Oxygen. *Angewandte Chemie-International Edition* **2020**, *59* (26), 10431-10435. DOI: 10.1002/anie.202002446.

(119) Arian, D.; Kovbasyuk, L.; Mokhir, A. 1,9-Dialkoxyanthracene as a O-1(2)-Sensitive Linker. *Journal of the American Chemical Society* **2011**, *133* (11), 3972-3980. DOI: 10.1021/ja108819c.

(120) Brega, V.; Scaletti, F.; Zhang, X.; Wang, L. S.; Li, P.; Xu, Q.; Rotello, V. M.; Thomas, S. W., 3rd. Polymer Amphiphiles for Photoregulated Anticancer Drug Delivery. *ACS Appl Mater Interfaces* **2019**, *11* (3), 2814-2820. DOI: 10.1021/acsami.8b18099 From NLM Medline.

(121) Baumes, J. M.; Gassensmith, J. J.; Giblin, J.; Lee, J. J.; White, A. G.; Culligan, W. J.; Leevy, W. M.; Kuno, M.; Smith, B. D. Storable, thermally activated, near-infrared chemiluminescent dyes and dye-stained microparticles for optical imaging. *Nat Chem* **2010**, *2* (12), 1025-1030. DOI: 10.1038/nchem.871 From NLM Medline.

(122) Collins, C. G.; Baumes, J. M.; Smith, B. D. Thermally-activated chemiluminescent squaraine rotaxane endoperoxide with green emission. *Chem Commun (Camb)* **2011**, *47* (45), 12352-12354. DOI: 10.1039/c1cc15550d From NLM PubMed-not-MEDLINE.

(123) Dong, S. Q.; Ong, A.; Chi, C. Y. Photochemistry of various acene based molecules. *Journal of Photochemistry and Photobiology C-Photochemistry Reviews* **2019**, *38*, 27-46. DOI: 10.1016/j.jphotochemrev.2018.12.002.

Chapter 2:

Multi-acene structures and their resistance to unwanted photo-oxidation

Reproduced in part with permission from:

Yan, Y.; Lamport, Z. A.; Kymissis, I.; Thomas, S. W., 3rd. Resistance to Unwanted Photo-Oxidation of Multi-Acene Molecules. *J Org Chem* **2020**, 85 (19), 12731-12739.

DOI: 10.1021/acs.joc.0c01890[28]

2.1 Introduction

Acenes, also known as linearly fused benzenes, have been frequently studied as building blocks for organic electronic devices.[2, 7] Besides, the interesting chemistry properties make acenes promising functional groups in applications[4, 60] such as drug delivery[120], stimuli-responsive materials[61, 62, 64], and singlet oxygen sensing[83, 84, 94-96]. However, the further development of acene-based materials is limited by their vulnerability towards unwanted photo-oxidation, mainly resulting from the self-sensitizing of singlet oxygen (**$^1O_2$**) and the following cycloaddition[76, 77, 124]. This problem is especially challenging for longer acenes due to the lower per-ring aromatic stabilization effect.[79]

Efforts have been made to address this issue via various approaches. For instance, Ogilby and co-workers have developed an acene-based singlet oxygen probe, Aarhus Senser Green (**ASG**).[96] The photo-sensitizing ability of **ASG** was decreased by adding fluorine atoms to the fluorophore, which protected the probe from **$^1O_2$**-mediated photo-oxidation. Other than cutting off the resource, acenes intrinsically inert to **$^1O_2$** have been developed. **TIPS-pentacene** is one of the most famous molecules among this kind.[18, 19] The triple bonds protected the acene core through a combination of altering the mechanism, physical quenching, and accelerating the reverse reaction.[3] Electronic effect and steric hindrance were also identified as major factors in the reactivity of acenes.[79, 81, 125] Moreover, as an alternative approach, kinetically blocking the reactive site of acenes by annulation was reported.[29, 32, 126]

2.2 Experimental design and synthesis of multi-acene structures

Inspired by the increasing volume of reports concerning multi-acene structures, which have been driven in large part by their potential in singlet fission[127-130] and thin film transistors[131]. We were interested in the singlet oxygen responsiveness of covalently-linked acenes. **Figure 2.1a** shows the first design of the original structure in which a conjugated carbon-carbon triple bond bridged an anthracene and a tetracene. However, the difficulty of unsymmetrical substitution of tetracene was very practically challenging.[132] Thus, we simplified the synthesis to the current design (**Figure 2.1b**). This structure can significantly reduce the load on synthesis because i) the anthracenes are symmetrically installed on both

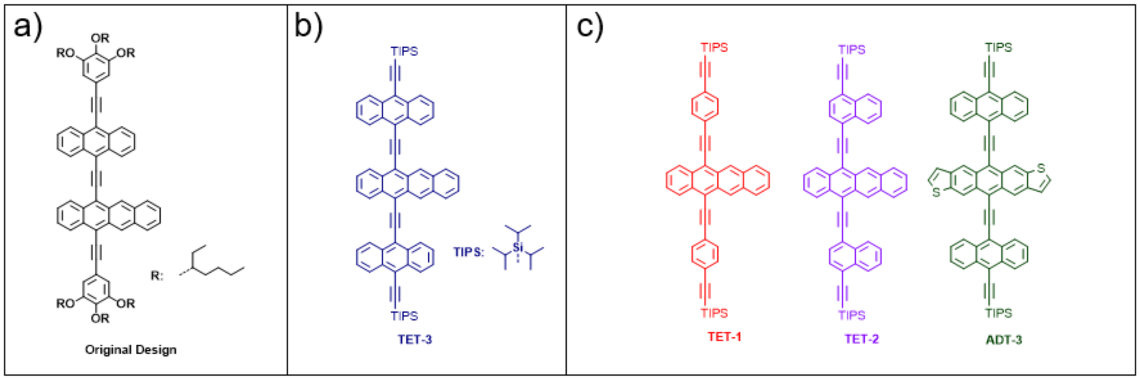

Figure 2.1: Chemical structures of our original design (a), the new design (b), and other developed molecules in this work. Figure reproduced from Ref.1.

sides of tetracene as pendants, ii) and the complicated solubilizing trialkoxy-benzene group was substituted by a triisopropyl-siliane (**TIPS**). Through an analysis of spectroscopy and reactivity, we show that the anthracene-substituted tetracene is highly stable to direct irradiation. We designed a set of controlled compounds to study such abnormalities, as shown in **Figure 2.1c**. With the same diethynyl tetracene core structure, we switched the

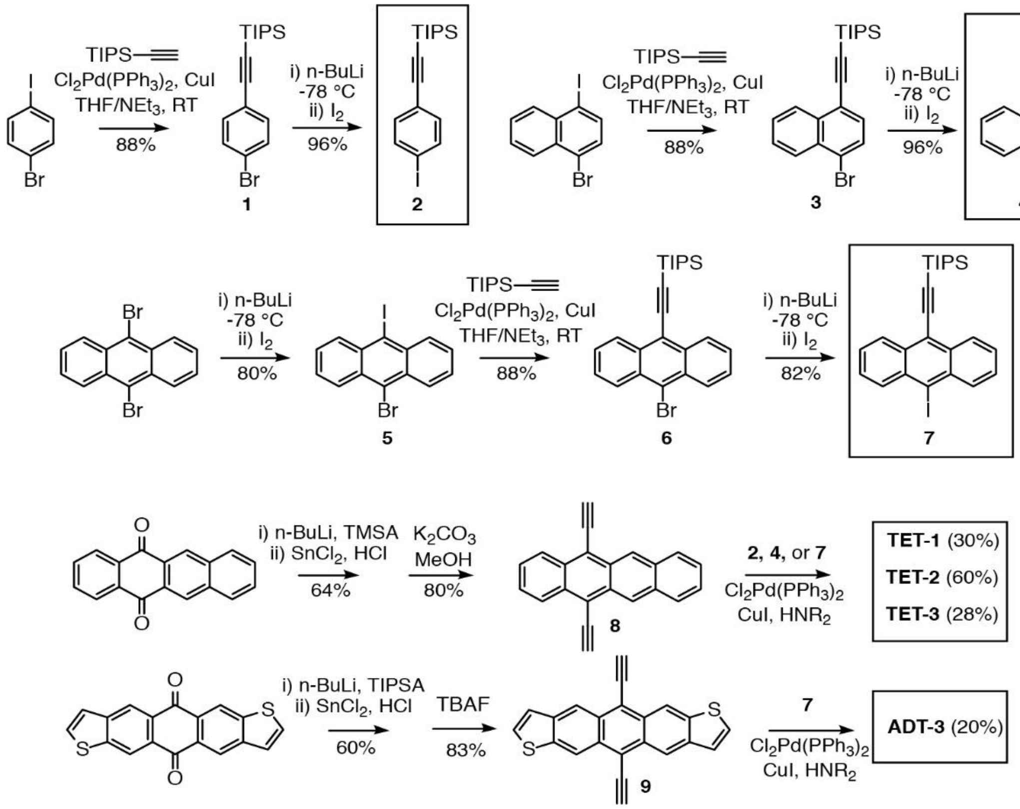

Scheme 2.1: Synthesis of developed acene-derivatives. Figure reproduced from Ref.1.

pendants to naphthalene or benzene to study the impact of side-chain length. Also, we made an anthradithiophene (**ADT**) control to investigate the effect of the core structure and the universality of the stabilization phenomenon.

The pendant and the core structures were synthesized separately and then linked via Sonogashira Coupling. For the tetracenes, we followed a reported synthetic pathway to get diethynyl acene from acene quinone.[132] In detail, trimethylsilyl acetylene (**TMSA**) was deprotonated by organolithium reagent, and the resulting ions attacked the quinones to form a diol intermedia. Tin chloride in diluted hydrochloride acid was then added as a reducer to assist the aromatization of acenes. On the other hand, the pendants were synthesized from unsymmetrical arene dihalides.[133] We utilized the different reactivity of iodide and bromide towards Sonogashira Coupling to obtain the mono-ethynylated arene halide.

2.3 Optical properties of developed acenes

Table 2.1: Photo-physical properties of developed acene derivatives.

Name	λ_{onset}, nm	λ_{max}, nm	ε^a, $M^{-1}cm^{-1}$	λ_{max}(em), nm	Φ_F	τ_{av}, ns	k_{rel}^b
TET-1	665	567*, 363, 293	29,600	581	0.33	6.3	5.5
TET-2	690	581*, 403, 295	37,700	600	0.34	3.6 s	4.1
TET-3	700	590*, 459, 262	53,400	657	< 0.001	-	4.5
ADT-3	730	612*, 466, 263	56,900	672	< 0.003	-	4.1

[a] Measured at the maximum of the longest wavelength band, indicated with an asterisk. [b] Disappearance of acene upon irradiation of **MB**, relative to rate measured for 9,10-diphenylanthracene (DPA, $k_{rel} = 1$) under identical conditions.

All four final compounds were at least moderately soluble; **ADT-3** resisted dissolution the most of the four, although it was sufficiently soluble in THF, toluene, and chlorobenzene to enable full spectroscopic characterization. To understand the impact of multiple conjugated chromophores on the optical transitions of these acenes, we measured the electronic absorbance spectrum of each in solution. **Table 2.1** Photophysical properties of developed acene derivatives.

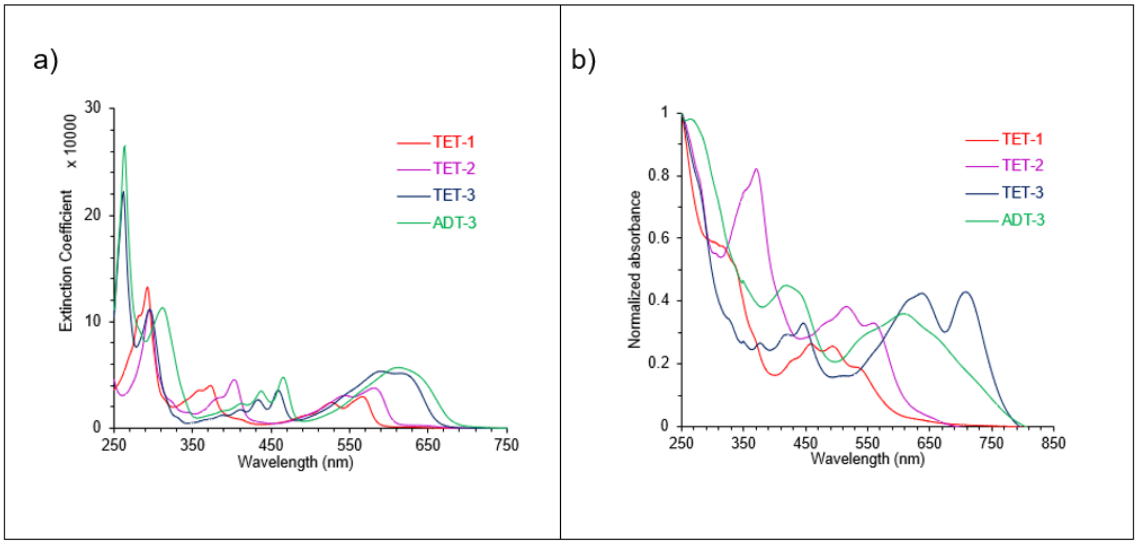

Figure 2.2: Absorbance spectra of developed molecules in (a) solution phase or in (b) solid phase. Figure reproduced from Ref.1.

Figure 2.2a shows the UV/vis spectra of these molecules in CH_2Cl_2 at low (10^{-5}-10^{-6} M) concentration, while **Table 2.1** summarizes their key spectroscopic parameters. These spectra share some common features of diethynyl-acenes[79], such as an intense and sharp transition in the UV and broad bands in the visible with some vibronic resolution. As the lengths of the acene pendants increase from benzene through anthracene, the onset of absorbance and λ_{max} of the lowest energy bands in the visible spectrum shifts to lower energy, with anthracene-conjugated **TET-3** showing λ_{max} of 590 and 620 nm.

In addition, **TET-3** and **ADT-3** show distinct, well-resolved bands from 360-480 nm, which isolated diethynyl-anthracene chromophores.[79] As drop-cast thin films (**Figure 2.2b**), **TET-1** and **TET-2** show spectral positions and features that, while broadened, are generally consistent with those in solution. In contrast, the solid-state absorbance of both **TET-3** and **ADT-3** stretch substantially to the red and in the case of **TET-3**, displays a new

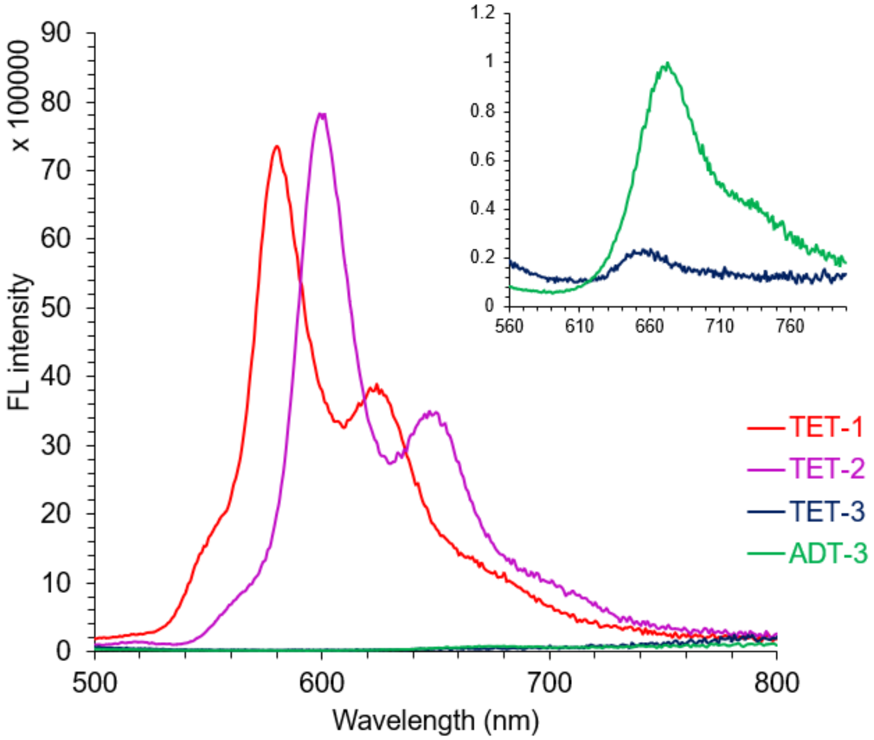

Figure 2.3: Photoluminescence spectra for developed acene derivatives. The inset displays spectra of **TET-3** and **ADT-3** measured with wider slit widths. Figure reproduced from Ref.1.

intense band at 720 nm. Preliminarily, we attribute this to a combination of increased planarization and intermolecular aggregation of the anthracene-containing “triacenes” as solids.

Similar to the trend in UV/vis spectra, the maximum wavelength of fluorescence for these four compounds (**Figure 2.3**) shifts with increasing conjugation of the arene pendants, from 581 nm for **TET-1**, 600 nm for **TET-2**, and greater than 650 nm for both **TET-3** and **ADT-3**. Notably, anthracene-containing **TET-3** and **ADT-3** are only very weakly fluorescent ($\Phi_F < 0.003$). This observation is consistent with previously reported observations of weak fluorescence from ethynyl-bridged multi-acene structures with either two conjugated tetracenes[134] or three conjugated anthracenes.[135]

2.4 Singlet oxygen responsiveness of developed acenes

We began our investigation of the photochemical oxidation of these acenes by using methylene blue (**MB**) as an external sensitizer, which is soluble in CH_2Cl_2 and absorbs ~650 nm light. Irradiation of **MB** as an external photosensitizer allows us to compare the intrinsic reactivity of different acenes with $^1O_2$ and mitigates other variables that can complicate such comparisons upon direct irradiation of the acenes, such as their intrinsic efficiency of $^1O_2$ generation, the extinction coefficient of the acenes, and the flux of the light source used at different wavelengths. We use a 200W Hg/Xe lamp with a 630 nm long-pass filter to irradiate **MB** in the presence of an acene in CH_2Cl_2 at a concentration between 2-4 mM. We measure the concentration of the acene as a function of irradiation

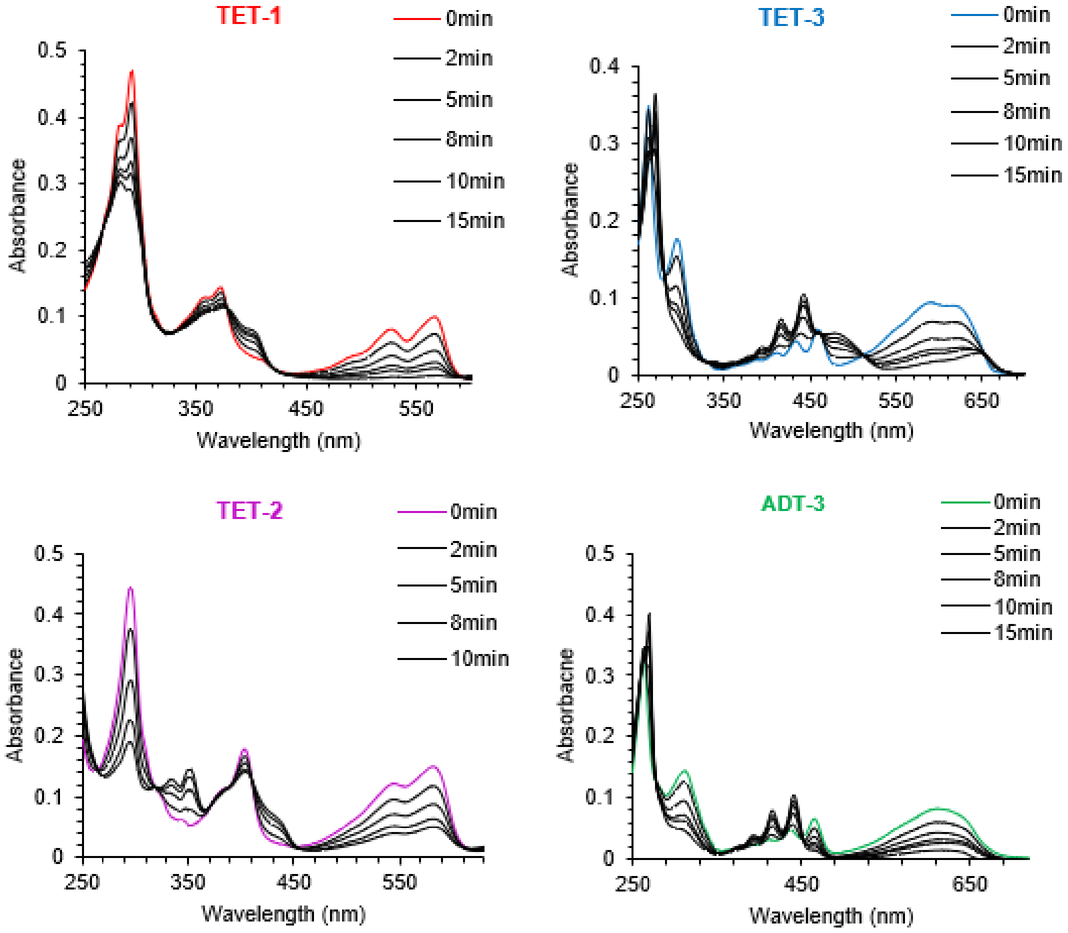

Figure 2.4: Pseudo first-order kinetics analysis of disappearance of acenes upon irradiation of **MB**. The reaction was monitored by UV-vis spectroscopy and each spectrum was taken at different time spot during the reaction. The initial absorbance spectrum of **MB** has been subtracted from each of these spectra. Figure reproduced from Ref.1.

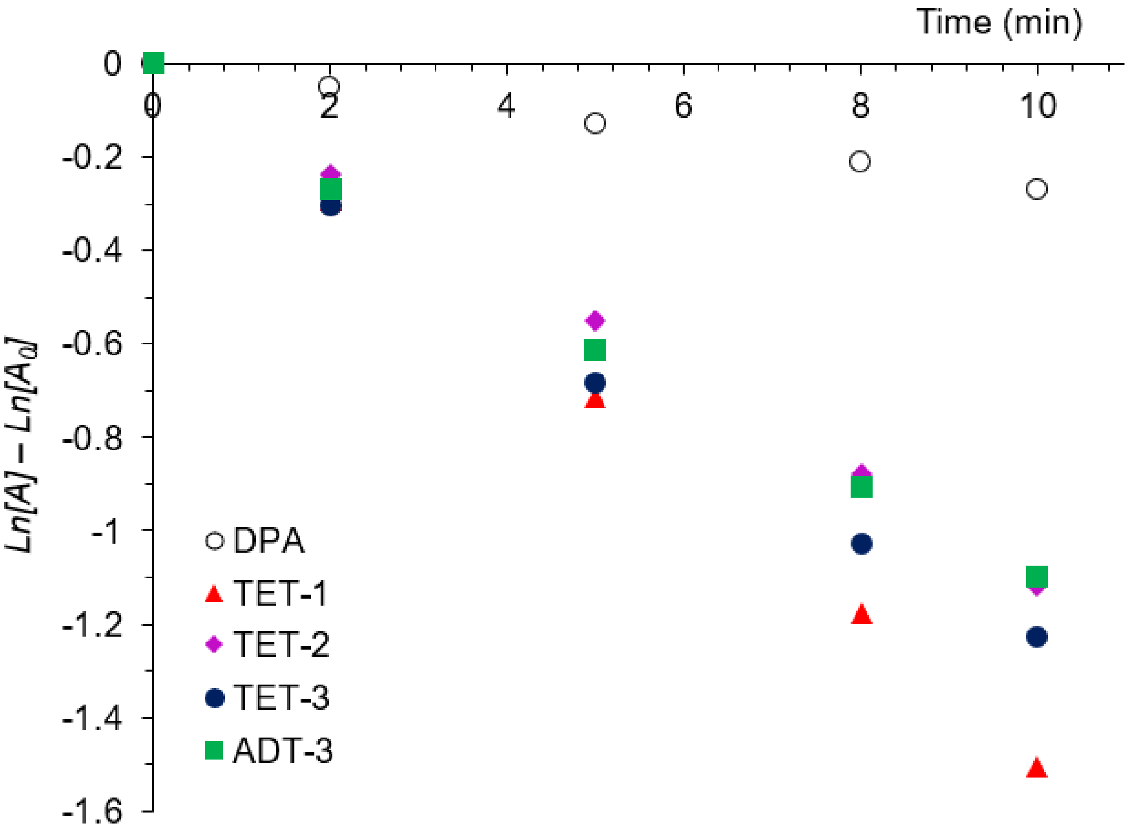

Figure 2.5: Pseudo first-order kinetics curves of cycloaddition. Rate constants relative to **DPA** (k_{rel}) for the four acenes range between 4-6. Figure reproduced from Ref.1.

time using UV/vis spectrophotometry. With constant light flux and sensitizer absorbance, we assume a steady-state concentration of $^1\mathbf{O_2}$ while irradiating and therefore fit the resulting data to a pseudo first-order kinetic model. We also monitored the disappearance of 9,10-diphenylanthracene (**DPA**) in a separate experiment under identical conditions as an external standard, as it has a known bimolecular rate constant for endoperoxide formation with $^1\mathbf{O_2}$ (1-3x10^6 $M^{-1}s^{-1}$) and resembles the reactive anthracene unit in $^1\mathbf{O_2}$-sensitive fluorophores **DPAX**[82] and Aarhus Sensor Green[96].

Figure 2.4 and **Figure 2.5** summarize the results of these experiments and analyses, which show that the four acenes all have similar reactivities with $^1O_2$. Relative to the rate constant of **DPA**, these acenes have relative rate constants (k_{rel}) of 4-6. This range is consistent with the reactivity of the previously reported compound from our group, **DE-TET**, which reacts ~5 times faster than a similar 9,10-diaryl anthracene. Therefore, neither the extended arylene-ethynylene linkers nor the conjugated naphthalene or anthracene pendants noticeably impact the intrinsic reactivity of these diethynyl-acenes with $\mathbf{^1O_2}$. The evolution of the optical spectra of these four acenes as they react is consistent with oxidation of the long central acene moiety: i) all show a diminution of the longest wavelength band and the sharp band at approximately 300 nm; ii) the tetracenes retain of the fully conjugated arylene-ethynylene linker when the tetracene is oxidized across the unsubstituted 6 and 11 positions; iii) the structured absorbance of **TET-3, ADT-3** after oxidation indicates the persistence of the diethynyl-anthracene side groups under the photo-oxidation conditions. Broad absorbance between 400-500 nm, which we attribute to a combination of retention of the fully conjugated arylene-ethynylene linker when the tetracene is oxidized across the unsubstituted 6 and 11 positions (*vide infra*); iii) the structured absorbance of **TET-3, ADT-3** after oxidation indicates the persistence of the diethynylanthracene side groups under the photo-oxidation conditions.

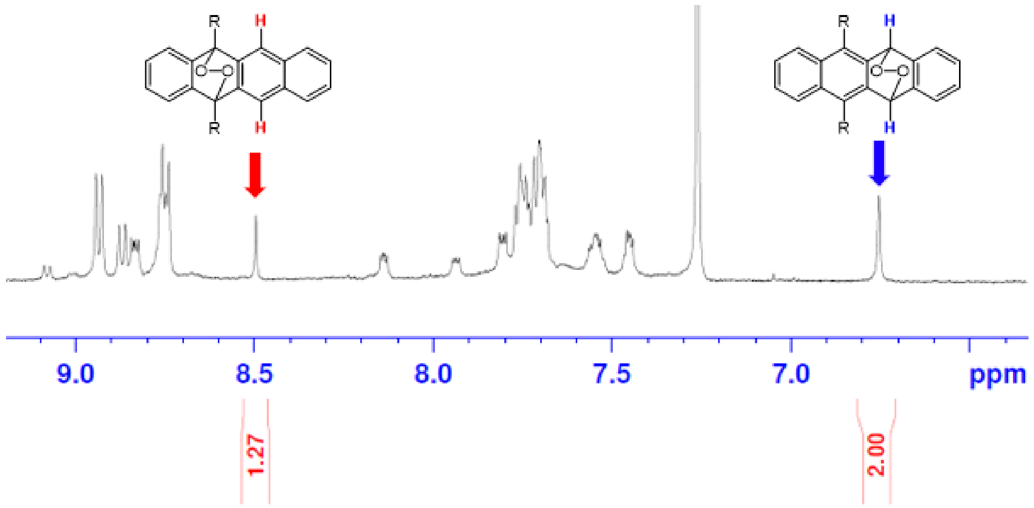

Figure 2.6: NMR spectrum of product mixture of cycloaddition of singlet oxygen on **TET-3.** Figure reproduced from Ref.1.

NMR spectroscopy (**Figure 2.6**) of **TET-3** upon photo-oxidation at higher acene concentration (~ 1 mM) using **MB** as photosensitizer provides further support for endoperoxide formation. As shown in **Figure 2.6**, ^{1}H resonances consistent with the two expected regioisomeric endoperoxides appear, along the disappearance of **TET-3** resonances. Based on the chemical shifts of the singlets associated with the hydrogens on the unsubstituted 6 and 11 positions of the tetracene core, we approximate a 2: 1 molar ratio of the 6,11-endoperoxide to the 5,12-endoperoxide; this preference for oxidation at the non-ethynylated position of tetracene agrees with previous work of our group.[87]

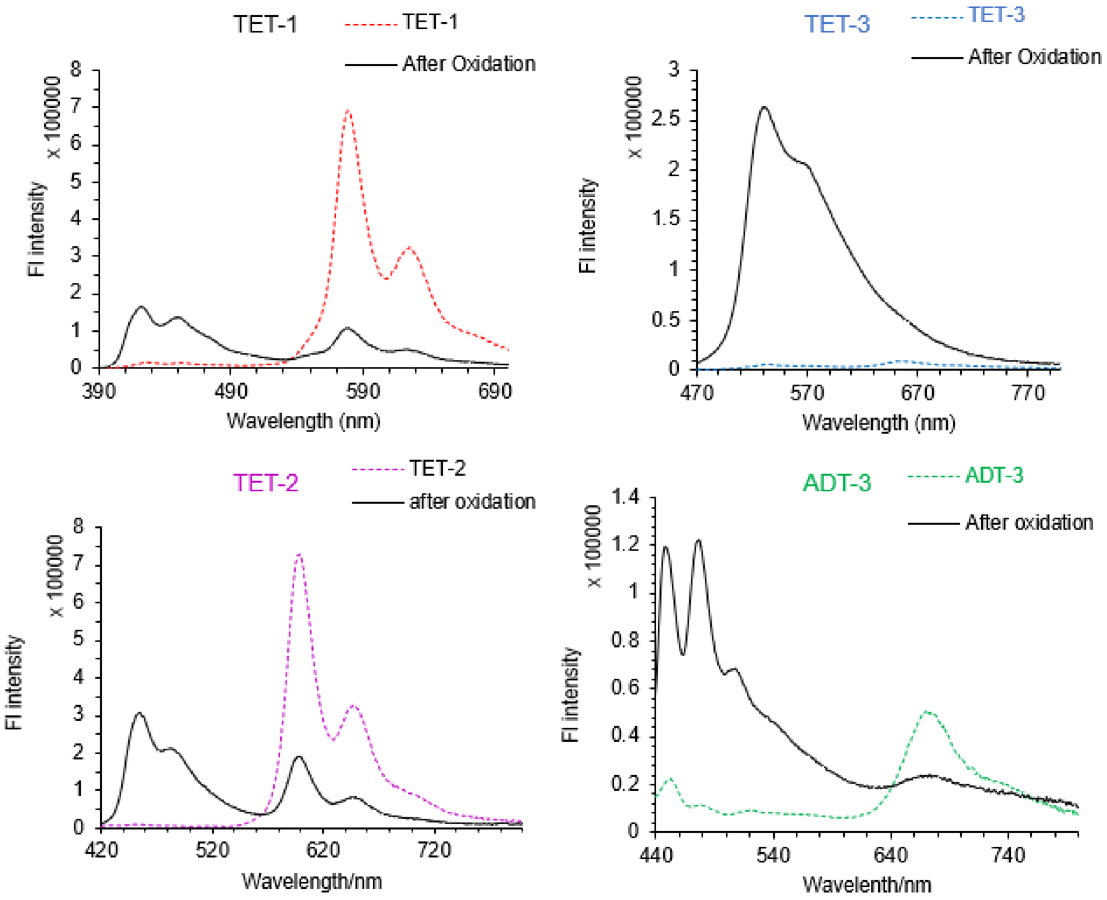

Figure 2.7: Fluorescent response of multi-chromophore acenes to $^1\mathbf{O_2}$ generated through irradiation of methylene blue in CH_2Cl_2. Figure reproduced from Ref.1.

A key design feature of these acenes is the presence of a visible emitting chromophore upon oxidation of the tetracene or anthradithiophene. As shown in **Figure 2.7**, **TET-1** (582 nm) and **TET-2** (601 nm) show ratiometric responses: initial acene fluorescence decreases in intensity as the tetracene oxidizes, while fluorescence from the mixture of regioisomeric endoperoxides emerges. In contrast, the very weakly emissive **TET-3** shows a “turn-on” of fluorescence. Comparing the fluorescence of the three mixtures of oxidized tetracenes, longer pendant arenes yield bathochromic ally shifted final fluorescence: **TET-1** (benzene) at 425 nm, **TET-2** (naphthalene) at 452 nm, and **TET-3** (anthracene) at 537 nm. We attribute these fluorescence spectra to the tetracenes oxidized across the 6 and 11 positions, which retain a conjugated chromophore along the entire molecule. In contrast, even though **ADT-3** has anthracene pendants, endoperoxidation is more likely across the central anthradithiophene ring, interrupting conjugation along the arylene-ethynylene chromophore, yielding blue-shifted emission upon oxidation (478 nm).

2.5 Direct irradiation reactivities of developed acenes

For the development of sensor materials for ^{1}**O$_2$**, the inherent reactivity with ^{1}**O$_2$** of acenes is critical to their function. For both ^{1}**O$_2$** sensing materials and the more popular applications of acenes based in organic electronics, preventing photo-oxidation of acenes upon direct irradiation is crucial. For organic electronics, chromophore oxidation can inhibit performance, and is likely to arise from direct irradiation of the active materials that can sensitize ^{1}**O$_2$** and other reactive oxygen species (ROS). Highly reactive acenes such as pentacene and rubrene suffer from this feature, while physical quenching of ^{1}**O$_2$** bestows TIPS-pentacene with slow inherent reactivity. For fluorogenic sensing materials for ^{1}**O$_2$**, direct irradiation of the fluorophore is necessary to measure luminescent response; if the fluorophore itself generates ^{1}**O$_2$** or other ROS, false positives can occur. This drawback is a reported characteristic of the commercially available Singlet Oxygen Sensor Green

(**SOSG**).[95, 107] Therefore, approaches to preventing "self-sensitization" of ROS acenes while preserving their inherent reactivity are important for improving the performance of such responsive fluorophores.

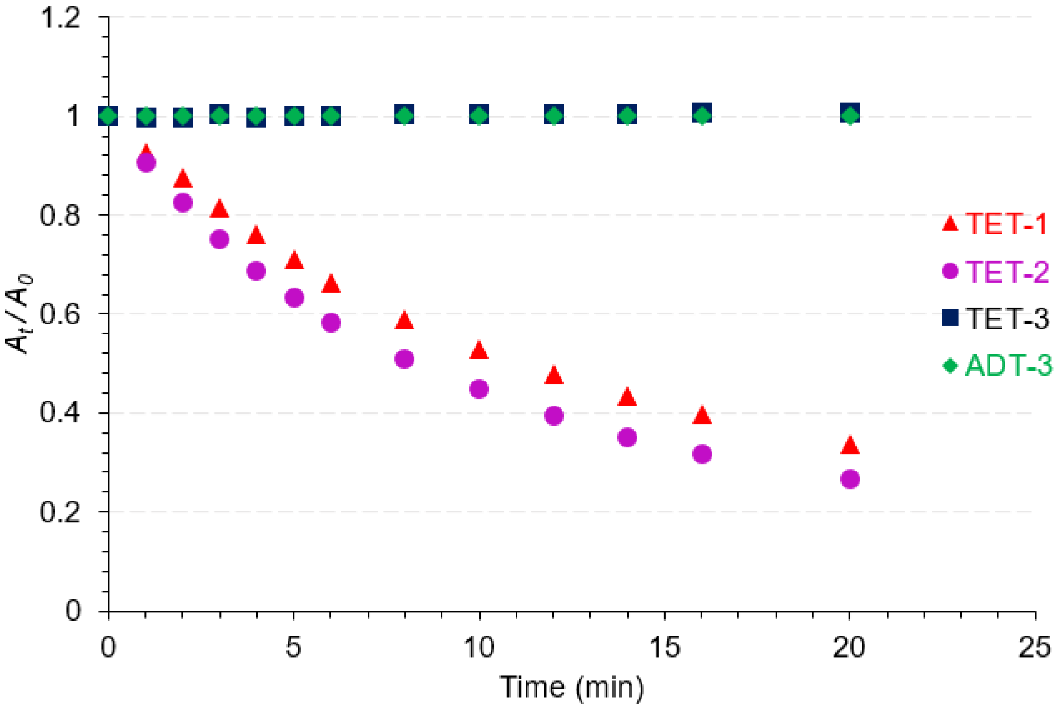

Figure 2.8: Photochemical bleaching of acenes during direct irradiation of each acene at 546 nm (12 mW/cm^2) in aerated $CHCl_3$. Figure reproduced from Ref.1.

To assess the impact of chemical structure on self-sensitized photo-oxidation, we monitored the concentration of these four extended acenes in $CHCl_3$, in the absence of any external sensitizer while irradiating them directly at 546 nm (12 mW/cm^2); the initial absorbance of all samples was 0.45 at 546 nm. As **Figure 2.8** shows, the highly fluorescent **TET-1** and **TET-2** degrade rapidly, with half-lives of 8-12 minutes. In contrast, highly quenched **TET-3** and **ADT-3** show no noticeable degradation, even after 20 minutes of irradiation. Our previous observation that the rates of reactions with $^1O_2$ for these four acenes are nearly identical makes it unlikely that physical quenching of $^1O_2$ by **TET-3** or **ADT-3** contributes to their persistence during direct irradiation, as is the case for TIPS-pentacene. Instead, consistent with the rapid non-radiative relaxation of their excited states that we infer from Φ_F<0.003, we attribute the persistence of **TET-3** and **ADT-3** to poor efficiency of photosensitization of **ROS**.

2.6 Determining key mechanisms of photostability

Inspired by Linker group's study on TIPS-pentacene, we tested the $^1O_2$ quenching capabilities of **TET-3** and **ADT-3** to determine if the abnormal stability originated from physical quenching. We executed similar kinetics tests on **DA-TET**, a more reactive acene derivative reported by our group[79], using **MB** as the photosensitizer. Three parallel experiments were carried out with i) just **DA-TET**, ii) **DA-TET** and **TET-3**, and iii) **DA-TET** and **ADT-3**. As shown in **Figure 2.9**, the rate constants did not display noticeable differences, which indicated physical quenching should not be the dominant mechanism of the photostability.

Next, we compared the photosensitization performance of **TET-3** and our previously reported, highly fluorescent diethynyltetracene **DE-TET** in the oxidation of the more highly reactive **DA-TET**. In detail, **DA-TET** was added to solutions of either **TET-3** or **DE-TET** in chloroform. Then, the solutions were irradiated with a lamp equipped with a long pass at 530 nm beyond the absorbance range of **DA-TET**. Thus, the self-sensitizing process of **TET-3** or **DE-TET** was the only resource of $^1O_2$. As shown in **Figure 2.10**, irradiation of **DE-TET** completely oxidized **DA-TET** within three minutes by UV/vis spectrophotometry, while irradiation of **TET-3** under otherwise identical conditions showed less than 50% oxidation of **DA-TET** after thirty minutes of irradiation. The poor performance of **TET-3** as a photosensitizer, therefore, explains its persistence (and that of **ADT-3**) under direct irradiation

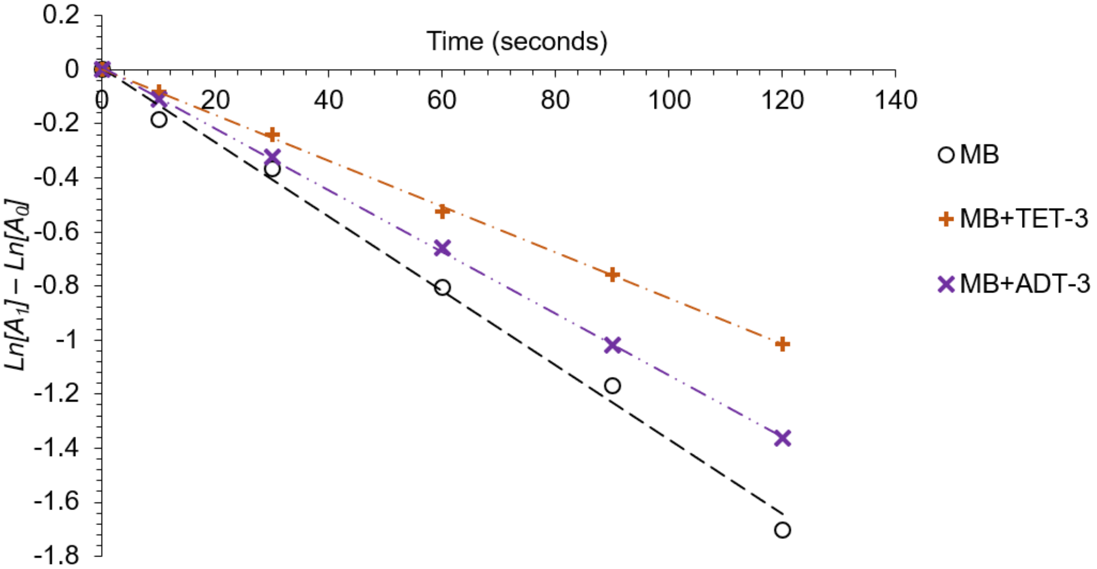

2.7 Theoretical calculations

Figure 2.9: Pseudo first-order kinetics curves of cycloaddition with or without stable acenes as potential singlet oxygen quencher. Figure reproduced from Ref.1.

Given the multi-chromophore nature of several of these compounds and the complexity of their UV/vis spectra, we calculated their molecular orbitals and optical transitions using density functional theory (DFT) and time-dependent DFT with the B3LYP functional and the 6-31G+(d,p) basis set, using a polarizable dielectric continuum model for CH_2Cl_2.[136] Geometry optimization at this level of theory shows a lack of coplanarity for the three acenes in **TET-3** and **ADT-3**, with torsional angles of 32-35°. Previously, molecules with three anthracenes connected through ethynyl linkers have shown similarly twisted lowest-energy torsions.[135] We attribute this twisting out of planarity to non-bonding steric interactions between the C-H bonds on acene rings adjacent to the ethynyl linkages—**TET-2** (20-24° torsional angles) and **TET-1** (0° torsional angles) show improved planarity along the phenylene-ethynylene chain. **Figure 2.11** shows the HOMO-2 through LUMO+2 wavefunctions for **TET-3**, and the appendix at the end of this chapter contains images of

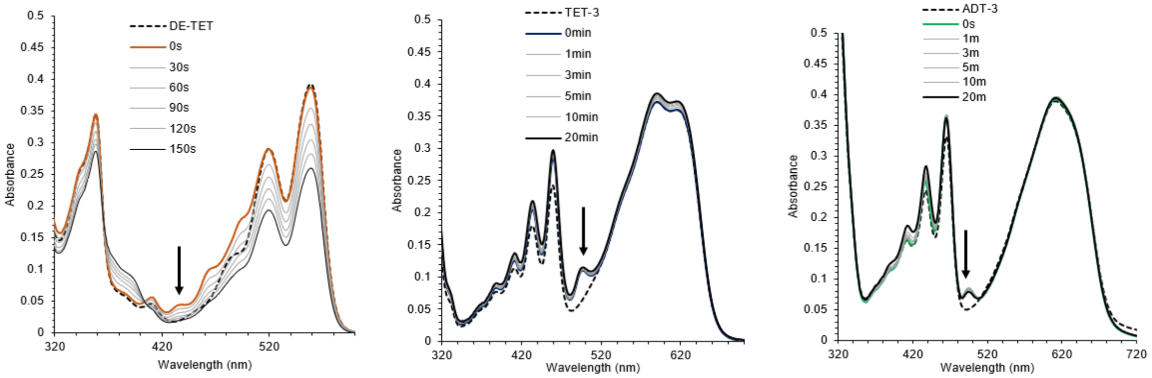

Figure 2.10: Experiment on photo-sensitizing capabilities. From left to right, the photosensitizer used was **DE-TET**, **TET-3** and **ADT-3**. Figure reproduced from Ref.1.

analogous orbitals for the other molecules. For all four molecules, the lowest energy transition with non-zero oscillator strength is HOMO-LUMO in nature, with the electronic density for each mostly on the central long acenes, with some occupancy along the entire π-conjugated system. The trends in calculated transition energies for these transition follows that observed experimentally, with longer acene pendants yielding lower energy transitions. Also in agreement with our experimental observation is the presence of a higher energy calculated transition at 425 nm, which is mainly localized on the anthracene pendants (HOMO-1 to LUMO+1).

We have also run calculations on the potential cycloaddition products, the endo-peroxides, of **TET-3.** The geometry optimization suggested that the cycloaddition bent the oxidized site to 109.5˚. When the singlet oxygen attacks 5,12 positions, the conjugation is entirely interrupted, resulting in the localization of electrons on anthracene pendants. On

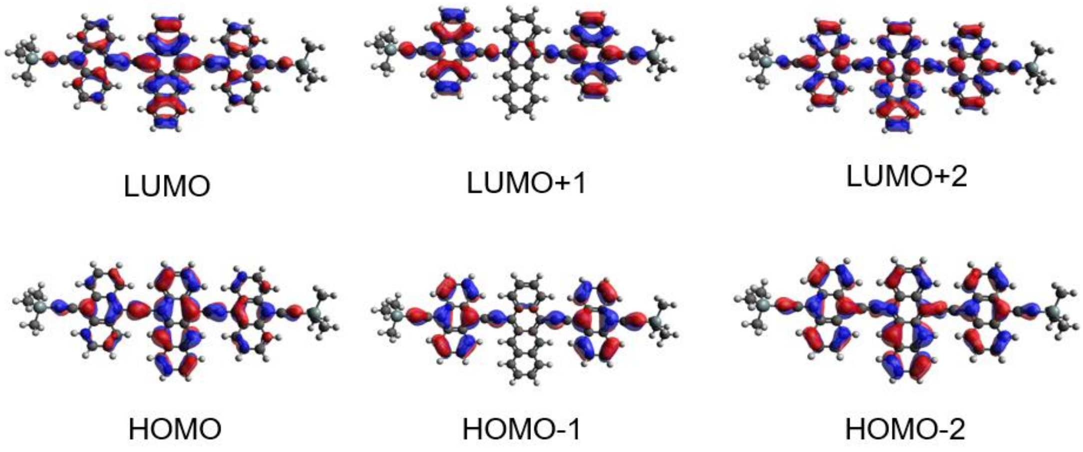

Figure 2.11: Frontier molecular orbitals of TET-3. Figure reproduced from Ref.1.

the other hand, when the reaction site is 6,11, the two anthracene pendants are still linked with a naphthalene-like conjugated linker. Time-dependent results indicated that the 6,11 product had a red-shifted absorbance, consistent with the broad, structureless peak around 490 nm in the experimentally obtained spectrum. Besides, the localization of electrons on the anthracene displayed in 5,12 endo-peroxide explained the anthracene-like vibronic features in the experimental results. An energetic analysis of the products showed that the 5,12 have a higher energy than the 6,11, indicating that the 6,11 was a thermodynamically stable product. The minor energy difference between the 5,12 product and **TET-3** gave a plausible explanation for the reversibility of this reaction, which has also been observed in other acenes reported by our group.[87]

2.8 Attempts on applications of TET-3

Due to its excellent photo-stability, our group believes **TET-3** could be a good candidate material for organic optoelectronic devices. Thus, collaborating with Kymissis group at Columbia University, we fabricated organic field-effect transistors (OFETs) in a bottom-gate, bottom-contact geometry using **TET-3** as a functional layer.[137] However, the tendency of this molecule to form small needles, shown in **Figure 2.12**, upon deposition limited the charge mobile abilities and the device's performance. Nonetheless, the material still displayed mobility around 10^{-4} cm^2/Vs. We believe that with a proper processing technique, this material may still be applicable.

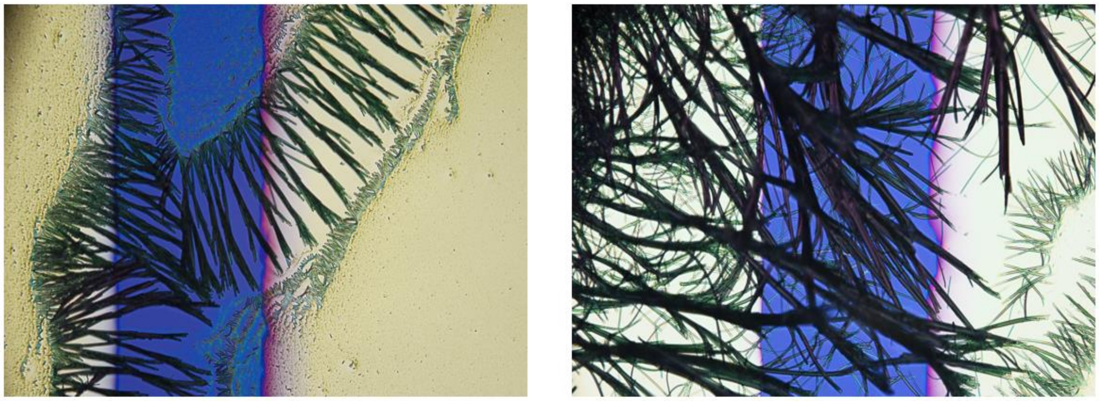

Figure 2.12: Microscope images of drop-cast device of **TET-3**. Reproduced from Ref.1.

2.9 Experimental section

General Information. All synthetic manipulations were performed under standard air-free conditions under an atmosphere of argon gas with magnetic stirring unless otherwise mentioned. Flash chromatography was performed using silica gel (230−400 mesh) as the stationary phase. NMR spectra were acquired on a 500 MHz spectrometer. Chemical shifts are reported relative to residual protonated solvent (7.26 ppm for $CHCl_3$ or 3.58 ppm for **THF**). High-resolution mass spectra (HRMS) were obtained using different ionization techniques and a peak-matching protocol to determine the mass and error range of the molecular ion.

Electronic absorbance spectra were acquired with a spectrophotometer in double-beam mode using a solvent-containing cuvette for background subtraction spectra. Fluorescence spectra were collected at a 90° angle from the incident irradiation (75W Xe lamp) and corrected for both fluctuations in the lamp intensity and the wavelength-dependent sensitivity of the photomultiplier tube detector. Fluorescence quantum yields were determined relative to coumarin 6 in ethanol.[138] Time-resolved fluorescence data were collected using a time-correlated single-photon counting instrument with a pulsed LED operating at 403 nm. Irradiation of methylene blue photosensitizer to generate $\mathbf{^1O_2}$ was performed with a 200 W Hg/Xe lamp equipped with a condensing lens, water filter, and manual shutter, with different long pass filters. Density functional theory calculations were performed using the Gaussian 09 software package[136], with optimized geometries and FMO energies determined at the B3LYP/6-31G (d,p) level of theory using a polarizable continuum solvent model for CH_2Cl_2. The time-dependent results of these optimized geometries were calculated with the same functional and basis set, using the Tamm−Dancoff approximation.

For fabrication of transistors, highly p-doped silicon was used as the bottom-gate electrode, and 285 nm thermally grown SiO_2 served as the gate dielectric. Cr/Au (5 nm/40nm) source and drain electrodes were evaporated through a shadow mask at 0.5 Å/s and functionalized with the self-assembled monolayer (SAM) pentafluoro-benzenethiol (**PFBT**) by vapor deposition at 70 °C for 2 hours. This SAM serves to shift the electrode work function away from the vacuum level, enhancing charge injection in p-type organic semiconductors.[139] To modify the surface energy and allow crystallites to form on the substrate, the silicon oxide layer was functionalized with trichloro(phenyl)silane by immersion in a 60 mM solution in chloroform for 1 hour, followed by immersion in fresh chloroform and a thorough rinse with 2-propanol. A 0.25 wt% solution of **TET-3** in chlorobenzene was then prepared and devices were formed using solvent-assisted crystallization[137], where the solution is drop-casted onto the patterned substrate in a covered petri dish with 100 μL chlorobenzene dispensed around the substrate. This technique creates a solvent-rich atmosphere such that the semiconductor solution evaporates more slowly, allowing for the formation of larger crystallites. Electrical measurements were then taken using two Keithley 2400 source-measure units in dark at ambient atmosphere.

Synthesis of developed acenes

5,12-bis[2-(trimethylsilyl)ethynyl]tetracene. This reaction was executed following a reported procedure.[132] In a flame-dried 2-neck round bottom flask, trimethylsilylacetylene (0.71 mL, 490 mg, 5.0 mmol) was dissolved in 20 mL of dry diethyl ether and cooled to 0°C in an ice-water bath. *n*-Butyllithium (2.2 mL, 4.8 mmol, 2.2 M in hexanes) was added dropwise. The colorless solution was allowed to warm to room temperature and stirred for 1 h, at which time napthacenequinone (520 mg, 2.0 mmol) was added as a solid. The suspension was stirred overnight and then neutralized with 1 M HCl (aq) and $SnCl_2•2H_2O$ (1.0 g, 4.4 mmol) was added to the mixture. After stirring for 3 h, the mixture was extracted using CH_2Cl_2 (3 x 10 mL), and the combined organic layers were dried over $MgSO_4$. The solvent was removed *in vacuo*, and the residue was purified through a plug of silica, eluted with hexanes to give 540 mg of the expected product ((65% yield) as a deep red powder .

^{1}H NMR (500 MHz $CDCl_3$): δ 9.20(s, 2H) 8.57-8.59 (dd , 2H), 8.08-8.10 (dd, 2H), 7.55-7.60 (dd, 2H), 7.47-7.49 (dd, 2 H), 0.54 (s, 18H). The chemical shifts are consistent with those reported in the literature.[132]

5,12-diethynyltetracene. 5,12-bis[2-(trimethylsilyl)ethynyl]tetracene (210 mg, 0.50 mmol) was dissolved in 10 mL CH_2Cl_2/methanol (1:1, v/v). To the solution, potassium carbonate (210 mg, 1.5 mmol) was added. The suspension was stirred at room temperature for 4 h. The solvent was removed, and the residue was extracted with CH_2Cl_2 (3 x 10 mL). The combined organic phase was sequentially washed with water and brine, and dried over $MgSO_4$. In syntheses of **TET-1**, **TET-2**, and **TET-3**, the crude product was used immediately after removing the solvent.

^{1}H NMR (500 MHz $CDCl_3$): δ 9.22 (s, 2H), 8.60-8.62 (dd, 2H), 8.08-8.10 (dd, 2H), 7.55-7.57 (dd, 2H), 7.48-7.50 (dd, 2H), 4.22 (s, 2H). ^{13}C NMR (125 MHz $CDCl_3$): δ 132.8, 130.4, 130.2, 128.5, 127.2, 126.9, 126.2, 125.9, 90.7, 80.7.

*1-bromo-4-(2-triisopropyl)ethynyl-benzene***.** Triisopropylsilylacetylene (0.22 mL, 180 mg, 1.0 mmol) of triisopropylsilyl acetylene was dissolved in 30 mL THF/triethylamine (2:1 v/v). The solution was deoxygenated with argon gas for 1 h. To another flame-dried two-neck round bottom flask, 1-iodo-4-bromobenzene (283 mg 1.0 mmol), bis(triphenylphosphine)palladium(II) dichloride (35 mg, 0.05 mmol), and copper (I) iodide (10 mg, 0.05 mmol) was added. Then, the degassed solution was transferred to the flask containing solids via cannula. The mixture was stirred overnight at room temperature. The solvent was removed *in vacuo*. The resultant solid was purified by flash column chromatography (hexanes) to yield the desired product as a colorless oil (320 mg, 95% yield).

^{1}H NMR (500 MHz $CDCl_3$): δ 7.42-7.44 (d, 2 H), 7.32-7.34 (d, 2 H), 1.09-1.12 (m, 21 H), The resonances are consistent with those reported previously in the literature.[140]

*1-iodo-4-(2-triisopropyl)ethynyl-benzene***.** In a flame-dried two-neck round bottom flask, 1-bromo-4-(2-triisopropyl)ethynyl-benzene (870 mg, 2.6 mmol) was dissolved in 10 mL of dry diethyl ether. *n*-butyllithium (1.14 mL, 2.8 mmol, 2.5 M in hexanes) was added dropwise after cooling the solution to -78 °C. The solution was stirred at -78 °C for 1 h. I_2 was added as a solid (857 mg, 3.4 mmol) and the mixture was allowed to warm up to ambient temperature. The reaction was then stirred for 8 h followed by quenching with 10 mL saturated ammonium chloride solution. The mixture was then extracted with CH_2Cl_2 and dried over $MgSO_4$. The crude product (870 mg, 87% yield) was directly used after removing the solvent without any further purification.

5,12-bis[((4-triisopropylethynyl)phenyl)ethynyl]tetracene (**TET-1**)**.** In a round bottom flask, 1-iodo-4-(2-triisopropyl)ethynyl-benzene (670 mg, 1.7 mmol) was dissolved in 9 mL toluene/diisopropylamine (2:1 v/v). The solution was deoxygenaged by bubbling with argon for 1 h. To another flame dried two-neck round bottom flask equipped with a condenser, 5,12-diethynyltetracene (180 mg, 0.63 mmol), $Cl_2Pd(PPh_3)_2$ (30 mg, 0.04

mmol), and CuI (10 mg, 0.05 mmol) was added. The degassed solution was then transferred to the flask via a syringe. The mixture was then stirred at 80 °C for 36 h. The solvent was removed *in vacuo*, and the residue was purified via flash column chromatography (CH_2Cl_2/hexanes 1:1 v/v). The crude product was recrystallized from $CHCl_3$/MeOH to yield **TET-1** (150 mg, 30% yield) as a purple solid.

^{1}H NMR (500 MHz $CDCl_3$): δ 1.17-1.18 (m, 42 H), 7.49-7.51 (dd, 2 H), 7.58-7.59 (m, 6 H), 7.60 (d, 4H), 8.11-8.12 (dd, 2H), 8.64-8.65 (dd, 2H), 9.25 (s, 2H).

^{13}C NMR (125 MHz $CDCl_3$): δ 132.4, 132.2, 131.5, 129.9, 128.6, 127.4, 126.8, 126.2, 126.1, 123.9, 123.3, 118.3, 106.7, 103.2, 93.4, 89.0, 18.7, 11.4.

HRMS (TOF, EI): m/z calcd for $C_{56}H_{60}Si_2$ (M^+) 788.4234, found 788.4212.

*1-bromo-4-(2-triisopropyl)ethynyl-naphthalene***.** A flame-dried round bottom flask was charged with 1-iodo-4-bromonaphthalene (1.2 g, 3.7 mmol) and 30 mL of degassed THF/NEt_3 (2:1 v/v). $Pd(PPh_3)_2Cl_2$ (100 mg, 0.14 mmol) and CuI (0.2 mmol, 40 mg) was added to the solution. With a syringe, triisopropylsilylacetylene (0.82 mL, 3.7 mmol) was added to the solution. The reaction was stirred overnight before purification by elution through a plug of silica with hexanes. After removing the solvent under vacuum, 1.25 g of the desired product was obtained as a pale-yellow oil. (88% yield).

^{1}H NMR (500 MHz $CDCl_3$): δ 8.40-8.41 (m, 1H), 8.24-8.26 (m, 1H), 7.72-7.73 (d, 1H), 7.62-7.65 (m, 2 H), 7.54-7.56 (d, 1 H), 1.19-1.20 (m, 21 H),

^{13}C NMR (125 MHz $CDCl_3$): δ 134.5, 132.8, 131.7, 130.9, 129.3, 127.7, 127.5, 126.8, 123.6, 121.3, 104.1, 97.3, 18.8 11.4.

1-iodo-4-(2-triisopropyl)ethynyl-naphthalene. In a flame dried round bottom flask, 1-bromo-4-(2-triisopropyl)ethynyl-naphthalene (1.25 g, 3.3 mmol) was dissolved in 10 mL of dry THF. The solution was cooled to -78 °C using an acetone/dry ice bath. With a syringe, *n*-butylithium solution (2.0 mL, 5.0 mmol, 2.5 M in hexanes) was added dropwise. The solution was stirred at -78 °C for 1 h, and then I_2 (1.5 g, 6 mmol) was added as a solid. The reaction was stirred overnight, and then quenched with aqueous NaS_2O_3. The mixture was extracted with CH_2Cl_2 three times, and the combined organic layers were dried over $MgSO_4$. Then, the solvent was removed *in vacuo* to yield 1.38 g yellow oil. This crude product was directly used in the next step without further purification (96% yield).

5,12-bis[((4-triisopropylethynyl)naphthyl)ethynyl]tetracene (**TET-2**). A round bottom flask was charged with a solution of 1-iodo-4-(2-triisopropyl)ethynyl-naphthalene (1.0 g, 2.3 mmol) dissolved in 14 mL of a toluene/diisopropylamine (4:3 v/v) mixture. The solution was then deoxygenated by bubbling with argon for 1 h. This solution was transferred by cannula into a flamed dried round bottom flask containing compound **8** (280 mg, 1.0 mmol), $Pd(PPh_3)_2Cl_2$ (35 mg, 0.05 mmol), and CuI (10 mg, 0.05 mmol). The reaction was heated to 80 °C and stirred for 20 h. The mixture was first purified by flash column chromatography (gradient elution 1:4 CH_2Cl_2/hexane to 100% CH_2Cl_2). Finally, 530 mg of pure **TET-2** was isolated by recrystallization from chloroform/methanol as a purple solid (60% yield).

^{1}H NMR (500 MHz $CDCl_3$): δ 9.39 (s, 2H), 8.76-8.80 (m, 4 H), 8.51-8.53 (m, 2 H), 8.08-8.10 (dd, 2 H), 7.99-8.00 (d, 2H), 7.81-7.83 (d, 2H), 7.71-7.76 (m, 6H), 7.62-7.64 (dd, 2 H), 7.49-7.51 (dd, 2 H), 1.24-1.28 (m, 42 H).

^{13}C NMR (125 MHz $CDCl_3$): δ 133.0, 132.4, 132.3, 130.5, 130.1, 130.0, 128.6, 127.53, 127.50, 126.9, 126.8, 126.2, 122.3, 121.8, 118.6, 104.8, 101.8, 98.5, 93.7, 18.8, 11.5.

HRMS (MALDI, matrix: DCTB): m/z calcd for $C_{64}H_{64}Si_2$ (M^+) 888.4547, found 888.4537.

*9-iodo-10-bromo-anthracene***.** In a flame-dried round bottom flask, 9,10-dibromoanthracene (1.0 g, 3.0 mmol) was added to 30 mL of dry THF and cooled to -78 °C. To the suspension, *n*-butyllithium (1.3 mL, 3.3 mmol, 2.5 M in hexanes) was added dropwise. The resulting solution was allowed to warm to room temperature and stirred for another 3 hours. The flask was cooled to -78°C again followed by the addition of 1.0 g of

I_2 (3.9 mmol). After stirring at room temperature for 20 h, the solution was concentrated *in vacuo* to approximately 10% of its original volume. Sodium thiosulfate aqueous solution (20 mL, 20% w/v) was mixed into the residue, and the resulting precipitate was collected by vacuum filtration to afford the desired product as needle-shaped yellow crystals (1.04 g, 91% yield)

^{1}H NMR (500 MHz $CDCl_3$): δ 8.56-8.58 (m, 4 H), 7.61-7.63 (m, 4H). The chemical shifts are consistent with those reported previously in the literature.[133]

*9-bromo-10-(2-triisopropyl)ethynyl-anthracene***.** A flame-dried round bottom flask was charged with a solution of 9-iodo-10-bromo-anthracene (1.04 g, 2.7 mmol) dissolved in 30 mL of a degassed THF/ NEt_3 (2:1, v/v) mixture. $Pd(PPh_3)_2Cl_2$ (98 mg, 0.14 mmol) and CuI (26 mg, 0.14 mmol) were added to the solution. With a syringe, triisopropylsilyl acetylene (0.61 mL, 2.7 mmol) was added to the solution. The mixture was stirred overnight at ambient temperature. The solvent was then removed *in vacuo* and the residue was purified by flash column chromatography (hexanes) to afford 1.10 g of the desired product as a pale yellow oil (93% yield).

^{1}H NMR (500 MHz $CDCl_3$): δ 8.54-8.68 (m, 4H), 7.60-7.64 (m, 4H), 1.25-1.30 (m, 21 H). The resonances are consistent with those reported previously.[141]

9-iodo-10-(2-triisopropyl)ethynyl-anthracene. In a flame-dried round bottom flask, 9-bromo-10-(2-triisopropyl)ethynyl-anthracene (600 mg, 1.4 mmol) was dissolved in 10 mL of dry diethyl ether. The solution was then cooled to -78°C. *n*-butyllithium (1.1 mL, 2.1 mmol, 2.2 M in hexanes) was added dropwise to the solution. The mixture was stirred for 1 h at -78°C, after which solid I_2 (630 mg, 2.5 mmol) was added to the mixture, and the reaction was allowed to warm to room temperature and stirred overnight. After quenching by adding sodium thiosulfate aqueous solution (20% w/v), the mixture was extracted with diethyl ether three times. The combined organic layers were dried over $MgSO_4$ and the solvent was removed under vacuum to afford the desired product as a red oil, (626 mg, 93% yield) which was used for the next step without further purification.

5,12-bis[((10-triisopropylethynyl)anthracenyl)ethynyl]tetracene **(TET-3).** A round bottom flask was charged with 9-iodo-10-(2-triisopropyl)ethynyl-anthracene (490 mg, 1.0 mmol) dissolved in 5 mL of a toluene/diisopropylamine mixture (3:2 v/v). The solution was then deoxygenated by bubbling with argon for 1 h. To a flame-dried round bottom flask, compound **8** (130 mg, 0.5 mmol), $Pd(PPh3)_2Cl_2$ (14 mg, 0.02 mmol) and CuI (10 mg, 0.05 mmol) were added as solids. The degassed solution was transferred into the flask containing solids using a cannula.. After stirring in the dark for 24 hours at 80 °C, the solvent was removed *in vacuo*. The residue was passed through a plug of silica with CH_2Cl_2

to remove highly polar impurities. The product was then recrystallized from acetone to yield 140 mg of **TET-3** as a blue solid (28% yield).

^{1}H NMR (500 MHz **THF**-*d8*): δ 9.48 (s, 2H), 8.99-9.01 (dd, 4H), 8.84-8.86 (dd, 2H), 8.70-8.72 (dd, 4H), 8.05-8.07 (dd, 2H), 7.66-7.71 (m, 10 H), 7.49-7.51 (dd, 2 H), 1.34-1.35 (m, 42 H).

^{13}C NMR (125 MHz **THF**-*d8*): δ 11.6, 18.4, 100.4,100.8, 103.7, 105.0, 118.6, 118.8, 126.1, 126.3, 127.0, 127.07, 127.10, 127.14, 127.3, 128.4, 129.8, 132.1, 132.3, 132.4, 132.5.

HRMS (MALDI matrix: **DCTB**): m/z calcd for $C_{72}H_{68}Si_2$ (M^+) 988.4860, found 988.4817.

Anthradithiophene-5,11-dione. 1,4-cyclohexanedione (0.84 g, 7.5 mmol) was added to a solution of 2,3-thiophene dicarbaldehyde (2.1 g, 15 mmol) in 100 mL ethanol. 6 mL of 15% (w/v) KOH aqueous solution was then added dropwise. The reaction was stirred at ambient temperature for four hours. The resulting precipitate was collected by vacuum filtration and washed with ethanol to obtain the product as a yellow solid. (2.4 g, 99% yield), which was used directly without any purification.

5,11-bis[2-(trimethylsilyl)ethynyl]-anthradithiophene. In a flame-dried round bottom flask, triisopropylsilylacetylene (1.1 mL, 5.0 mmol) was dissolved in 20 mL of dry diethyl ether and cooled to 0 °C. A solution of *n*-BuLi (5 mmol, 2.0 mL 2.5 M in hexanes) was added dropwise. The mixture was stirred at 0 °C for 30 minutes and stirred at room temperature for another hour. Then, anthradithiophene-5,11-dione (640 mg, 2.0 mmol) was added as a solid. The reaction was stirred at room temperature overnight. The pH of the reaction was tuned to approximately 7 using a 0.1 M HCl aqueous solution, and then 1.0 g of $SnCl_2 \cdot 2H_2O$ was added to the mixture. This mixture was stirred in the dark for 3 hours. The mixture was extracted with diethyl ether 3 times and the combined organic phases were dried over $MgSO_4$. The crude product was purified using column chromatography (hexanes) to obtain the desired product (850 mg, 60% yield).

^{1}H NMR (300 MHz, $CDCl_3$): δ 9.20 (s, 2H), 9.16 (s, 2H), 7.55-7.56 (d, 2H), 7.43-7.44 (d, 2H), 1.32-1.38 (m, 42H), These resonances are consistent with those reported in the literature.[142]

5,11-diethynylanthradithiophene. In a round bottom flask, 5,11-bis[2-(trimethylsilyl) ethynyl]-anthradithiophene (130 mg 0.20 mmol) was dissolved in 5 mL of THF and cooled to -78 °C. 2.0 mL of TBAF solution (1 M in THF) was added dropwise. In the dark, the reaction was stirred for 5 min at -78 °C and stirred for another hour at room temperature. After quenching the reaction with 10 mL of water, the precipitate was filtered and washed with water and cold methanol to afford the desired product as a red solid. (340 mg, 83% yield)

^{1}H NMR (300 MHz $CDCl_3$): δ = 9.19 (s, 2H), 9.12 (s, 2H), 7.56-7.58 (d, 2H), 7.48-7.49 (d, 2H). 4.24-4.29 (m, 2H). The solubility of this compound is very low in solvents for NMR spectroscopy. Thus, the ^{13}C NMR spectrum could not be obtained with high quality.

5,11-Bis[((10-triisopropylethynyl)anthracenyl)ethynyl]anthradithiophene (**ADT-3**). In a round bottom flask, 9-iodo-10-(2-triisopropyl)ethynyl-anthracene (1.20 g, 2.5 mmol) was dissolved in 15 mL of THF/diisopropylamine (2:1 v/v). The solution was then deoxygenated by bubbling with argon gas for 1 h. In another flame-dried flask, of 5,11-diethynylanthradithiophene (340 mg, 1.0 mmol), $Pd(PPh3)_2Cl_2$ (35 mg, 0.05 mmol), and CuI (10 mg, 0.05 mmol) were added as solids. The degassed solution was then added to the flask with solids using a cannula. The reaction was stirred at 80 °C for 24 hours. After removal of solvent *in vacuo*, the residue was passed through a plug of silica with CH_2Cl_2 eluent. The product was recrystallized from acetone twice and then chloroform/methanol twice to yield **ADT-3** as a dark green solid. (250 mg, 25% yield).

^{1}H NMR (500 MHz THF-*d8*): δ 9.00-9.07 (m, 4H), 8.73-8.74 (m, 4H), 8.58-8.60 (m, 4H), 7.60 (m, 2H), 7.56 (m, 4H), 7.25 (m, 4 H), 6.92 (m, 2 H), 1.38-1.4 (m, 42 H). **HRMS** (**MALD**I matrix: **DCTB**): m/z calcd for $C_{72}H_{66}S_2Si_2$ (M^+) 1050.4144, found 1050.4104. The product is a mixture of slightly soluble trans-/cis- isomers, so the multiplicity of signals cannot be distinguished. However, the structure can be confirmed by the HRMS and 2D-NMR. The solubility of **ADT-3** is very low in solvents for ^{13}C NMR spectroscopy.

References

(1) Yan, Y.; Lamport, Z. A.; Kymissis, I.; Thomas, S. W., 3rd. Resistance to Unwanted Photo-Oxidation of Multi-Acene Molecules. J Org Chem 2020, 85 (19), 12731-12739. DOI: 10.1021/acs.joc.0c01890.

(2) Anthony, J. E. The larger acenes: Versatile organic semiconductors. Angewandte Chemie-International Edition 2008, 47 (3), 452-483. DOI: 10.1002/anie.200604045.

(3) Anthony, J. E. Functionalized acenes and heteroacenes for organic electronics. Chemical Reviews 2006, 106 (12), 5028-5048. DOI: 10.1021/cr050966z.

(4) Brega, V.; Yan, Y.; Thomas, S. W., 3rd. Acenes beyond organic electronics: sensing of singlet oxygen and stimuli-responsive materials. Org Biomol Chem 2020, 18 (45), 9191-9209. DOI: 10.1039/d0ob01744b.

(5) Van Damme, J.; Du Prez, F. Anthracene-containing polymers toward high-end applications. Progress in Polymer Science 2018, 82, 92-119. DOI: 10.1016/j.progpolymsci.2018.02.002.

(6) Brega, V.; Scaletti, F.; Zhang, X.; Wang, L. S.; Li, P.; Xu, Q.; Rotello, V. M.; Thomas, S. W., 3rd. Polymer Amphiphiles for Photoregulated Anticancer Drug Delivery. ACS Appl Mater Interfaces 2019, 11 (3), 2814-2820. DOI: 10.1021/acsami.8b18099.

(7) Claus, T. K.; Telitel, S.; Welle, A.; Bastmeyer, M.; Vogt, A. P.; Delaittre, G.; Barner-Kowollik, C. Light-driven reversible surface functionalization with anthracenes: visible light writing and mild UV erasing. Chemical Communications 2017, 53 (10), 1599-1602. DOI: 10.1039/c6cc09897e.

(8) Li, J.; Shiraki, T.; Hu, B.; Wright, R. A. E.; Zhao, B.; Moore, J. S. Mechanophore Activation at Heterointerfaces. Journal of the American Chemical Society 2014, 136 (45), 15925-15928. DOI: 10.1021/ja509949d.

(9) Sulkanen, A. R.; Sung, J.; Robb, M. J.; Moore, J. S.; Sottos, N. R.; Liu, G. Y. Spatially Selective and Density-Controlled Activation of Interfacial Mechanophores. Journal of the American Chemical Society 2019, 141 (9), 4080-4085. DOI: 10.1021/jacs.8b10257.

(10) Kim, S.; Fujitsuka, M.; Majima, T. Photochemistry of Singlet Oxygen Sensor Green. Journal of Physical Chemistry B 2013, 117 (45), 13985-13992. DOI: 10.1021/jp406638g.

(11) Pedersen, S. K.; Holmehave, J.; Blaikie, F. H.; Gollmer, A.; Breitenbach, T.; Jensen, H. H.; Ogilby, P. R. Aarhus Sensor Green: A Fluorescent Probe for Singlet Oxygen. Journal of Organic Chemistry 2014, 79 (7), 3079-3087. DOI: 10.1021/jo500219y.

(12) Altinok, E.; Frausto, F.; Thomas, S. W. Water-Soluble Fluorescent Polymers that Respond to Singlet Oxygen. Journal of Polymer Science Part a-Polymer Chemistry 2016, 54 (16), 2526-2535. DOI: 10.1002/pola.28130.

(13) Frausto, F.; Thomas, S. W., 3rd. Ratiometric Singlet Oxygen Detection in Water Using Acene-Doped Conjugated Polymer Nanoparticles. ACS Appl Mater Interfaces 2017, 9 (18), 15768-15775. DOI: 10.1021/acsami.7b02034 From NLM PubMed-not-MEDLINE.

(14) Zhang, J. J.; Sarrafpour, S.; Pawle, R. H.; Thomas, S. W. Acene-linked conjugated

polymers with ratiometric fluorescent response to O-1(2). Chemical Communications 2011, 47 (12), 3445-3447. DOI: 10.1039/c0cc05770c.

(15) Enko, B.; Borisov, S. M.; Regensburger, J.; Bäumler, W.; Gescheidt, G.; Klimant, I. Singlet Oxygen-Induced Photodegradation of the Polymers and Dyes in Optical Sensing Materials and the Effect of Stabilizers on These Processes. The Journal of Physical Chemistry A 2013, 117 (36), 8873-8882. DOI: 10.1021/jp4046462 (acccessed 2023-06-01T01:02:10).

(16) Maliakal, A.; Raghavachari, K.; Katz, H.; Chandross, E.; Siegrist, T. Photochemical stability of pentacene and a substituted pentacene in solution and in thin films. Chemistry of Materials 2004, 16 (24), 4980-4986. DOI: 10.1021/cm049060k.

(17) Scurlock, R. D.; Wang, B.; Ogilby, P. R.; Sheats, J. R.; Clough, R. L. Singlet Oxygen as a Reactive Intermediate in the Photodegradation of an Electroluminescent Polymer. Journal of the American Chemical Society 1995, 117 (41), 10194-10202. DOI: 10.1021/ja00146a004 (acccessed 2023-06-01T01:03:12).

(18) Zhang, J.; Smith, Z. C.; Thomas, S. W., 3rd. Electronic effects of ring fusion and alkyne substitution on acene properties and reactivity. J Org Chem 2014, 79 (21), 10081-10093. DOI: 10.1021/jo501696d From NLM PubMed-not-MEDLINE.

(19) Anthony, J. E.; Brooks, J. S.; Eaton, D. L.; Parkin, S. R. Functionalized pentacene: Improved electronic properties from control of solid-state order. Journal of the American Chemical Society 2001, 123 (38), 9482-9483. DOI: 10.1021/ja0162459.

(20) Chen, J. H.; Martin, D. C.; Anthony, J. E. Morphology and molecular orientation of thin-film bis(triisopropylsilylethynyl) pentacene. Journal of Materials Research 2007, 22 (6), 1701-1709. DOI: 10.1557/jmr.2007.0220.

(21) Fudickar, W.; Linker, T. Why Triple Bonds Protect Acenes from Oxidation and Decomposition. Journal of the American Chemical Society 2012, 134 (36), 15071-15082. DOI: 10.1021/ja306056x.

(22) Zhang, J.; Pawle, R. H.; Haas, T. E.; Thomas, S. W. Combining Electronic and Steric Effects for Highly Stable Unsymmetric Pentacenes. Chemistry - A European Journal 2014, 20 (20), 5880-5884. DOI: 10.1002/chem.201402003 (acccessed 2023-06-01T01:52:14).

(23) Baral, R. N.; Thomas, S. W. Steric and Electronic Substituent Effects Influencing Regioselectivity of Tetracene Endoperoxidation. Journal of Organic Chemistry 2015, 80 (21), 11086-11091. DOI: 10.1021/acs.joc.5b01692.

(24) Bheemireddy, S. R.; Ubaldo, P. C.; Rose, P. W.; Finke, A. D.; Zhuang, J. P.; Wang, L. C.; Plunkett, K. N. Stabilizing Pentacene By Cyclopentannulation. Angewandte Chemie-International Edition 2015, 54 (52), 15762-15766. DOI: 10.1002/anie.201508650.

(25) Murata, M.; Togo, M.; Mishima, D.; Harada, A.; Muraoka, M. Benzo- and Thieno-Annulated Tetracenes: A One-Pot Synthesis via Cross-Dehydrogenative Annulation. Organic Letters 2020, 22 (11), 4160-4163. DOI: 10.1021/acs.orglett.0c01244.

(26) Dai, G. L.; Chang, J. J.; Luo, J.; Dong, S. Q.; Aratani, N.; Zheng, B.; Huang, K. W.;

Yamada, H.; Chi, C. Y. Z-Shaped Pentaleno-Acene Dimers with High Stability and Small Band Gap. Angewandte Chemie-International Edition 2016, 55 (8), 2693-2696. DOI: 10.1002/anie.201508919.

(27) Fuemmeler, E. G.; Sanders, S. N.; Pun, A. B.; Kumarasamy, E.; Zeng, T.; Miyata, K.; Steigerwald, M. L.; Zhu, X. Y.; Sfeir, M. Y.; Campos, L. M.; et al. A Direct Mechanism of Ultrafast Intramolecular Singlet Fission in Pentacene Dimers. Acs Central Science 2016, 2 (5), 316-324. DOI: 10.1021/acscentsci.6b00063.

(28) Hetzer, C.; Guldi, D. M.; Tykwinski, R. R. Pentacene Dimers as a Critical Tool for the Investigation of Intramolecular Singlet Fission. Chemistry-a European Journal 2018, 24 (33), 8245-+. DOI: 10.1002/chem.201705355.

(29) Korovina, N. V.; Das, S.; Nett, Z.; Feng, X. T.; Joy, J.; Haiges, R.; Krylov, A. I.; Bradforth, S. E.; Thompson, M. E. Singlet Fission in a Covalently Linked Cofacial Alkynyltetracene Dimer. Journal of the American Chemical Society 2016, 138 (2), 617-627. DOI: 10.1021/jacs.5b10550.

(30) Korovina, N. V.; Joy, J.; Feng, X. T.; Feltenberger, C.; Krylov, A. I.; Bradforth, S. E.; Thompson, M. E. Linker-Dependent Singlet Fission in Tetracene Dimers. Journal of the American Chemical Society 2018, 140 (32), 10179-10190. DOI: 10.1021/jacs.8b04401.

(31) Dell'Aquila, A.; Marinelli, F.; Tey, J.; Keg, P.; Lam, Y. M.; Kapitanchuk, O. L.; Mastrorilli, P.; Nobile, C. F.; Cosma, P.; Marchenko, A.; et al. 9,10-ter-anthrylene-ethynylene: a new molecular architecture for solution processed anthracene-based thin film transistors. Journal of Materials Chemistry 2008, 18 (7), 786-791. DOI: 10.1039/b714865h.

(32) Iwanaga, T.; Yamamoto, Y.; Nishioka, K.; Toyota, S. Efficient Synthesis and Electronic Spectra of Unsymmetrical 5,12-Diethynyltetracene Derivatives. Synthesis-Stuttgart 2015, 47 (24), 3997-4007. DOI: 10.1055/s-0035-1560474.

(33) Nesterov, E. E.; Zhu, Z. G.; Swager, T. M. Conjugation enhancement of intramolecular exciton migration in poly(p-phenylene ethynylene)s. Journal of the American Chemical Society 2005, 127 (28), 10083-10088. DOI: 10.1021/ja051936g.

(34) Barlier, V. S.; Schlenker, C. W.; Chin, S. W.; Thompson, M. E. Acetylide-bridged tetracene dimers. Chemical Communications 2011, 47 (13), 3754-3756. DOI: 10.1039/c0cc05164k.

(35) Toyota, S.; Karashima, S.; Iwanaga, T. Synthesis and Properties of Extended pi-Conjugated Compounds with 9,10-Bis(phenylethynyl)anthracene Units. Bulletin of the Chemical Society of Japan 2015, 88 (1), 192-199. DOI: 10.1246/bcsj.20140279.

(36) Tanaka, K.; Miura, T.; Umezawa, N.; Urano, Y.; Kikuchi, K.; Higuchi, T.; Nagano, T. Rational design of fluorescein-based fluorescence probes, mechanism-based design of a maximum fluorescence probe for singlet oxygen. Journal of the American Chemical Society 2001, 123 (11), 2530-2536. DOI: 10.1021/ja0035708.

(37) Zhang, J.; Sarrafpour, S.; Haas, T. E.; Müller, P.; Thomas, S. W. Structure, photophysics, and photooxidation of crowded diethynyltetracenes. Journal of Materials

Chemistry 2012, 22 (13), 6182. DOI: 10.1039/c2jm16173g (acccessed 2023-06-01T01:51:58).

(38) Ragas, X.; Jimenez-Banzo, A.; Sanchez-Garcia, D.; Batllori, X.; Nonell, S. Singlet oxygen photosensitisation by the fluorescent probe Singlet Oxygen Sensor Green (R). Chemical Communications 2009, (20), 2920-2922. DOI: 10.1039/b822776d.

(39) M. J. T. Frisch, G. W.; Schlegel, H. B.; Scuseria, G. E.; Robb, M. A.; Cheeseman, J. R.; Scalmani, G.; Barone, V.; Petersson, G. A.; Nakatsuji, H.; Li, X.; Caricato, M.; Marenich, A.; Bloino, J.; Janesko, B. G.; Gomperts, R.; Mennucci, B.; Hratchian, H. P.; Ortiz, J. V.; Izmaylov, A. F.; Sonnenberg, J. L.; Williams-Young, D.; Ding, F.; Lipparini, F.; Egidi, F.; Goings, J.; Peng, B.; Petrone, A.; Henderson, T.; Ranasinghe, D.; Zakrzewski, V. G.; Gao, J.; Rega, N.; Zheng, G.; Liang, W.; Hada, M.; Ehara, M.; Toyota, K.; Fukuda, R.; Hasegawa, J.; Ishida, M.; Nakajima, T.; Honda, Y.; Kitao, O.; Nakai, H.; Vreven, T.; Throssell, K.; Montgomery, J. A., Jr.; Peralta, J. E.; Ogliaro, F.; Bearpark, M. J.; Heyd, J. J.; Brothers, E. N.; Kudin, K. N.; Staroverov, V. N.; Keith, T. A.; Kobayashi, R.; Normand, J.; Raghavachari, K.; Rendell, A. P.; Burant, J. C.; Iyengar, S. S.; Tomasi, J.; Cossi, M.; Millam, J. M.; Klene, M.; Adamo, C.; Cammi, R.; Ochterski, J. W.; Martin, R. L.; Morokuma, K.; Farkas, O.; Foresman, J. B.; Fox, D. J. Gaussian 09, Revision D.01; Gaussian, Inc.: Wallingford CT, 2016.Frisch, MJEA

(40) Lamport, Z. A.; Haneef, H. F.; Anand, S.; Waldrip, M.; Jurchescu, O. D. Tutorial: Organic field-effect transistors: Materials, structure and operation. Journal of Applied Physics 2018, 124 (7). DOI: 10.1063/1.5042255.

(41) Brouwer, A. M. Standards for photoluminescence quantum yield measurements in solution (IUPAC Technical Report). Pure and Applied Chemistry 2011, 83 (12), 2213-2228. DOI: 10.1351/pac-rep-10-09-31.

(42) de Boer, B.; Hadipour, A.; Mandoc, M. M.; van Woudenbergh, T.; Blom, P. W. M. Tuning of Metal Work Functions with Self-Assembled Monolayers. Advanced Materials 2005, 17 (5), 621-625. DOI: 10.1002/adma.200401216 (acccessed 2020/04/13).

(43) Urushibara, K.; Yamada, T.; Yokoyama, A.; Mori, H.; Masu, H.; Azumaya, I.; Kagechika, H.; Yokozawa, T.; Tanatani, A. Development of Helical Aromatic Amide Foldamers with a Diphenylacetylene Backbone. Journal of Organic Chemistry 2020, 85 (4), 2019-2039. DOI: 10.1021/acs.joc.9b02758.

(44) de Montigny, F.; Argouarch, G.; Lapinte, C. New route to unsymmetrical 9,10-disubstituted ethynylanthracene derivatives. Synthesis-Stuttgart 2006, (2), 293-298. DOI: 10.1055/s-2005-918512.

(45) Payne, M. M.; Odom, S. A.; Parkin, S. R.; Anthony, J. E. Stable, crystalline acenedithiophenes with up to seven linearly fused rings. Organic Letters 2004, 6 (19), 3325-3328. DOI: 10.1021/ol048686d.

Chapter 2 Appendix

Theoretical calculation results

NMR spectra

Theoretical calculated electron orbitals of TET-1, TET-2, and ADT-3.

TET-1

167
LUMO+2
-1.461eV

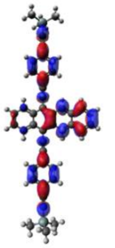

166
LUMO+1
-1.541eV

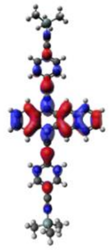

165
LUMO
-2.817eV

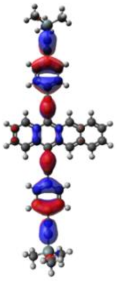

163
HOMO-2
-6.230eV

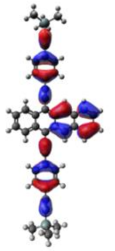

163
HOMO-1
-6.043eV

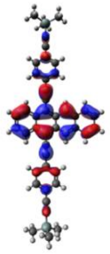

164
HOMO
-4.918eV

TET-2

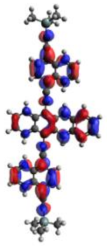

193
LUMO+2
-1.817eV

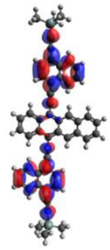

192
LUMO+1
-1.877eV

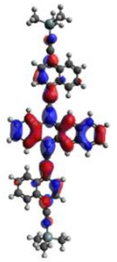

191
LUMO
-2.859eV

188
HOMO-2
-5.846eV

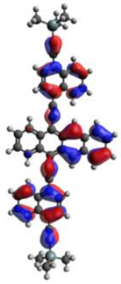

189
HOMO-1
-5.838eV

190
HOMO
-4.901eV

ADT-3

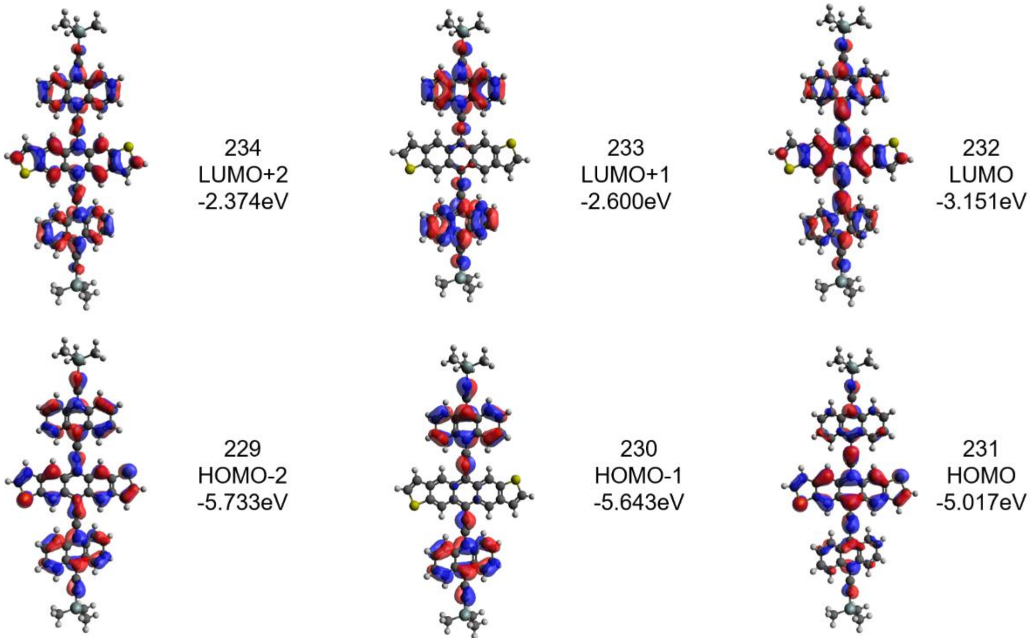

Theoretical calculated electron orbitals of endo-peroxides generated from cyclo- addition of **TET-3**.

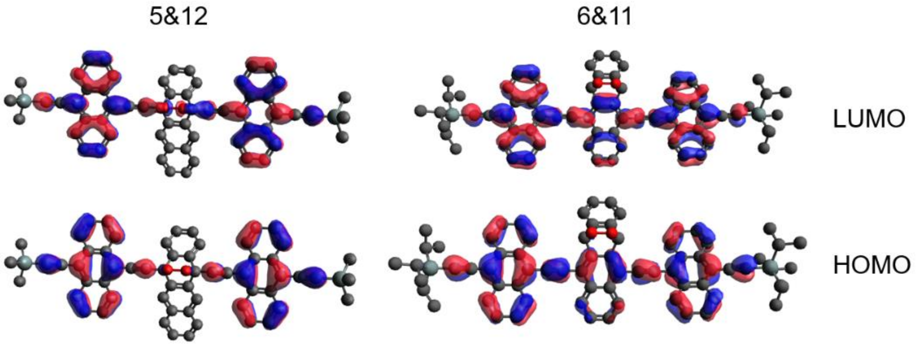

Cartesian Coordinates and Free Energies

Cartesian Coordinates and Free Energies of All Optimized Structures Cartesian coordinates (in Angstroms) and free energies (in a.u.) of all optimized structures used in the **HOMO** and **LUMO** calculations. All **DFT** calculations were performed at PCM-(CH_2Cl_2) with the Gaussian 09 software package, at the B3LYP/6-31G(d,p) level of theory.[136]

TET-1

Energy=-2277.35234483 A.U.

Cartesian Coordinates:

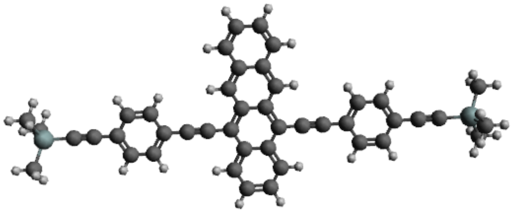

C	24.9628	-26.58	-0.0371
C	26.3392	-26.9448	-0.0431
C	27.3094	-25.9786	-0.0307
C	26.974	-24.5886	-0.0115
C	25.5794	-24.219	-0.005
C	24.5991	-25.2601	-0.0187
C	27.9757	-23.5846	0.001
C	27.6104	-22.1978	0.0224
C	26.2115	-21.8271	0.0286
C	25.207	-22.8506	0.0144
C	28.5812	-21.1799	0.0378

C	28.2387	-19.8281	0.0586
C	26.8403	-19.4576	0.0638
C	25.8729	-20.4621	0.0487
C	29.2255	-18.7893	0.0751
C	28.8548	-17.4723	0.0951
C	27.4725	-17.106	0.0999
C	26.4979	-18.0664	0.0847
C	23.8385	-22.4882	0.0206
C	29.344	-23.9477	-0.0093
C	22.6599	-22.1712	0.0266
C	30.5244	-24.2575	-0.0207
C	21.2874	-21.8064	0.0343
C	31.8977	-24.6192	-0.0358
C	20.9027	-20.4476	0.0527
C	19.5622	-20.0926	0.0607
C	18.5557	-21.0811	0.0509
C	18.9391	-22.4387	0.0322
C	20.2792	-22.7953	0.024
C	32.2851	-25.977	-0.0608
C	33.6264	-26.3292	-0.0769
C	34.6308	-25.3386	-0.0687
C	34.2447	-23.9819	-0.0431
C	32.9039	-23.6282	-0.027
C	17.1772	-20.7159	0.0607
C	36.01	-25.7008	-0.0872
C	15.9949	-20.4042	0.0701
C	37.193	-26.0096	-0.1044
Si	14.208	-19.936	0.0859
Si	38.981	-26.473	-0.1325
C	13.5549	-19.9987	-1.6847
C	14.0537	-18.1885	0.7828
C	13.2779	-21.1671	1.1736
C	39.6461	-26.4083	1.6336
C	39.9002	-25.2394	-1.2266
C	39.1353	-28.2201	-0.8303
H	24.2014	-27.3538	-0.0472

H	26.6173	-27.9941	-0.0574
H	28.3581	-26.2537	-0.035
H	23.5519	-24.9791	-0.014
H	29.6296	-21.4595	0.0334
H	24.8237	-20.1852	0.0528
H	30.275	-19.0702	0.0714
H	29.6107	-16.6929	0.1075
H	27.2019	-16.0545	0.1158
H	25.4471	-17.7902	0.0885
H	21.6676	-19.6783	0.0606
H	19.2784	-19.0457	0.0751
H	18.1734	-23.2071	0.0245
H	20.5617	-23.8426	0.0098
H	31.5218	-26.7479	-0.068
H	33.9122	-27.3755	-0.0965
H	35.0089	-23.212	-0.0366
H	32.6193	-22.5816	-0.0076
H	14.0948	-19.3019	-2.3339
H	12.4937	-19.7259	-1.7078
H	13.6532	-21.0025	-2.1104
H	14.6102	-17.4669	0.1761
H	14.434	-18.1331	1.8078
H	13.0033	-17.8766	0.7964
H	13.3746	-22.1885	0.7916
H	12.2109	-20.919	1.2025
H	13.6535	-21.1538	2.2018
H	39.5476	-25.4048	2.0599
H	40.7083	-26.6777	1.6494
H	39.1128	-27.1067	2.2864
H	39.803	-24.2182	-0.8443
H	39.5179	-25.2541	-2.2523
H	40.9678	-25.4844	-1.2624
H	38.5853	-28.9433	-0.2197
H	40.1865	-28.5289	-0.8514
H	38.748	-28.2767	-1.8527

TET-2

Energy: -2584.64537077 A.U.

Cartesian Coordinates:

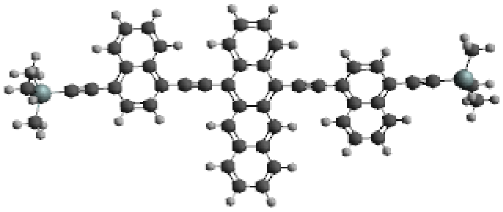

C	8.9095	-16.0917	0.3484
C	8.8593	-17.5144	0.361
C	10.0167	-18.2457	0.3355
C	11.2974	-17.6108	0.2969
C	11.3484	-16.1689	0.3029
C	10.1157	-15.4442	0.3212
C	12.4978	-18.3649	0.2551
C	13.7694	-17.701	0.2574
C	13.8206	-16.255	0.2836
C	12.6002	-15.502	0.2856
C	14.9774	-18.4213	0.2338
C	16.2199	-17.7878	0.2499
C	16.2713	-16.3429	0.2947
C	15.0769	-15.6228	0.3098
C	17.4516	-18.5195	0.2292
C	18.6537	-17.8663	0.2542
C	18.7044	-16.4379	0.3022
C	17.5517	-15.7007	0.3222
C	12.6481	-14.0871	0.264
C	12.4491	-19.7791	0.2058
C	12.6833	-12.8667	0.2347
C	12.425	-20.9989	0.1523
C	12.6982	-11.4474	0.2233
C	12.4241	-22.4177	0.1104
C	13.847	-10.7199	-0.2557
C	13.8363	-9.2888	-0.2212
C	12.6733	-8.6021	0.2781

C	11.5776	-9.3417	0.716
C	11.5896	-10.7425	0.6902
C	14.991	-11.3819	-0.7714
C	16.0819	-10.67	-1.2197
C	16.0767	-9.2572	-1.1726
C	14.9773	-8.5846	-0.6868
C	11.2639	-23.1487	-0.3346
C	11.2938	-24.58	-0.3358
C	12.486	-25.2629	0.0951
C	13.5904	-24.5196	0.5035
C	13.5603	-23.119	0.5123
C	10.0897	-22.49	-0.7817
C	8.9886	-23.2056	-1.1981
C	9.0137	-24.6189	-1.1872
C	10.1422	-25.2882	-0.7679
C	12.629	-7.1786	0.3261
C	12.5501	-26.6864	0.105
C	12.5778	-5.9573	0.3722
C	12.6191	-27.9077	0.1172
Si	12.4886	-4.1127	0.4451
Si	12.7351	-29.752	0.1385
C	12.9822	-3.4251	-1.2424
C	13.6791	-3.5071	1.7795
C	10.717	-3.6192	0.8697
C	14.5089	-30.2426	-0.2809
C	11.5383	-30.4381	-1.1503
C	12.27	-30.3625	1.8636
H	7.9863	-15.5208	0.3648
H	7.8984	-18.0186	0.3934
H	9.9805	-19.3288	0.3596
H	10.1573	-14.3608	0.3169
H	14.9378	-19.5053	0.2073
H	15.1153	-14.5397	0.3569
H	17.4102	-19.6046	0.194
H	19.5814	-18.4302	0.2381
H	19.6698	-15.9414	0.3224
H	17.5877	-14.6154	0.3579
H	10.7019	-8.8217	1.0887
H	10.7251	-11.2908	1.0485

H	14.9863	-12.4653	-0.821
H	16.9472	-11.1945	-1.6132
H	16.9403	-8.7018	-1.5254
H	14.965	-7.5003	-0.6549
H	14.4879	-25.0368	0.8252
H	14.4329	-22.568	0.8457
H	10.0781	-21.4057	-0.8036
H	8.0995	-22.6835	-1.5382
H	8.1421	-25.1771	-1.5149
H	10.1695	-26.3727	-0.7638
H	12.3082	-3.7792	-2.029
H	14.001	-3.7225	-1.5111
H	12.9432	-2.3299	-1.2341
H	14.7096	-3.8046	1.5605
H	13.4128	-3.9094	2.7622
H	13.6515	-2.4136	1.8451
H	10.0101	-3.9812	0.1163
H	10.6279	-2.528	0.9174
H	10.4132	-4.0234	1.8407
H	14.7946	-29.8873	-1.2762
H	14.6137	-31.3334	-0.2702
H	15.2193	-29.8299	0.4425
H	11.7851	-30.0775	-2.1541
H	10.5058	-30.1475	-0.9311
H	11.5828	-31.5329	-1.1662
H	12.9473	-29.9612	2.6243
H	12.3248	-31.4561	1.9076
H	11.2501	-30.0662	2.129

TET-3

Energy=-2891.92862728 A.U.

Cartesian Coordinates：

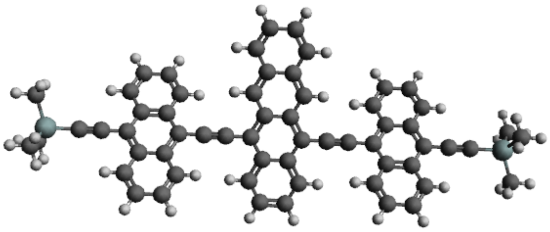

C	29.35	-16.8941	1.1821
C	29.3633	-18.3173	1.1854
C	30.5056	-18.9973	0.8555
C	31.7037	-18.3074	0.4912
C	31.6913	-16.865	0.4913
C	30.4803	-16.1948	0.8511
C	32.8892	-19.0091	0.1502
C	34.0834	-18.2897	-0.1884
C	34.0719	-16.8424	-0.1839
C	32.8659	-16.1437	0.156
C	35.2705	-18.9559	-0.5432
C	36.4377	-18.2681	-0.8773
C	36.4263	-16.8218	-0.8724
C	35.2484	-16.1549	-0.5336
C	37.6492	-18.945	-1.2329
C	38.7749	-18.2386	-1.5592
C	38.7635	-16.8087	-1.5548
C	37.6267	-16.1229	-1.2238
C	32.853	-14.728	0.1548
C	32.8956	-20.4245	0.139
C	32.8449	-13.5058	0.1514
C	32.8984	-21.6468	0.1218
C	32.8336	-12.0885	0.1453
C	32.892	-23.0636	0.0974
C	33.9998	-11.3679	0.5318
C	33.9902	-9.9296	0.516
C	32.8124	-9.2328	0.1283
C	31.6448	-9.9512	-0.2509
C	31.6565	-11.3896	-0.2496
C	31.6965	-23.7616	-0.242
C	31.6892	-25.1998	-0.2645
C	32.8796	-25.9193	0.0349
C	34.0745	-25.2238	0.3703
C	34.0794	-23.7859	0.4108
C	35.1892	-12.0365	0.9504
C	36.3101	-11.334	1.3139
C	36.3052	-9.9136	1.284
C	35.1771	-9.2348	0.8999

C	30.4483	-9.2785	-0.6449
C	29.3315	-9.9783	-1.0228
C	29.3474	-11.399	-1.0346
C	30.4773	-12.0805	-0.6611
C	35.2828	-25.9196	0.6776
C	36.427	-25.2424	1.0125
C	36.4277	-23.8227	1.0678
C	35.2865	-23.1193	0.7776
C	30.4931	-23.07	-0.5731
C	29.3434	-23.7504	-0.8844
C	29.3318	-25.171	-0.8911
C	30.4729	-25.8715	-0.595
C	32.8025	-7.8098	0.1176
C	32.8749	-27.3418	-0.0035
C	32.7933	-6.5856	0.1067
C	32.8695	-28.5654	-0.0405
Si	32.7784	-4.737	0.0945
Si	32.8628	-30.413	-0.1051
C	33.2543	-4.144	-1.6339
C	31.0388	-4.1547	0.5406
C	34.027	-4.1245	1.3711
C	31.6277	-30.957	-1.4248
C	32.3544	-31.0719	1.5895
C	34.6021	-30.9962	-0.5501
H	28.4424	-16.3635	1.4533
H	28.4664	-18.8633	1.4606
H	30.5231	-20.0808	0.8803
H	30.478	-15.111	0.8702
H	35.2731	-20.0404	-0.5699
H	35.234	-15.0702	-0.5522
H	37.6548	-20.0315	-1.2365
H	39.6886	-18.7612	-1.8253
H	39.6686	-16.2695	-1.818
H	37.6146	-15.0365	-1.2204
H	35.187	-13.1201	0.9874
H	37.2038	-11.8634	1.6303
H	37.1973	-9.366	1.5721
H	35.1661	-8.1506	0.883
H	30.4433	-8.1942	-0.6407

H	28.4324	-9.4473	-1.3196
H	28.4621	-11.945	-1.3446
H	30.4948	-13.1643	-0.6835
H	35.2747	-27.0034	0.6426
H	37.3352	-25.7908	1.2426
H	37.335	-23.2948	1.3449
H	35.2813	-22.0366	0.836
H	30.5068	-21.9861	-0.5843
H	28.4387	-23.2032	-1.1307
H	28.4163	-25.7012	-1.1367
H	30.4717	-26.9557	-0.6071
H	32.5493	-4.5075	-2.3884
H	34.2551	-4.4899	-1.9115
H	33.2541	-3.0486	-1.6727
H	30.298	-4.5198	-0.1782
H	30.9932	-3.0598	0.5431
H	30.7461	-4.5055	1.5354
H	35.0389	-4.4722	1.139
H	33.7714	-4.4744	2.3765
H	34.0449	-3.0289	1.3909
H	30.6163	-30.6064	-1.1956
H	31.5971	-32.0505	-1.4891
H	31.9044	-30.5703	-2.4109
H	31.3532	-30.7267	1.8664
H	33.0515	-30.7478	2.3689
H	32.3425	-32.1677	1.5831
H	34.9134	-30.608	-1.5252
H	34.6357	-32.0905	-0.5974
H	35.3362	-30.6699	0.1937

ADT-3

Energy=-3687.09397545 A.U.

Cartesian Coordinates:

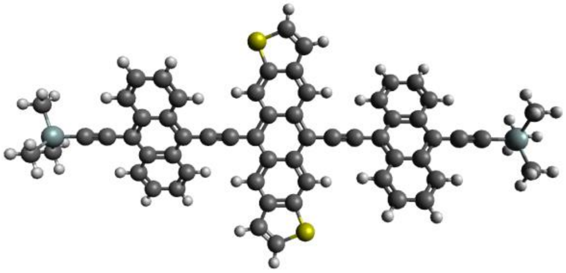

C	29.1697	-16.7584	-0.095
C	29.1605	-18.196	-0.1262
C	30.3219	-18.927	-0.1345
C	31.5778	-18.2586	-0.1144
C	31.6064	-16.813	-0.1134
C	30.3824	-16.0963	-0.0899
C	32.7996	-18.9924	-0.097
C	34.0543	-18.311	-0.1022
C	34.0828	-16.8659	-0.1376
C	32.861	-16.1318	-0.1313
C	35.2784	-19.0272	-0.0686
C	36.4909	-18.3655	-0.0953
C	36.4999	-16.9289	-0.16
C	35.3385	-16.1982	-0.1796
C	32.8913	-14.7164	-0.1396
C	32.7686	-20.4075	-0.0697
C	32.9184	-13.4944	-0.1423
C	32.7379	-21.6291	-0.0404
C	32.9479	-12.0774	-0.1412
C	32.7005	-23.0453	-0.0001
C	34.0209	-11.3901	0.4963
C	34.0521	-9.952	0.4928
C	33.0032	-9.222	-0.1318
C	31.9278	-9.9068	-0.7626

C	31.9034	-11.345	-0.7756
C	31.6312	-23.7078	0.6691
C	31.5908	-25.1452	0.7056
C	32.6271	-25.899	0.0881
C	33.6988	-25.2388	-0.5743
C	33.7323	-23.8017	-0.6268
C	35.0738	-12.0919	1.1557
C	36.1079	-11.4218	1.7583
C	36.1467	-10.0017	1.7412
C	35.1458	-9.2913	1.1298
C	30.8612	-9.2001	-1.3962
C	29.8346	-9.8673	-2.0137
C	29.8187	-11.2877	-2.0404
C	30.825	-12.0013	-1.4407
C	34.7528	-25.9696	-1.2016
C	35.7759	-25.3263	-1.8495
C	35.8009	-23.9072	-1.9148
C	34.8067	-23.1708	-1.3224
C	30.5911	-22.9812	1.322
C	29.5605	-23.6276	1.9557
C	29.5126	-25.0473	1.9781
C	30.5011	-25.781	1.3742
C	33.0295	-7.7992	-0.1248
C	32.5909	-27.3209	0.1344
C	33.0522	-6.5752	-0.1178
C	32.5575	-28.5439	0.1766
Si	33.0859	-4.7269	-0.1049
Si	32.496	-30.3902	0.2494
C	34.8872	-4.1654	-0.1602
C	32.153	-4.1055	-1.6237
C	32.2523	-4.1233	1.478
C	30.8701	-30.8923	1.0666
C	32.5891	-31.0639	-1.5115
C	33.9636	-30.9992	1.2691
C	37.83	-18.9083	-0.0731
C	38.7889	-17.9542	-0.1227
S	38.1548	-16.3119	-0.1992
C	27.8308	-16.2151	-0.0788
C	26.8717	-17.1701	-0.1016

S	27.5055	-18.8137	-0.143
H	30.3041	-20.01	-0.1649
H	30.4084	-15.0129	-0.0599
H	35.2525	-20.1097	-0.0137
H	35.356	-15.1162	-0.2351
H	35.035	-13.175	1.1827
H	36.8984	-11.9767	2.2541
H	36.9697	-9.4797	2.2194
H	35.1667	-8.2072	1.1209
H	30.8824	-8.1161	-1.3804
H	29.0333	-9.3106	-2.4898
H	29.0084	-11.8082	-2.5416
H	30.8222	-13.0849	-1.4747
H	34.7248	-27.0525	-1.1561
H	36.5676	-25.901	-2.3203
H	36.6083	-23.4061	-2.4397
H	34.8163	-22.0884	-1.3851
H	30.6372	-21.8982	1.319
H	28.7799	-23.0541	2.4459
H	28.6924	-25.5506	2.4808
H	30.4731	-26.8647	1.3953
H	35.3862	-4.5197	-1.0679
H	35.449	-4.5384	0.7023
H	34.945	-3.0711	-0.1504
H	32.6193	-4.4598	-2.5487
H	32.1498	-3.0099	-1.6472
H	31.1117	-4.4437	-1.6187
H	32.7735	-4.4913	2.3676
H	31.2116	-4.4582	1.5331
H	32.2557	-3.028	1.5151
H	30.009	-30.5341	0.4934
H	30.7936	-30.4877	2.081
H	30.798	-31.9837	1.1343
H	31.7536	-30.704	-2.1203
H	32.5508	-32.159	-1.5007
H	33.52	-30.7652	-2.0041
H	33.9297	-30.6044	2.2896
H	34.9152	-30.696	0.8208
H	33.9547	-32.0933	1.3311

H	38.0424	-19.9699	-0.0236
H	39.8614	-18.096	-0.1205
H	27.6185	-15.1526	-0.053
H	25.7992	-17.0282	-0.0975

NMR Spectra

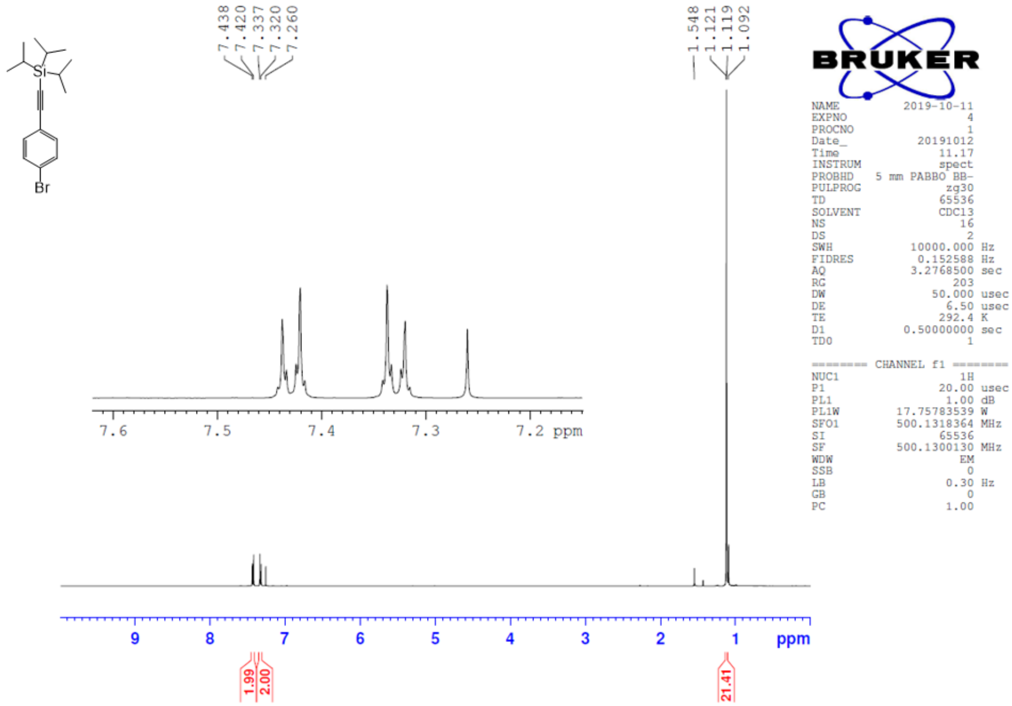

```
NAME          2019-10-11
EXPNO                  4
PROCNO                 1
Date_           20191012
Time               11.17
INSTRUM            spect
PROBHD   5 mm PABBO BB-
PULPROG             zg30
TD                 65536
SOLVENT            CDCl3
NS                    16
DS                     2
SWH            10000.000 Hz
FIDRES          0.152588 Hz
AQ             3.2768500 sec
RG                   203
DW                50.000 usec
DE                  6.50 usec
TE                 292.4 K
D1            0.50000000 sec
TD0                    1

======= CHANNEL f1 =======
NUC1                  1H
P1                 20.00 usec
PL1                 1.00 dB
PL1W         17.75783539 W
SFO1         500.1318364 MHz
SI                 65536
SF           500.1300130 MHz
WDW                   EM
SSB                    0
LB                  0.30 Hz
GB                     0
PC                  1.00
```

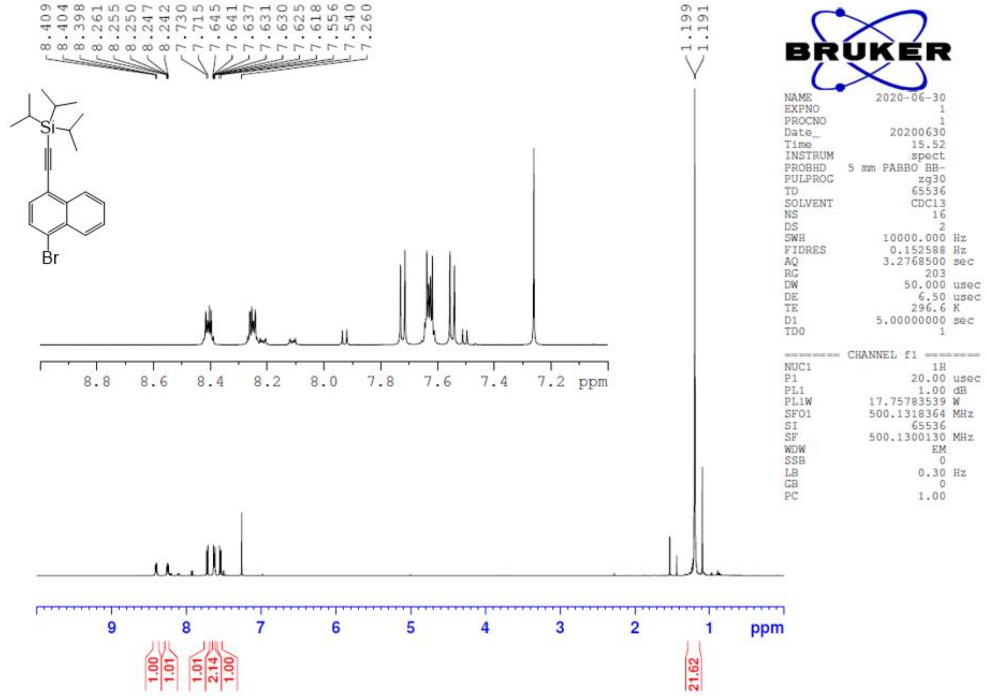

```
NAME          2020-06-30
EXPNO                  1
PROCNO                 1
Date_           20200630
Time               15.52
INSTRUM            spect
PROBHD   5 mm PABBO BB-
PULPROG             zg30
TD                 65536
SOLVENT            CDCl3
NS                    16
DS                     2
SWH            10000.000 Hz
FIDRES          0.152588 Hz
AQ             3.2768500 sec
RG                   203
DW                50.000 usec
DE                  6.50 usec
TE                 296.6 K
D1            5.00000000 sec
TD0                    1

======= CHANNEL f1 =======
NUC1                  1H
P1                 20.00 usec
PL1                 1.00 dB
PL1W         17.75783539 W
SFO1         500.1318364 MHz
SI                 65536
SF           500.1300130 MHz
WDW                   EM
SSB                    0
LB                  0.30 Hz
GB                     0
PC                  1.00
```

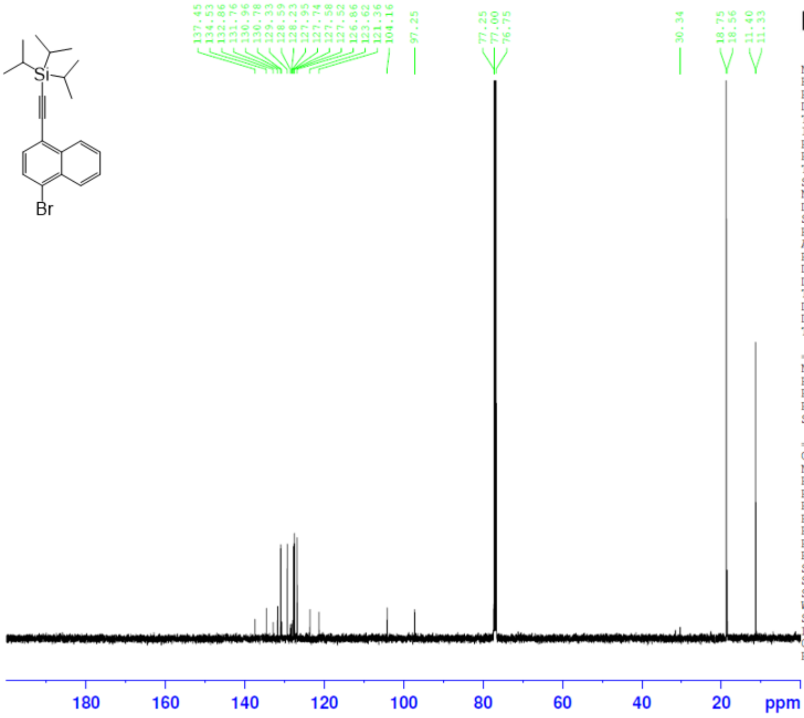

```
NAME          2020-06-30
EXPNO                  2
PROCNO                 1
Date_           20200630
Time               16.11
INSTRUM            spect
PROBHD   5 mm PABBO BB-
PULPROG           zgpg30
TD                 65536
SOLVENT            CDCl3
NS                  1039
DS                     4
SWH            29761.904 Hz
FIDRES          0.454131 Hz
AQ             1.1010548 sec
RG                   203
DW                16.800 usec
DE                  6.50 usec
TE                 298.3 K
D1            0.50000000 sec
D11           0.03000000 sec
TD0                    4

======= CHANNEL f1 =======
NUC1                 13C
P1                  9.50 usec
PL1                 0.00 dB
PL1W         89.92553711 W
SFO1         125.7703643 MHz

======= CHANNEL f2 =======
CPDPRG2          waltz16
NUC2                  1H
PCPD2              80.00 usec
PL2                 1.00 dB
PL12               13.04 dB
PL13               16.80 dB
PL2W         17.75783539 W
PL12W         1.11017132 W
PL13W         0.46707872 W
SFO2         500.1320005 MHz
SI                 65536
SF           125.7577890 MHz
WDW                   EM
SSB                    0
LB                  1.00 Hz
GB                     0
PC                  1.40
```

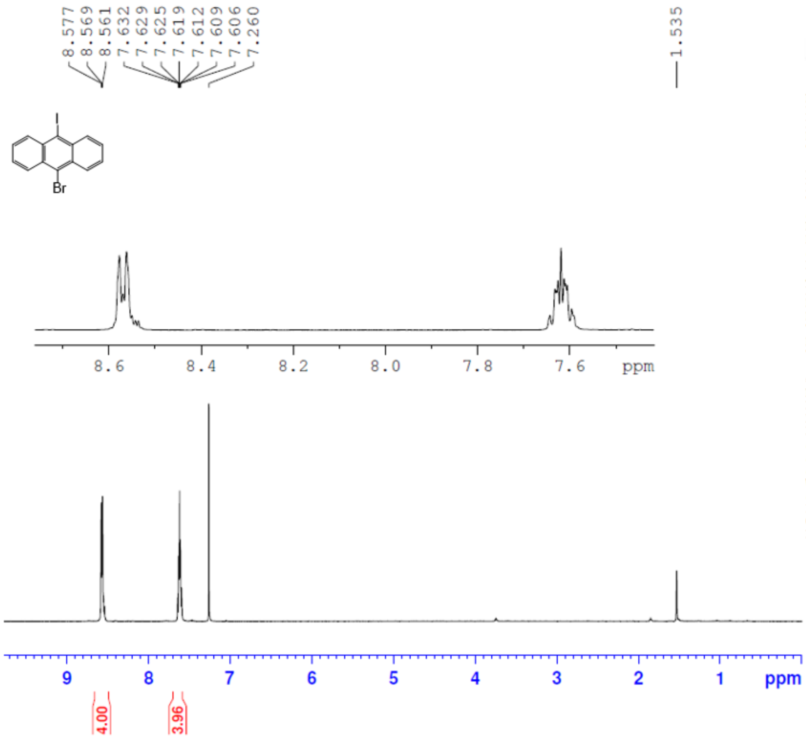

```
NAME            2019-6-8
EXPNO                  1
PROCNO                 1
Date_           20190609
Time               14.23
INSTRUM            spect
PROBHD   5 mm PABBO BB-
PULPROG             zg30
TD                 65536
SOLVENT            CDCl3
NS                    16
DS                     2
SWH            10000.000 Hz
FIDRES          0.152588 Hz
AQ             3.2768500 sec
RG                   203
DW                50.000 usec
DE                  6.50 usec
TE                 294.1 K
D1            5.00000000 sec
TD0                    1

======= CHANNEL f1 =======
NUC1                  1H
P1                 20.00 usec
PL1                 1.00 dB
PL1W         17.75783539 W
SFO1         500.1318364 MHz
SI                 65536
SF           500.1300133 MHz
WDW                   EM
SSB                    0
LB                  0.30 Hz
GB                     0
PC                  1.00
```

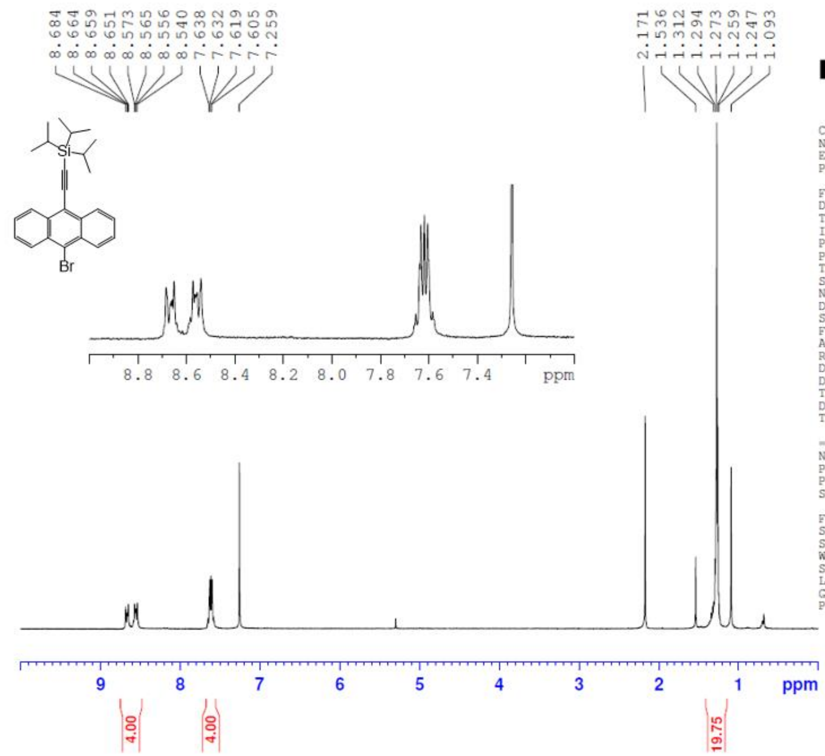

```
Current Data Parameters
NAME                2019-4-3
EXPNO                      1
PROCNO                     1

F2 - Acquisition Parameters
Date_               20190403
Time                   16.37
INSTRUM                spect
PROBHD   5 mm QNP 1H/13
PULPROG                 zg30
TD                     32768
SOLVENT                CDCl3
NS                        16
DS                         2
SWH                 6218.905 Hz
FIDRES              0.189786 Hz
AQ                 2.6345973 sec
RG                     724.1
DW                    80.400 usec
DE                      6.00 usec
TE                     300.0 K
D1                5.00000000 sec
TD0                        1

======= CHANNEL f1 =======
NUC1                      1H
P1                     12.00 usec
PL1                     0.00 dB
SFO1             300.3418547 MHz

F2 - Processing parameters
SI                     32768
SF               300.3400043 MHz
WDW                       EM
SSB                        0
LB                      0.30 Hz
GB                         0
PC                      1.00
```

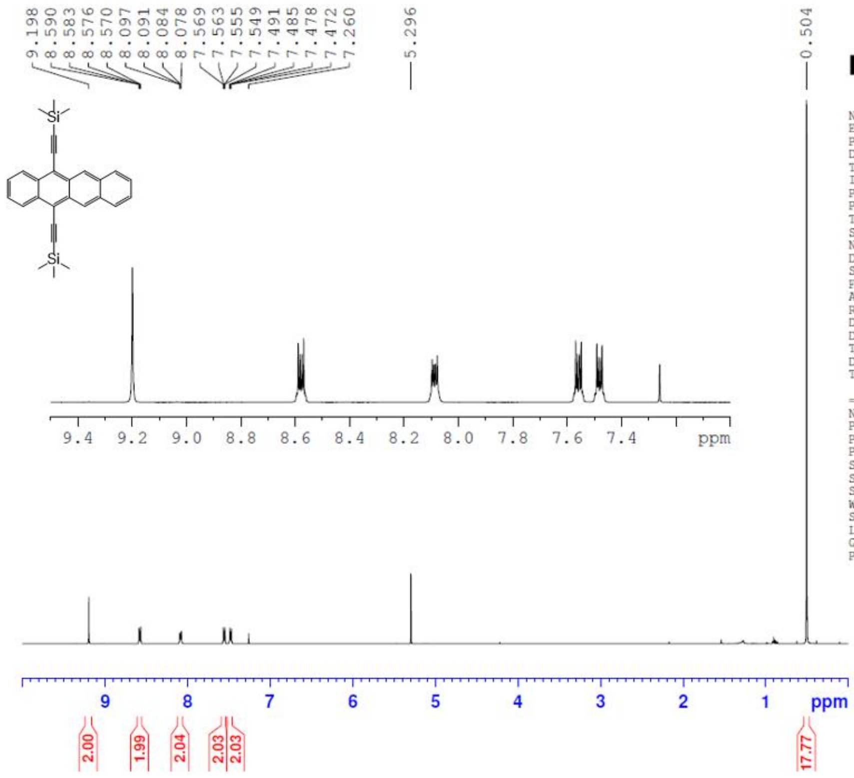

```
NAME               2018-7-25
EXPNO                      1
PROCNO                     1
Date_               20180725
Time                   11.22
INSTRUM                spect
PROBHD   5 mm PABBO BB-
PULPROG                 zg30
TD                     65536
SOLVENT                CDCl3
NS                        16
DS                         2
SWH                10000.000 Hz
FIDRES              0.152588 Hz
AQ                 3.2768500 sec
RG                       128
DW                    50.000 usec
DE                      6.50 usec
TE                     293.0 K
D1                0.50000000 sec
TD0                        1

======= CHANNEL f1 =======
NUC1                      1H
P1                     20.00 usec
PL1                     1.00 dB
PL1W             17.75783539 W
SFO1             500.1318364 MHz
SI                     65536
SF               500.1300131 MHz
WDW                       EM
SSB                        0
LB                      0.30 Hz
GB                         0
PC                      1.00
```

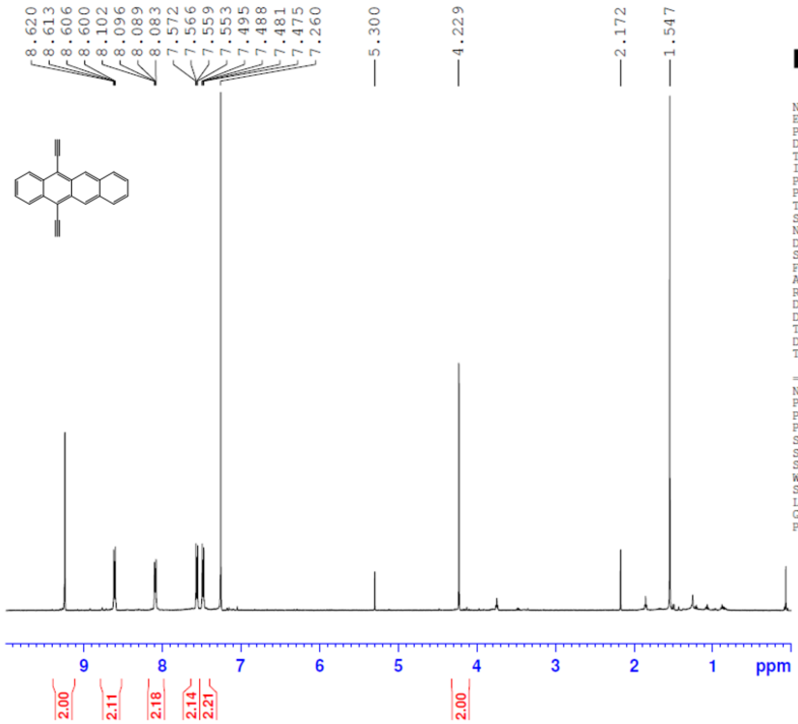

```
NAME           2019-4-25
EXPNO                  1
PROCNO                 1
Date_           20190425
Time               14.59
INSTRUM            spect
PROBHD   5 mm PABBO BB-
PULPROG             zg30
TD                 65536
SOLVENT            CDCl3
NS                    16
DS                     2
SWH            10000.000 Hz
FIDRES          0.152588 Hz
AQ             3.2768500 sec
RG                   203
DW                50.000 usec
DE                  6.50 usec
TE                 292.5 K
D1            5.00000000 sec
TD0                    1

======= CHANNEL f1 =======
NUC1                  1H
P1                 20.00 usec
PL1                 1.00 dB
PL1W         17.75783539 W
SFO1         500.1318364 MHz
SI                 65536
SF           500.1300130 MHz
WDW                   EM
SSB                    0
LB                  0.30 Hz
GB                     0
PC                  1.00
```

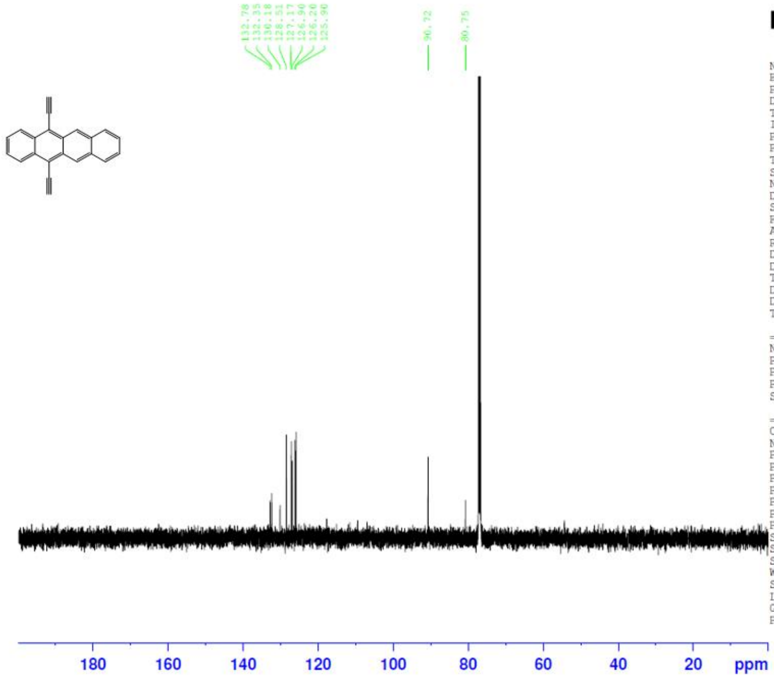

```
NAME           2019-4-25
EXPNO                  2
PROCNO                 1
Date_           20190425
Time               15.30
INSTRUM            spect
PROBHD   5 mm PABBO BB-
PULPROG           zgpg30
TD                 65536
SOLVENT            CDCl3
NS                  1024
DS                     4
SWH            29761.904 Hz
FIDRES          0.454131 Hz
AQ             1.1010548 sec
RG                   203
DW                16.800 usec
DE                  6.50 usec
TE                 294.8 K
D1            0.50000000 sec
D11           0.03000000 sec
TD0                    1

======= CHANNEL f1 =======
NUC1                 13C
P1                  9.50 usec
PL1                 0.00 dB
PL1W         89.92553711 W
SFO1         125.7703643 MHz

======= CHANNEL f2 =======
CPDPRG2          waltz16
NUC2                  1H
PCPD2              80.00 usec
PL2                 1.00 dB
PL12               13.04 dB
PL13               16.80 dB
PL2W         17.75783539 W
PL12W         1.11017132 W
PL13W         0.46707872 W
SFO2         500.1320005 MHz
SI                 65536
SF           125.7577890 MHz
WDW                   EM
SSB                    0
LB                  1.00 Hz
GB                     0
PC                  1.40
```

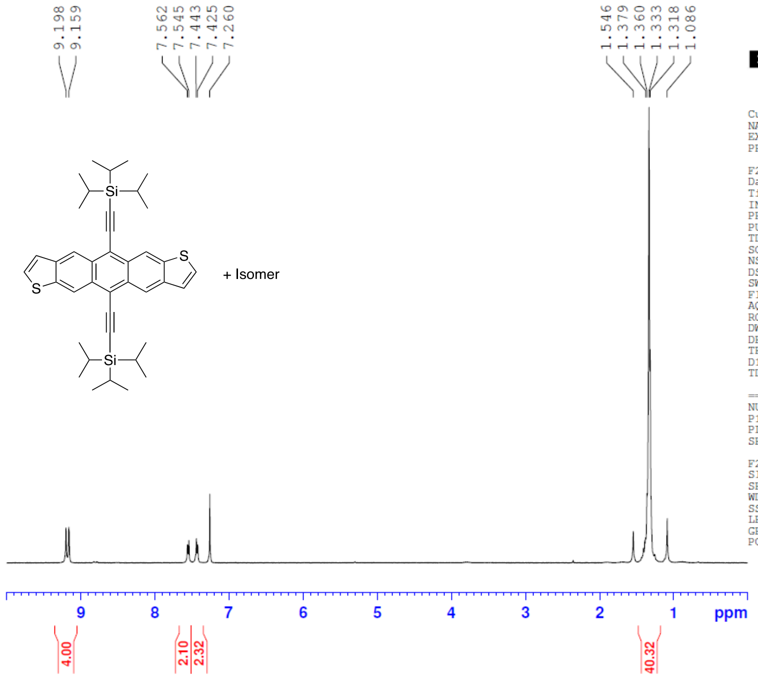

```
Current Data Parameters
NAME              2019-9-11
EXPNO                     1
PROCNO                    1

F2 - Acquisition Parameters
Date_              20190911
Time                   9.16
INSTRUM               spect
PROBHD   5 mm QNP 1H/13
PULPROG                zg30
TD                    32768
SOLVENT               CDCl3
NS                       16
DS                        2
SWH                6218.905 Hz
FIDRES             0.189786 Hz
AQ                2.6345973 sec
RG                    574.7
DW                   80.400 usec
DE                     6.00 usec
TE                    300.0 K
D1               5.00000000 sec
TD0                       1

======= CHANNEL f1 =======
NUC1                     1H
P1                    12.00 usec
PL1                    0.00 dB
SFO1            300.3418547 MHz

F2 - Processing parameters
SI                    32768
SF              300.3400040 MHz
WDW                      EM
SSB                       0
LB                     0.30 Hz
GB                        0
PC                     1.00
```

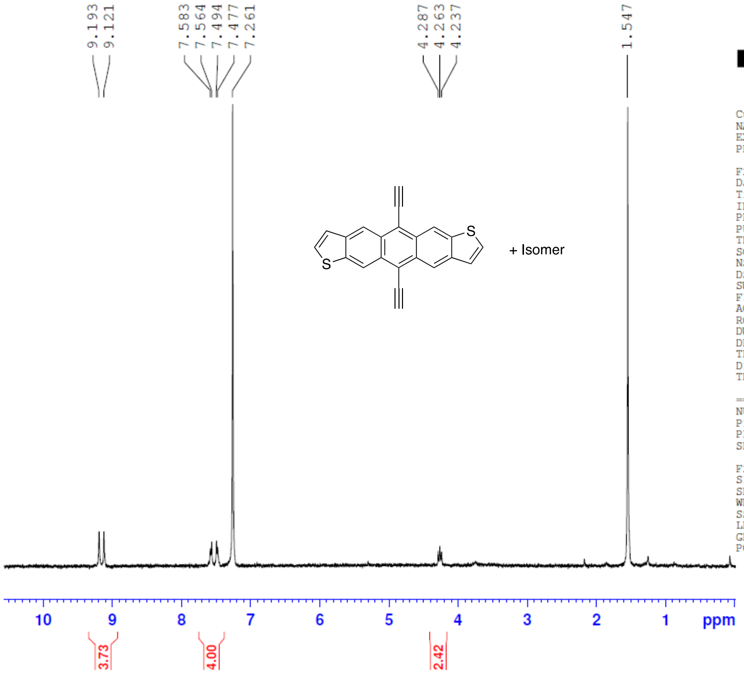

```
Current Data Parameters
NAME              2019-9-13
EXPNO                     1
PROCNO                    1

F2 - Acquisition Parameters
Date_              20190913
Time                  13.21
INSTRUM               spect
PROBHD   5 mm QNP 1H/13
PULPROG                zg30
TD                    32768
SOLVENT               CDCl3
NS                       16
DS                        2
SWH                6218.905 Hz
FIDRES             0.189786 Hz
AQ                2.6345973 sec
RG                    912.3
DW                   80.400 usec
DE                     6.00 usec
TE                    300.0 K
D1               5.00000000 sec
TD0                       1

======= CHANNEL f1 =======
NUC1                     1H
P1                    12.00 usec
PL1                    0.00 dB
SFO1            300.3418547 MHz

F2 - Processing parameters
SI                    32768
SF              300.3400040 MHz
WDW                      EM
SSB                       0
LB                     0.30 Hz
GB                        0
PC                     1.00
```

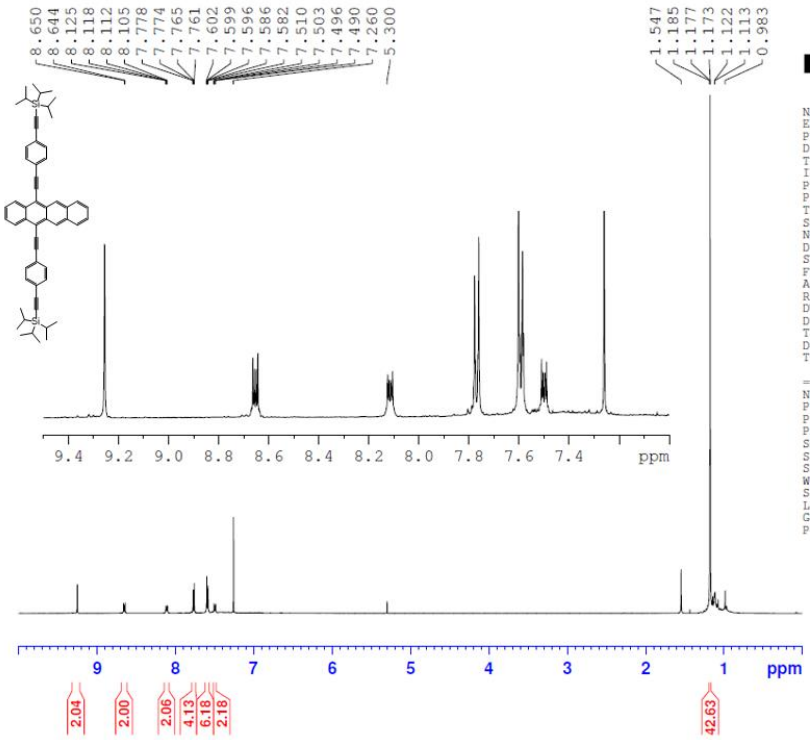

```
NAME          2019-11-1
EXPNO                 1
PROCNO                1
Date_          20191101
Time              17.04
INSTRUM           spect
PROBHD   5 mm PABBO BB-
PULPROG            zg30
TD                65536
SOLVENT           CDCl3
NS                   16
DS                    2
SWH           10000.000 Hz
FIDRES         0.152588 Hz
AQ            3.2768500 sec
RG                  203
DW               50.000 usec
DE                 6.50 usec
TE                292.4 K
D1           5.00000000 sec
TD0                   1

======= CHANNEL f1 =======
NUC1                 1H
P1                20.00 usec
PL1                1.00 dB
PL1W        17.75783539 W
SFO1        500.1318364 MHz
SI                65536
SF          500.1300133 MHz
WDW                  EM
SSB                   0
LB                 0.30 Hz
GB                    0
PC                 1.00
```

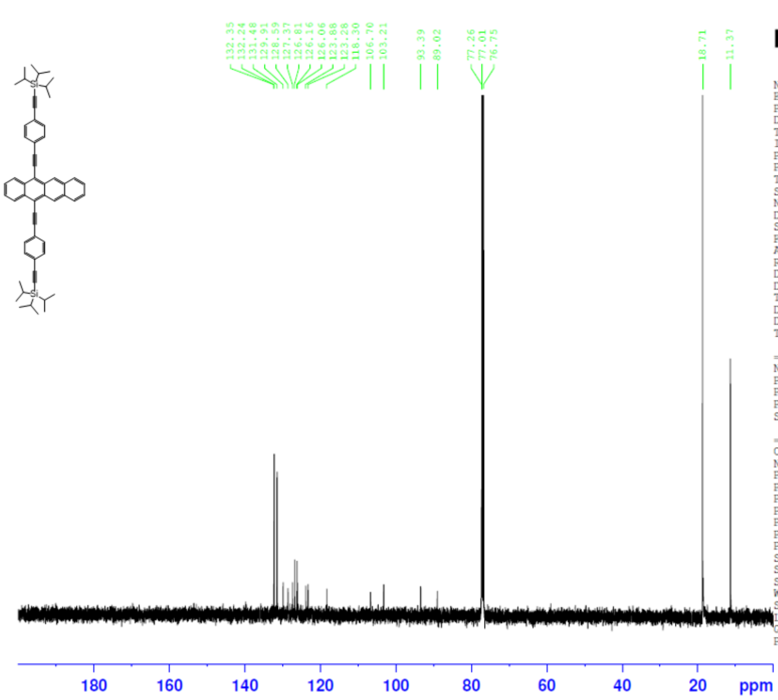

```
NAME          2019-11-1
EXPNO                 3
PROCNO                1
Date_          20191101
Time              17.52
INSTRUM           spect
PROBHD   5 mm PABBO BB-
PULPROG          zgpg30
TD                65536
SOLVENT           CDCl3
NS                 1024
DS                    4
SWH           29761.904 Hz
FIDRES         0.454131 Hz
AQ            1.1010548 sec
RG                  203
DW               16.800 usec
DE                 6.50 usec
TE                294.7 K
D1           0.50000000 sec
D11          0.03000000 sec
TD0                   1

======= CHANNEL f1 =======
NUC1                13C
P1                 9.50 usec
PL1                0.00 dB
PL1W        89.92553711 W
SFO1        125.7703643 MHz

======= CHANNEL f2 =======
CPDPRG2         waltz16
NUC2                 1H
PCPD2             80.00 usec
PL2                1.00 dB
PL12              13.04 dB
PL13              16.80 dB
PL2W        17.75783539 W
PL12W        1.11017132 W
PL13W        0.46707872 W
SFO2        500.1320005 MHz
SI                65536
SF          125.7577890 MHz
WDW                  EM
SSB                   0
LB                 1.00 Hz
GB                    0
PC                 1.40
```

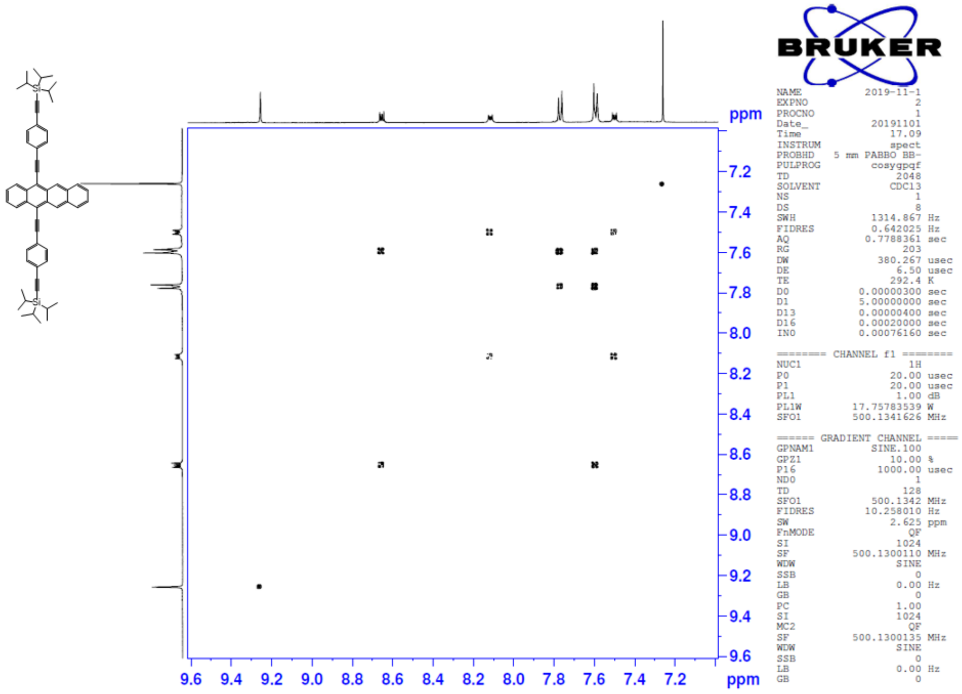

```
NAME           2019-11-1
EXPNO                  2
PROCNO                 1
Date_           20191101
Time               17.09
INSTRUM            spect
PROBHD   5 mm PABBO BB-
PULPROG          cosygpqf
TD                  2048
SOLVENT            CDC13
NS                     1
DS                     8
SWH             1314.867 Hz
FIDRES          0.642025 Hz
AQ             0.7788361 sec
RG                   203
DW               380.267 usec
DE                  6.50 usec
TE                 292.4 K
D0            0.00000300 sec
D1            5.00000000 sec
D13           0.00000400 sec
D16           0.00020000 sec
IN0           0.00076160 sec

======= CHANNEL f1 =======
NUC1                  1H
P0                 20.00 usec
P1                 20.00 usec
PL1                 1.00 dB
PL1W         17.75783539 W
SFO1         500.1341626 MHz

===== GRADIENT CHANNEL ====
GPNAM1          SINE.100
GPZ1               10.00 %
P16              1000.00 usec
ND0                    1
TD                   128
SFO1            500.1342 MHz
FIDRES         10.258010 Hz
SW                 2.625 ppm
FnMODE                QF
SI                  1024
SF           500.1300110 MHz
WDW                 SINE
SSB                    0
LB                  0.00 Hz
GB                     0
PC                  1.00
SI                  1024
MC2                   QF
SF           500.1300135 MHz
WDW                 SINE
SSB                    0
LB                  0.00 Hz
GB                     0
```

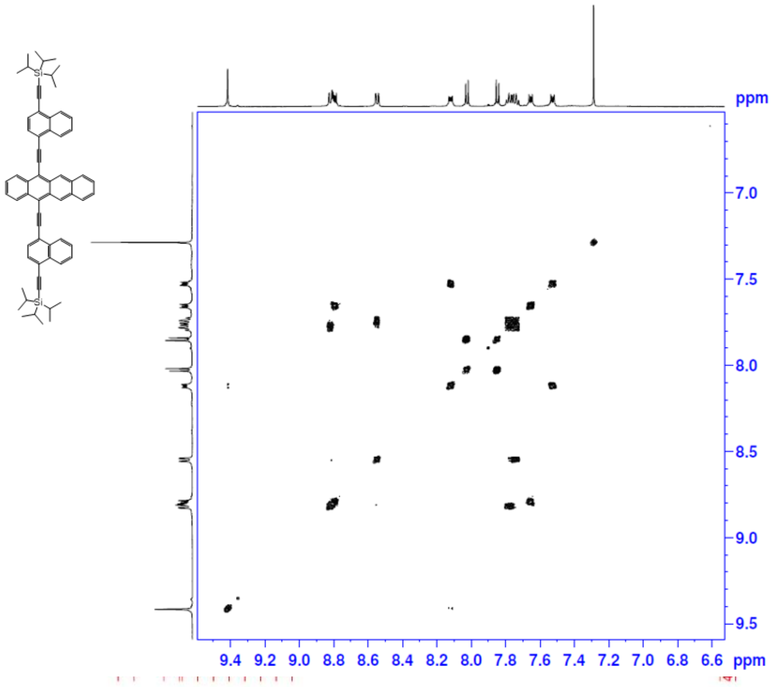

```
NAME            2019-12-10
EXPNO                    3
PROCNO                   1
Date_             20191210
Time                 14.46
INSTRUM              spect
PROBHD   5 mm PABBO BB-
PULPROG           cosygpqf
TD                    2048
SOLVENT              CDCl3
NS                       1
DS                       8
SWH               1533.742 Hz
FIDRES            0.748898 Hz
AQ               0.6676980 sec
RG                     203
DW                 326.000 usec
DE                    6.50 usec
TE                   292.0 K
D0              0.00000300 sec
D1              0.50000000 sec
D13             0.00000400 sec
D16             0.00020000 sec
IN0             0.00065280 sec

======= CHANNEL f1 =======
NUC1                    1H
P0                   20.00 usec
P1                   20.00 usec
PL1                   1.00 dB
PL1W           17.75783539 W
SFO1           500.1340305 MHz

===== GRADIENT CHANNEL ====
GPNAM1            SINE.100
GPZ1                 10.00 %
P16                1000.00 usec
ND0                      1
TD                     128
SFO1               500.134 MHz
FIDRES           11.967678 Hz
SW                   3.063 ppm
FnMODE                  QF
SI                    1024
SF             500.1300000 MHz
WDW                   SINE
SSB                      0
LB                    0.00 Hz
GB                       0
PC                    1.00
SI                    1024
MC2                     QF
SF             500.1300000 MHz
WDW                   SINE
SSB                      0
LB                    0.00 Hz
GB                       0
```

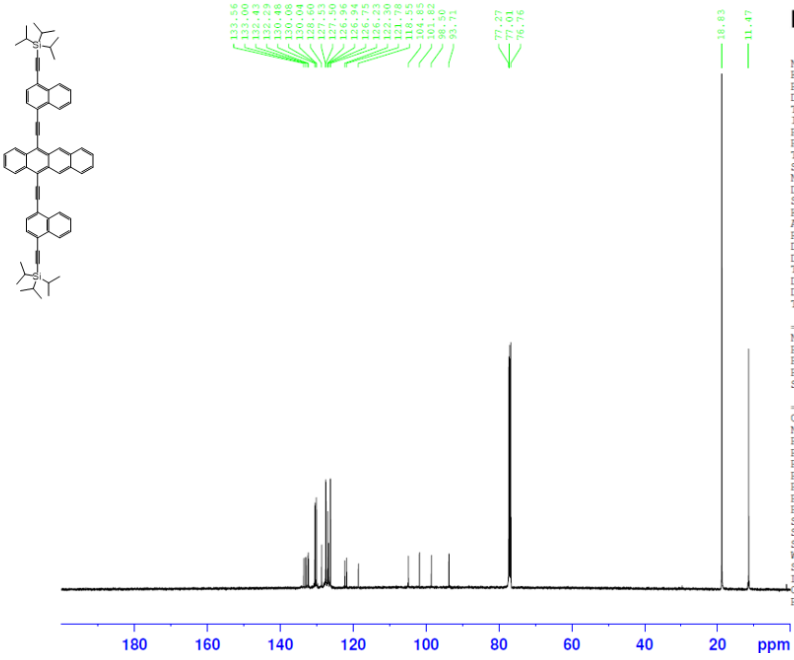

```
NAME            2019-12-11
EXPNO                    1
PROCNO                   1
Date_             20191211
Time                 18.46
INSTRUM              spect
PROBHD   5 mm PABBO BB-
PULPROG               zgpg
TD                   65536
SOLVENT              CDCl3
NS                   30720
DS                       4
SWH              29761.904 Hz
FIDRES            0.454131 Hz
AQ               1.1010548 sec
RG                     203
DW                  16.800 usec
DE                    6.50 usec
TE                   293.4 K
D1              0.50000000 sec
D11             0.03000000 sec
TD0                     30

======== CHANNEL f1 ========
NUC1                   13C
P1                    9.50 usec
PL1                   0.00 dB
PL1W           89.92553711 W
SFO1           125.7703643 MHz

======== CHANNEL f2 ========
CPDPRG2            waltz16
NUC2                    1H
PCPD2                80.00 usec
PL2                   1.00 dB
PL12                 13.04 dB
PL13                 16.80 dB
PL2W           17.75783539 W
PL12W           1.11017132 W
PL13W           0.46707872 W
SFO2           500.1320005 MHz
SI                   65536
SF             125.7577890 MHz
WDW                     EM
SSB                      0
LB                    1.00 Hz
GB                       0
PC                    1.40
```

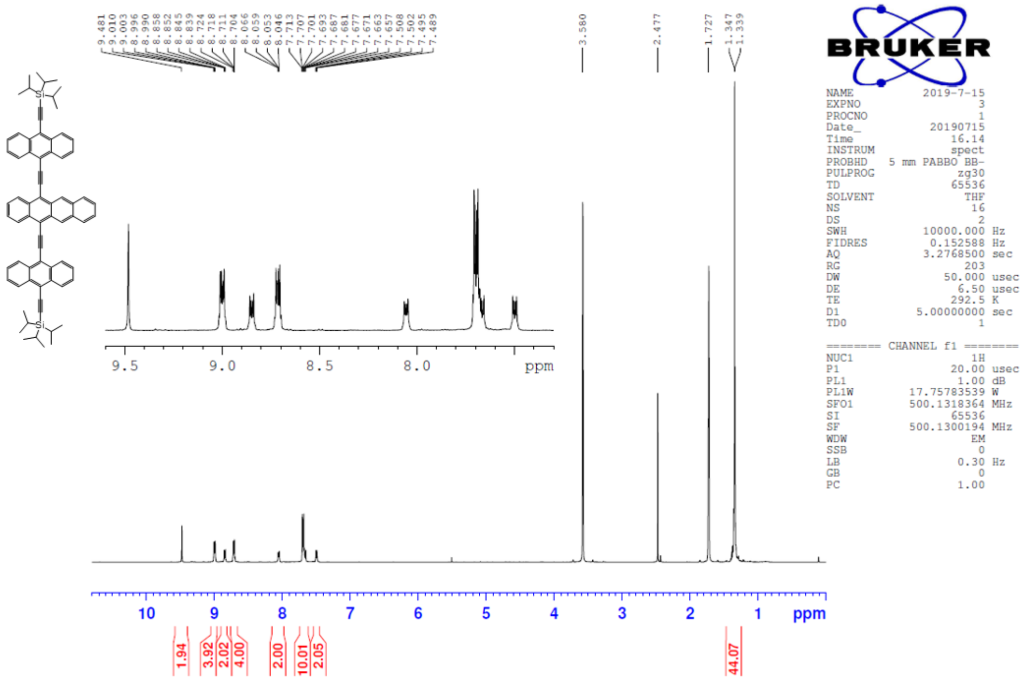
9.481
9.010
9.003
8.996
8.990
8.858
8.852
8.845
8.839
8.724
8.718
8.711
8.704
8.066
8.059
8.053
8.046
7.713
7.707
7.701
7.693
7.687
7.681
7.677
7.671
7.663
7.657
7.508
7.502
7.495
7.489
3.580
2.477
1.727
1.347
1.339
Si
Si
9.5
9.0
8.5
8.0
ppm
10
9
8
7
6
5
4
3
2
1
ppm
1.94
3.92
2.02
4.00
2.00
10.01
2.05
44.07
BRUKER
NAME 2019-7-15
EXPNO 3
PROCNO 1
Date_ 20190715
Time 16.14
INSTRUM spect
PROBHD 5 mm PABBO BB-
PULPROG zg30
TD 65536
SOLVENT THF
NS 16
DS 2
SWH 10000.000 Hz
FIDRES 0.152588 Hz
AQ 3.2768500 sec
RG 203
DW 50.000 usec
DE 6.50 usec
TE 292.5 K
D1 5.00000000 sec
TD0 1
======= CHANNEL f1 =======
NUC1 1H
P1 20.00 usec
PL1 1.00 dB
PL1W 17.75783539 W
SFO1 500.1318364 MHz
SI 65536
SF 500.1300194 MHz
WDW EM
SSB 0
LB 0.30 Hz
GB 0
PC 1.00

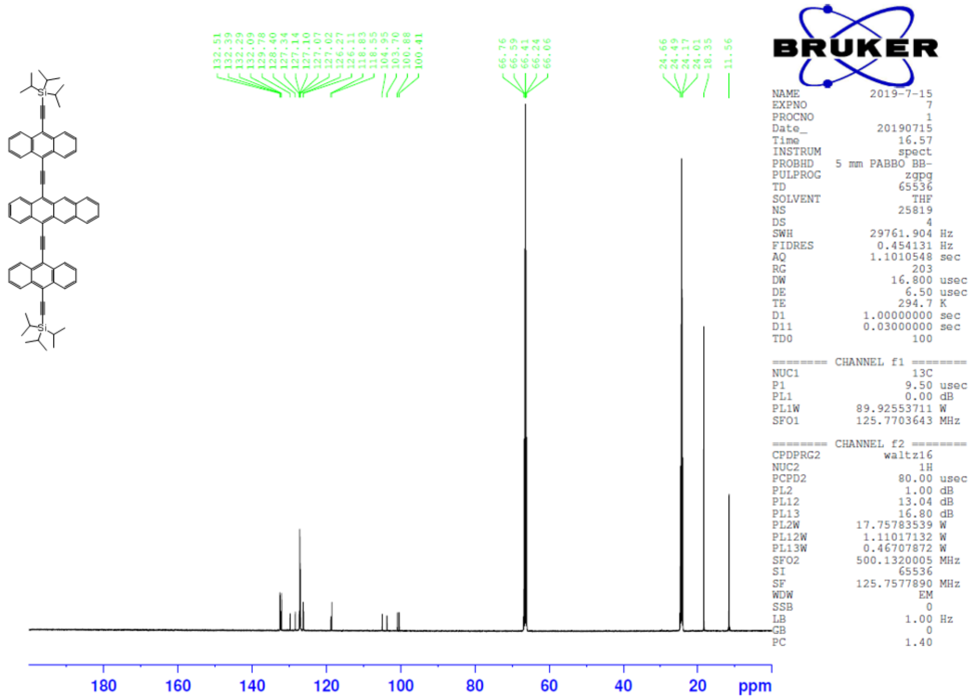
132.51
132.39
132.29
132.09
129.78
128.40
127.34
127.14
127.10
127.07
127.02
126.27
126.11
118.83
118.55
104.95
103.70
100.88
100.41
66.76
66.59
66.41
66.24
66.06
24.66
24.49
24.17
24.01
18.35
11.56
Si
Si
180
160
140
120
100
80
60
40
20
ppm
BRUKER
NAME 2019-7-15
EXPNO 7
PROCNO 1
Date_ 20190715
Time 16.57
INSTRUM spect
PROBHD 5 mm PABBO BB-
PULPROG zgpg
TD 65536
SOLVENT THF
NS 25819
DS 4
SWH 29761.904 Hz
FIDRES 0.454131 Hz
AQ 1.1010548 sec
RG 203
DW 16.800 usec
DE 6.50 usec
TE 294.7 K
D1 1.00000000 sec
D11 0.03000000 sec
TD0 100
======= CHANNEL f1 =======
NUC1 13C
P1 9.50 usec
PL1 0.00 dB
PL1W 89.92553711 W
SFO1 125.7703643 MHz
======= CHANNEL f2 =======
CPDPRG2 waltz16
NUC2 1H
PCPD2 80.00 usec
PL2 1.00 dB
PL12 13.04 dB
PL13 16.80 dB
PL2W 17.75783539 W
PL12W 1.11017132 W
PL13W 0.46707872 W
SFO2 500.1320005 MHz
SI 65536
SF 125.7577890 MHz
WDW EM
SSB 0
LB 1.00 Hz
GB 0
PC 1.40

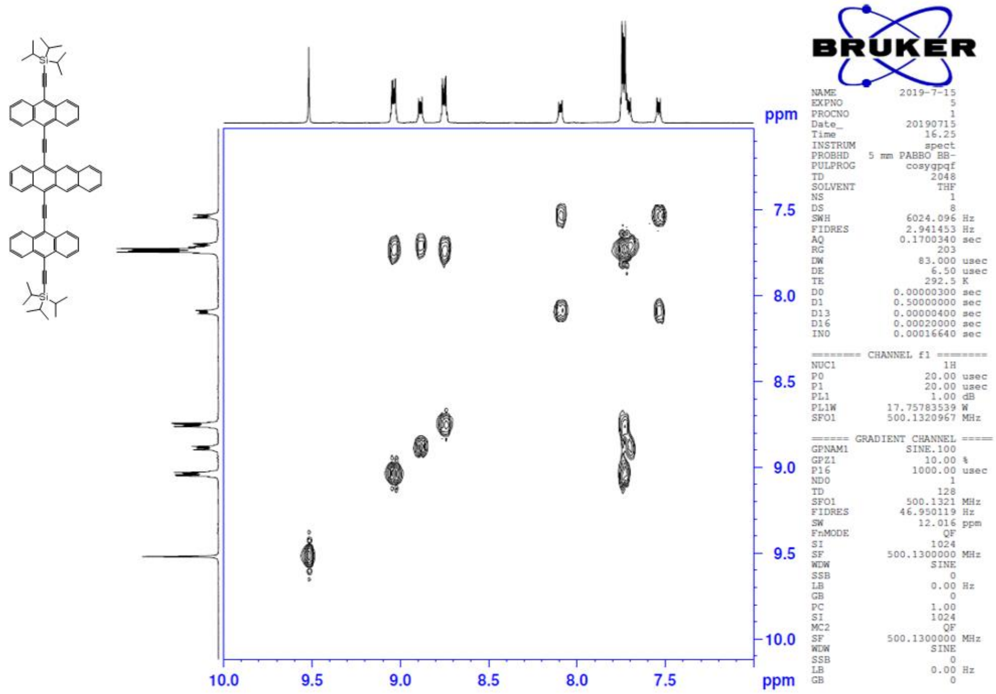

```
NAME          2019-7-15
EXPNO                 5
PROCNO                1
Date_          20190715
Time              16.25
INSTRUM           spect
PROBHD   5 mm PABBO BB-
PULPROG        cosygpqf
TD                 2048
SOLVENT             THF
NS                    1
DS                    8
SWH            6024.096 Hz
FIDRES         2.941453 Hz
AQ            0.1700340 sec
RG                  203
DW               83.000 usec
DE                 6.50 usec
TE                292.5 K
D0           0.00000300 sec
D1           0.50000000 sec
D13          0.00000400 sec
D16          0.00020000 sec
IN0          0.00016640 sec

======= CHANNEL f1 =======
NUC1                 1H
P0                20.00 usec
P1                20.00 usec
PL1                1.00 dB
PL1W        17.75783539 W
SFO1        500.1320967 MHz

===== GRADIENT CHANNEL ====
GPNAM1         SINE.100
GPZ1              10.00 %
P16             1000.00 usec
ND0                   1
TD                  128
SFO1           500.1321 MHz
FIDRES        46.950119 Hz
SW               12.016 ppm
FnMODE               QF
SI                 1024
SF          500.1300000 MHz
WDW                SINE
SSB                   0
LB                 0.00 Hz
GB                    0
PC                 1.00
SI                 1024
MC2                  QF
SF          500.1300000 MHz
WDW                SINE
SSB                   0
LB                 0.00 Hz
GB                    0
```

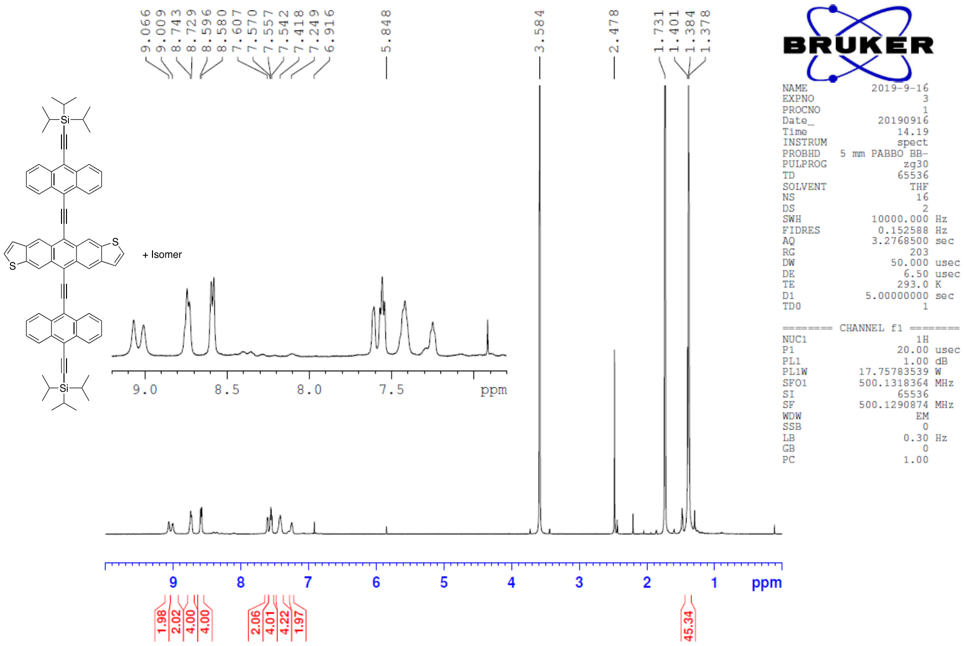

```
NAME          2019-9-16
EXPNO                 3
PROCNO                1
Date_          20190916
Time              14.19
INSTRUM           spect
PROBHD   5 mm PABBO BB-
PULPROG            zg30
TD                65536
SOLVENT             THF
NS                   16
DS                    2
SWH           10000.000 Hz
FIDRES         0.152588 Hz
AQ            3.2768500 sec
RG                  203
DW               50.000 usec
DE                 6.50 usec
TE                293.0 K
D1           5.00000000 sec
TD0                   1

======== CHANNEL f1 ========
NUC1                 1H
P1                20.00 usec
PL1                1.00 dB
PL1W        17.75783539 W
SFO1        500.1318364 MHz
SI                65536
SF          500.1290874 MHz
WDW                  EM
SSB                   0
LB                 0.30 Hz
GB                    0
PC                 1.00
```

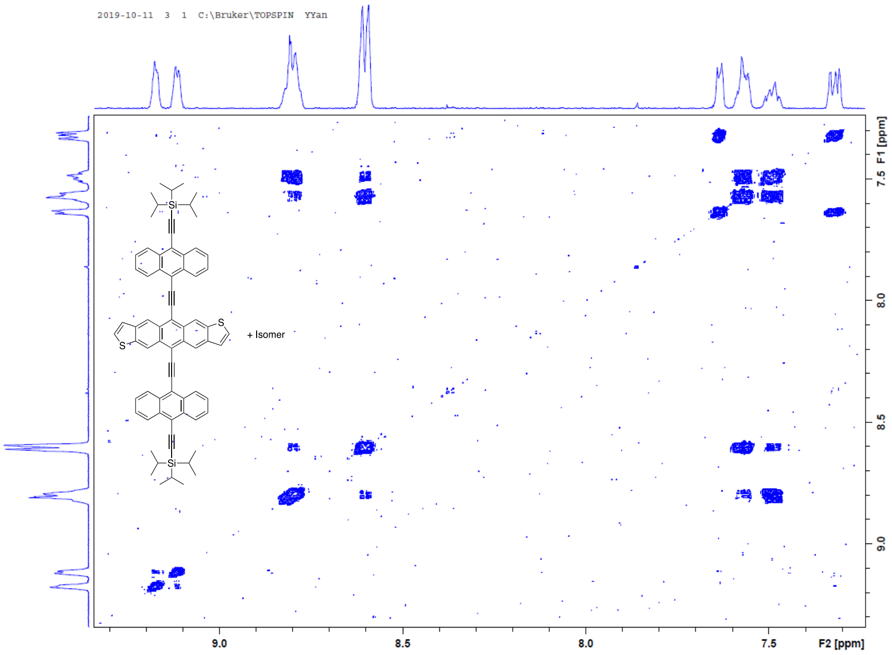

Chapter 3:

Tuning the fluorescence and singlet oxygen responsiveness of ethynylated tetracenes by electron-donating or withdrawing effect

3.1 Introduction

Acenes, or linearly fused benzenes, are commonly studied as a kind of building block of organic electronics because of their favored electronic properties.[2, 7, 18] In recent years, the discovery of stable longer acene derivatives, especially TIPS-pentacene, considerably triggered research in this field[19, 143]. On the other hand, acenes can participate in various interesting chemical reactions, allowing them to be used in applications beyond organic electronics.[4] Among these applications, singlet oxygen sensing is one of the prominent directions due to the significance of singlet oxygen in biosystems and material degradation[78].

Probes based on acenes have been developed, such as the commercially available singlet oxygen sensing green (**SOSG**)[95], FRET-based conjugated polymers[27, 84], and water-dispersible nanoparticles[83, 99, 104]. Rapid cycloaddition reactions between acenes and singlet oxygen results in changes in energies of frontier molecular orbitals of the incorporated acenes, and then the signal is reported in absorbance or fluorescence. To further improve the performance of these probes or to develop new ones, it is vital to understand the property-structure relationship between the acenes and their photo-physical and chemical properties.

An excellent candidate for a singlet oxygen probe should have: i) favorable reaction kinetics with singlet oxygen, ii) significant change in fluorescent properties, iii) high fluorescent quantum yield (FLQY), and iv) reasonable photo-stability. For biological systems, v) red-shifted fluorescence is also required to avoid artifacts from autofluorescence and larger tissue penetration depth.[144-147] Our group has carefully studied the impact of length of acenes[79, 88], triple bond substitution following the work of Linker group[3], and steric hindrance[81]. Recently, we have also found that the aromatic pendants spaced by ethynyl groups could still affect the spectroscopic properties of acenes and the photo-stabilities.[28] Such a finding agrees with Anthony group's work on the impact of single atom switching in acetylene side-chains of acenes.[89]

3.2 Experimental design:

In this work, we studied the electronic effects, namely electron-donating and electron-withdrawing effects, by introducing aromatic pendants on both sides of ethynylated tetracene and testing photo-physical properties and kinetics of singlet oxygen cycloaddition. As the backbone structure, ethynylated tetracene is reported to have a favorable reaction rate with singlet oxygen and a relatively high fluorescent quantum yield.[3, 79, 87] The electron donating/withdrawing groups are selected because of their capability of red-shifting the absorbance and emission of organic fluorescent dyes by forming donor-acceptor (D-A) systems and narrowing the HOMO-LUMO gaps.[145] **Figure 3.1** displays the chemical structures of all the molecules developed in this work and **1D** from our group's past work. We select thiophene (**ED1**), dimethyl aniline (**ED2**), and triphenylamine (**ED3**) as the electron-donating groups; pyridine (**EW2**), pyrazine (**EW2**), and benzothiadiazole (**EW3**) as electron-withdrawing groups. We have also installed tetraphenyl ethylene (**F1**), a famous moiety that triggers aggregation-induced emission effect (AIE)[148], because we reported the rapid rotation might increase the photo-stability of the acenes.[28] As a reference , we include **1D** from our group's 2012 work[87], which has two phenyl substitutions at the end of triple bonds. Interestingly, although many of the anthracene-based or pentacene-based analogs of these molecules have been studied,[149-152] the studies about substituted tetracenes are very

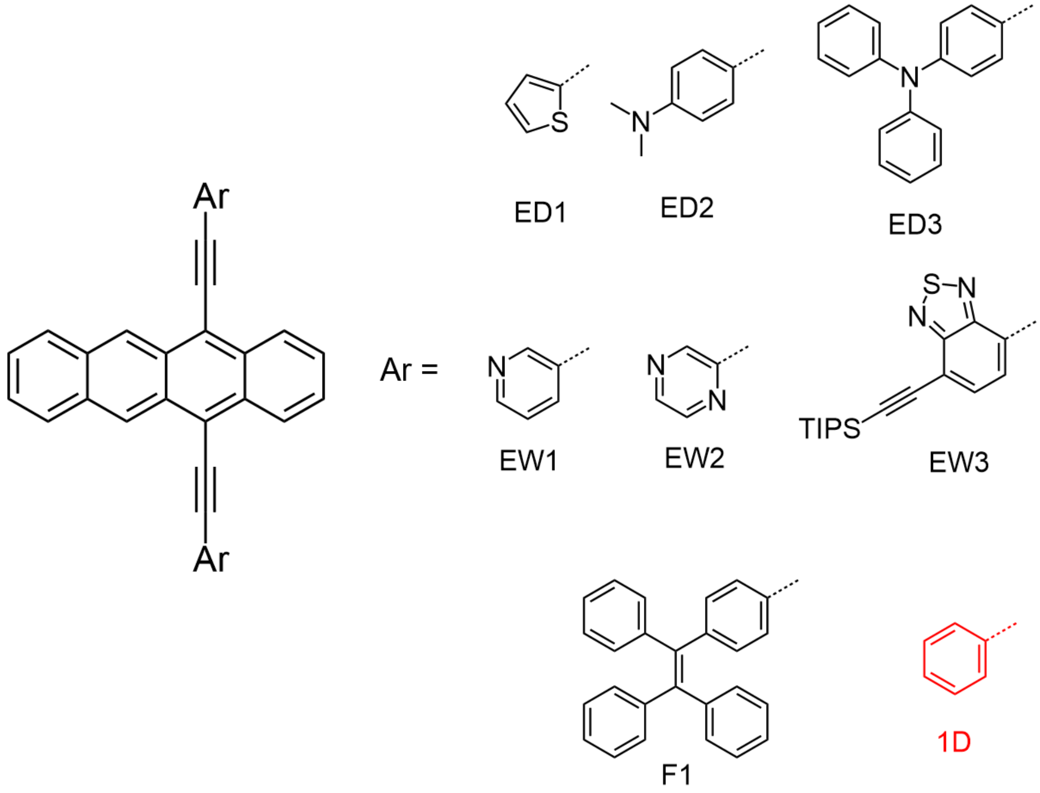

Figure 3.1: Molecular structure of the tetracene derivatives studied in this work. The molecule **1D** is reported by our group in 2012.

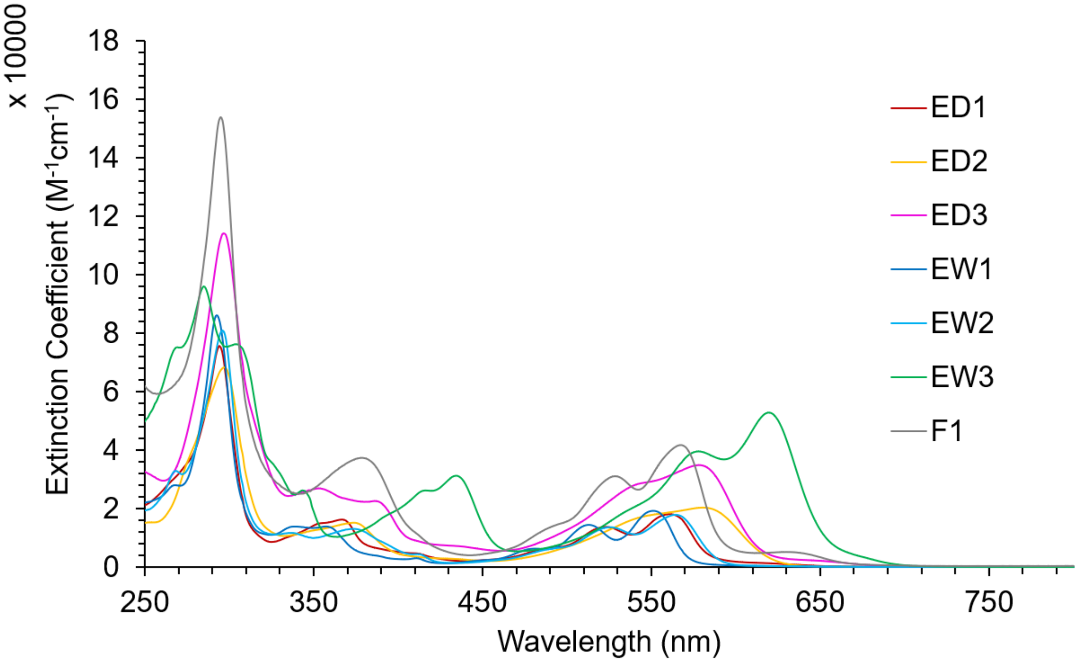

Figure 3.2: Absorbance spectra of tetracene derivatives studied in this work.

limited[153]. Also, instead of focusing on electronic properties and device properties, this work focuses more on the fundamental physical organic chemistry of these acenes.

3.3 Spectroscopic analysis of developed molecules

Figure 3.2 shows the absorbance spectra of developed molecules. All the molecules exhibit a strong absorbance peak in the visible range and a sharp absorbance peak in the ultraviolet. Vibrational features are observed in most molecules, except **ED2** and **ED3**, which contain amine substitutions. As we expected, the absorbance maxima are red-shifted with the introduction of either electron-donating or withdrawing functional groups, compared with the relatively electron-neutral benzene substitution. Among these molecules,

EW3 shows the most red-shifted absorbance (68 nm from **1D**) and the highest extinction coefficient due to the stronger electron-withdrawing ability and longer conjugation of the benzothiadiazole side chain. Besides, the other two molecules with larger conjugation systems, **ED3** and **F1**, also exhibit higher extinction coefficients. The extinction coefficients of the rest molecules are all very similar, agreeing with their similarities in conjugation. The key parameters of photo-physical properties are summarized in **Table 3.1**.

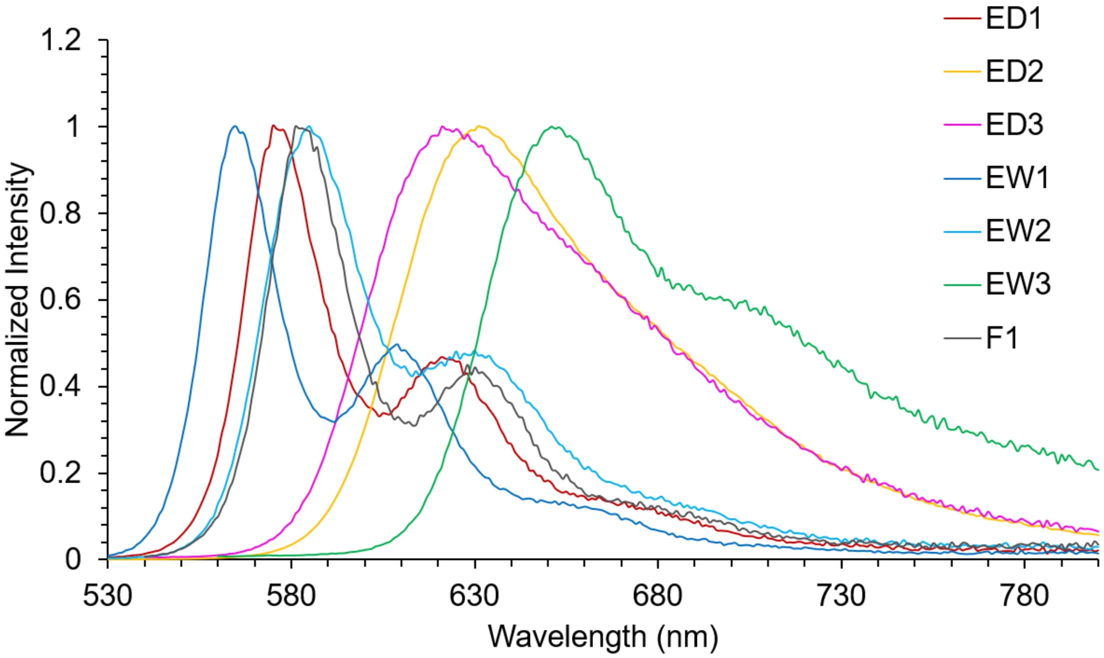

Figure 3.3: Photoluminescence spectra of tetracene derivatives studied in this work.

The electronic impacts are more significant on the photoluminescence properties, as shown in **Figure 3.3**. Again, **EW3** displays the most bathochromic shift of 88 nm from **1D**. Comparing **EW1** and **EW2**, switching from pyridine to pyrazine substitution results in a bathochromic shift in fluorescence of 20 nm, which is consistent with our past work[154]. Notably, **ED2** has a larger red shift in the spectrum than **ED3**, indicating a stronger electron-donating ability of dimethyl aniline than triphenylamine. All the molecules are sufficiently emissive. Even the least fluorescent compound, **EW3** has a FLQY as high as 26%. The **ED3** and **EW2** have FLQY higher than 80%, which is rare for red-emitting organic dyes.

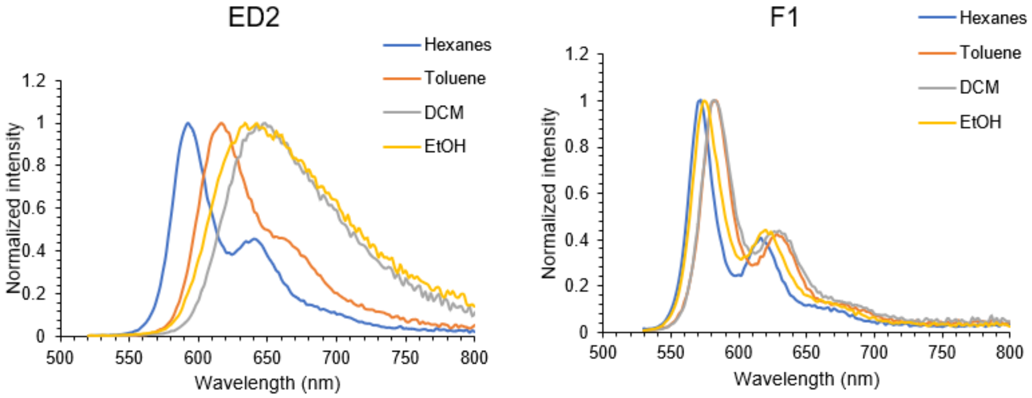

Figure 3.4: Solvatochromism effect of **ED2** and **F1** in emission spectra.

Solvatochromism of these molecules is tested by dissolving in a set of solvents with different polarities, namely hexanes, toluene, dichloromethane, and ethanol. **Figure 3.4** shows the results of **ED2** and **F1**. The spectra of **ED2** display the largest positive solvatochromism, indicating the strong D-A feature of the molecule.[155, 156] On the other hand, the non-D-A molecule **F1** did not show significant solvatochromic features. For molecules except **EW2** (impacted by hydrogen bonding in EtOH), the largest difference is observed between the **DCM** solution (red-shifted) and the solution of hexanes. The emission maximum shift is summarized in **Table 3.1**. We believe this value reflects the fraction of D-A features within the developed tetracene derivatives.

Table 3.1: Key photophysical parameters of tetracene derivatives studied in this paper. The solvatochromism lists the emission maximum difference between solutions of DCM and Hexanes

Name	$\lambda_{abs,max}$ (nm)	Extinction coefficient (M^{-1} cm^{-1})	$\lambda_{FL,max}$ (nm)	FLQY	Solvatochromism (nm, cm^{-1})
1D	552	23000	565	0.76	10, 320
ED1	561	18000	575	0.70	12, 369
ED2	580	20300	632	0.55	56, 1459
ED3	578	34900	621	0.87	34, 929
EW1	551	19700	565	0.77	12, 383
EW2	564	18400	585	0.81	16, 485
EW3	620	51700	653	0.26	24, 583
F1	567	42600	581	0.68	10, 300

We have also tested the AIEE effect of F1.[148] No AIEE effect is observed for this molecule, unlike its analog without triple bonds.[157] We attribute this to the additional distance created by triple bonds between the chromophore and AIE-gens.

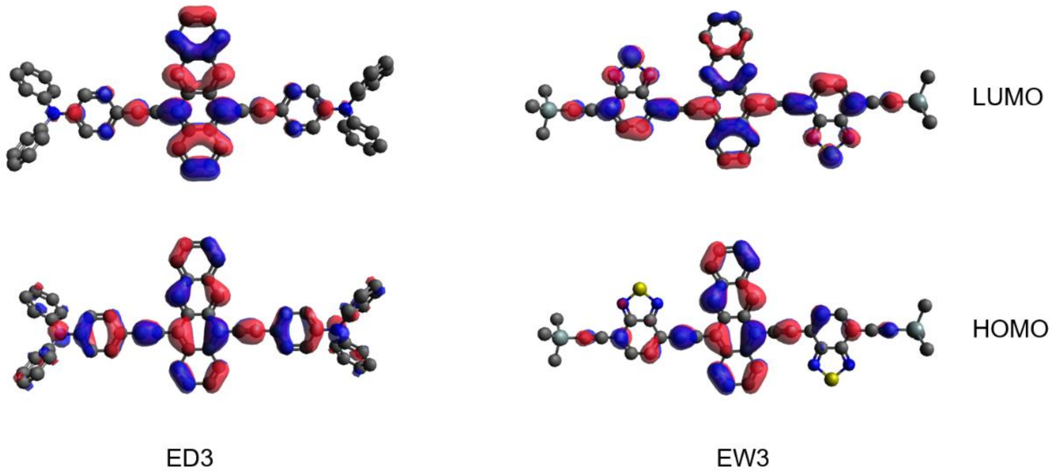

Figure 3.5: Calculated FMOs of **ED3** and **EW3**.

3.4 Theoretical calculations and electrochemistry

To better understand the photo-physical phenomena, we performed density functional theory (DFT) and time-dependent density functional theory (TD-DFT) calculations on these molecules.[136] The geometries are optimized with the B3LYP functional and the 6-31G+(d,p) basis set, using a polarizable dielectric continuum model for chloroform, and the frontier molecular orbitals (FMO) and excitation states are then calculated on optimized structure with the 6-311+(d,p) basis set using Tamm-Dancoff Approximation.

In general, the molecule with electron-donating groups has elevated HOMO and LUMO energies, and the ones with electron-withdrawing groups have lower energies. However, introducing both kinds of substitutions result in narrowing the bandgap.[158, 159] From the TD-DFT calculation, we also find the major excited state of each molecule is the

Table 3.2: Calculated FMO energies, experimental HOMO energies by cyclic voltammetry, and experimental relative rate constants of singlet oxygen cycloaddition of developed tetracene derivatives in this work.

Name	LUMO (eV)	$HOMO_{DFT}$ (eV)	$HOMO_{CV}$ (eV)	k_{rel}
1D	-3.01	-5.18	-5.19	1.00± 0.02
ED1	-3.04	-5.12	-5.20	1.19± 0.04
ED2	-2.74	-4.72	-4.89	4.44± 0.15
ED3	-2.90	-4.90	-5.05	1.73± 0.23
EW1	-3.14	-5.30	-5.29	0.87± 0.00
EW2	-3.32	-5.43	-5.41	0.44± 0.02
EW3	-3.48	-5.26	-5.17	0.69± 0.06
F1	-2.98	-5.15	-5.17	1.31± 0.13

transition between HOMO and LUMO. Thus, analyzing where the electrons are located could help us understand the red-shifting of spectra.

Cyclic voltammetry (CV) is performed on all of the developed acenes to determine the oxidation potentials. Compared with an external ferrocene reference, the first oxidation potential, which equals the HOMO energy of a molecule, can be calculated from the onset of the first oxidation peak of each curve.[18] The results are listed in **Table 3.2**, whose trend agrees with the theoretical calculation results. For instance, the **ED2** also displays the highest HOMO energy, while the **EW2** still displays the lowest HOMO energy.

Figure 3.5 displays the FMOs of ED3 and EW3, the intramolecular electron transfer is clearly observed. For **ED3**, electron clouds are located all over the phenyl ring connected to the triple bonds in HOMO. But in LUMO, there are almost no electron clouds on the same ring. Such change indicates a push-and-pull effect upon the excitation of the molecules. On the other hand, **EW3** displays a similar effect in opposite directions. Compared with those of **ED3** and **EW3**, calculation results of **ED2** also display a considerable charge transfer character, while the results of **ED1** and **EW2** only show minor charge transfer characters, and the results of **EW1**, **F1**, and **1D** show almost no electron transfer effects. Such a trend aligns well with the gap between HOMOs and LUMOs calculated and is also consistent with the degree of red shift in spectra.

3.5 Singlet oxygen responsiveness and kinetic analysis

Given the capability of tuning photo-physical properties through the electron-donating/ withdrawing effect, the next step is to determine the impact of these functional substitutions on the chemical properties of tetracenes, especially on the singlet oxygen responsiveness. We first evaluated the reaction rate between the developed tetracene derivatives and singlet oxygen by performing a kinetic experiment.[27] In detail, we selectively irradiate an external singlet oxygen photo-sensitizer, Methylene Blue (**MB**), in the solution of acenes. Under constant irradiation and constant concentration of **MB**, the concentration of singlet oxygen in the reaction system is constant, making this reaction a pseudo-first-order reaction. Thus, the relative rate constant of each molecule can be obtained by monitoring the reaction by absorbance and fitting the data to a first-order equation.

Table 3.2 lists the rate constant relative to the rate constant of **1D** ($k_{rel} = 1.0$). Each molecule has been subjected to the kinetic test three times, and a standard error of the mean is calculated. In general, introducing electron-donating groups accelerates the reaction rate, and the level of acceleration is dependent on the electron donation capability, which could be estimated by calculated HOMO energies and solvatochromic effects. For instance, **ED2** has a reaction rate about 4.4 times faster than **1D** and higher than **ED1** ($k_{rel} = 1.2$) and **ED3** ($k_{rel} = 1.7$). Meanwhile, the calculated HOMO energy of **ED2**, which is -4.72 eV, is elevated compared with the calculated HOMO energies of **1D** (-5.18 eV), **ED1**(-5.12 eV) and **ED3** (-4.90 eV). A similar trend is observed in the set of electron-withdrawing functionalized tetracenes. With stronger electron-withdrawing capability (lower HOMO), the molecule reacts slower with singlet oxygen. This relationship between the HOMO level and the reaction kinetics of singlet oxygen cycloaddition is consistent with Linker group's statement[3] and consistent with our group's past works. [87]

Besides the change in absorbance, all the molecules show a significant change in fluorescence after reacting with singlet oxygen. Such changes give potentials of singlet oxygen sensing applications to the molecules. Among the molecules, **ED3** and **EW3** display favorable ratiometric fluorescent signals, with emission peaks fully separated before and after the reaction and maintenance of their strong fluorescent intensity. **Figure 3.6** displays the fluorescent responsiveness of **ED3** and **EW3**.

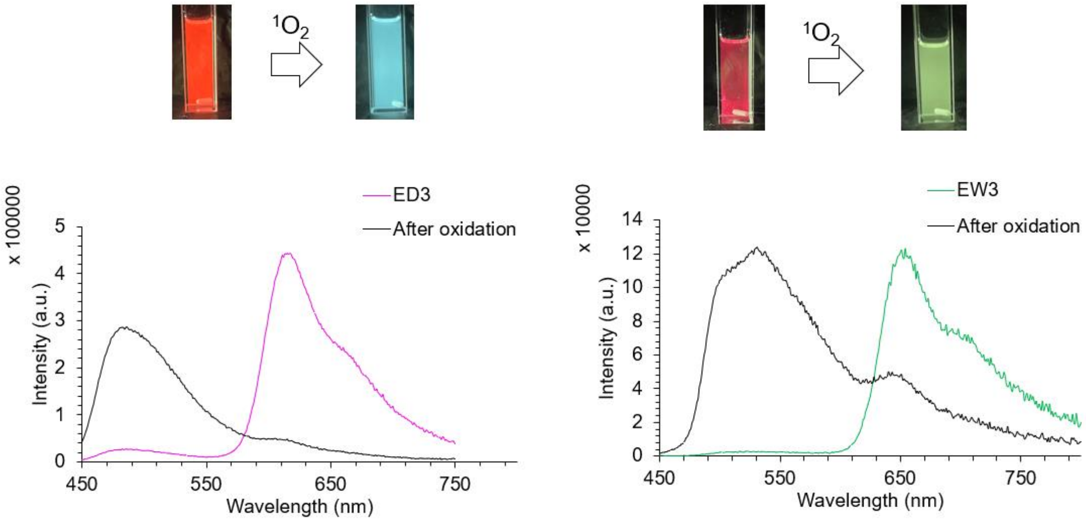

Figure 3.6: Ratiometric fluorescent singlet oxygen responsiveness of **ED3** (left) and **EW3** (right). The picture above is the photos under UV lamp.

3.6 Photo-stability

Photo-stability is a critical challenge of organic small molecule dyes. Photo-beaching of fluorescence hindered the organic dyes from being used in many applications, such as organic electronics[90] and bio-imaging.[160] In the field of singlet oxygen sensing, low photo-stability could also result in artifacts giving false positive signals upon irradiation.[96, 107] Common strategies include installing an electron-withdrawing group on the reactive sites to lower the oxidative potential[161, 162], kinetically blocking the reactive site[31], and suppressing the photosensitizing process.[28] In this work, we study the impact of ethyne-spaced electron-donating/withdrawing groups on the stability of tetracenes.

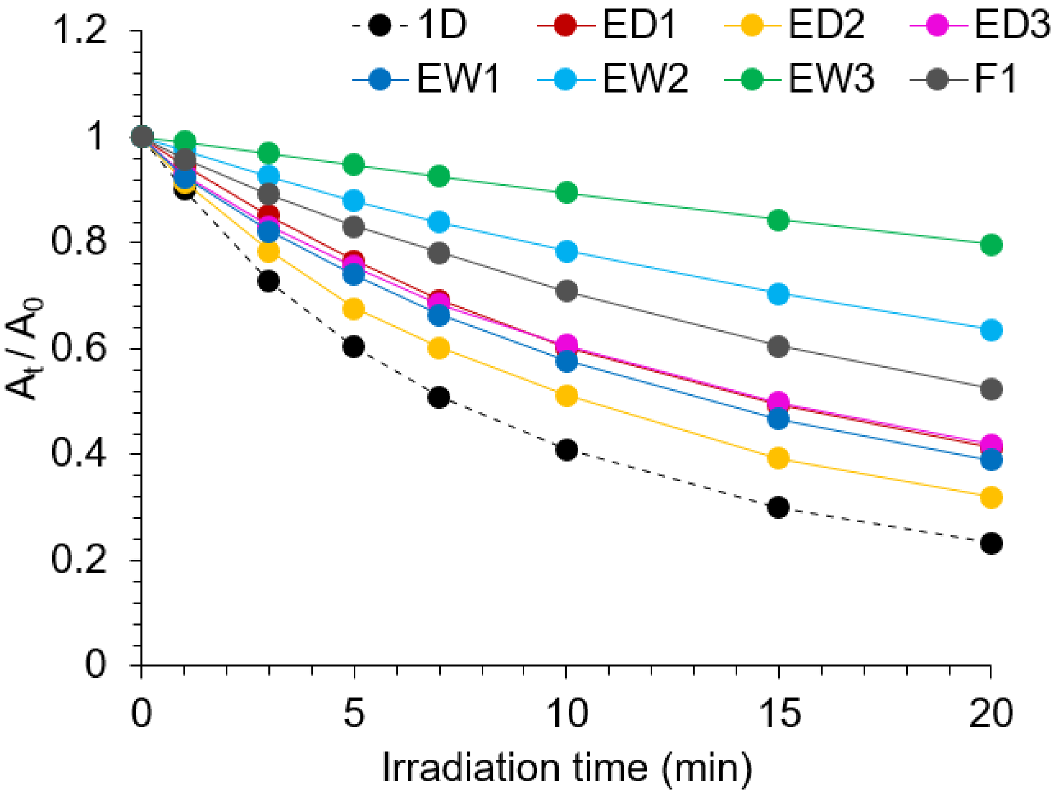

Figure 3.7: Photo-stability test of developed tetracene derivatives.

Although it is difficult to control the number of photons absorbed due to the variation of absorbance of samples under testing, we limit the errors by using a 546 nm bandpass and controlling the optical density of the sample at 546 nm to be nearly identical (~0.4). **Figure 3.7** shows the degradation of each molecule upon irradiation. Surprisingly, both electron-donating and electron-withdrawing groups stabilize the molecule. Compared with **1D**, all the molecules show a slower degradation rate. This is especially unexpected for **ED1**, **ED2**, and **ED3**, which have faster singlet oxygen responsiveness using external sensitizers. As reported by Anthony group, the photo-stability of acenes also relates to the enthalpy of oxidation reaction, the ability of photo-sensitizing, and other factors.[90] Here, we hypothesize that the electron donating/withdrawing effect is lowering the ability of photo-sensitizing of developed tetracene derivatives.

3.7 Fabricating acene-doped singlet oxygen sensing CPNs

Given the favorable photo-physical can chemical properties of the developed tetracene derivatives, we explored the possibility of applying them in the singlet oxygen sensing platform based on conjugated polymer nanoparticles. **EW3** is selected as the first acene to examine due to its red-shifted emission in the NIR-I window. [144]

Following a nano-precipitation method reported by McNeill group[101, 163, 164] and our group[83], we doped **EW3** into a matrix of poly(9,9-dioctylfluorene-alt-benzothiadiazole)

(**F8BT**), with various weight percentages. **Figure 3.8** shows the emission of the CPNs with different dopant levels. With 3% (w/w) of dopant, the original emission of **F8BT** is almost fully quenched by Fröster resonance energy transfer (FRET)[165], and the majority of emission is from the dopant, peaking at 660 nm.

Then, we directly irradiate the CPN to generate singlet oxygen by self-sensitizing. The process is monitored by fluorescence spectroscopy. Upon irradiation, a more than 120 nm hypochromic shift is observed. Although more experiments are still ongoing, these results validate the application potential of **EW3** in ratiometric fluorescent singlet oxygen sensing.

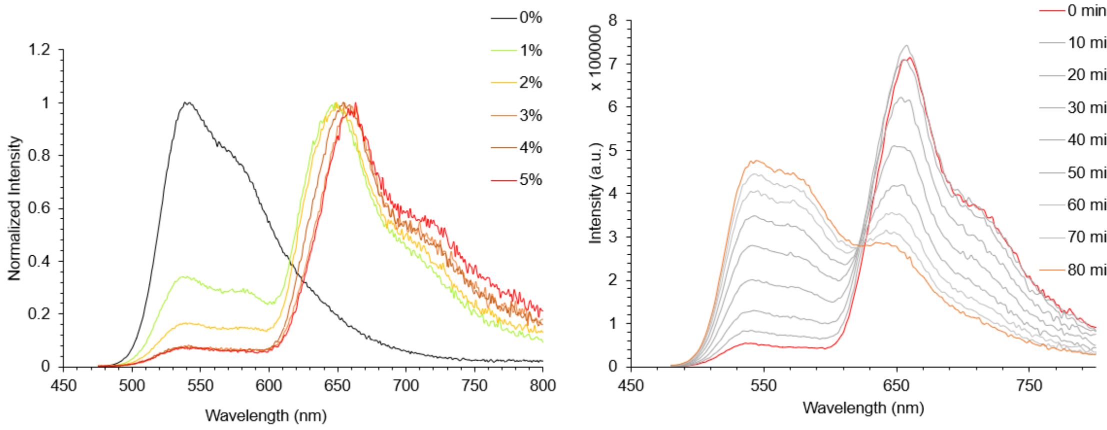

Figure 3.8: Emission spectra of **F8BT** CPNs with different dopant percentage,(left) and emission shifting of 3% doped CPN under irradiation.

3.8 Conclusions

In this work, we design and synthesize seven new tetracene derivatives comprised of electron-donating/ withdrawing functional groups and ethynylated tetracenes. Both photo-physical and chemical properties are tuned by electronic effects. We find the electron donating/ withdrawing groups can significantly red-shift the absorbance and emission of tetracene by forming donor-acceptor systems and extending the π-conjugation. Also, even spaced by triple bonds, these functional groups display considerable effects on the kinetics of singlet oxygen cycloaddition reactions. The observed relative constant can be tuned in a range between 4.5 times faster with electron donors and 2.5 times slower with electron acceptors relative to plain benzene substitution. Such phenomena can be explained by the modulation of HOMO levels with electronic effects. Also, we notice that the photo-stabilities are enhanced by introducing these functional groups. Finally, we fabricated a CPN-based singlet sensing platform with **EW3** and proved its candidacy as a novel singlet oxygen responsive material.

3.9 Experimental section

Synthesis of tetracene derivatives

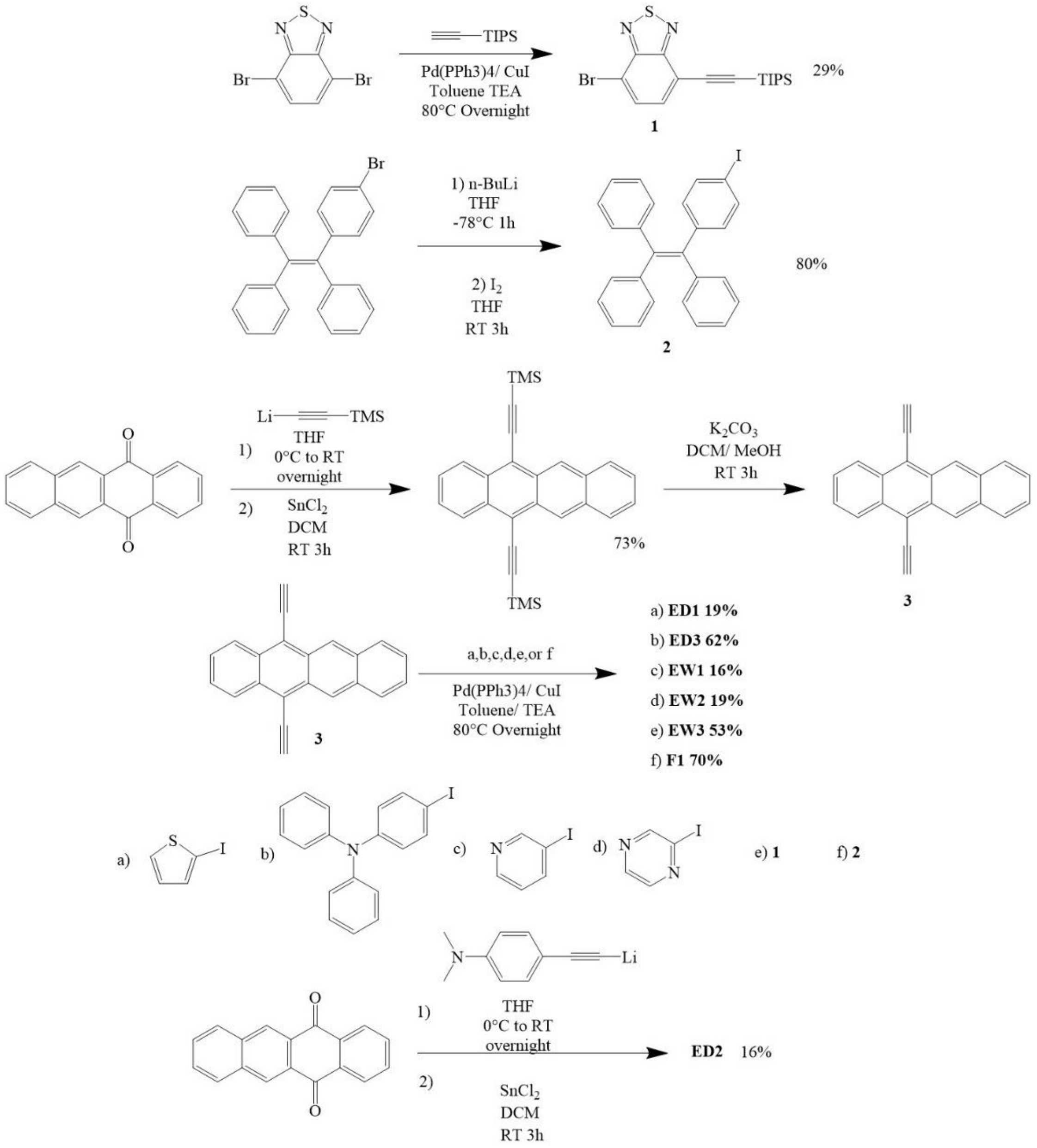

Scheme 3.1: Synthesis of developed tetracene derivatives in this work.

All synthetic manipulations were performed under standard air-free conditions under an atmosphere of argon gas with magnetic stirring unless otherwise mentioned. Flash chromatography was performed using silica gel (230−400 mesh) as the stationary phase. NMR spectra were acquired on a 500 MHz spectrometer. Chemical shifts are reported relative to residual protonated solvent (7.28 ppm for CHCl3).

4-Bromo-7-[2-[tris(1-methylethyl)silyl]ethynyl]-2,1,3-benzothiadiazole (**1**). Triisopropylsilylacetylene (1 mL, 800 mg, 4.4 mmol) was added to a mixture of 20 mL THF and 10 mL of triethyl amine in a round-bottom flask. The solution was then degassed by bubbling argon for one hour. 4,7-dibromo-2,1,3- benzothiadiazole (1000 mg, 3.4 mmol), tetrakis(triphenylphosphinepalladium(0) (120 mg, 0.12 mmol), and copper(I) iodide (35 mg, 0.17 mmol) were added to the flash as solids. The reaction was then stirred overnight under room temperature. Then, the solvent was removed by rotary evaporation. The residue was purified by column chromatography using DCM: Hexanes (1: 2, v: v) as eluent. 388 mg of yellow oil (0.97 mmol 29% yield) was collected as desired product, and 548 mg white solid (1.1 mmol 32% yield) was identified as side product (**1B**) with substitution on both sides of benzothadiazole.

^{1}H NMR (1) (500 MHz $CDCl_3$): δ 7.82-7.80 (d, 1H) 7.64-7.63 (d , 1H), 1.21-1.20 (m, 21H).

^{1}H NMR (1B) (500 MHz $CDCl_3$): δ 7.69 (s, 2H)), 1.21-1.20 (m, 21H).

The chemical shifts are consistent with those reported in the literature. [166]

1-Iodo-4-(1,2,2-triphenylethenyl)benzene (**2**). In a flame-dried round bottom flask, 10 ml of dry THF and 1-bromo-4-(1,2,2-triphenylethenyl)benzene (411 mg, 1 mmol) were added. The solution was then cooled down to -78°C via aceton/ dry ice bath. To the mixture, n-butyl lithium solution (0.6 mL, 1.5 mmol, 2.5M in Hexane) was added dropwise. The mixture was stirred for one hour under cold bath followed by quenching with solid iodine (500 mg, 2 mmol). The reaction was allowed to warm up to room temperature and further stirred for three hours. Then, the reaction was quenched by saturated aqueous sodium thiosulfate solution and extracted by DCM for three times. The combined organic layer was washed by diluted sodium thiosulfate solution, water, and brine before being dried by magnesium sulfate and filtration. 366 mg of brown solid (0.8 mmol, 80% yield) was collected after removing the solvent by rotavap. The product was directly added to the next step without further purification.

5,12-bis[2-(trimethylsilyl)ethynyl]tetracene. In a flame-dried 2-neck round bottom flask, trimethylsilylacetylene (0.71 mL, 490 mg, 5.0 mmol) was dissolved in 20 mL of dry diethyl ether and cooled to 0°C in an ice-water bath. *n*-Butyllithium (2.2 mL, 4.8 mmol, 2.2 M in hexanes) was added dropwise. The colorless solution was allowed to warm to room temperature and stirred for one hour, at which time napthacenequinone (520 mg, 2.0 mmol) was added as a solid. The suspension was stirred overnight and then neutralized with 1 M HCl (aq) and $SnCl_2$•$2H_2O$ (1.0 g, 4.4 mmol) was added to the mixture. After stirring for 3 h, the mixture was extracted using CH_2Cl_2 (3 x 10 mL), and the combined organic layers were dried over $MgSO_4$. The solvent was removed *in vacuo*, and the residue was purified through a plug of silica, eluted with hexanes to give 540 mg of the expected product (65% yield) as a deep red powder.

^{1}H NMR (500 MHz $CDCl_3$): δ 9.20(s, 2H) 8.57-8.59 (dd , 2H), 8.08-8.10 (dd, 2H), 7.55-7.60 (dd, 2H), 7.47-7.49 (dd, 2 H), 0.54 (s, 18H).

The chemical shifts are consistent with those reported in the literature.[22]

5,12-Diethynylnaphthacene (**3**). 5,12-bis[2-(trimethylsilyl)ethynyl]tetracene (420 mg, 1 mmol) was dissolved in 10 mL of DCM/ MeOH mixture (1: 1, v: v). Potassium carbonate (270 mg, 2 mmol) was added to the solution. The suspension was stirred for 3 h at room temperature. Then, the mixture was washed by 1M HCl solution in an open flask and extracted by DCM 3 times. The combined organic layer was washed by water and brine, dried over $MgSO_4$, and filtered. 270 mg crude product (1 mmol, 99% yield) was collected after removing the solvent as a red solid. The product was directly added to the next step without further purification.

The synthesis of **ED1**, **ED3**, **EW1**, **EW2**, **EW3**, and **F1** was carried out with a general procedure of Sonogashira coupling reaction. In general, the starting materials were dissolved in a toluene/ Et_3N (2: 1, v: v) mixture and the solution was degassed via freeze-pump-thaw method. Then, the catalysts, $Pd(PPh_3)_4$ and CuI, were added with 0.05 eq. as solids. The reaction was stirred overnight under 80°C before subjected to work-up and purifications.

ED1. 2-iodothiophene (210 mg, 1 mmol) and **3** (110 mg, 0.4 mmol) were subjected to a general Sonogashira coupling reaction. The reaction was worked up by removing the solvent *in vacuo.* The residue was passed through a silica plug using DCM as eluent and recrystallized from chloroform / hexanes to afford 35 mg of purple solid (0.08 mmol, 19% yield).

^{1}H NMR (500 MHz $CDCl_3$): δ 9.25(s, 2H) 8.63-8.65 (dd , 2H), 8.13-8.15 (dd, 2H), 7.62 (d,2H),7.60-7.62 (dd, 2H), 7.52-7.53 (dd, 2 H), 7.51-7.52 (d, 2H), 7.18-7.20 (t, 2H), 0.54 (s, 18H).

^{13}C [^{1}H] NMR (125 MHz, $CDCl_3$): *δ* 132.3, 132.3, 132.2, 129.8, 128.6, 128.1, 127.5, 127.3, 126.8, 126.1, 1260, 123.5, 118.1, 96.5, 91.1.

ED3. 1-diphenylmethy-4-iodo-benzene (560 mg, 1.5 mmol) and **3** (170 mg, 0.6 mmol) were added to a round bottom flask and then a general Sonogashira coupling reaction was executed. The residue was purified via column chromatography using hexanes/ DCM (1: 1, v: v) as eluent and recrystallized from chloroform/ MeOH to afford 280 mg of purple solid (0.36 mmol, 60% yield).

^{1}H NMR (500 MHz $CDCl_3$): δ 9.31(s, 2H) 8.68-8.70 (dd , 2H), 8.10-8.12 (dd, 2H), 7.70-7.72 (d, 4H), 7.30-7.37 (m, 8H), 7.56-7.58 (dd, 2H), 7.47-7.50 (dd, 2 H), 7.10-7.23 (m, 16H).

^{13}C [^{1}H] NMR (125 MHz, $CDCl_3$): *δ* 148.4, 147.2, 132.7, 132.2, 130.0, 129.5, 129.4, 128.6, 127.5, 126.4, 125.9, 125.2, 123.8, 122.4, 118.3, 116.3, 103.8, 86.7.

EW1. 3-iodopyridine (204 mg, 1 mmol) and **3** (110 mg, 0.4 mmol) were subjected to a general Sonogashira coupling reaction. The reaction was worked up by removing the solvent *in vacuo.* The residue was passed through a silica plug using DCM as eluent and recrystallized from chloroform / hexanes to afford 28 mg of purple solid (0.06 mmol, 16% yield).

^{1}H NMR (500 MHz $CDCl_3$): δ 9.28 (s, 2H), 9.15 (s, 2H), 8.66-8.68 (m , 4H), 8.14-8.19 (m, 4H), 7.64-7.66 (dd, 2H), 7.50-7.56 (m, 4H).

^{13}C [^{1}H] NMR (125 MHz, $CDCl_3$): *δ* 151.8, 148.6, 138.9, 132.4, 132.1, 129.8, 128.5, 127.2, 127.1, 126.5, 125.9, 123.5, 120.9, 118.1, 99.7, 90.5.

EW2. 2-iodopyrazine (205 mg, 1 mmol) and **3** (110 mg, 0.4 mmol) were subjected to a general Sonogashira coupling reaction. The reaction was worked up by removing the solvent *in vacuo.* The residue was passed through a silica plug using DCM as eluent and recrystallized from chloroform / hexanes to afford 33 mg of purple solid (0.08 mmol, 19% yield).

^{1}H NMR (500 MHz $CDCl_3$): δ 9.37(s, 2H), 9.13 (s, 2H), 8.73-8.75 (m , 4H), 8.64 (s 2H), 8.17-8.19 (dd, 2H), 7.67-7.69 (dd, 2H), 7.55-7.57 (dd, 2 H).

^{13}C [^{1}H] NMR (125 MHz, $CDCl_3$): *δ* 148.0, 144.8, 143.2, 140.5, 132.9, 132.6, 129.9, 128.6, 127.6, 127.2, 126.6, 126.0, 117.9, 99.8, 90.6.

EW3. **1** (380 mg, 0.95 mmol) and **3** (110 mg, 0.4 mmol) were subjected to a general Sonogashira coupling reaction. The reaction was worked up by removing the solvent *in vacuo.* The residue was passed through a silica plug using DCM as eluent and recrystallized from chloroform / MeOH to afford 180 mg of blue-black solid (0.2 mmol, 53% yield).

^{1}H NMR (500 MHz $CDCl_3$): δ 9.67(s, 2H) 8.92-8.94 (dd , 2H), 8.23-8.25 (dd, 2H), 8.01-8.03(d, 2H), 7.87-7.89 (d, 2H), 7.69-7.72 (dd, 2H), 7.56-7.58 (dd, 2 H), 1.21-1.31 (m, 42H).

^{13}C [^{1}H] NMR (125 MHz, $CDCl_3$): *δ* 154.8, 154.7, 133.1, 132.5, 131.5, 130.0, 128.6, 127.4, 127.1, 126.5, 126.1, 118.6, 117.5, 102.5, 100.9, 100.2, 95.9.

F1. **2** (366 mg, 0.8 mmol) and **3** (85 mg, 0.3 mmol) were subjected to a general Sonogashira coupling reaction. The reaction was worked up by removing the solvent *in vacuo.* The residue was passed through a silica plug using DCM as eluent and recrystallized from chloroform / MeOH to afford 190mg of purple solid (0.2 mmol, 70% yield).

^{1}H NMR (500 MHz $CDCl_3$): δ 9.24(s, 2H) 8.63-8.65 (dd , 2H), 8.08-8.10 (dd, 2H), 7.59-7.61(d, 4H), 7.54-7.56 (dd, 2H), 7.47-7.49 (dd, 2 H), 7.09-7.23 (m, 34H).

^{13}C [^{1}H] NMR (125 MHz, $CDCl_3$): *δ* 144.5, 143.5, 143.5, 143.4, 141.9, 140.3, 132.3, 131.7, 131.6, 131.4, 131.4, 131.3, 131.2, 131.1, 129.9, 128.6, 127.8, 127.7, 127.4, 126.8, 126.7, 126.6, 126.6, 126.1, 126.0, 121.4, 118.3, 103.8, 87.6.

ED2. In a flame-dried 2-neck round bottom flask, 4-ethynyl-N,N-dimethylaniline (145 mg, 1 mmol) was dissolved in 20 mL of dry THF and cooled to 0°C in an ice-water bath. *n*-Butyllithium (0.4 mL, 1 mmol, 2.5 M in hexanes) was added dropwise. The solution was allowed to warm to room temperature and stirred for one hour, at which time napthacenequinone (100 mg, 0.4 mmol) was added as a solid. The suspension was stirred overnight and then neutralized with 1 M HCl (aq). $SnCl_2 \cdot 2H_2O$ (400 mg, 2 mmol) was added to the mixture. After stirring for 3 h, the mixture was extracted using CH_2Cl_2 (3 x 10 mL), and the combined organic layers were dried over $MgSO_4$. The solvent was removed *in vacuo*, and the residue was purified via column chromatography, eluted with DCM, and recrystallized from chloroform/ hexanes to give 30 mg of black solid (0.06 mmol. 16% yield).

^{1}H NMR (500 MHz $CDCl_3$): δ 9.33 (s, 2H) 8.72-8.73 (dd , 2H), 8.12-8.14 (dd, 2H), 7.74-7.76 (d, 4H), 7.56-7.57 (dd, 2H), 7.47-7.49 (dd, 2 H), 6.83-6.85 (d, 4H), 3.10 (s, 12H).

^{13}C [^{1}H] NMR (125 MHz, $CDCl_3$): *δ* 132.9, 132.0, 130.0, 128.6, 127.6, 126.2, 126.1, 125.6, 118.3, 112.1, 104.7, 85.8, 40.3.

Instrumental analysis and theoretical calculations

Electronic absorbance spectra were acquired with a spectrophotometer in double-beam mode using a solvent-containing cuvette for background subtraction spectra. Fluorescence spectra were collected at a 90° angle from the incident irradiation (75W Xe lamp) and corrected for both fluctuations in the lamp intensity and the wavelength-dependent sensitivity of the photomultiplier tube detector. Fluorescence quantum yields were determined relative to coumarin 6 in ethanol or crestyl violet in ethanol.[138] Irradiation of methylene blue photosensitizer to generate **$^1O_2$** was performed with a 200 W Hg/Xe lamp equipped with a condensing lens, water filter, and manual shutter, with different filters. Density functional theory calculations were performed using the Gaussian 09 software package[136], with optimized geometries and FMO energies determined at the B3LYP/6-31G (d,p) level of theory using a polarizable continuum solvent model for chloroform. The time-dependent results of these optimized geometries were calculated at the B3LYP/6-311+G (d,p) level of theory, using the Tamm−Dancoff approximation. Cyclic voltammograms were acquired using a three-electrode setup with platinum working and counter electrodes and a non-aqueous (DCM) Ag/AgCl reference electrode and were reported relative to the ferrocene/ferrocenium redox couple measured as an external standard under identical conditions.[51] The concentrations of acenes and ferrocene standard were around 2 mg/mL in degassed DCM with 0.1 M tetrabutylammonium hexafluorophosphate as the electrolyte at room temperature.

Fabrication of conjugated polymer nanoparticles (CPNs)

The CPNs were fabricated using a reported method.[101] First, the 20 ppm THF solution was prepared for both dopant and **F8BT** polymer. For a non-doping CPN, 2 ml of **F8BT** 20 ppm solution was injected into 8 mL of DI water under sonication. The THF was then removed via rotavap. The size was determined by Dynamic light scattering (DLS) measurements with a Malvern Zetasizer Nano-ZS. The doped CPN was made by injecting a mixture with ration of desired to the water under same conditions, followed by rotavap.

Reference

(1) Anthony, J. E. Functionalized acenes and heteroacenes for organic electronics. *Chemical Reviews* **2006**, *106* (12), 5028-5048. DOI: 10.1021/cr050966z.

(2) Anthony, J. E.; Brooks, J. S.; Eaton, D. L.; Parkin, S. R. Functionalized pentacene: Improved electronic properties from control of solid-state order. *Journal of the American Chemical Society* **2001**, *123* (38), 9482-9483. DOI: 10.1021/ja0162459.

(3) Anthony, J. E. The larger acenes: Versatile organic semiconductors. *Angewandte Chemie-International Edition* **2008**, *47* (3), 452-483. DOI: 10.1002/anie.200604045.

(4) Chen, J. H.; Martin, D. C.; Anthony, J. E. Morphology and molecular orientation of thin-film bis(triisopropylsilylethynyl) pentacene. *Journal of Materials Research* **2007**, *22* (6), 1701-1709. DOI: 10.1557/jmr.2007.0220.

(5) Kaur, I.; Jia, W. L.; Kopreski, R. P.; Selvarasah, S.; Dokmeci, M. R.; Pramanik, C.; McGruer, N. E.; Miller, G. P. Substituent Effects in Pentacenes: Gaining Control over HOMO-LUMO Gaps and Photooxidative Resistances. *Journal of the American Chemical Society* **2008**, *130* (48), 16274-16286. DOI: 10.1021/ja804515y.

(6) Brega, V.; Yan, Y.; Thomas, S. W., 3rd. Acenes beyond organic electronics: sensing of singlet oxygen and stimuli-responsive materials. *Org Biomol Chem* **2020**, *18* (45), 9191-9209. DOI: 10.1039/d0ob01744b From NLM PubMed-not-MEDLINE.

(7) Thomas, S.; Altinok, E.; Zhang, J. Cycloadditions of Singlet Oxygen for Responsive Fluorescent Polymers. *Synlett* **2015**, *27* (03), 355-368. DOI: 10.1055/s-0035-1560725.

(8) Kim, S.; Fujitsuka, M.; Majima, T. Photochemistry of Singlet Oxygen Sensor Green. *Journal of Physical Chemistry B* **2013**, *117* (45), 13985-13992. DOI: 10.1021/jp406638g.

(9) Altinok, E.; Smith, Z. C.; Thomas, S. W. Two-Dimensional, Acene-Containing Conjugated Polymers That Show Ratiometric Fluorescent Response to Singlet Oxygen. *Macromolecules* **2015**, *48* (19), 6825-6831. DOI: 10.1021/acs.macromol.5b01076.

(10) Zhang, J. J.; Sarrafpour, S.; Pawle, R. H.; Thomas, S. W. Acene-linked conjugated polymers with ratiometric fluorescent response to O-1(2). *Chemical Communications* **2011**, *47* (12), 3445-3447. DOI: 10.1039/c0cc05770c.

(11) Frausto, F.; Thomas, S. W., 3rd. Ratiometric Singlet Oxygen Detection in Water Using Acene-Doped Conjugated Polymer Nanoparticles. *ACS Appl Mater Interfaces* **2017**, *9* (18), 15768-15775. DOI: 10.1021/acsami.7b02034 From NLM PubMed-not-MEDLINE.

(12) Frausto, F.; Thomas, S. W. Tuning the Key Properties of Singlet Oxygen-Responsive Acene-Doped Conjugated Polymer Nanoparticles. *ChemPhotoChem* **2018**, *2* (7), 632-639. DOI: 10.1002/cptc.201800039.

(13) Brega, V.; Thomas, S. W., 3rd. Red-Emitting, Acene-Doped Conjugated Polymer Nanoparticles that Respond Ratiometrically to Photogenerated (1)O(2). *ACS Appl Mater Interfaces* **2021**, *13* (11), 13658-13665. DOI: 10.1021/acsami.0c22313 From NLM PubMed-not-MEDLINE.

(14) Escobedo, J. O.; Rusin, O.; Lim, S.; Strongin, R. M. NIR dyes for bioimaging

applications. *Curr Opin Chem Biol* **2010**, *14* (1), 64-70. DOI: 10.1016/j.cbpa.2009.10.022 From NLM Medline.

(15) Chen, C.; Fang, C. Devising Efficient Red-Shifting Strategies for Bioimaging: A Generalizable Donor-Acceptor Fluorophore Prototype. *Chem Asian J* **2020**, *15* (10), 1514-1523. DOI: 10.1002/asia.202000175 From NLM Medline.

(16) Wu, J. X.; Shi, Z. X.; Zhu, L. L.; Li, J.; Han, X.; Xu, M.; Hao, S. P.; Fan, Y. B.; Shao, T.; Bai, H.; et al. The Design and Bioimaging Applications of NIR Fluorescent Organic Dyes with High Brightness. *Adv Opt Mater* **2022**, *10* (8). DOI: ARTN 2102514 10.1002/adom.202102514.

(17) Ran, C.; Mansfield, J. R.; Bai, M.; Viola, N. T.; Mahajan, A.; Delikatny, E. J. Practical Guidance for Developing Small-Molecule Optical Probes for In Vivo Imaging. *Mol Imaging Biol* **2023**, *25* (1), 240-264. DOI: 10.1007/s11307-023-01800-1 From NLM Medline.

(18) Zhang, J.; Smith, Z. C.; Thomas, S. W., 3rd. Electronic effects of ring fusion and alkyne substitution on acene properties and reactivity. *J Org Chem* **2014**, *79* (21), 10081-10093. DOI: 10.1021/jo501696d From NLM PubMed-not-MEDLINE.

(19) Brega, V.; Kanari, S. N.; Doherty, C. T.; Che, D.; Sharber, S. A.; Thomas, S. W. Spectroscopy and Reactivity of Dialkoxy Acenes. *Chemistry-a European Journal* **2019**, *25* (44), 10400-10407. DOI: 10.1002/chem.201901258.

(20) Fudickar, W.; Linker, T. Why Triple Bonds Protect Acenes from Oxidation and Decomposition. *Journal of the American Chemical Society* **2012**, *134* (36), 15071-15082. DOI: 10.1021/ja306056x.

(21) Baral, R. N.; Thomas, S. W. Steric and Electronic Substituent Effects Influencing Regioselectivity of Tetracene Endoperoxidation. *Journal of Organic Chemistry* **2015**, *80* (21), 11086-11091. DOI: 10.1021/acs.joc.5b01692.

(22) Yan, Y.; Lamport, Z. A.; Kymissis, I.; Thomas, S. W., 3rd. Resistance to Unwanted Photo-Oxidation of Multi-Acene Molecules. *J Org Chem* **2020**, *85* (19), 12731-12739. DOI: 10.1021/acs.joc.0c01890 From NLM PubMed-not-MEDLINE.

(23) Thorley, K. J.; Benford, M.; Song, Y.; Parkin, S. R.; Risko, C.; Anthony, J. E. What is special about silicon in functionalised organic semiconductors? *Materials Advances* **2021**, *2* (16), 5415-5421. DOI: 10.1039/d1ma00447f.

(24) Zhang, J.; Sarrafpour, S.; Haas, T. E.; Müller, P.; Thomas, S. W. Structure, photophysics, and photooxidation of crowded diethynyltetracenes. *Journal of Materials Chemistry* **2012**, *22* (13), 6182. DOI: 10.1039/c2jm16173g (acccessed 2023-06-01T01:51:58).

(25) Chen, Y.; Lam, J. W. Y.; Kwok, R. T. K.; Liu, B.; Tang, B. Z. Aggregation-induced emission: fundamental understanding and future developments. *Materials Horizons* **2019**, *6* (3), 428-433. DOI: 10.1039/c8mh01331d.

(26) Fudickar, W.; Bauch, M.; Ihmels, H.; Linker, T. DNA-Triggered Enhancement of

Singlet Oxygen Production by Pyridinium Alkynylanthracenes. *Chemistry* **2021**, *27* (54), 13591-13604. DOI: 10.1002/chem.202101918 From NLM Medline.

(27) Xue, T.; Zhao, D.; Hao, T.; Li, X.; Wang, T.; Nie, J. Synthesis, one/two-photon optical and electrochemical properties and the photopolymerization-sensitizing effect of anthracene-based dyes: influence of the donor groups. *New Journal of Chemistry* **2019**, *43* (17), 6737-6745. DOI: 10.1039/c8nj06520a.

(28) Tao, J.; Liu, D.; Jing, J.; Dong, H.; Liu, L.; Xu, B.; Tian, W. Organic Single Crystals with High Photoluminescence Quantum Yields Close to 100% and High Mobility for Optoelectronic Devices. *Adv Mater* **2021**, *33* (48), e2105466. DOI: 10.1002/adma.202105466 From NLM PubMed-not-MEDLINE.

(29) Hur, J. A.; Kim, S. J.; Kim, K. H.; Lee, T. W.; Kim, K.; Shin, J.; Hwang, K. S.; Chin, B. D.; Choi, D. H. Two-dimensional extended π-conjugated anthracene-based molecules bearing 4-ethynyl-7-(5-hexylthiophen-2-yl)benzo[c][1,2,5]thiadiazole at 2,6- and 9,10-substitution positions. *Synthetic Metals* **2012**, *161* (23-24), 2776-2784. DOI: 10.1016/j.synthmet.2011.10.019.

(30) Odom, S. A.; Parkin, S. R.; Anthony, J. E. Tetracene derivatives as potential red emitters for organic LEDs. *Org Lett* **2003**, *5* (23), 4245-4248. DOI: 10.1021/ol035415e From NLM PubMed-not-MEDLINE.

(31) Mullin, W. J.; Müller, P.; Schaefer, A. J.; Guzman, E.; Wheeler, S. E.; Thomas Iii, S. W. Crystal engineering of heterocyclic arylene(ethynylene) oligomers through programmed aromatic stacking. *Journal of Materials Chemistry C* **2022**, *10* (31), 11199-11210. DOI: 10.1039/d2tc01292h (acccessed 2022-11-28T20:54:48).

(32) Effenberger, F.; Wuerthner, F.; Steybe, F. Synthesis and solvatochromic properties of donor-acceptor-substituted oligothiophenes. *The Journal of Organic Chemistry* **1995**, *60* (7), 2082-2091.

(33) Qiu, Q.; Xu, P.; Zhu, Y.; Yu, J.; Wei, M.; Xi, W.; Feng, H.; Chen, J.; Qian, Z. Rational Design of Dual-State Emission Luminogens with Solvatochromism by Combining a Partially Shared Donor–Acceptor Pattern and Twisted Structures. *Chemistry – A European Journal* **2019**, *25* (70), 15983-15987. DOI: 10.1002/chem.201903857 (acccessed 2023-07-07T15:39:03).

(34) Liu, B. Q.; Nie, H.; Zhou, X. B.; Hu, S. B.; Luo, D. X.; Gao, D. Y.; Zou, J. H.; Xu, M.; Wang, L.; Zhao, Z. J.; et al. Manipulation of Charge and Exciton Distribution Based on Blue Aggregation-Induced Emission Fluorophors: A Novel Concept to Achieve High-Performance Hybrid White Organic Light-Emitting Diodes. *Advanced Functional Materials* **2016**, *26* (5), 776-783. DOI: 10.1002/adfm.201503368.

(35) Frisch, M. J.; Trucks, G. W.; Schlegel, H. B.; Scuseria, G. E.; Robb, M. A.; Cheeseman, J. R.; Scalmani, G.; Barone, V.; Petersson, G. A.; Nakatsuji, H.; Li, X.; Caricato, M.; Marenich, A.; Bloino, J.; Janesko, B. G.; Gomperts, R.; Mennucci, B.; Hratchian, H. P.; Ortiz, J. V.; Izmaylov, A. F.; Sonnenberg, J. L.; Williams-Young, D.; Ding, F.; Lipparini, F.;

Egidi, F.; Goings, J.; Peng, B.; Petrone, A.; Henderson, T.; Ranasinghe, D.; Zakrzewski, V. G.; Gao, J.; Rega, N.; Zheng, G.; Liang, W.; Hada, M.; Ehara, M.; Toyota, K.; Fukuda, R.; Hasegawa, J.; Ishida, M.; Nakajima, T.; Honda, Y.; Kitao, O.; Nakai, H.; Vreven, T.; Throssell, K.; Montgomery, J. A., Jr.; Peralta, J. E.; Ogliaro, F.; Bearpark, M. J.; Heyd, J. J.; Brothers, E. N.; Kudin, K. N.; Staroverov, V. N.; Keith, T. A.; Kobayashi, R.; Normand, J.; Raghavachari, K.; Rendell, A. P.; Burant, J. C.; Iyengar, S. S.; Tomasi, J.; Cossi, M.; Millam, J. M.; Klene, M.; Adamo, C.; Cammi, R.; Ochterski, J. W.; Martin, R. L.; Morokuma, K.; Farkas, O.; Foresman, J. B.; Fox, D. J. Gaussian 09, Revision D.01; Gaussian, Inc.: Wallingford CT, 2016.Frisch, MJEA

(36) Serevicius, T.; Skaisgiris, R.; Dodonova, J.; Kazlauskas, K.; Jursenas, S.; Tumkevicius, S. Minimization of solid-state conformational disorder in donor-acceptor TADF compounds. *Phys Chem Chem Phys* **2019**, *22* (1), 265-272. DOI: 10.1039/c9cp05907e From NLM PubMed-not-MEDLINE.

(37) Li, C.; Duan, R.; Liang, B.; Han, G.; Wang, S.; Ye, K.; Liu, Y.; Yi, Y.; Wang, Y. Deep-Red to Near-Infrared Thermally Activated Delayed Fluorescence in Organic Solid Films and Electroluminescent Devices. *Angew Chem Int Ed Engl* **2017**, *56* (38), 11525-11529. DOI: 10.1002/anie.201706464 From NLM PubMed-not-MEDLINE.

(38) Thorley, K. J.; Le, H.; Song, Y.; Anthony, J. E. Unravelling the major factors in photo-oxidative stability of anthradithiophene derivatives. *Journal of Materials Chemistry C* **2022**, *10* (42), 15861-15871. DOI: 10.1039/d2tc02922g.

(39) Toutchkine, A.; Nguyen, D. V.; Hahn, K. M. Merocyanine dyes with improved photostability. *Org Lett* **2007**, *9* (15), 2775-2777. DOI: 10.1021/ol070780h

(40) Pedersen, S. K.; Holmehave, J.; Blaikie, F. H.; Gollmer, A.; Breitenbach, T.; Jensen, H. H.; Ogilby, P. R. Aarhus Sensor Green: A Fluorescent Probe for Singlet Oxygen. *Journal of Organic Chemistry* **2014**, *79* (7), 3079-3087. DOI: 10.1021/jo500219y.

(41) Ragas, X.; Jimenez-Banzo, A.; Sanchez-Garcia, D.; Batllori, X.; Nonell, S. Singlet oxygen photosensitisation by the fluorescent probe Singlet Oxygen Sensor Green (R). *Chemical Communications* **2009**, (20), 2920-2922. DOI: 10.1039/b822776d.

(42) Samanta, A.; Vendrell, M.; Das, R.; Chang, Y. T. Development of photostable near-infrared cyanine dyes. *Chem Commun (Camb)* **2010**, *46* (39), 7406-7408. DOI: 10.1039/c0cc02366c From NLM Medline.

(43) Gut, A.; Łapok, Ł.; Jamróz, D.; Gorski, A.; Solarski, J.; Nowakowska, M. Photophysics and redox properties of aza-BODIPY dyes with electron-withdrawing groups. *New Journal of Chemistry* **2017**, *41* (20), 12110-12122.

(44) Shi, X. L.; Chi, C. Y. Different Strategies for the Stabilization of Acenes and Acene Analogues. *Chemical Record* **2016**, *16* (3), 1690-1700. DOI: 10.1002/tcr.201600031.

(45) Wu, C.; Szymanski, C.; Mcneill, J. Preparation and Encapsulation of Highly Fluorescent Conjugated Polymer Nanoparticles. *Langmuir* **2006**, *22* (7), 2956-2960. DOI: 10.1021/la060188l (acccessed 2023-06-01T17:04:55).

(46) Tian, Z.; Yu, J.; Wu, C.; Szymanski, C.; Mcneill, J. Amplified energy transfer in conjugated polymer nanoparticle tags and sensors. *Nanoscale* **2010**, *2* (10), 1999. DOI: 10.1039/c0nr00322k (acccessed 2023-06-01T17:05:37).

(47) Jiang, Y.; McNeill, J. Light-harvesting and amplified energy transfer in conjugated polymer nanoparticles. *Chemical reviews* **2017**, *117* (2), 838-859.

(48) Frausto, F.; Thomas, S. W. Tuning the Key Properties of Singlet Oxygen-Responsive Acene-Doped Conjugated Polymer Nanoparticles. *Chemphotochem* **2018**, *2* (7), 632-639. DOI: 10.1002/cptc.201800039.

(49) Ince, M.; Yum, J.-H.; Kim, Y.; Mathew, S.; Grätzel, M.; Torres, T.; Nazeeruddin, M. K. Molecular Engineering of Phthalocyanine Sensitizers for Dye-Sensitized Solar Cells. *The Journal of Physical Chemistry C* **2014**, *118* (30), 17166-17170. DOI: 10.1021/jp502447y.

(50) Brouwer, A. M. Standards for photoluminescence quantum yield measurements in solution (IUPAC Technical Report). *Pure and Applied Chemistry* **2011**, *83* (12), 2213-2228. DOI: 10.1351/pac-rep-10-09-31.

(51) Hou, J.; Zhang, B.; Li, D.; Fu, Y.; Liu, D.; Chen, Y. Enabling superior stretchable resistive switching memory via polymer-functionalized graphene oxide nanosheets. *Journal of Materials Chemistry C* **2019**,*7*(46) 14664-14671.

Chapter 3 Appendix

DFT results

Solvatochromism

Cyclic Voltammetry

NMR spectra

Calculated FMOs for developed tetracene derivatives

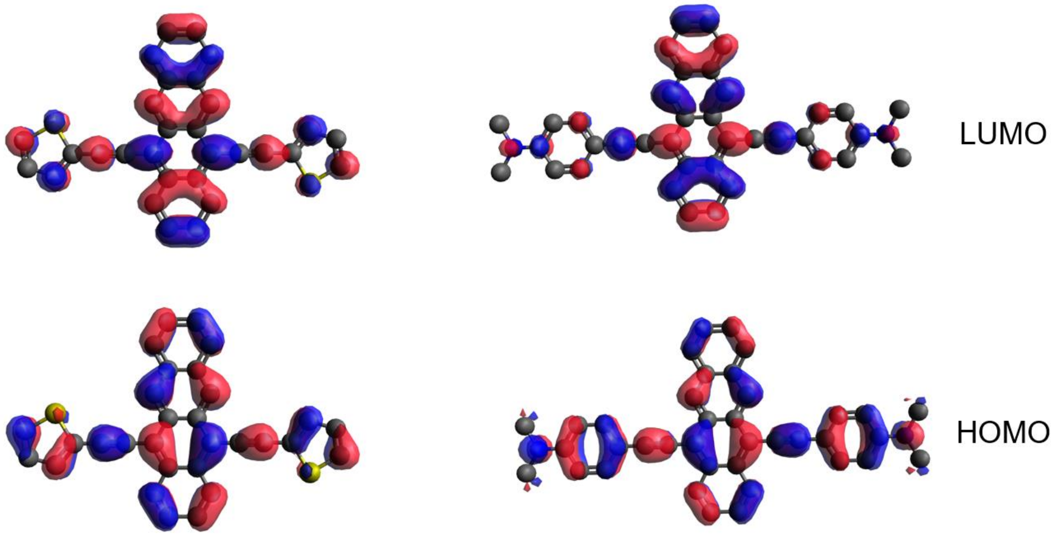

ED1 ED2

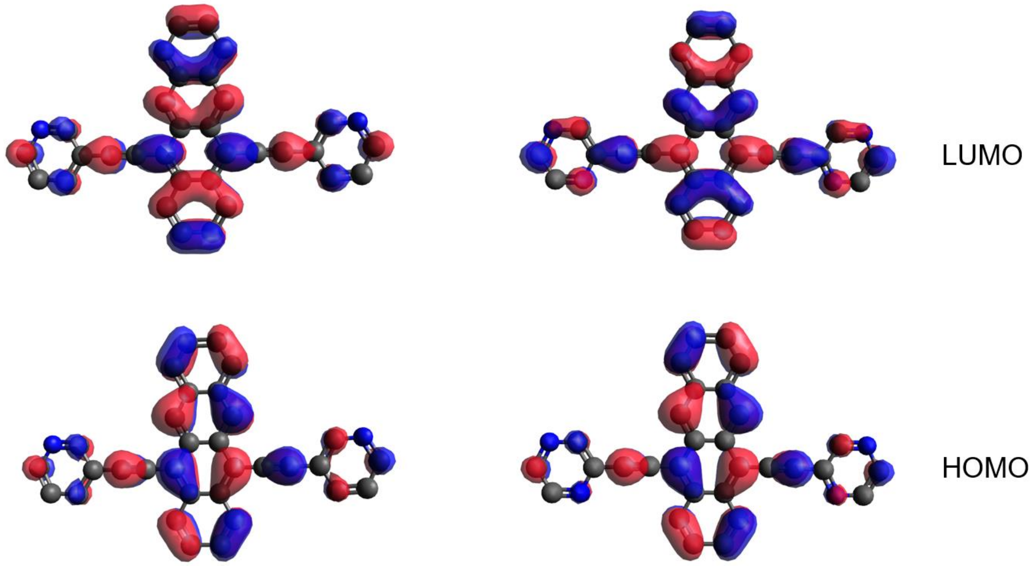

EW1 EW2

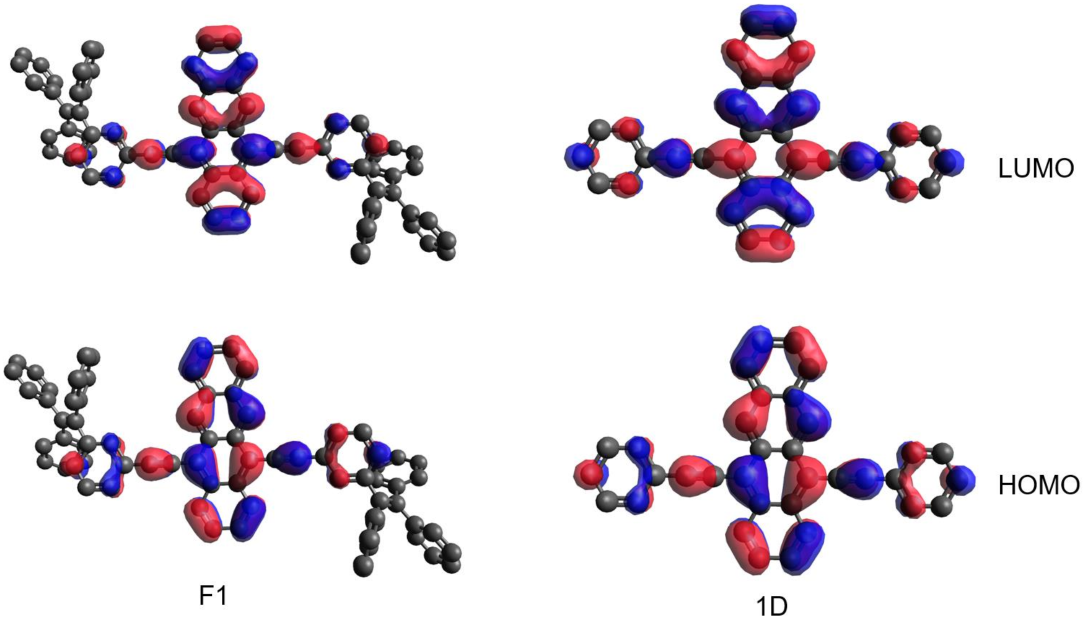

Solvatochromism

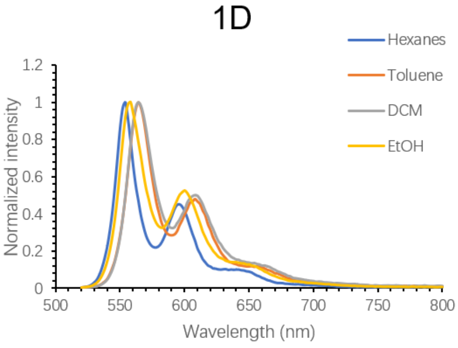

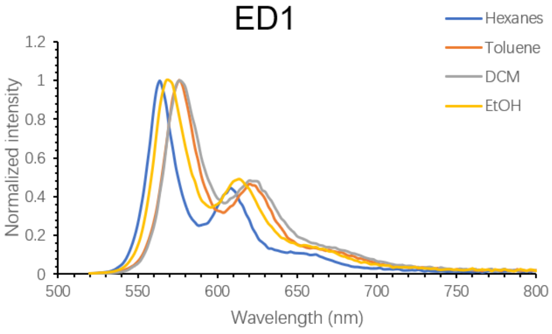

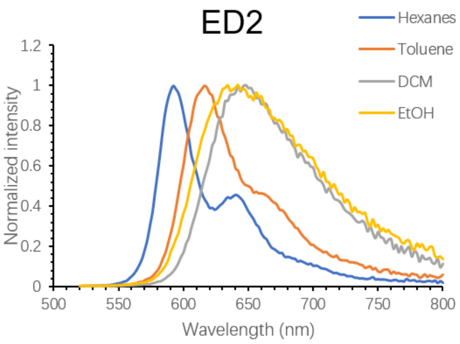

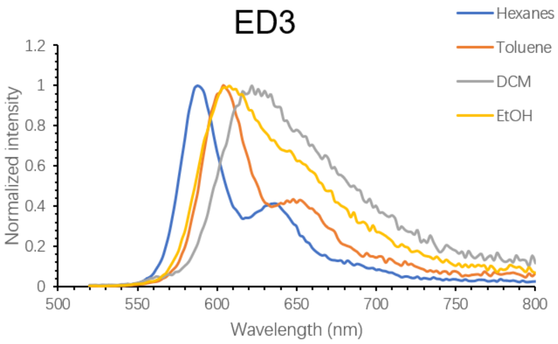

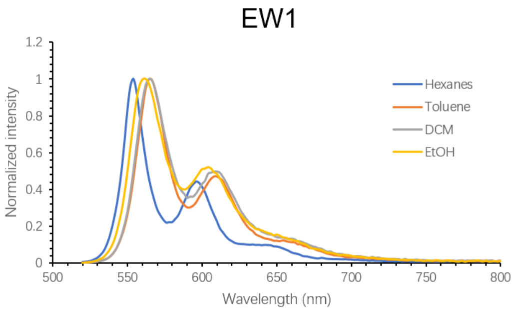
EW1
Normalized intensity
0
0.2
0.4
0.6
0.8
1
1.2
500
550
600
650
700
750
800
Wavelength (nm)
Hexanes
Toluene
DCM
EtOH

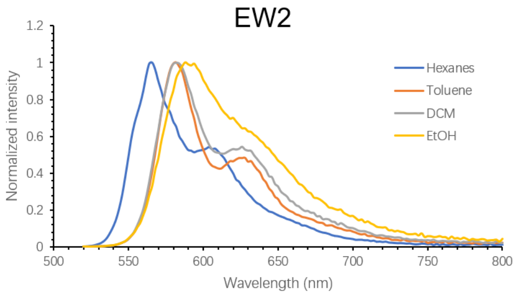
EW2
Normalized intensity
0
0.2
0.4
0.6
0.8
1
1.2
500
550
600
650
700
750
800
Wavelength (nm)
Hexanes
Toluene
DCM
EtOH

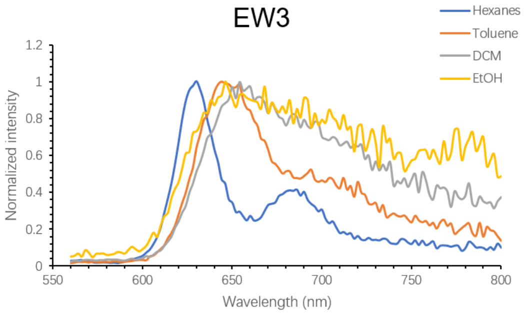
EW3
Normalized intensity
0
0.2
0.4
0.6
0.8
1
1.2
550
600
650
700
750
800
Wavelength (nm)
Hexanes
Toluene
DCM
EtOH

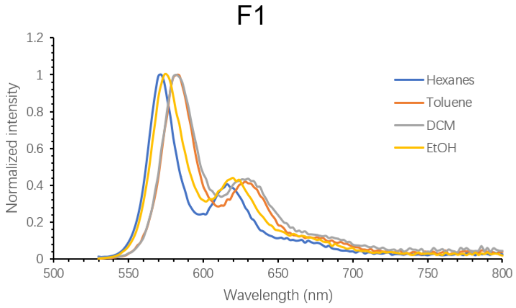
F1
Normalized intensity
0
0.2
0.4
0.6
0.8
1
1.2
500
550
600
650
700
750
800
Wavelength (nm)
Hexanes
Toluene
DCM
EtOH

Cyclic Voltammetry Results

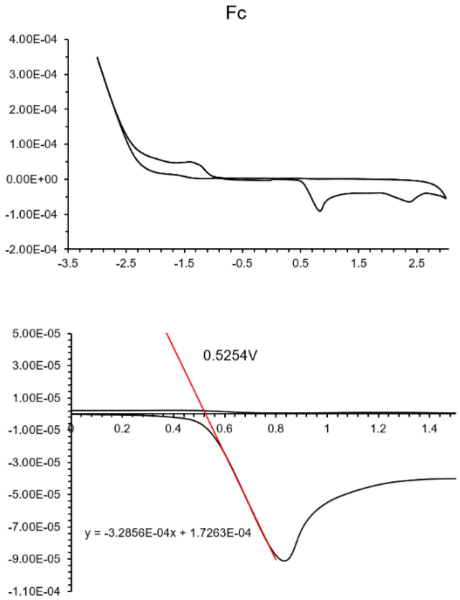

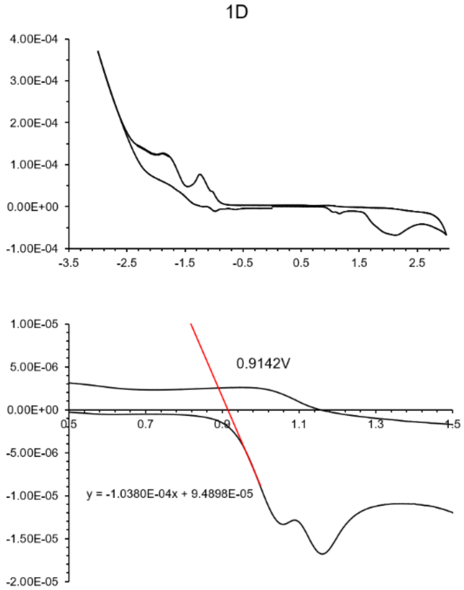

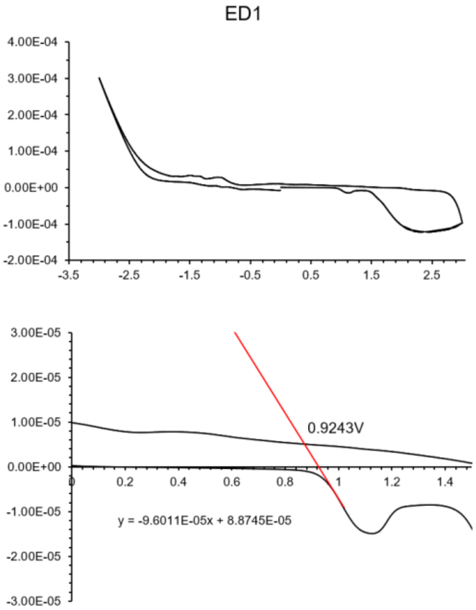

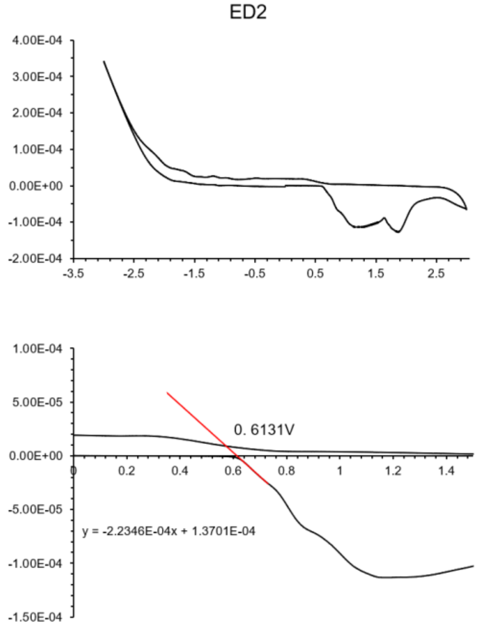

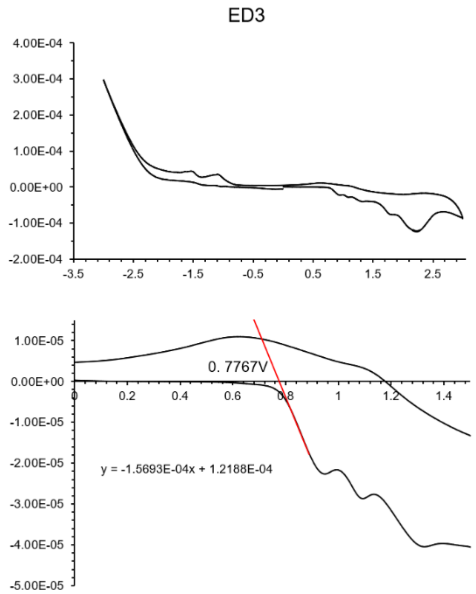

ED3

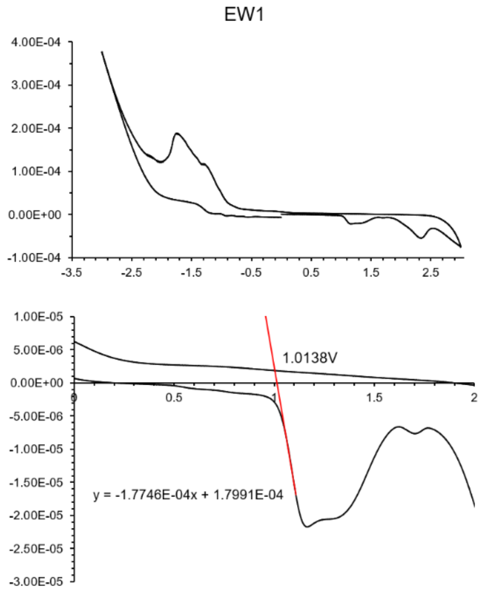

EW1

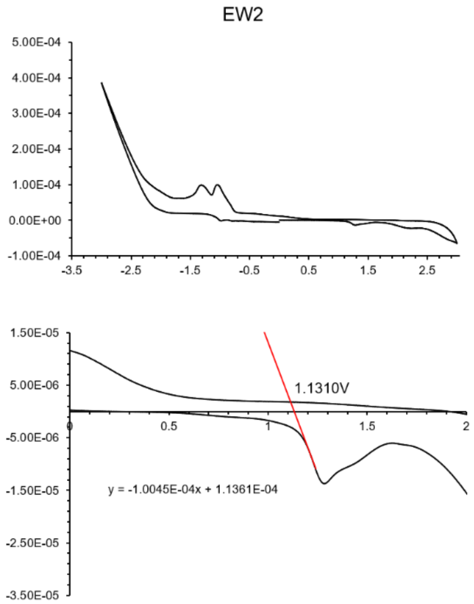

EW2

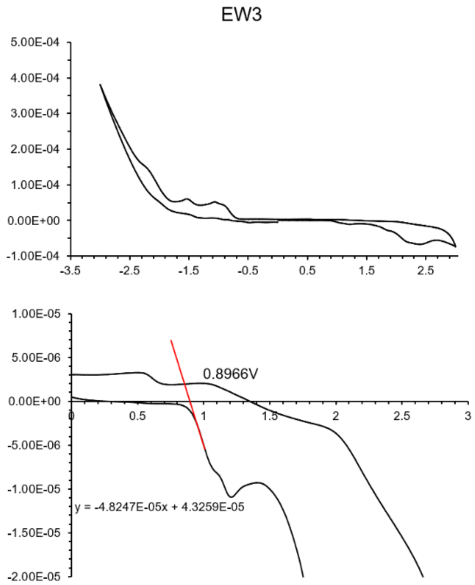

EW3

F1

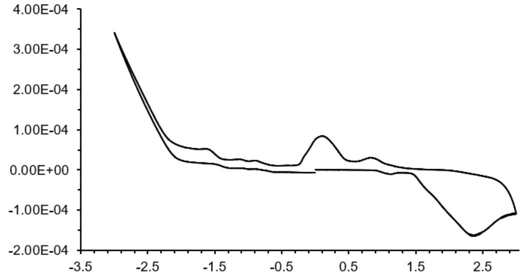

4.00E-04
3.00E-04
2.00E-04
1.00E-04
0.00E+00
-1.00E-04
-2.00E-04
-3.5
-2.5
-1.5
-0.5
0.5
1.5
2.5

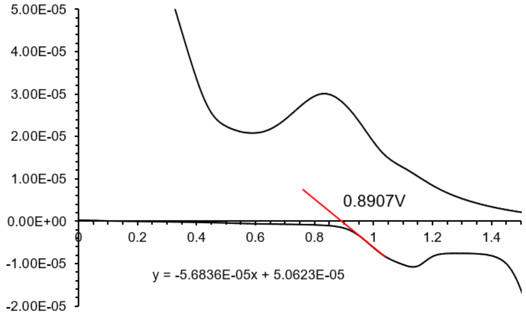

5.00E-05
4.00E-05
3.00E-05
2.00E-05
1.00E-05
0.00E+00
-1.00E-05
-2.00E-05
0
0.2
0.4
0.6
0.8
1
1.2
1.4
0.8907V
y = -5.6836E-05x + 5.0623E-05

NMR spectra

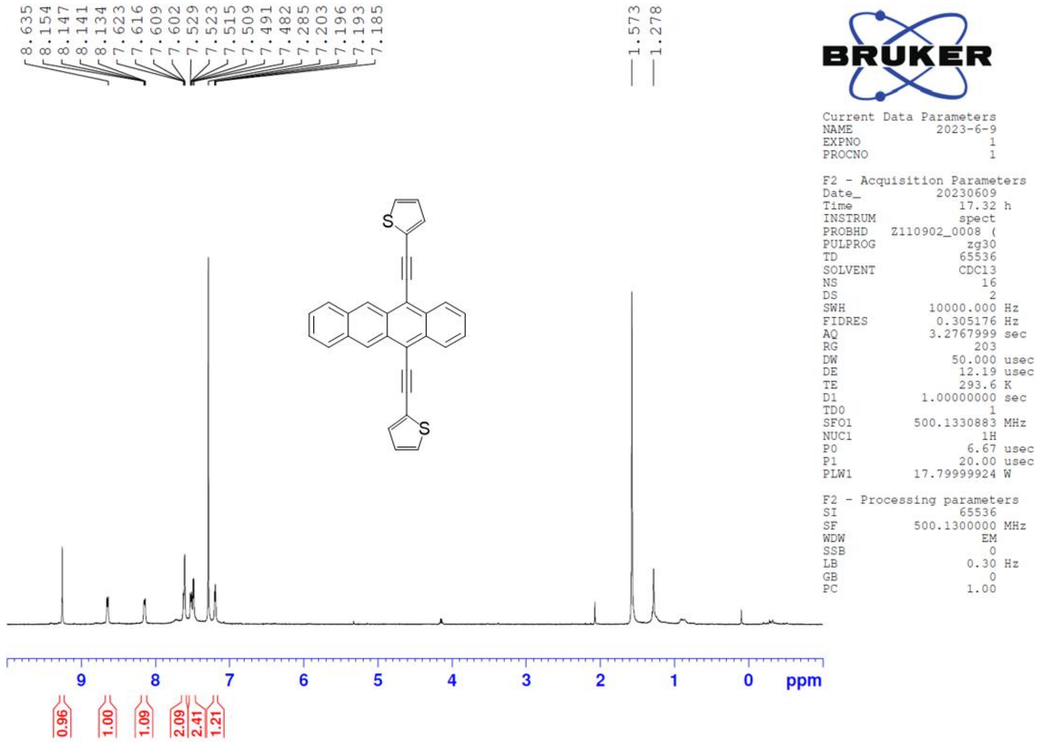

```
Current Data Parameters
NAME              2023-6-9
EXPNO                    1
PROCNO                   1

F2 - Acquisition Parameters
Date_             20230609
Time                 17.32 h
INSTRUM              spect
PROBHD   Z110902_0008 (
PULPROG               zg30
TD                   65536
SOLVENT              CDCl3
NS                      16
DS                       2
SWH              10000.000 Hz
FIDRES            0.305176 Hz
AQ               3.2767999 sec
RG                     203
DW                  50.000 usec
DE                   12.19 usec
TE                   293.6 K
D1              1.00000000 sec
TD0                      1
SFO1           500.1330883 MHz
NUC1                    1H
P0                    6.67 usec
P1                   20.00 usec
PLW1           17.79999924 W

F2 - Processing parameters
SI                   65536
SF             500.1300000 MHz
WDW                     EM
SSB                      0
LB                    0.30 Hz
GB                       0
PC                    1.00
```

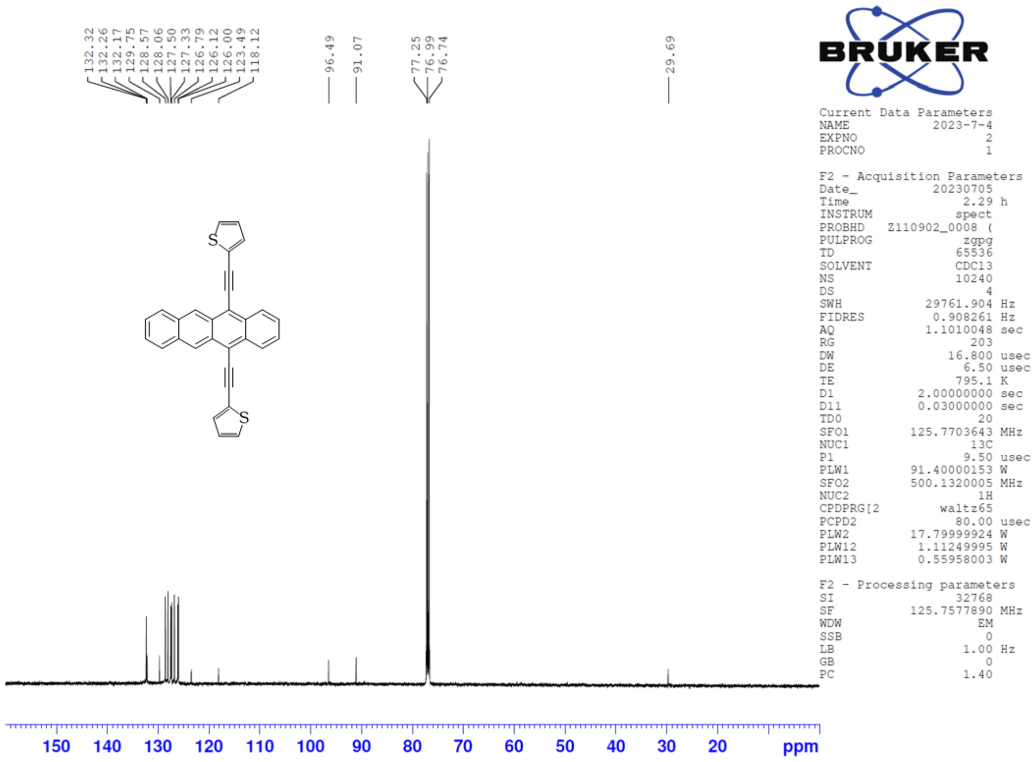

```
Current Data Parameters
NAME              2023-7-4
EXPNO                    2
PROCNO                   1

F2 - Acquisition Parameters
Date_             20230705
Time                  2.29 h
INSTRUM              spect
PROBHD   Z110902_0008 (
PULPROG               zgpg
TD                   65536
SOLVENT              CDCl3
NS                   10240
DS                       4
SWH              29761.904 Hz
FIDRES            0.908261 Hz
AQ               1.1010048 sec
RG                     203
DW                  16.800 usec
DE                    6.50 usec
TE                   795.1 K
D1              2.00000000 sec
D11             0.03000000 sec
TD0                     20
SFO1           125.7703643 MHz
NUC1                   13C
P1                    9.50 usec
PLW1           91.40000153 W
SFO2           500.1320005 MHz
NUC2                    1H
CPDPRG[2           waltz65
PCPD2                80.00 usec
PLW2           17.79999924 W
PLW12           1.11249995 W
PLW13           0.55958003 W

F2 - Processing parameters
SI                   32768
SF             125.7577890 MHz
WDW                     EM
SSB                      0
LB                    1.00 Hz
GB                       0
PC                    1.40
```

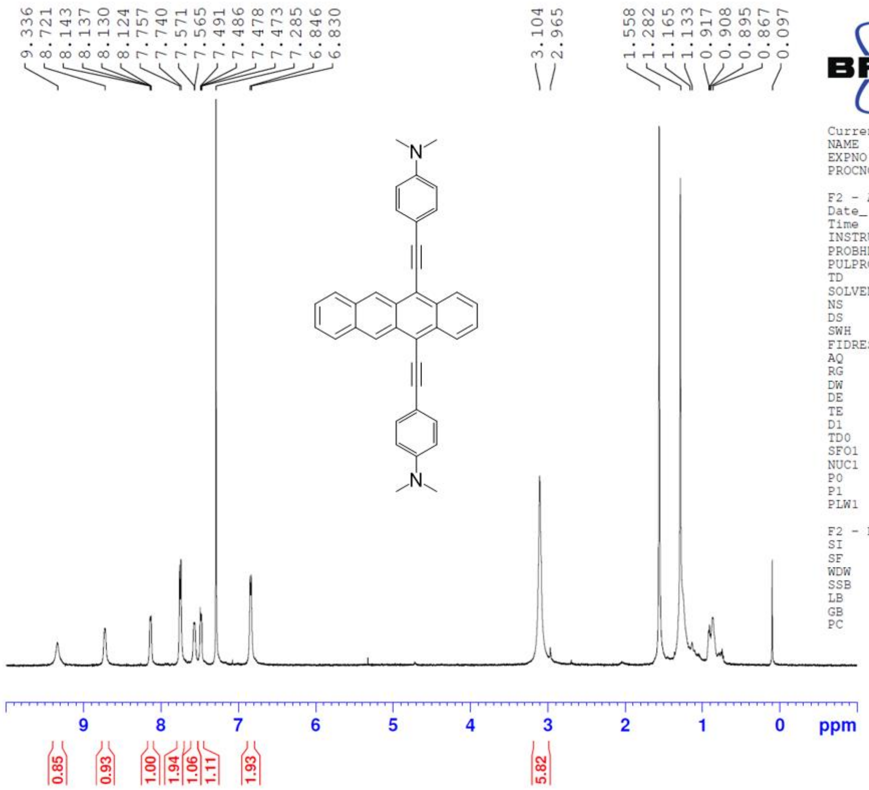

```
Current Data Parameters
NAME             2023-6-27
EXPNO                    3
PROCNO                   1

F2 - Acquisition Parameters
Date_             20230627
Time                 18.20 h
INSTRUM              spect
PROBHD   Z110902_0008 (
PULPROG               zg30
TD                   65536
SOLVENT              CDCl3
NS                      16
DS                       2
SWH              10000.000 Hz
FIDRES            0.305176 Hz
AQ               3.2767999 sec
RG                     203
DW                  50.000 usec
DE                   12.19 usec
TE                  1057.9 K
D1              1.00000000 sec
TD0                      1
SFO1           500.1330883 MHz
NUC1                    1H
P0                    6.67 usec
P1                   20.00 usec
PLW1           17.79999924 W

F2 - Processing parameters
SI                   65536
SF             500.1300000 MHz
WDW                     EM
SSB                      0
LB                    0.30 Hz
GB                       0
PC                    1.00
```

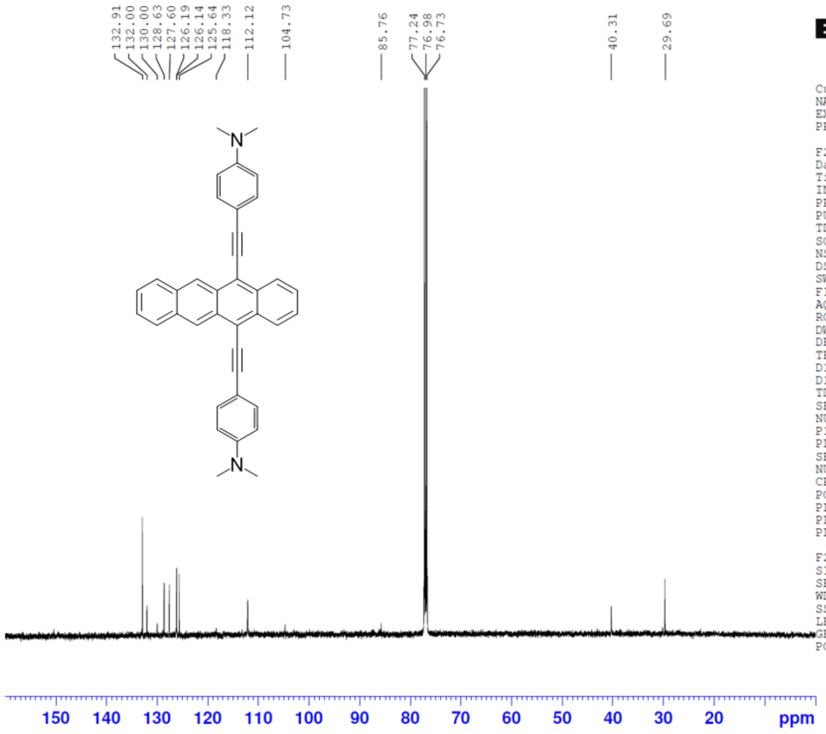

```
Current Data Parameters
NAME             2023-6-27
EXPNO                    5
PROCNO                   1

F2 - Acquisition Parameters
Date_             20230628
Time                  1.52 h
INSTRUM              spect
PROBHD   Z110902_0008 (
PULPROG               zgpg
TD                   65536
SOLVENT              CDCl3
NS                    8192
DS                       4
SWH              29761.904 Hz
FIDRES            0.908261 Hz
AQ               1.1010048 sec
RG                     203
DW                  16.800 usec
DE                    6.50 usec
TE                  1066.5 K
D1              2.00000000 sec
D11             0.03000000 sec
TD0                     16
SFO1           125.7703643 MHz
NUC1                   13C
P1                    9.50 usec
PLW1           91.40000153 W
SFO2           500.1320005 MHz
NUC2                    1H
CPDPRG[2           waltz65
PCPD2                80.00 usec
PLW2           17.79999924 W
PLW12           1.11249995 W
PLW13           0.55958003 W

F2 - Processing parameters
SI                   32768
SF             125.7577890 MHz
WDW                     EM
SSB                      0
LB                    1.00 Hz
GB                       0
PC                    1.40
```

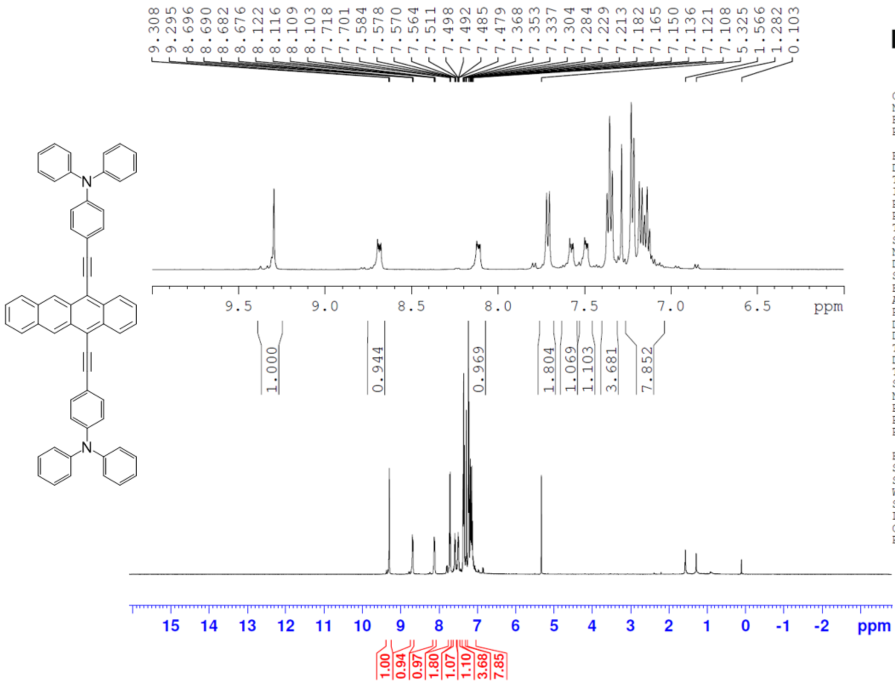

```
Current Data Parameters
NAME              2023-1-9
EXPNO                    1
PROCNO                   1

F2 - Acquisition Parameters
Date_             20230109
Time                 12.10 h
INSTRUM               spect
PROBHD    Z110902_0008 (
PULPROG               zg30
TD                   65536
SOLVENT              CDCl3
NS                      16
DS                       2
SWH              10000.000 Hz
FIDRES            0.305176 Hz
AQ               3.2767999 sec
RG                     203
DW                  50.000 usec
DE                   12.19 usec
TE                   292.6 K
D1              1.00000000 sec
TD0                      1
SFO1           500.1330883 MHz
NUC1                    1H
P0                    6.67 usec
P1                   20.00 usec
PLW1           17.79999924 W

F2 - Processing parameters
SI                   65536
SF             500.1300000 MHz
WDW                     EM
SSB                      0
LB                    0.30 Hz
GB                       0
PC                    1.00
```

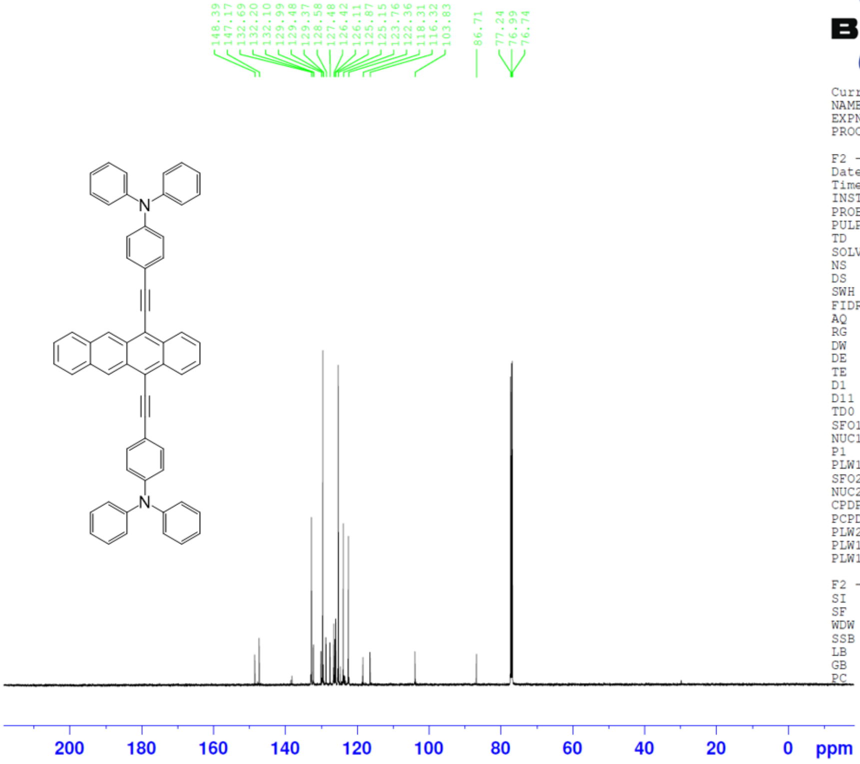

```
Current Data Parameters
NAME              2023-7-7
EXPNO                    2
PROCNO                   1

F2 - Acquisition Parameters
Date_             20230708
Time                  5.12 h
INSTRUM               spect
PROBHD    Z110902_0008 (
PULPROG               zgpg
TD                   65536
SOLVENT              CDCl3
NS                   12288
DS                       4
SWH              29761.904 Hz
FIDRES            0.908261 Hz
AQ               1.1010048 sec
RG                     203
DW                  16.800 usec
DE                    6.50 usec
TE                   845.1 K
D1              2.00000000 sec
D11             0.03000000 sec
TD0                     24
SFO1           125.7703643 MHz
NUC1                   13C
P1                    9.50 usec
PLW1           91.40000153 W
SFO2           500.1320005 MHz
NUC2                    1H
CPDPRG[2           waltz65
PCPD2                80.00 usec
PLW2           17.79999924 W
PLW12           1.11249995 W
PLW13           0.55958003 W

F2 - Processing parameters
SI                   32768
SF             125.7577890 MHz
WDW                     EM
SSB                      0
LB                    1.00 Hz
GB                       0
PC                    1.40
```

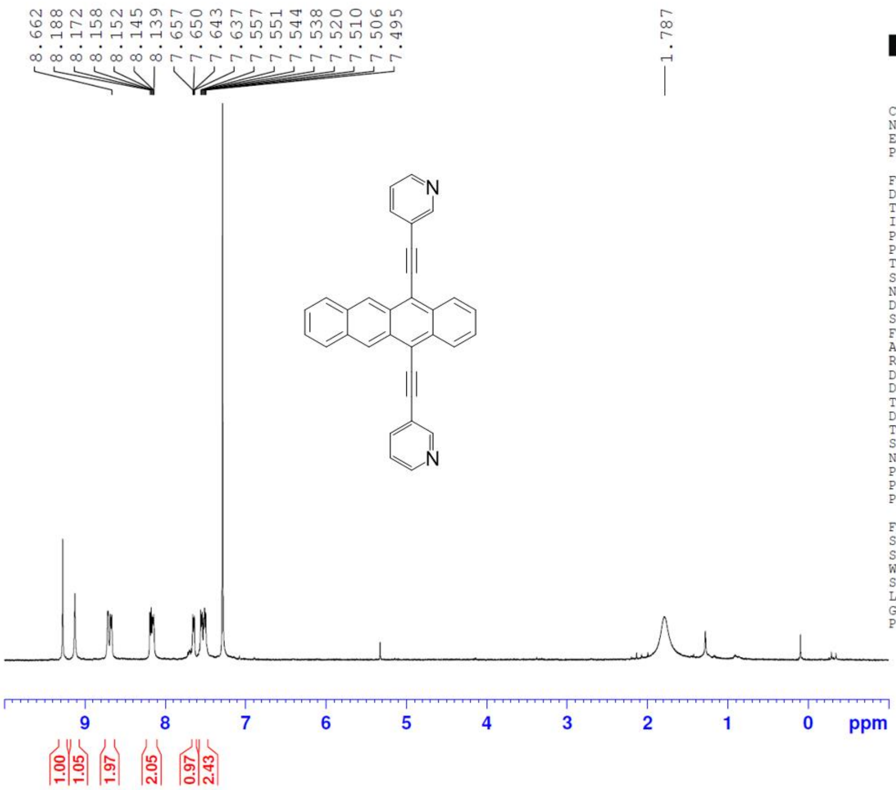

```
Current Data Parameters
NAME             2023-6-10
EXPNO                    1
PROCNO                   1

F2 - Acquisition Parameters
Date_             20230610
Time                 16.52 h
INSTRUM              spect
PROBHD   Z110902_0008 (
PULPROG               zg30
TD                   65536
SOLVENT              CDCl3
NS                      16
DS                       2
SWH              10000.000 Hz
FIDRES            0.305176 Hz
AQ               3.2767999 sec
RG                     203
DW                  50.000 usec
DE                   12.19 usec
TE                   294.2 K
D1              1.00000000 sec
TD0                      1
SFO1           500.1330883 MHz
NUC1                    1H
P0                    6.67 usec
P1                   20.00 usec
PLW1           17.79999924 W

F2 - Processing parameters
SI                   65536
SF             500.1300000 MHz
WDW                     EM
SSB                      0
LB                    0.30 Hz
GB                       0
PC                    1.00
```

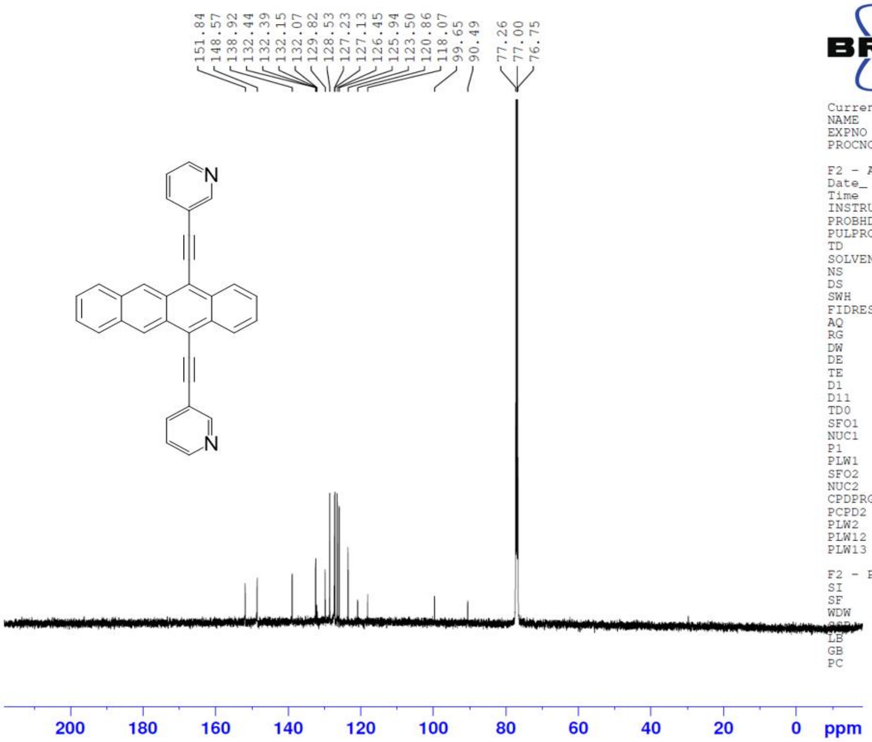

```
Current Data Parameters
NAME             2023-6-10
EXPNO                    3
PROCNO                   1

F2 - Acquisition Parameters
Date_             20230611
Time                  9.42 h
INSTRUM              spect
PROBHD   Z110902_0008 (
PULPROG               zgpg
TD                   65536
SOLVENT              CDCl3
NS                   18910
DS                       4
SWH              29761.904 Hz
FIDRES            0.908261 Hz
AQ               1.1010048 sec
RG                     203
DW                  16.800 usec
DE                    6.50 usec
TE                   295.8 K
D1              2.00000000 sec
D11             0.03000000 sec
TD0                     64
SFO1           125.7703643 MHz
NUC1                   13C
P1                    9.50 usec
PLW1           91.40000153 W
SFO2           500.1320005 MHz
NUC2                    1H
CPDPRG[2           waltz65
PCPD2                80.00 usec
PLW2           17.79999924 W
PLW12           1.11249995 W
PLW13           0.55958003 W

F2 - Processing parameters
SI                   32768
SF             125.7577890 MHz
WDW                     EM
SSB                      0
LB                    1.00 Hz
GB                       0
PC                    1.40
```

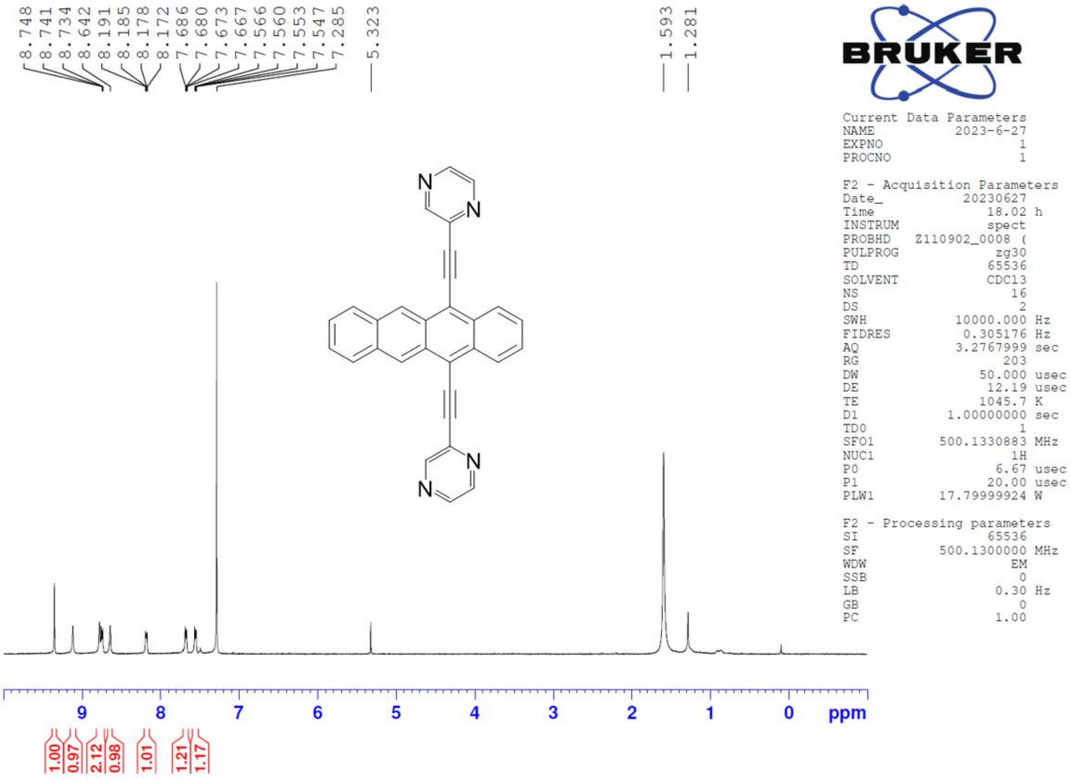

```
Current Data Parameters
NAME            2023-6-27
EXPNO                   1
PROCNO                  1

F2 - Acquisition Parameters
Date_            20230627
Time                18.02 h
INSTRUM             spect
PROBHD    Z110902_0008 (
PULPROG              zg30
TD                  65536
SOLVENT             CDCl3
NS                     16
DS                      2
SWH             10000.000 Hz
FIDRES           0.305176 Hz
AQ              3.2767999 sec
RG                    203
DW                 50.000 usec
DE                  12.19 usec
TE                 1045.7 K
D1             1.00000000 sec
TD0                     1
SFO1          500.1330883 MHz
NUC1                   1H
P0                   6.67 usec
P1                  20.00 usec
PLW1          17.79999924 W

F2 - Processing parameters
SI                  65536
SF            500.1300000 MHz
WDW                    EM
SSB                     0
LB                   0.30 Hz
GB                      0
PC                   1.00
```

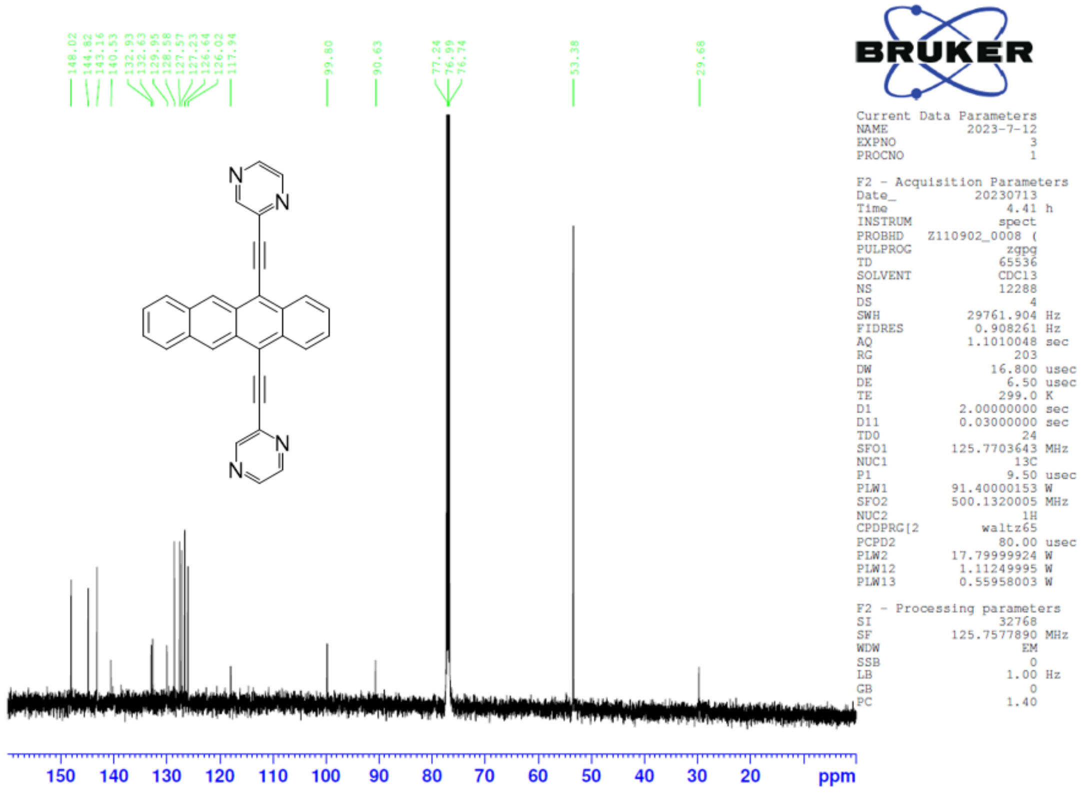

```
Current Data Parameters
NAME            2023-7-12
EXPNO                   3
PROCNO                  1

F2 - Acquisition Parameters
Date_            20230713
Time                 4.41 h
INSTRUM             spect
PROBHD    Z110902_0008 (
PULPROG              zgpg
TD                  65536
SOLVENT             CDCl3
NS                  12288
DS                      4
SWH             29761.904 Hz
FIDRES           0.908261 Hz
AQ              1.1010048 sec
RG                    203
DW                 16.800 usec
DE                   6.50 usec
TE                  299.0 K
D1             2.00000000 sec
D11            0.03000000 sec
TD0                    24
SFO1          125.7703643 MHz
NUC1                  13C
P1                   9.50 usec
PLW1          91.40000153 W
SFO2          500.1320005 MHz
NUC2                   1H
CPDPRG[2          waltz65
PCPD2               80.00 usec
PLW2          17.79999924 W
PLW12          1.11249995 W
PLW13          0.55958003 W

F2 - Processing parameters
SI                  32768
SF            125.7577890 MHz
WDW                    EM
SSB                     0
LB                   1.00 Hz
GB                      0
PC                   1.40
```

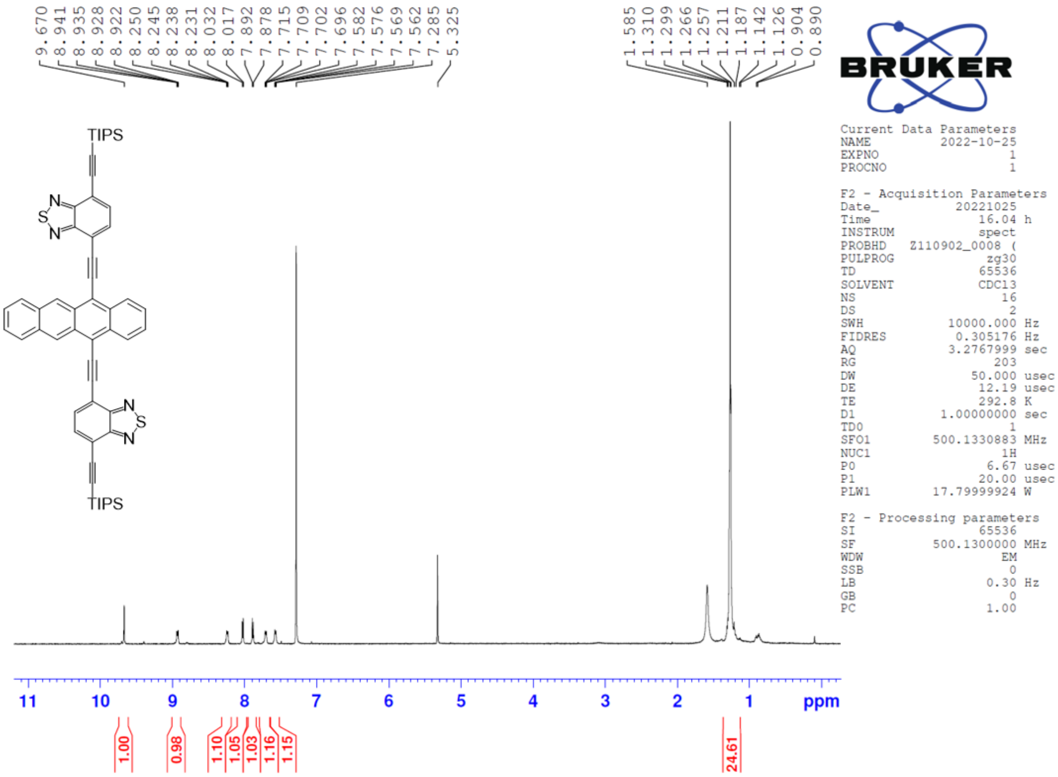

```
Current Data Parameters
NAME             2022-10-25
EXPNO                     1
PROCNO                    1

F2 - Acquisition Parameters
Date_              20221025
Time                16.04 h
INSTRUM               spect
PROBHD   Z110902_0008 (
PULPROG                zg30
TD                    65536
SOLVENT               CDCl3
NS                       16
DS                        2
SWH              10000.000 Hz
FIDRES            0.305176 Hz
AQ               3.2767999 sec
RG                      203
DW                  50.000 usec
DE                   12.19 usec
TE                   292.8 K
D1              1.00000000 sec
TD0                       1
SFO1           500.1330883 MHz
NUC1                     1H
P0                    6.67 usec
P1                   20.00 usec
PLW1           17.79999924 W

F2 - Processing parameters
SI                    65536
SF             500.1300000 MHz
WDW                      EM
SSB                       0
LB                     0.30 Hz
GB                        0
PC                     1.00
```

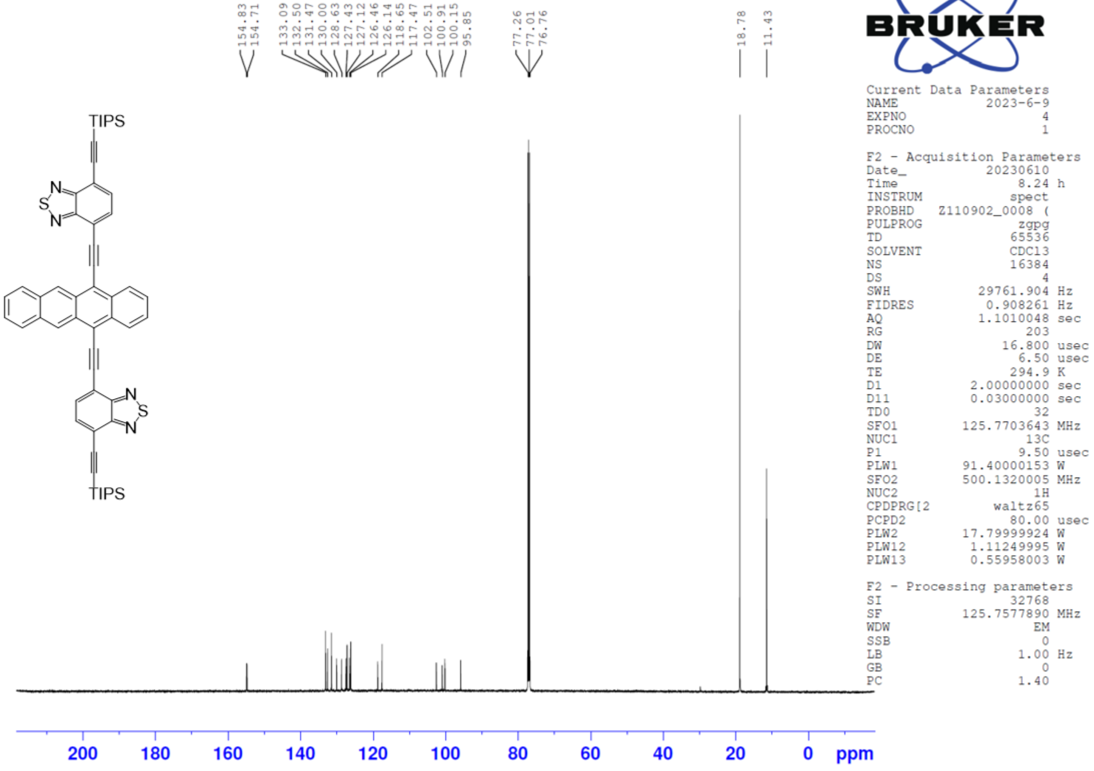

```
Current Data Parameters
NAME               2023-6-9
EXPNO                     4
PROCNO                    1

F2 - Acquisition Parameters
Date_              20230610
Time                 8.24 h
INSTRUM               spect
PROBHD   Z110902_0008 (
PULPROG                zgpg
TD                    65536
SOLVENT               CDCl3
NS                    16384
DS                        4
SWH              29761.904 Hz
FIDRES            0.908261 Hz
AQ               1.1010048 sec
RG                      203
DW                  16.800 usec
DE                    6.50 usec
TE                   294.9 K
D1              2.00000000 sec
D11             0.03000000 sec
TD0                      32
SFO1           125.7703643 MHz
NUC1                    13C
P1                    9.50 usec
PLW1           91.40000153 W
SFO2           500.1320005 MHz
NUC2                     1H
CPDPRG[2            waltz65
PCPD2                80.00 usec
PLW2           17.79999924 W
PLW12           1.11249995 W
PLW13           0.55958003 W

F2 - Processing parameters
SI                    32768
SF             125.7577890 MHz
WDW                      EM
SSB                       0
LB                     1.00 Hz
GB                        0
PC                     1.40
```

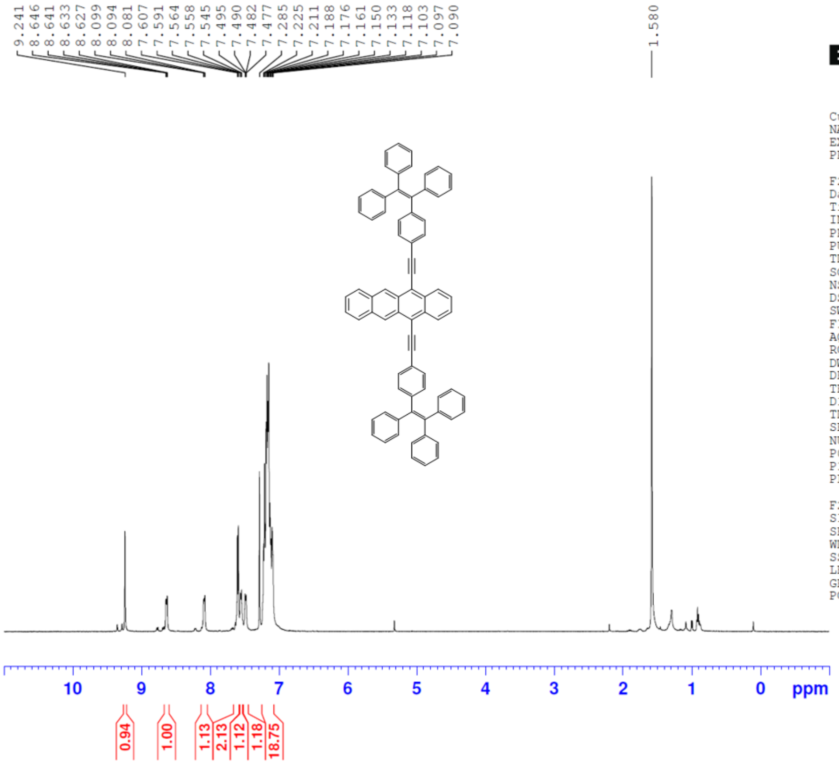

```
Current Data Parameters
NAME            2023-7-2
EXPNO                  2
PROCNO                 1

F2 - Acquisition Parameters
Date_           20230702
Time             17.44 h
INSTRUM            spect
PROBHD   Z110902_0008 (
PULPROG             zg30
TD                 65536
SOLVENT            CDCl3
NS                    16
DS                     2
SWH        10000.000 Hz
FIDRES      0.305176 Hz
AQ         3.2767999 sec
RG                   203
DW            50.000 usec
DE             12.19 usec
TE              1107.0 K
D1        1.00000000 sec
TD0                    1
SFO1     500.1330883 MHz
NUC1                  1H
P0              6.67 usec
P1             20.00 usec
PLW1      17.79999924 W

F2 - Processing parameters
SI                 65536
SF       500.1300000 MHz
WDW                   EM
SSB                    0
LB               0.30 Hz
GB                     0
PC                  1.00
```

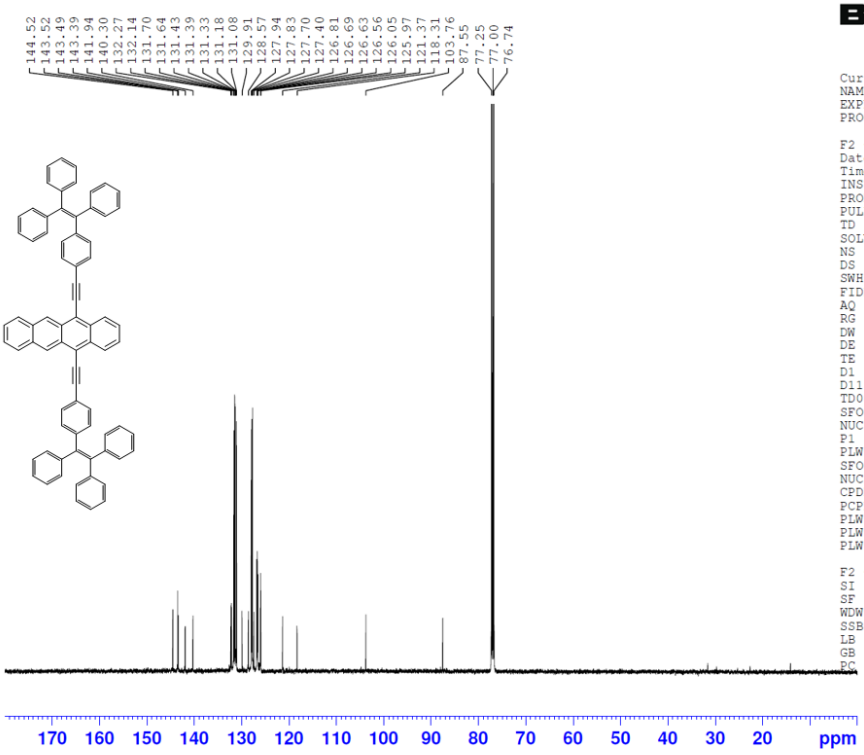

```
Current Data Parameters
NAME            2023-7-2
EXPNO                  3
PROCNO                 1

F2 - Acquisition Parameters
Date_           20230703
Time              2.48 h
INSTRUM            spect
PROBHD   Z110902_0008 (
PULPROG             zgpg
TD                 65536
SOLVENT            CDCl3
NS                 10240
DS                     4
SWH        29761.904 Hz
FIDRES      0.908261 Hz
AQ         1.1010048 sec
RG                   203
DW            16.800 usec
DE              6.50 usec
TE              1101.1 K
D1        2.00000000 sec
D11       0.03000000 sec
TD0                   20
SFO1     125.7703643 MHz
NUC1                 13C
P1              9.50 usec
PLW1      91.40000153 W
SFO2     500.1320005 MHz
NUC2                  1H
CPDPRG[2         waltz65
PCPD2          80.00 usec
PLW2      17.79999924 W
PLW12      1.11249995 W
PLW13      0.55958003 W

F2 - Processing parameters
SI                 32768
SF       125.7577890 MHz
WDW                   EM
SSB                    0
LB               1.00 Hz
GB                     0
PC                  1.40
```

Chapter 4:

Directing the crystallization of acene-based materials

4.1 Introduction

As a frequently used building block in organic electronics, acenes, especially longer acenes, have favorable electronic properties.[2, 7] Devices, such as organic thin-film transistors (OTFT),[18] based on acene-based materials have displayed comparable performances to traditional devices using traditional materials, such as silicon or metal oxides.[19] Besides, pure organic materials are advantaged in precision atomic modification, flexibility, and solution-processabilities.[167, 168]

However, the rational design of suitable materials for applications in organic electronics is still challenging. One of the major issues is the gap between the commonly used solution-phase characterizations and simulations and the solid-phase nature of devices.[169] The way molecules stack could dramatically change the overall properties and affect the performance of devices. Such stacking patterns are highly related to intermolecular and intramolecular interactions, including but not limited to hydrogen bonding, static electric interaction, steric hindrance, chalcogen bonding, halogen bonding, and π-π interactions.[170-172] It has been reported that even a small modification, such as a switch with one single atom in the molecule, can result in significant consequences.[173] Understanding these interactions and carefully analyzing them is highly desired in developing novel materials.

Despite the difficulties caused by the numerous interactions, we could harness them by intentionally introducing an interaction into our molecular design to direct the solid-state structure and tune the material's properties.[174, 175] Our group has practiced this idea and designed a method to direct the crystallization of conjugated materials through non-covalent interactions, namely ArF-ArH interactions, as shown in **Figure 4.1**.[176] The electronegative fluorine substitutions polarized the benzene ring's π systems, generating a partial positive potential at the center and a partial negative potential at the edges.[177, 178] Thus, perfluorinated benzenes favor a co-facial, center-to-center stacking with regular benzenes through quadrupole interactions.

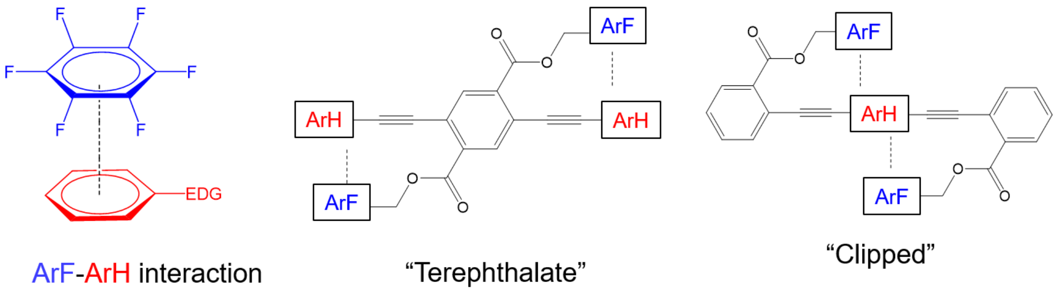

ArF-ArH interaction

"Terephthalate"

"Clipped"

Figure 4.1: ArF-ArH interaction (left), Terephthalate (middle) and Clipped (right) structure of designed molecule.

Our group carefully studied this ArF-ArH interaction in a model of phenylene-ethynylene trimers.[176, 179, 180] As shown in **Figure 4.1**, the side chains of interest were installed either on the central phenyl ring as a "terephthalate ester" or on the peripheral phenyl rings as a "clipped structure." A methylene group was intentionally added to break the conjugation of the side chain, which can minimize the impact of different arenes on the electronic properties of the products. In both cases, we have observed shifts in the solid-state spectra of the molecules when switching the ArF-ArH interaction on and off. Because the molecules displayed similar photophysical properties in solution-phase, we attribute such differences to altering inter- and intramolecular packing. Our hypothesis was further proved by the single-crystal X-ray diffraction (SCXRD) results, which showed the presence of ArF-ArH interactions and showed the twisting of the backbone of the trimer

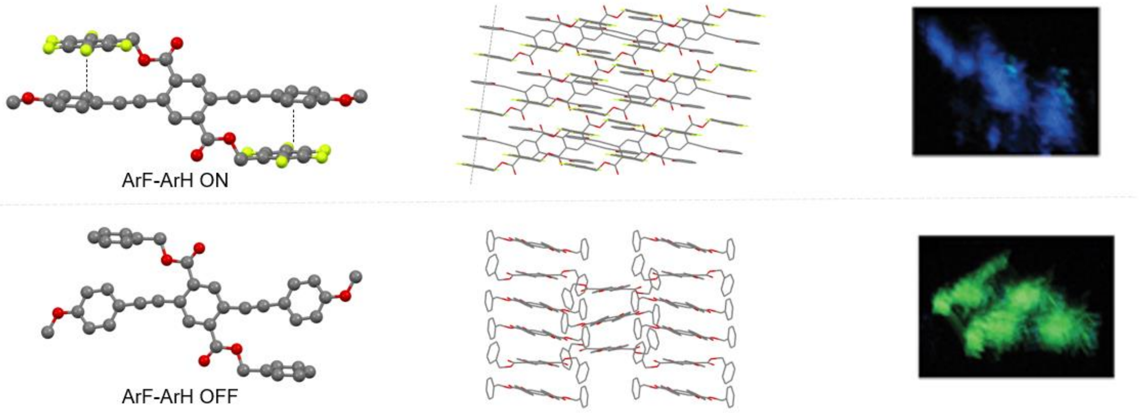

Figure 4.2: Crystal structures and fluorescent photos of phenylene-ethynylene trimers with ArF-ArH on and off. Left: the twisting of backbones by ArF-ArH interaction; Middle: the columnar packing of alternated phenyl and fluorophenyl rings; Right: the fluorescent color of crystals under UV-light. *Copyright 2014, Royal Society of Chemistry.*

driven by such interactions.[176]

In the recent five years, our group has adapted this method to other aromatic systems, including various substituted benzenes, heteroatom arenes, metal complexes, and polycyclic arenes.[154, 180, 181] In this work, we further adapted the “clipped structure” to acenes and studied the possibility of directing the crystallization of this kind of material.

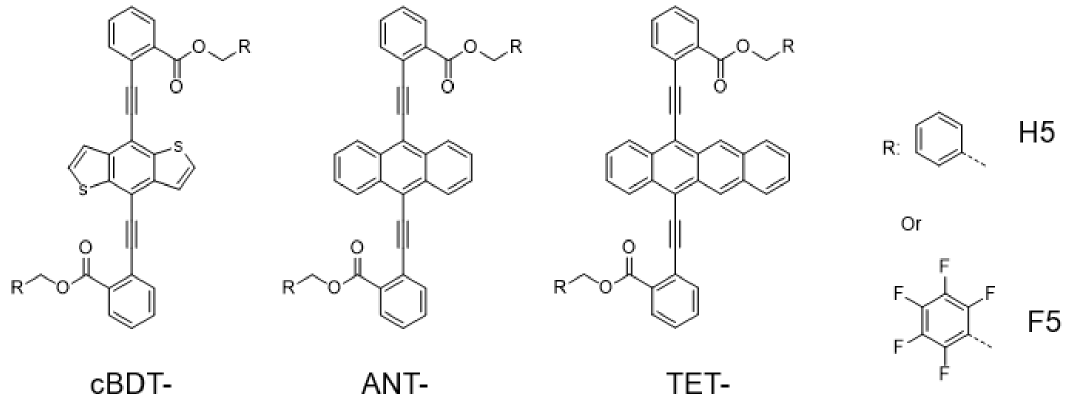

Scheme 4.1: Molecular structures that is discussed in this section. The first part of the name indicates the core structure: **cBDT** for central benzodithiophene, **ANT** for anthracene, and **TET** for tetracene. The postfix, F5 and H5 is indicating if the side chains are fluorinated or not, respectively.

4.2 Experimental design and synthesis of clipped acenes

This project is part of a collaborative project in which a large set of polycyclic aromatic systems with “clipped structures” was studied. However, in this dissertation, only six molecules are included indicating the author’s actual contribution to this project.

The molecular structures of developed clipped acenes are listed in **Scheme 4.1**. The side chains are installed at the central ring, perpendicular to the long axis of the acenes. The three sets of molecules were derivated from anthracene (**ANT**), tetracene (**TET**), and benzothiophene (**cBDT**), respectively. Besides, the feature of side chains was represented by either H5 (phenyl) or F5 (pentafluorophenyl). Following a reported procedure, we synthesized the side chains first with a single-step DCC coupling reaction to form esters. The iodinated side chain was then subjected to Sonogashira coupling reactions with either trimethylsilyl (**TMS**) acetylene to form an intermediate product or the ethylated acenes to form the final products. The **TMS**-protected side chains were then deprotected and added to another Sonogashira Coupling reaction with dibromoanthracenes to yield the final products. The synthesis is shown in **Scheme 4.2**.

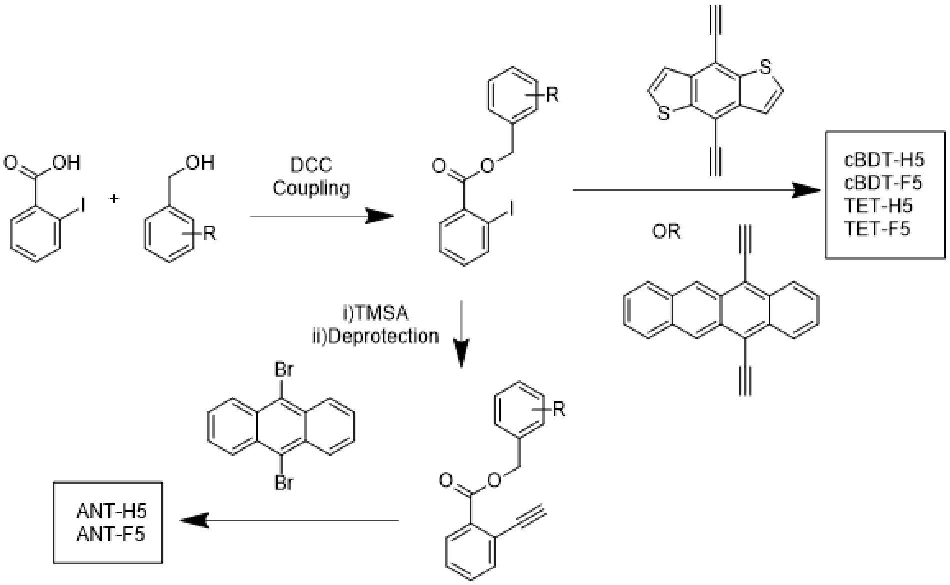

Scheme 4.2: Synthesis pathway of developed acene derivatives.

4.3 Solution phase properties and theoretical calculations

Table 4.1: The photophysical properties of developed acene derivatives in this work.

Name	$\lambda_{abs,max}$ (nm)	$\lambda_{Fl,max}$ (nm)	ε	FLQY (%)
ANTF5	460^{*}, 276	497	33350	67
ANTH5	476^{*},277	493	37600	72
cBDTF5	415^{*},297	457	33750	44
cBDTH5	414^{*},295	453	57500	47
TETF5	556^{*},295	584	35000	81
TETH5	566^{*},296	581	40300	79

The asterisk(*) indicates at which wavelength the extinction coefficients (ε) are reported.

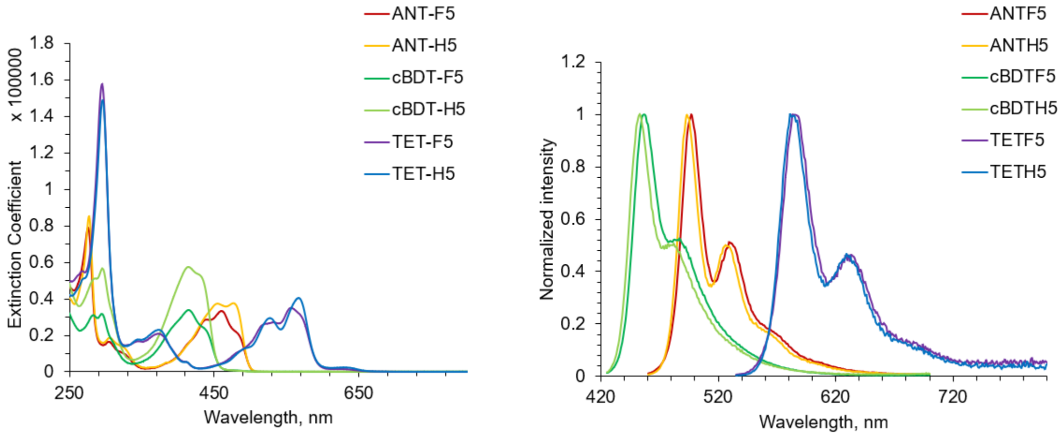

Figure 4.3: Absorbance spectra (left) and the normalized emission spectra (right) of developed acene derivatives.

Figure 4.3 displays the results of solution-phase absorbance and fluorescent spectroscopies. As expected, fluorination does not significantly affect the electronic structures due to the methylene spacer. As for photoluminescence, all six molecules display strong emission with fluorescent quantum yield (FLQY) between 40%-80% (**Table 4.1**). A slight emission red-shift is observed on the fluorinated molecules, which can be attributed to the inductive effect.[179]

Table 4.2: Theoretical calculation results of developed acene derivatives in this work.

Name	LUMO (eV)	HOMO (eV)	Gap (eV)	Excited States (eV)[a]
ANTF5	-2.614	-5.114	2.500	2.317
ANTH5	-2.552	-5.066	2.514	2.337
cBDTF5	-2.776	-5.609	2.833	2.543
cBDTH5	-2.696	-5.554	2.858	2.574
TETF5	-3.098	-5.173	2.075	1.940
TETH5	-2.717	-4.807	2.090	1.991

[a] The excited states are selected by the highest oscillator strength within the first 20 possible excited transitions from the TD-DFT calculations.

To better understand these photophysical properties, we performed theoretical calculations using Gaussian/g09.[136] The solution state geometries of the molecules were determined by DFT calculation at the B3LYP/6-31G(d,p) level of theory using a polarizable continuum solvent model for chloroform. Then, we performed TD-DFT at the B3LYP/6-311+G(d,p) level of theory on the optimized geometries to calculate the excitation states and frontier molecular orbitals (FMOs).

Figure 4.4 shows the results for **ANT-H5** and **ANT-F5**. The results show that the predominant excitation is from HOMO to LUMO, and this transition results in the absorbance peak at the longest wavelength. Notably, for both HOMO and LUMO of these anthracenes, the electron clouds are localized within the conjugated system but not spreading to the H5 or F5 rings inside side chains. Such findings support our data from spectroscopy and explain why fluorination had only minimal impact on the solution phase

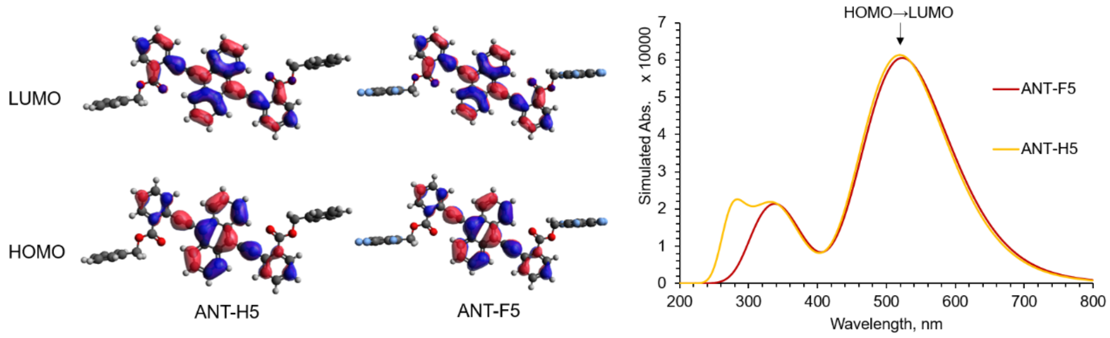

Figure 4.4: FMOs and simulated absorbance of **ANT-H5** and **ANT-F5**.

properties. The other two sets of molecules have similar results, and the key parameters were collected and summarized in **Table 4.2**.

4.4 Spectroscopy on thin films

Although fluorination does not impact the solution phase properties much, the difference between the solid-phase H5 and F5 versions is considerable, even with a single atomic substitution[173] or switching the position of fluorination[182]. To characterize the solid-state properties with spectroscopy, we fabricated thin films of the developed molecules either by spin-casting or drop-casting. Interestingly, spun-cast films give better reproductivity in terms of the color of emissions, which may result from more precise

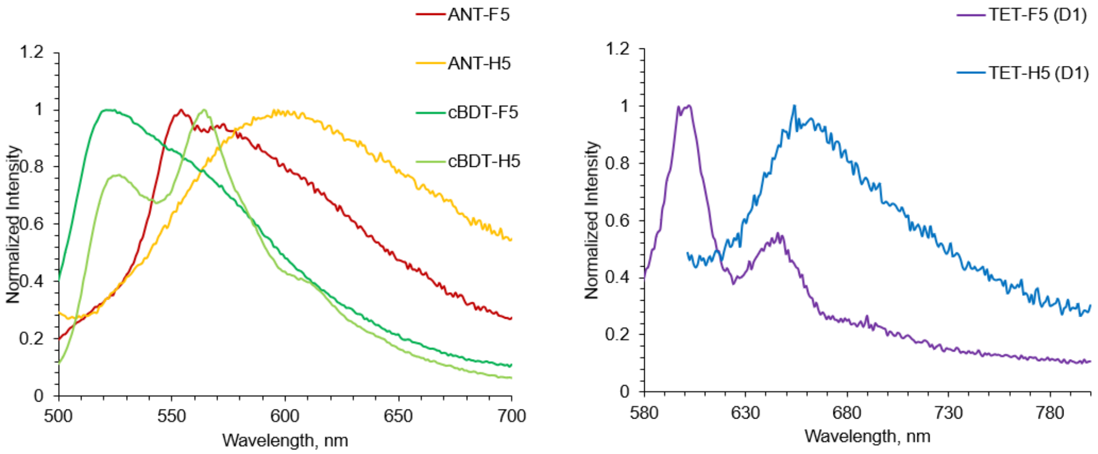

Figure 4.5: Fluorescent spectra of thin-films fabricated by developed acenes derivatives. The films of made by **TET-F5** and **TET-H5** are tested with larger band widths, and the results is not corrected due to the potential artifact in long-wavelength for less emissive samples.

control of film construction. The photophysical properties of fabricated films are collected in **Table 4.3**.

Table 4.3: Photophysical properties of fabricated thin films.

Name	Drop-Cast Film		Spun-Cast Film	
	$\lambda_{abs,max}$ (nm)	$\lambda_{Fl,max}$ (nm), FLQY(%)	$\lambda_{abs,max}$ (nm)	$\lambda_{Fl,max}$ (nm), FLQY(%)
ANTF5	507	551, 2.3	499	554, 3.1
ANTH5	515	556, 2.5	469	595, 4.5
cBDTF5	417	564, 42	457	521, 18
cBDTH5	466	537, 23	417	564, 11
TETF5	589	602, 0.04	586	602, 0.04
TETH5	609	661, 0.8	605	654, 0.04

Figure 4.5 shows the emission spectra of spun-cast films. Generally, the **F5** versions display a more than 40 nm hypochromic shift in emission compared to their H5 counterparts. However, we did not observe similar results from drop-cast films, which indicates a different mechanism from the "twisting" of the backbone, as our group observed in the past. More details will be discussed in the section on crystal structures. (*Vide infra*) Films constructed by **ANTs** and **cBDTs** are sufficiently emissive, with FLQY higher than

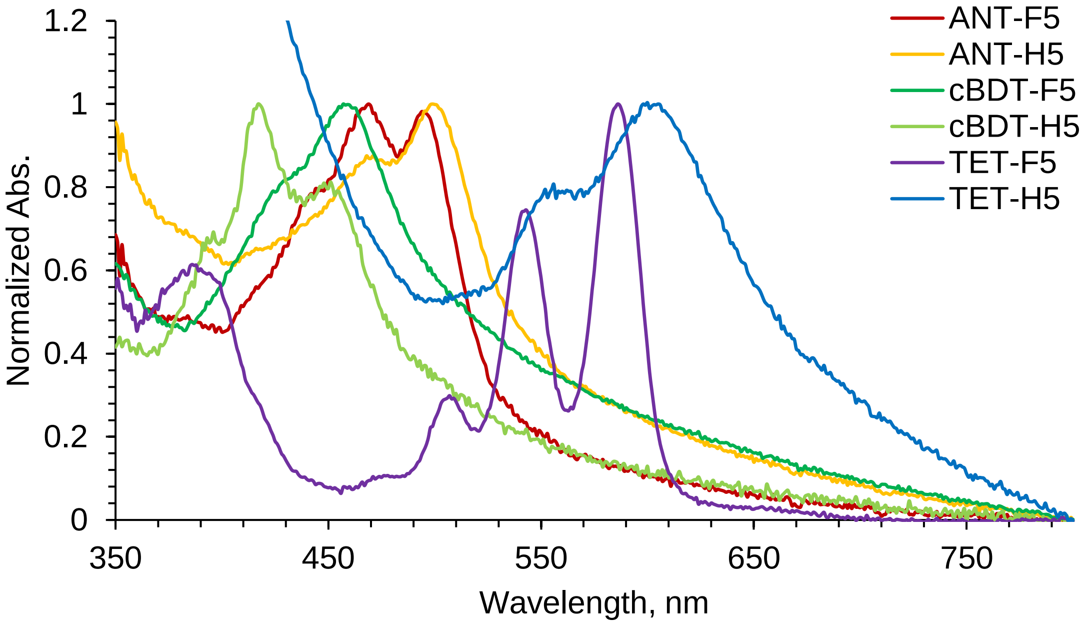

Figure 4.6: Absorbance spectra of spun-cast films of developed acene derivatives. The spectra were normalized by the peak at longest wavelength.

2% for **ANTs** and 10% for **cBDTs**. However, the **TETs** suffer from an aggregation-induced-quenching (ACQ) effect, and only poorly emitting with a FLQY lower than 1%, though the signals are still testable with larger slit-widths without mathematical correction.

The absorbance spectra do not display significant shifting between fluorinated and non-fluorinated acenes. However, as shown in **Figure 4.6**, the spectra of **TET-F5** and **TET-H5** exhibit a noticeable difference in shapes. The spectrum of **TET-F5** features a vibrational structure, while **TET-H5** does not. We attribute this phenomenon to the more rigid local environment within the **TET-F5** thin film.

4.5 Crystal structures and simulated ESP maps

To directly evaluate the impact of ArF-ArH interactions on the stacking, we performed single-crystal X-ray diffraction (SCXRD) test on the crystals of developed molecules. Unfortunately, **TETs** tend to form thin plates that are not testable by SCXRD experiments. On the other hand, the results of the **ANTs** and **cBDTs** are obtained in sufficient quality.

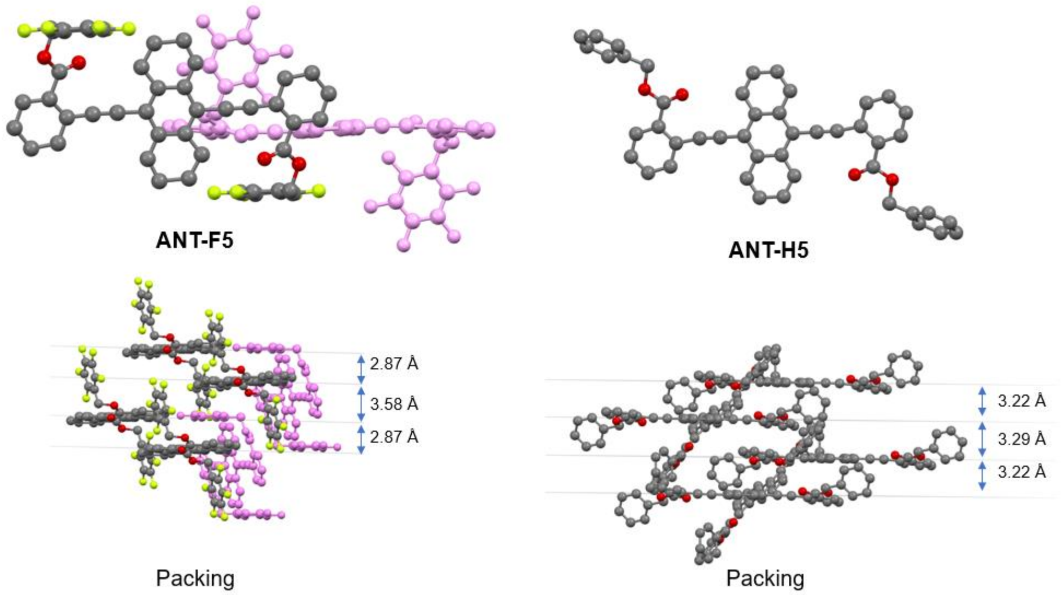

Figure 4.7: Crystal structure of **ANT-F5** and **ANT-H5**. The grey planes in packing displays are indicating the plane of anthracenes and the labeled distance are distance between planes.

As shown in **Figure 4.7**, the **ANT-F5** and **ANT-H5** display very different crystal structures. For **ANT-F5**, the anthracenes are almost perpendicularly staggered with each

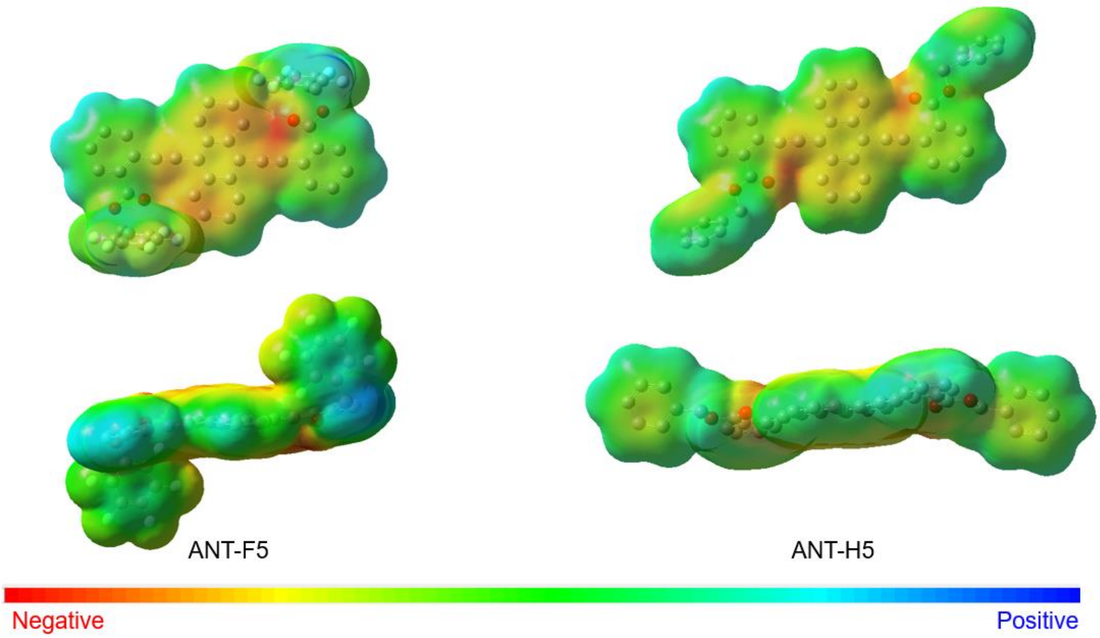

Figure 4.8: ESP Maps of **ANT-F5** and **ANT-H5**, with views perpendicular(top) or along (bottom) the plane of backbones.

other, and the dihedral angle was measured to be 85-96°. Also, the intramolecularly face-to-face stacking between the ArF and aromatic structure, which usually appears in our past works,[154, 179-181, 183] is absent in the crystal structure of **ANT-F5**, as well as the characteristic twisting between the side-chain and central arenes. Instead, the **ANT-F5** appears to have a highly coplanar molecular backbone with a torsion angle smaller than 5°. In addition, the ArF ring is 80-100° bent from the plane of the diethynyl anthracene backbone. Although there is no intramolecular ArF-ArH interaction observed, we find an intermolecularly short C•••C distance of 3.33 Å between anthracene and pentafluoro-benzene. The interacting carbon in anthracene also displays interaction with carbon on benzoic ester, located in a third molecule, with a C•••C distance of 3.34 Å. We also find interactions between the ArF ring and the carbonyl oxygen, with the shortest C•••O distance of 3.05 Å. Notably, this interaction could be identified as electrostatic interaction by simulated Electrostatic Potential (ESP) Maps. Combining these impacts, the ArF rings are actively participating in the formation of crystals and spacing the chromophores through competitive ArF-ArH interactions.

In the obtained crystal structure of **ANT-H5**, the benzene ring in the side chain shows no noticeable interactions or impacts on the stacking of anthracenes. The anthracenes display a herringbone stacking with a dihedral angle of 55-65°. Such stacking patterns are also observed in previous works of substituted anthracenes.[184-186] Short contacts are found between the benzoic ester and the anthracenes with a C•••O distance of 3.20 Å and a C•••C distance of 3.35 Å, which results in a parallel displaced stacking of the molecules. We have also estimated a Pitch (P) and Roll (R) distance of the two molecules[187]. For **ANT-F5**, the P and R distances are estimated to be 9.4 Å and 2.3 Å, which are significantly larger than those, 7.4 Å and 1.3 Å for **ANT-H5**. These results indicate the tighter packing of chromophores in **ANT-H5** crystals and explain why **ANT-H5** has a red-shifted emission compared with **ANT-F5**.

The **cBDT** set shows very similar crystal structures to **ANTs** (in the appendix). Given the reassembled electronic properties and size of the molecules, it is reasonable to see benzodithiophene exhibiting analogous results. Also, we hypothesize that it was because of the steric hindrance that blocked the rotation of ester bonds. In other words, the space is not enough for the bulky ArF-ring to point towards the inner direction of the molecule, towards the chromophore, due to the large size of **ANT** or **BDT**.

To further understand the stacking of these molecules, electrostatic potential (ESP) maps of ANTs are calculated by Gaussian/g09. [136]As shown in **Figure 4.8**, the flip of positive and negative potential by fluorination is clear. At the center of the benzene ring, the potential renders from negative (H5) to positive (F5). The most negative potential locates in carbonyl groups for both molecules, which results from the n-orbitals on the oxygen. These observations explain the strong electrostatic interaction between the ArF ring and the carbonyl oxygen of **ANT-F5**. At the same time, anthracene has a negative potential due to its electron-rich nature. Thus, the interactions are found between the anthracenes and ArF rings, too. However, there is no evidence to support the interaction between benzoic ester and anthracene as in **ANT-H5** being static electronic interactions.

4.6 Mechanochromism of ANTs

Although the molecules are not displaying a twisted structure as we normally observe in our other “clipped” structures, mechanochromism is still found in the **ANTs**. **Figure 4.9** shows the emission spectra of **ANTs**’ drop-cast films before smearing, after smearing, and after annealing on a hot plate at 80°C. Different from we opposite mechano-chromism effects we reported on other ArF-ArH molecules[170, 182], both **ANT-H5** and **ANT-F5** exhibit positive mechanochromism, red-shifting upon mechanic force. We attribute this change to the aggregation of anthracenes triggered by compressing of the crystallin films. Such a phenomenon was first reported by Tian's group and found in many anthracene-containing molecules.[172, 184]

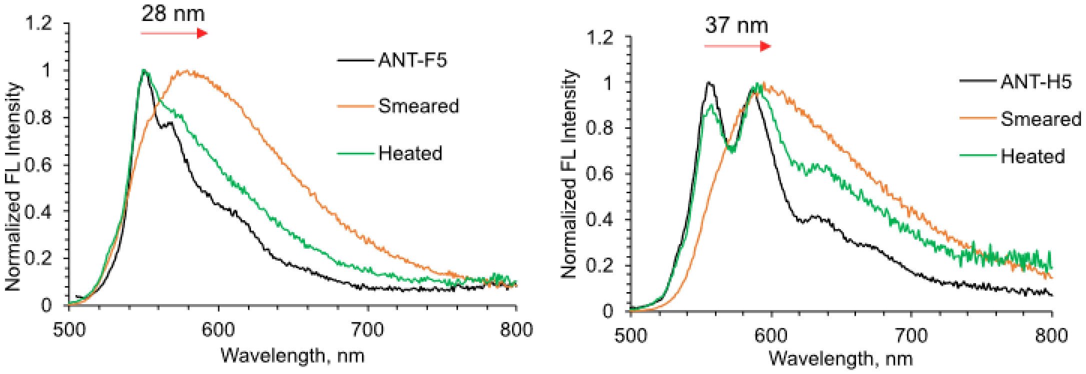

Figure 4.9: Mechanochromism of drop-cast films of ANT-F5(left) and ANT-H5(right), displayed by emission spectra.

4.7 Conclusion

In this work, we have successfully altered the stacking of acenes by intentionally introducing a non-covalent interaction, namely, ArF-ArH interaction. Compared with the non-fluorinated molecules, the ArF version of the acenes has very similar photophysical properties to their counterparts in solutions. However, the solid state properties are very different, such as a 40 nm blue-shifting in emission for **ANT-F5** films. Also, the crystals of developed acenes are grown and characterized by XRD, which provides direct evidence of impact on ArF-ArH interactions. We believe this work could inspire further research for organic electronic materials, and the development of organic electronic devices based on materials in this work is still ongoing.

4.8 Experimental section

General Information. All synthetic manipulations were performed under standard air-free conditions under an atmosphere of argon gas with magnetic stirring unless otherwise mentioned. Flash chromatography was performed using silica gel (230−400 mesh) as the stationary phase. NMR spectra were acquired on a 500 MHz spectrometer. Chemical shifts are reported relative to residual protonated solvent (7.26 ppm for $CHCl_3$ or 3.58 ppm for THF.

Electronic absorbance spectra were acquired with a spectrophotometer in double-beam mode using a solvent-containing cuvette for background subtraction spectra. Fluorescence spectra were collected at a 90° angle from the incident irradiation (75W Xe lamp) and corrected for both fluctuations in the lamp intensity, and the wavelength-dependent sensitivity of the photomultiplier tube detector Density functional theory calculations was performed using the Gaussian 09 software package[53], with optimized geometries and FMO energies determined at the B3LYP/6-31G (d,p) level of theory using a polarizable continuum solvent model for CH_2Cl_2. The time-dependent results of these optimized geometries were calculated with the same functional and basis set using the Tamm−Dancoff approximation.

Synthesis of acenes

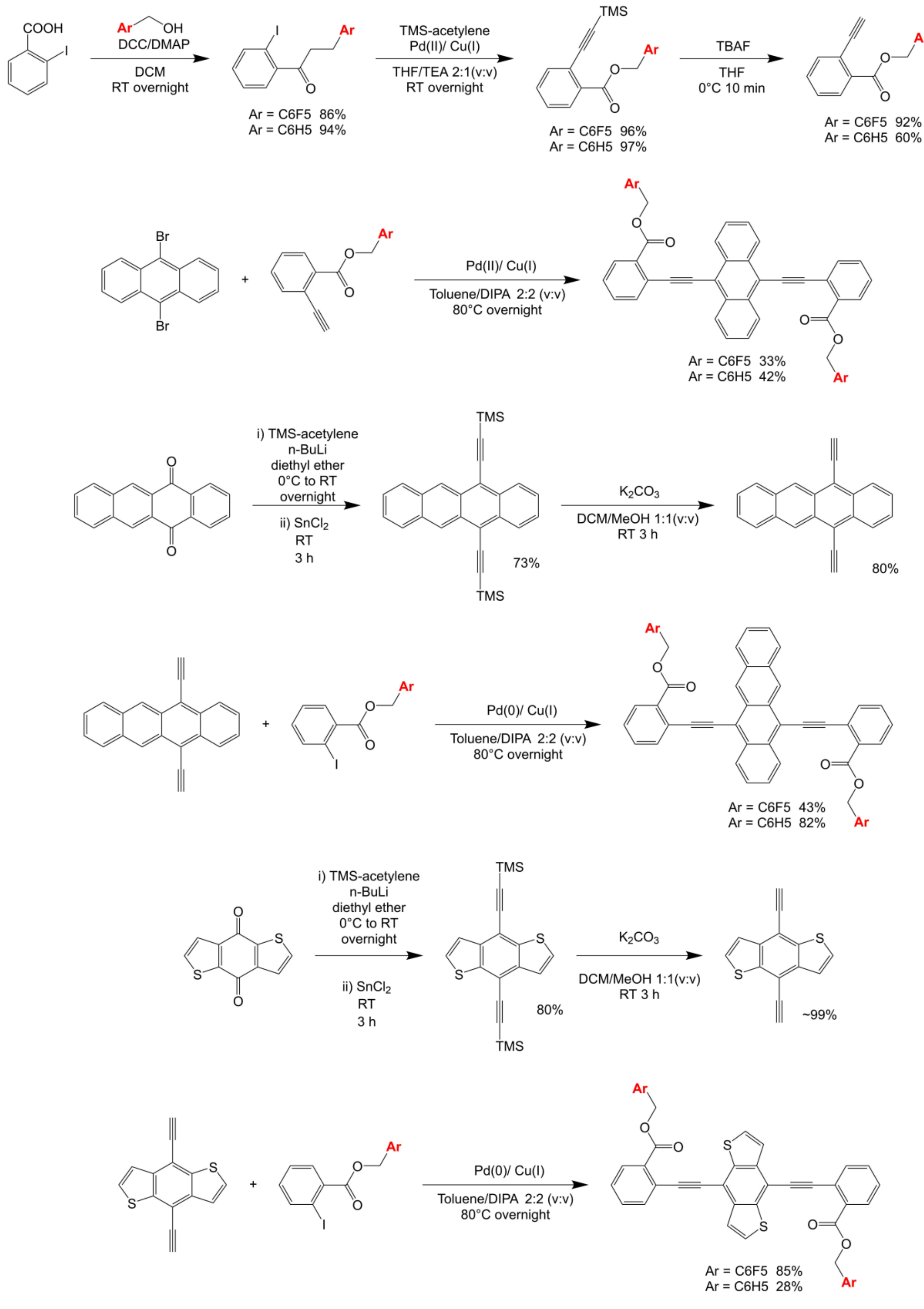

Scheme 4.3: Synthesis of developed molecules in this work.

(2,3,4,5,6-Pentafluorophenyl)methyl 2-iodobenzoate **(Y1-F5)** 2-Iodobenzoic acid (1.25 g, 5 mmol), dimethylaminopyridine (DMAP, 122mg, 1 mmol), and dicyclohexylcarbodiimide (DCC, 1.1 g 5.5 mmol) were loaded into a flame dried round bottom flask. A solution of pentafluorobenzyl alcohol (1 g 5.25 mmol) in 50 mL DCM was then added. The mixture was stirred at room temperature overnight, followed by Celite-assist filtration. The filtrate was washed with water and brine, dried over $MgSO_4$, filtered, and concentrated under a vacuum. The crude product was then purified through flash column chromatography on silica, using pure DCM as the eluent, to yield 2.00 g white solid (4.68 mmol, 93% yield).

^{1}HNMR (500 MHz, $CDCl_3$): δ 8.04-8.02 (d, 1H), 7.82-7.80 (d, 1H), 7.44-7.40 (t, 2H), 7.21-7.18 (t, 1H), 5.48 (s, 2H).

The peaks are consistent with those reported in the literature.[180]

Phenylmethyl 2-iodobenzoate **(Y1-H5)** Instead of pentafluorobenzyl alcohol, the reaction was carried out with benzyl alcohol under the same conditions. Then, the reaction was worked up via the same procedure to afford 1.6 g of a colorless oil. (4.7 mmol 94% yield).

^{1}HNMR: (500 MHz, $CDCl_3$): δ 8.02 (d, 1H), 8.01 (d, 1H), 7.50 (d ,2H), 7.44-7.40 (m, 4H), 7.18-7.15 (t, 1H), 5.40 (s, 2H).

The peaks are consistent with those reported in the literature.[180]

(2,3,4,5,6-Pentafluorophenyl)methyl 2-[2-(trimethylsilyl)ethynyl]benzoate **(Y2-F5)** Y1-F5 (850 mg, 2 mmol) was dissolved in 15 mL of THF/TEA mixture (2: 1,v: v). The solution was degassed by bubbling argon through for 30 minutes. Then, trimethylsilyl acetylene (300 mg, 3 mmol), Bis(triphenylphosphine)palladium(II) dichloride (70 mg 0.1 mmol), and copper(I) iodide (19 mg, 0.1 mmol) were added into the flask. The reaction was then heated up to 80°C and stirred overnight. The solvent was removed by rotatory evaporation. The crude product was purified via column chromatography using dichloromethane as an eluent. 765 mg of brown oil was collected (1.9 mmol, 96%yield)

^{1}HNMR (500 MHz, $CDCl_3$): δ 7.90-7.88 (d, 1H), 7.62-7.60 (d, 1H), 7.48-7.47 (t, 2H), 7.39-7.37 (t, 1H), 5.47 (s, 2H), 0.28 (s, 9H).

The peaks are consistent with those reported in the literature.[180]

Phenylmethyl 2-[2-(trimethylsilyl)ethynyl]benzoate **(Y2-H5) Y1-H5** (490 mg, 1.5 mmol) was subjected to Sonogashira Coupling and followed the same procedure for **Y1-F5**. 451 mg of black oil was collected (1.45 mol 97% yield)

^{1}HNMR (500 MHz, $CDCl_3$): δ 7.92-7.90 (d, 1H), 7.60-7.57(d, 1H), 7.47-7.30 (m, 7H), 5.38 (s, 2H), 0.22 (s, 9H).

The peaks are consistent with those reported in the literature.[180]

(2,3,4,5,6-Pentafluorophenyl)methyl 2-ethynyl benzoate **(Y3-F5) Y2-F5** (750 mg. 1.8 mmol) was dissolved in 10 mL of THF and cooled to 0°C. Tetra-n-butylammonium fluoride was added as a 1.0 M THF solution (2 mL, 2 mmol). The mixture was then stirred for 10 minutes under a cool bath. Then, the reaction was quenched by pouring into ice water. The product was extracted twice by diethyl ether, washed with brine, dried over $MgSO_4$, and concentrated by rotavap. The crude was passed through a silica plug using 1: 1 DCM/hexanes as eluent to afford 540 mg black oil as a product (1.65mmol 92%).

^{1}HNMR (500 MHz, $CDCl_3$): δ 7.95-7.93 (d, 1H), 7.66-7.64 (d, 1H), 7.54-7.50 (t, 2H), 7.45-7.41 (t, 1H), 5.48 (s, 2H), 3.38 (s, 1H).

The peaks are consistent with those reported in the literature.[180]

Phenylmethyl 2-ethynyl benzoate **(Y3-H5) Y2-H5** (450 mg 1.4 mmol) was deprotected by TBAF following the same procedure. 200 mg of black oil was collected after purification (200 mg, 60% yield)

^{1}HNMR (500 MHz, $CDCl_3$): δ 7.99 (d, 1H), 7.66-7.64(d, 1H), 7.52-7.36 (m, 7H), 5.41 (s, 2H), 3.38(s, 1H).

The peaks are consistent with those reported in the literature.[180]

ANT-F5. 9,10-dibromoanthracene (200 mg 0.6 mmol) and **Y3-F5** (540 mg 1.6 mmol) were dissolved in a 2: 1 mixture of Toluene and diisopropylamine. The solution was then degassed by freeze-pump-thaw three times. Copper(I) iodide (10 mg, 0.05 mmol) and tetrakis(triphenylphosphine)palladium(0) (30 mg, 0.03 mmol) were added. The flask was heated to 80°C and stirred overnight. The solvent was removed via rotavap, and the crude was recrystallized twice from a mixture of methanol/chloroform. 170 mg yellow powder was collected (0.2 mmol 33% yield).

^{1}HNMR (500 MHz, THF-d8): δ 8.89-8.87 (m, 4H), 8.12-8.10 (m, 2H), 8.01-7.99 (m, 2H), 7.69-7.66 (m, 6H), 7.52-7.54 (m, 2H), 5.56 (s, 4H).

Due to the low solubility of ANT-F5, the ^{13}CNMR spectrum is not accessible.,

ANT-H5. 9,10-dibromoanthracene (120 mg 0.35 mmol) and **Y3-H5** (200 mg 0.8 mmol) were dissolved in a 2: 1 mixture of Toluene and diisopropylamine. The solution was then degassed by freeze-pump-thaw three times. Copper(I) iodide (4 mg, 0.025 mmol) and tetrakis(triphenylphosphine)palladium(0) (20 mg, 0.02 mmol) were added. The flask was heated to 80°C and stirred overnight. The solvent was removed via rotavap, and the crude was purified via column chromatography with a gradient elution system from 1: 1 hexanes/DCM to pure DCM. After removing solvent via rotavap, the solid was recrystallized from hexanes/chloroform to yield 95 mg of orange needles (0.15 mmol 42% yield)

^{1}HNMR (500 MHz, $CDCl_3$): δ 8.88-8.86 (m, 4H), 8.16-8.14 (m, 2H), 7.98-7.96 (m, 2H), 7.67-7.63 (m, 6H), 7.50-7.45 (m, 6H), 7.26-7.25 (m, 6H), 5.51 (s, 4H).

^{13}C [^{1}H] NMR (125 MHz, $CDCl_3$): δ 165.9, 135.9, 134.5, 132.5, 131.9, 131.4, 130.8, 128.5, 128.2, 128.1, 127.4, 126.9, 124.2, 118.9, 101.1, 92.0, 67.1.

5,12-Bis[(trimethylsilyl)ethynyl]tetracene. The synthesis of this molecule followed the procedures reported by our group.[28] Trimethylsilyl acetylene (490 mg, 5 mmol) was dissolved in 10 mL of dry diethyl ether and the solution was cooled to 0°C via ice bath. N-butyl lithium (2 ml, 5 mmol) was slowly added as a 2.5 M solution in hexane via a syringe. The mixture was stirred for an hour under 0°C. Then, naphthacenequinone (516 mg, 2 mmol) was added as solids. The reaction was let warm to room temperature and stirred overnight, followed by quenching with 5% HCl solution. The mixture was extracted with ethyl acetate twice. To the combined organic layer, tin chloride dihydrate (1 g, 4.5mmol) was added, and the suspension was stirred for three hours until the color changed from yellow to deep red. The mixture was then washed with 5% HCl solution, water, and brine, dried over $MgSO_4$, and concentrated in *vacuo*. The crude product was purified by column chromatography with hexanes as eluent to yield 610 mg red solid (1.45 mmol, 73% yield).

^{1}**HNMR** (500 MHz, $CDCl_3$):δ 9.20 (s, 2H) 8.60−8.58 (dd, 2H), 8.11−8.10 (dd, 2H), 7.58−7.56 (dd, 2H), 7.51−7.49 (dd, 2 H), 0.50 (s, 18H).

The peaks are consistent with those reported in the literature.[28]

5,12-diethynyltetracene. 5,12-Bis[(trimethylsilyl)ethynyl]tetracene (210 mg, 0.5 mmol) was dissolved in a 1: 1 mixture of methanol and dichloromethane. Potassium carbonate (170 mg, 1.25 mmol) was added to the flask as a solid. The reaction was stirred for three hours, followed by washing with 5% HCl, water, and brine successively, dried over $MgSO_4$, and the solvent was removed by rotavap. 110 mg of red solid was collected. (0.4 mmol, 80% yield) The product was directly added to the next step due to the low stability.

^{1}**HNMR** (500 MHz, $CDCl_3$): δ 9.26 (s, 2H) 8.64−8.62 (dd, 2H), 8.12−8.10 (dd, 2H), 7.59−7.57 (dd, 2H), 7.52−7.49 (dd, 2H), 4.25 (s, 2H).

The peaks are consistent with those reported in the literature.[28]

TET-F5. 5,12-diethynyltetracene (110 mg, 0.4 mmol) and Y1-F5 (430 mg, 1 mmol) were dissolved in a 2: 1 mixture of Toluene and diisopropylamine. The solution was then degassed by freeze-pump-thaw three times. Copper(I) iodide (5 mg, 0.025 mmol) and tetrakis(triphenylphosphine)palladium(0) (25 mg, 0.025 mmol) were added. The flask was heated to 80°C and stirred overnight. The solvent was removed by rotary evaporation and the residue was passed through a column with DCM/hexanes (1: 1, v: v) as eluent. The crude product was then recrystallized from chloroform/hexanes and THF/hexanes to afford 150 mg purple solid. (0.17 mmol, 43% yield)

^{1}**HNMR** (500 MHz, $CDCl_3$): δ 9.50 (s, 2H) 8.78−8.76 (dd, 2H), 8.20−8.16 (m, 4H), 8.04−8.02 (d, 2H), 7.72−7.69 (t, 2H), 7.64−7.62 (dd, 2H), 7.55−7.52 (m, 4H), 5.56 (s, 4H).

Due to the low solubility of TET-F5, the ^{13}CNMR spectrum is not accessible.,

TET-H5. 5,12-diethynyltetracene (110 mg, 0.4 mmol) and Y1-H5 (337 mg, 1 mmol) were dissolved in a 2: 1 mixture of Toluene and diisopropylamine. The solution was then degassed by freeze-pump-thaw three times. Copper(I) iodide (5 mg, 0.025 mmol) and tetrakis(triphenylphosphine)palladium(0) (25 mg, 0.025 mmol) were added. The flask was heated to 80°C and stirred overnight. The solvent was removed by rotary evaporation, and the residue was passed through a column with DCM/hexanes (1: 1, v: v) as eluent. The crude product was then recrystallized from chloroform/hexanes to afford 230 mg purple solid. (0.33 mmol, 82% yield)

^{1}**HNMR** (500 MHz, $CDCl_3$): δ 9.61 (s, 2H) 8.84−8.82 (dd, 2H), 8.18−8.15 (m, 4H), 8.02−8.00 (d, 2H), 7.66−7.59 (t, 2H), 7.59−7.57 (m, 2H), 7.50−7.44 (m, 8H), 7.23−7.21 (m, 6H), 5.53 (s, 4H).

^{13}C [^{1}H] NMR (125 MHz, $CDCl_3$): δ 165.9, 135.9, 134.5, 132.8, 132.5, 132.0, 131., 130.9, 130.4, 128.8, 128.5, 128.3, 128.2, 128.2, 127.5, 126.7, 126.5, 125.9, 124.4, 118.9, 102.1, 92.7, 67.1.

*4,8-Bis[2-(trimethylsilyl)ethynyl]benzo[1,2-*b*:4,5-*b*']dithiophene.* Trimethylsilyl acetylene (490 mg, 5 mmol) was dissolved in 20 mL of dry diethyl ether in a flame-dried round bottom flask. The solution was cooled by an ice-water bath. To the flask, n-butyl lithium was added as a 2.5 M hexane solution (2 mL, 5 mmol) dropwise. The mixture was stirred under a cold bath for one hour, followed by adding benzo[1,2-*b*:4,5-*b′*]dithiophene-4,8-dione (440 mg, 2 mmol) as a solid. The mixture was then let to warm up to room temperature and stirred overnight. The reaction was quenched with 5% HCl aqueous solution. The product was extracted with ethyl acetate twice, washed with water and brine, and dried over magnesium sulfate. Tin chloride dihydride (1g, 4.5 mmol) was added to the organic solution. The suspension was stirred for three hours before being washed by diluted HCl solution, water, and brine, dried over $MgSO_4$, and concentrated *in vacuo*. The residue was purified by a gradient column using 0% to 100% DCM in hexanes as the eluent system. 620 mg of yellow powder was collected as the product (1.6 mmol 80% yield)

^{1}HNMR (500 MHz, $CDCl_3$): δ 7.63-7.61(d, 2H), 7.58-7.56 (d, 2H), 0.38 (s, 18H).

The peaks are consistent with those reported in the literature.[188]

4,8-Diethynylbenzo[1,2-*b*:4,5-*b*′]dithiophene4,8-Bis[2-(trimethylsilyl)ethynyl]-benzo[1,2-*b*:4,5-*b*′]dithiophene (230 mg, 0.6 mmol) and potassium carbonate (200 mg, 1.5 mmol) was added to a round bottom flask. 20 mL of 1: 1 mixture of dichloromethane and methanol was added to the flask, and the suspension was stirred for three hours at room temperature. The product was then extracted by DCM twice. The combined organic layer was washed with diluted HCl solution, dried over magnesium sulfate, and concentrated *in vacuo* to afford 140 mg of yellow powder. (0.6 mmol, 99% yield) The product was directly added to the next step without any further purification.

^{1}HNMR (500 MHz, $CDCl_3$): δ 7.66-7.64(d, 2H), 7.61-7.60 (d, 2H), 3.87 (s, 2H).

The peaks are consistent with those reported in the literature.[189]

cBDT-F5. 4,8-Diethynylbenzo[1,2-*b*:4,5-*b*′]dithiophene (140 mg, 0.6 mmol) and Y1-F5 (640 mg, 1.5 mmol) was dissolved in a 2: 1 mixture of Toluene and diisopropylamine. The solution was then degassed by bubbling argon for one hour. Copper(I) iodide (6 mg, 0.03 mmol) and tetrakis(triphenylphosphine)palladium(0) (35 mg, 0.03 mmol) were added. The flask was heated to 80°C and stirred overnight. The solvent was removed by rotary evaporation and the residue recrystallized from chloroform/methanol and hexanes to afford 427 mg yellow solid (0.5 mmol, 85% yield).

^{1}HNMR (500 MHz, $CDCl_3$): δ 8.10-8.08 (d, 2H), 7.89-7.87 (m, 4H), 7.87-7.85 (m, 4H), 7.65-7.64 (t, 2H), 5.53 (s, 4H).

Due to the low solubility of cBDT-F5, the ^{13}CNMR spectrum is not accessible.

cBDT-H5. 4,8-Diethynylbenzo[1,2-*b*:4,5-*b′*]dithiophene (140 mg, 0.6 mmol) and Y1-H5 (507 mg, 1.5 mmol) was dissolved in a 2: 1 mixture of Toluene and diisopropylamine. The solution was then degassed by bubbling argon for one hour. Copper(I) iodide (6 mg, 0.03 mmol) and tetrakis(triphenylphosphine)palladium(0) (35 mg, 0.03 mmol) were added. The reaction was refluxed for one hour and stirred overnight at room temperature. The solvent was removed by rotary evaporation and the residue recrystallized from chloroform/methanol and hexanes to afford 110 mg yellow solid (0.17 mmol, 28% yield).

^{1}HNMR: (500 MHz, $CDCl_3$): δ 8.10-8.08 (d, 2H), 7.90-7.86 (m, 4H), 7.62-7.59 (m, 4H), 7.49-7.45 (m, 6H), 7.29-7.26 (m, 6H), 5.49 (s, 4H).

^{13}C [^{1}H] NMR (125 MHz, $CDCl_3$): δ 165.7, 140.6, 138.9, 135.9, 134.5, 131.9, 130.7, 128.5, 128.4, 128.3, 128.1, 123.6, 112.3, 98.0, 90.8, 67.1

References

(1) Anthony, J. E. Functionalized acenes and heteroacenes for organic electronics. *Chemical Reviews* 2006, *106* (12), 5028-5048. DOI: 10.1021/cr050966z.

(2) Anthony, J. E. The larger acenes: Versatile organic semiconductors. *Angewandte Chemie-International Edition* 2008, *47* (3), 452-483. DOI: 10.1002/anie.200604045.

(3) Anthony, J. E.; Brooks, J. S.; Eaton, D. L.; Parkin, S. R. Functionalized pentacene: Improved electronic properties from control of solid-state order. *Journal of the American Chemical Society* 2001, *123* (38), 9482-9483. DOI: 10.1021/ja0162459.

(4) Chen, J. H.; Martin, D. C.; Anthony, J. E. Morphology and molecular orientation of thin-film bis(triisopropylsilylethynyl) pentacene. *Journal of Materials Research* 2007, *22* (6), 1701-1709. DOI: 10.1557/jmr.2007.0220.

(5) Wang, C. L.; Dong, H. L.; Hu, W. P.; Liu, Y. Q.; Zhu, D. B. Semiconducting pi-Conjugated Systems in Field-Effect Transistors: A Material Odyssey of Organic Electronics. *Chemical Reviews* 2012, *112* (4), 2208-2267. DOI: 10.1021/cr100380z.

(6) Matsui, H.; Takeda, Y.; Tokito, S. Flexible and printed organic transistors: From materials to integrated circuits. *Organic Electronics* 2019, *75*. DOI: ARTN 105432 10.1016/j.orgel.2019.105432.

(7) Henson, Z. B.; Müllen, K.; Bazan, G. C. Design strategies for organic semiconductors beyond the molecular formula. *Nature Chemistry* 2012, *4* (9), 699-704. DOI: 10.1038/nchem.1422 (acccessed 2023-06-26T14:01:57).

(8) Sharber, S. A.; Mullin, W. J.; Thomas, S. W. Bridging the Void: Halogen Bonding and Aromatic Interactions to Program Luminescence and Electronic Properties of π-Conjugated Materials in the Solid State. *Chemistry of Materials* 2021, *33* (17), 6640-6661. DOI: 10.1021/acs.chemmater.1c01969 (acccessed 2022-11-28T21:02:45).

(9) Mullin, W. J.; Sharber, S. A.; Thomas, S. W. Optimizing the self-assembly of conjugated polymers and small molecules through structurally programmed non-covalent control. *Journal of Polymer Science* 2021, *59* (15), 1643-1663. DOI: 10.1002/pol.20210290.

(10) Ma, S.; Du, S.; Pan, G.; Dai, S.; Xu, B.; Tian, W. Organic molecular aggregates: From aggregation structure to emission property. *Aggregate* 2021, *2* (4). DOI: 10.1002/agt2.96.

(11) Sharber, S. A.; Thomas, S. W., 3rd. Small Changes With Big Consequences: Swapping Two Atoms In Side Chains Changes Phenylene-Ethynylene Packing And Fluorescence. *Chemistry* 2018, *24* (64), 16987-16991. DOI: 10.1002/chem.201804648 From NLM PubMed-not-MEDLINE.

(12) Dou, J.-H.; Zheng, Y.-Q.; Yao, Z.-F.; Yu, Z.-A.; Lei, T.; Shen, X.; Luo, X.-Y.; Sun, J.; Zhang, S.-D.; Ding, Y.-F.; et al. Fine-Tuning of Crystal Packing and Charge Transport Properties of BDOPV Derivatives through Fluorine Substitution. *Journal of the American*

Chemical Society 2015, *137* (50), 15947-15956. DOI: 10.1021/jacs.5b11114 (acccessed 2023-06-26T14:04:44).

(13) Yao, Z.-F.; Wang, J.-Y.; Pei, J. Control of π–π Stacking via Crystal Engineering in Organic Conjugated Small Molecule Crystals. *Crystal Growth & Design* 2018, *18* (1), 7-15. DOI: 10.1021/acs.cgd.7b01385 (acccessed 2023-06-26T14:08:25).

(14) Pawle, R. H.; Haas, T. E.; Müller, P.; Thomas Iii, S. W. Twisting and piezochromism of phenylene-ethynylenes with aromatic interactions between side chains and main chains. *Chem. Sci.* 2014, *5* (11), 4184-4188. DOI: 10.1039/c4sc01466a.

(15) Wheeler, S. E.; Houk, K. N. Substituent Effects in the Benzene Dimer are Due to Direct Interactions of the Substituents with the Unsubstituted Benzene. *Journal of the American Chemical Society* 2008, *130* (33), 10854-10855. DOI: 10.1021/ja802849j (acccessed 2023-06-26T15:05:05).

(16) Wheeler, S. E. Local Nature of Substituent Effects in Stacking Interactions. *Journal of the American Chemical Society* 2011, *133* (26), 10262-10274. DOI: 10.1021/ja202932e (acccessed 2023-06-26T15:09:47).

(17) Sharber, S. A.; Baral, R. N.; Frausto, F.; Haas, T. E.; Muller, P.; Thomas Iii, S. W. Substituent Effects That Control Conjugated Oligomer Conformation through Non-covalent Interactions. *J Am Chem Soc* 2017, *139* (14), 5164-5174. DOI: 10.1021/jacs.7b00878 From NLM PubMed-not-MEDLINE.

(18) Mullin, W. J.; Pawle, R. H.; Sharber, S. A.; Müller, P.; Thomas, S. W. Programmed twisting of phenylene–ethynylene linkages from aromatic stacking interactions. *Journal of Materials Chemistry C* 2019, *7* (5), 1198-1207. DOI: 10.1039/c8tc05612a.

(19) Mullin, W. J.; Qin, H.; Mani, T.; Muller, P.; Panzer, M. J.; Thomas, S. W. Turning on solid-state phosphorescence of platinum acetylides with aromatic stacking. *Chem Commun (Camb)* 2020, *56* (50), 6854-6857. DOI: 10.1039/d0cc02119a From NLM PubMed-not-MEDLINE.

(20) Mullin, W. J.; Müller, P.; Schaefer, A. J.; Guzman, E.; Wheeler, S. E.; Thomas Iii, S. W. Crystal engineering of heterocyclic arylene(ethynylene) oligomers through programmed aromatic stacking. *Journal of Materials Chemistry C* 2022, *10* (31), 11199-11210. DOI: 10.1039/d2tc01292h (acccessed 2022-11-28T20:54:48).

(21) Frisch, M. J.; Trucks, G. W.; Schlegel, H. B.; Scuseria, G. E.; Robb, M. A.; Cheeseman, J. R.; Scalmani, G.; Barone, V.; Petersson, G. A.; Nakatsuji, H.; Li, X.; Caricato, M.; Marenich, A.; Bloino, J.; Janesko, B. G.; Gomperts, R.; Mennucci, B.; Hratchian, H. P.; Ortiz, J. V.; Izmaylov, A. F.; Sonnenberg, J. L.; Williams-Young, D.; Ding, F.; Lipparini, F.; Egidi, F.; Goings, J.; Peng, B.; Petrone, A.; Henderson, T.; Ranasinghe, D.; Zakrzewski, V. G.; Gao, J.; Rega, N.; Zheng, G.; Liang, W.; Hada, M.; Ehara, M.; Toyota, K.; Fukuda, R.;

Hasegawa, J.; Ishida, M.; Nakajima, T.; Honda, Y.; Kitao, O.; Nakai, H.; Vreven, T.; Throssell, K.; Montgomery, J. A., Jr.; Peralta, J. E.; Ogliaro, F.; Bearpark, M. J.; Heyd, J. J.; Brothers, E. N.; Kudin, K. N.; Staroverov, V. N.; Keith, T. A.; Kobayashi, R.; Normand, J.; Raghavachari, K.; Rendell, A. P.; Burant, J. C.; Iyengar, S. S.; Tomasi, J.; Cossi, M.; Millam, J. M.; Klene, M.; Adamo, C.; Cammi, R.; Ochterski, J. W.; Martin, R. L.; Morokuma, K.; Farkas, O.; Foresman, J. B.; Fox, D. J. Gaussian 09, Revision D.01; Gaussian, Inc.: Wallingford CT, 2016.Frisch, MJEA

(22) Sharber, S. A.; Thomas, S. W. Side Chain Regioisomers that Dictate Optical Properties and Mechanofluorochromism through Crystal Packing. *Chemistry of Materials* 2020, *32* (13), 5785-5801. DOI: 10.1021/acs.chemmater.0c01676.

(23) Sharber, S. A.; Mann, A.; Shih, K. C.; Mullin, W. J.; Nieh, M. P.; Thomas, S. W., 3rd. Directed Polymorphism and Mechanofluorochromism of Conjugated Materials through Weak Non-Covalent Control. *J Mater Chem C Mater* 2019, *7* (27), 8316-8324. DOI: 10.1039/c9tc01301f From NLM PubMed-not-MEDLINE.

(24) Dong, Y.; Xu, B.; Zhang, J.; Tan, X.; Wang, L.; Chen, J.; Lv, H.; Wen, S.; Li, B.; Ye, L.; et al. Piezochromic Luminescence Based on the Molecular Aggregation of 9,10-Bis((<i>E</i>)-2-(pyrid-2-yl)vinyl)anthracene. *Angewandte Chemie International Edition* 2012, *51* (43), 10782-10785. DOI: 10.1002/anie.201204660 (acccessed 2023-07-03T22:55:45).

(25) Yan, L.; Zhao, Y.; Yu, H.; Hu, Z.; He, Y.; Li, A.; Goto, O.; Yan, C.; Chen, T.; Chen, R.; et al. Influence of heteroatoms on the charge mobility of anthracene derivatives. *Journal of Materials Chemistry C* 2016, *4* (16), 3517-3522. DOI: 10.1039/c6tc01088a (acccessed 2023-07-03T22:58:45).

(26) Hisamatsu, S.; Masu, H.; Takahashi, M.; Kishikawa, K.; Kohmoto, S. Pairwise Packing of Anthracene Fluorophore: Hydrogen-Bonding-Assisted Dimer Emission in Solid State. *Crystal Growth & Design* 2015, *15* (5), 2291-2302. DOI: 10.1021/acs.cgd.5b00081 (acccessed 2023-07-03T22:59:49).

(27) Curtis, M. D.; Cao, J.; Kampf, J. W. Solid-state packing of conjugated oligomers: from pi-stacks to the herringbone structure. *J Am Chem Soc* 2004, *126* (13), 4318-4328. DOI: 10.1021/ja0397916 From NLM PubMed-not-MEDLINE.

(28) Yan, Y.; Lamport, Z. A.; Kymissis, I.; Thomas, S. W., 3rd. Resistance to Unwanted Photo-Oxidation of Multi-Acene Molecules. *J Org Chem* 2020, *85* (19), 12731-12739. DOI: 10.1021/acs.joc.0c01890 From NLM PubMed-not-MEDLINE.

(29) Wang, Y.; Parkin, S. R.; Watson, M. D. Benzodichalcogenophenes with Perfluoroarene Termini. *Organic Letters* 2008, *10* (20), 4421-4424. DOI: 10.1021/ol801569m.

(30) Zhu, E.; Ge, G.; Shu, J.; Yi, M.; Bian, L.; Hai, J.; Yu, J.; Liu, Y.; Zhou, J.; Tang, W.

Direct access to 4,8-functionalized benzo[1,2-b:4,5-b′]dithiophenes with deep low-lying HOMO levels and high mobilities. *J. Mater. Chem. A* 2014, *2* (33), 13580-13586. DOI: 10.1039/c4ta01226g.

Chapter 4 Appendix

Crystal structure of cBDTs

Theoretical calculation results

NMR spectra

Crystal structures of cBDT-F5 and cBDT-H5

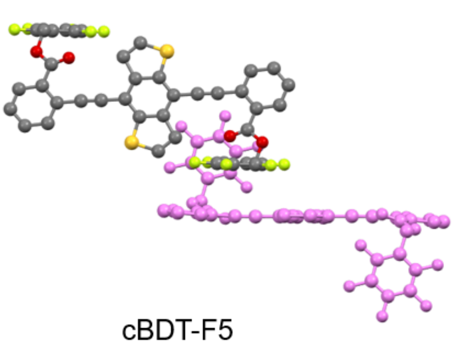

cBDT-F5

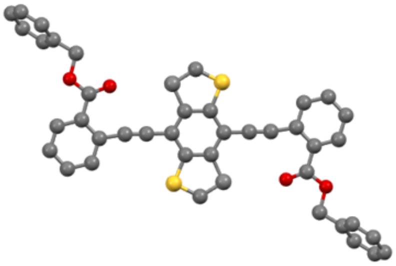

cBDT-H5

Calculated FMOs for cBDTs and TETs

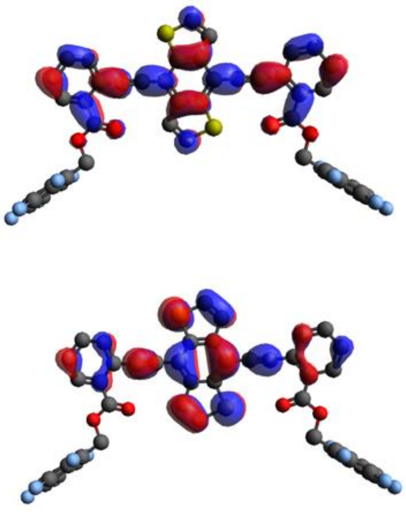

cBDT-F5

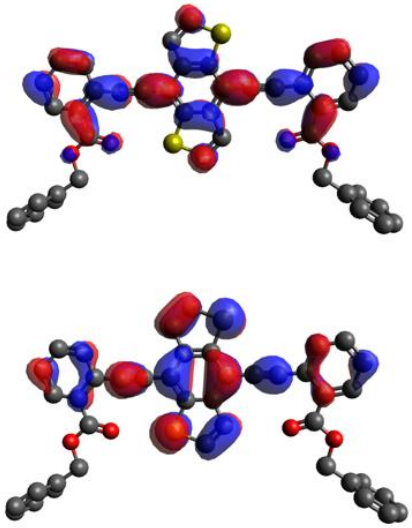

cBDT-H5

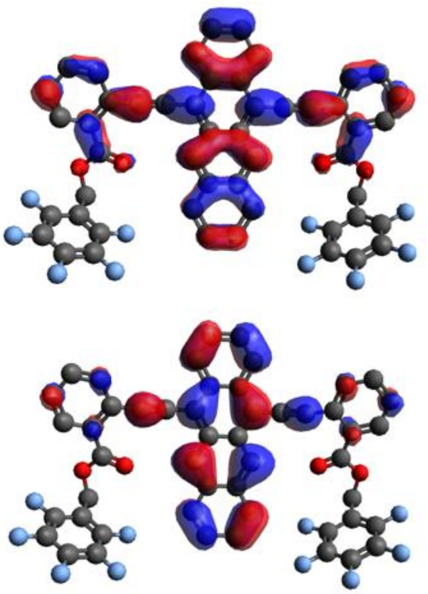

TET-F5

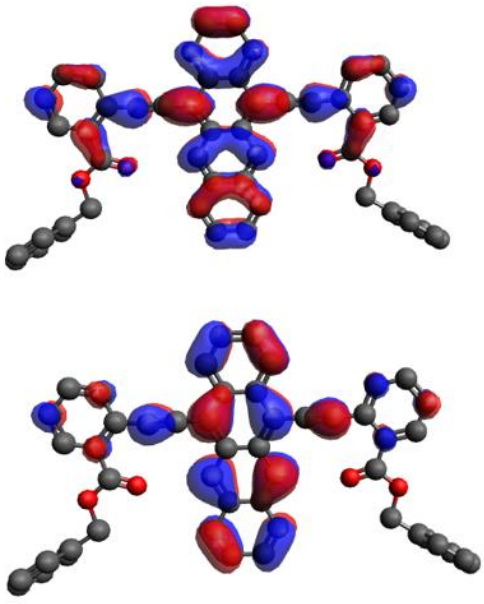

TET-H5

NMR Spectra

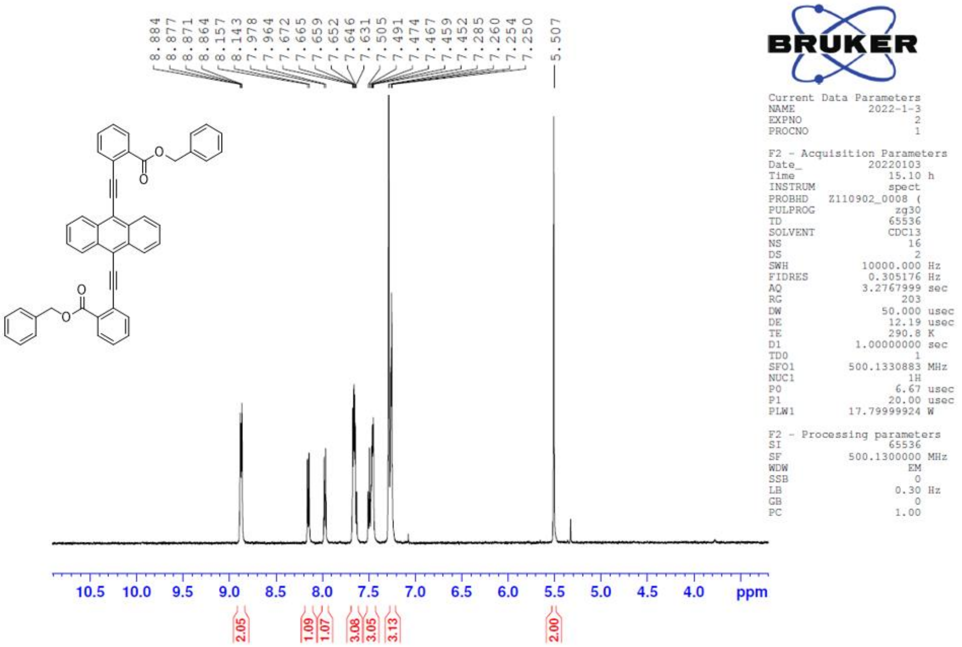

```
Current Data Parameters
NAME            2022-1-3
EXPNO                  2
PROCNO                 1

F2 - Acquisition Parameters
Date_           20220103
Time               15.10 h
INSTRUM            spect
PROBHD   Z110902_0008 (
PULPROG             zg30
TD                 65536
SOLVENT            CDC13
NS                    16
DS                     2
SWH            10000.000 Hz
FIDRES          0.305176 Hz
AQ             3.2767999 sec
RG                   203
DW                50.000 usec
DE                 12.19 usec
TE                 290.8 K
D1            1.00000000 sec
TD0                    1
SFO1         500.1330883 MHz
NUC1                  1H
P0                  6.67 usec
P1                 20.00 usec
PLW1         17.79999924 W

F2 - Processing parameters
SI                 65536
SF           500.1300000 MHz
WDW                   EM
SSB                    0
LB                  0.30 Hz
GB                     0
PC                  1.00
```

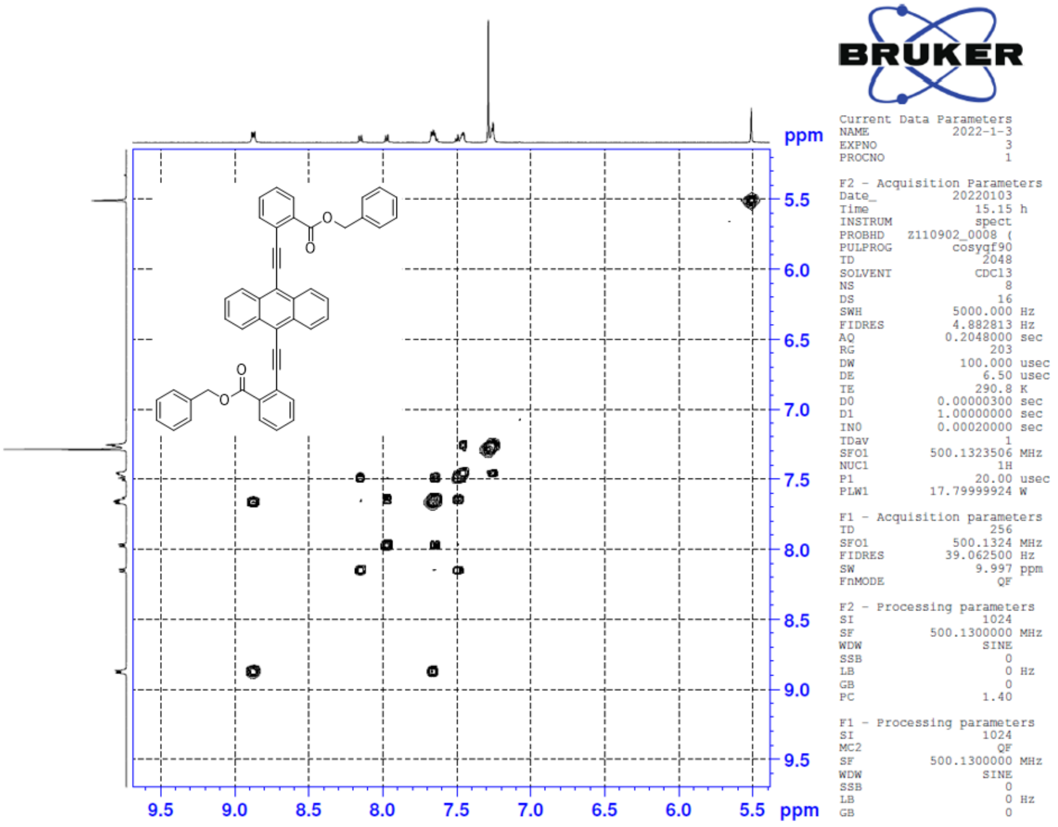

```
Current Data Parameters
NAME            2022-1-3
EXPNO                  3
PROCNO                 1

F2 - Acquisition Parameters
Date_           20220103
Time               15.15 h
INSTRUM            spect
PROBHD   Z110902_0008 (
PULPROG         cosygf90
TD                  2048
SOLVENT            CDC13
NS                     8
DS                    16
SWH             5000.000 Hz
FIDRES          4.882813 Hz
AQ             0.2048000 sec
RG                   203
DW               100.000 usec
DE                  6.50 usec
TE                 290.8 K
D0            0.00000300 sec
D1            1.00000000 sec
IN0           0.00020000 sec
TDav                   1
SFO1         500.1323506 MHz
NUC1                  1H
P1                 20.00 usec
PLW1         17.79999924 W

F1 - Acquisition parameters
TD                   256
SFO1            500.1324 MHz
FIDRES         39.062500 Hz
SW                 9.997 ppm
FnMODE                QF

F2 - Processing parameters
SI                  1024
SF           500.1300000 MHz
WDW                 SINE
SSB                    0
LB                     0 Hz
GB                     0
PC                  1.40

F1 - Processing parameters
SI                  1024
MC2                   QF
SF           500.1300000 MHz
WDW                 SINE
SSB                    0
LB                     0 Hz
GB                     0
```

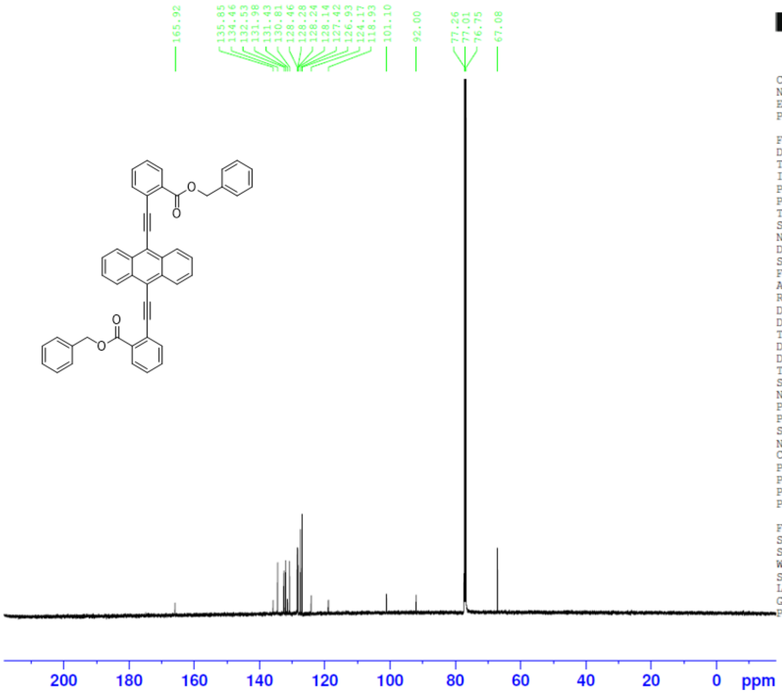

```
Current Data Parameters
NAME          2022-1-20
EXPNO                 3
PROCNO                1

F2 - Acquisition Parameters
Date_          20220121
Time               6.51 h
INSTRUM           spect
PROBHD   Z110902_0008 (
PULPROG            zgpg
TD                65536
SOLVENT           CDCl3
NS                14476
DS                    4
SWH           29761.904 Hz
FIDRES         0.908261 Hz
AQ            1.1010048 sec
RG                  203
DW               16.800 usec
DE                 6.50 usec
TE                292.7 K
D1           2.00000000 sec
D11          0.03000000 sec
TD0                  50
SFO1        125.7703643 MHz
NUC1                13C
P1                 9.50 usec
PLW1        91.40000153 W
SFO2        500.1320005 MHz
NUC2                 1H
CPDPRG[2        waltz65
PCPD2             80.00 usec
PLW2        17.79999924 W
PLW12        1.11249995 W
PLW13        0.55958003 W

F2 - Processing parameters
SI                32768
SF          125.7577890 MHz
WDW                  EM
SSB                   0
LB                 1.00 Hz
GB                    0
PC                 1.40
```

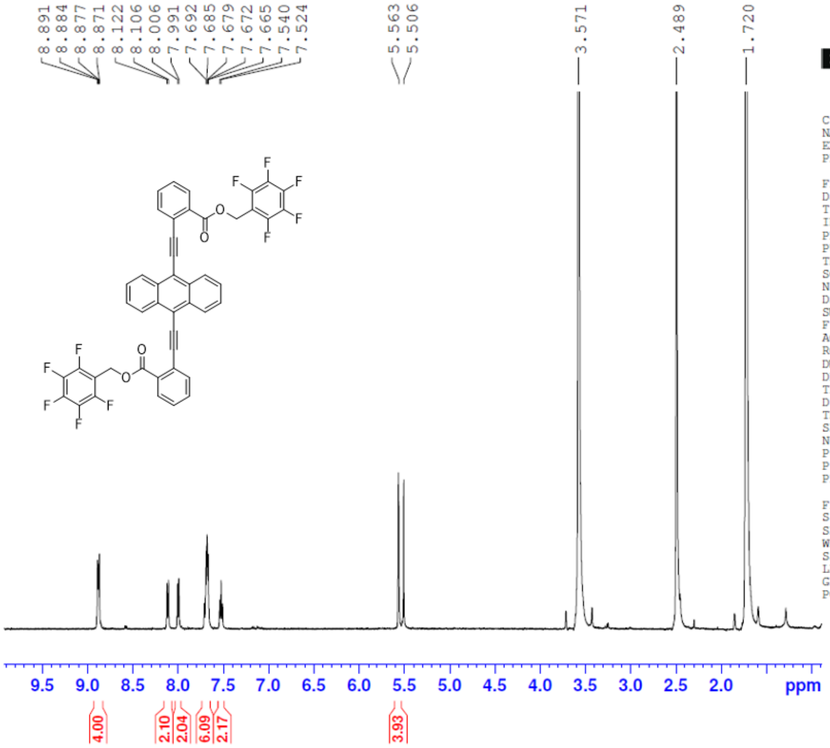

```
Current Data Parameters
NAME          2022-1-13
EXPNO                 4
PROCNO                1

F2 - Acquisition Parameters
Date_          20220113
Time              17.11 h
INSTRUM           spect
PROBHD   Z110902_0008 (
PULPROG            zg30
TD                65536
SOLVENT             THF
NS                   16
DS                    2
SWH           10000.000 Hz
FIDRES         0.305176 Hz
AQ            3.2767999 sec
RG                  203
DW               50.000 usec
DE                12.19 usec
TE                291.0 K
D1           1.00000000 sec
TD0                   1
SFO1        500.1330883 MHz
NUC1                 1H
P0                 6.67 usec
P1                20.00 usec
PLW1        17.79999924 W

F2 - Processing parameters
SI                65536
SF          500.1290934 MHz
WDW                  EM
SSB                   0
LB                 0.30 Hz
GB                    0
PC                 1.00
```

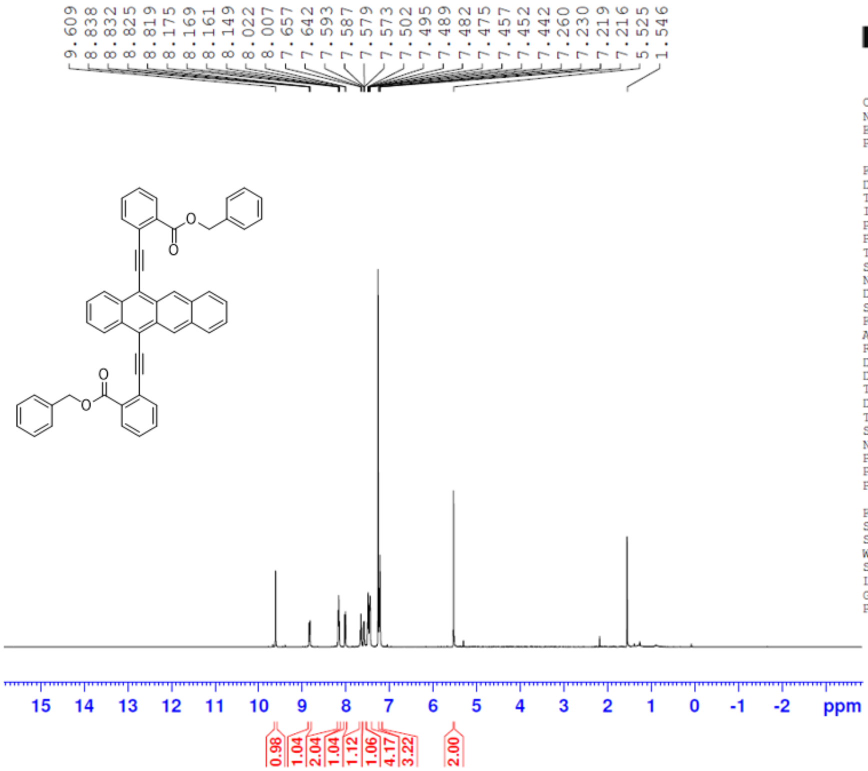

```
Current Data Parameters
NAME              2022-2-3
EXPNO                    1
PROCNO                   1

F2 - Acquisition Parameters
Date_             20220203
Time                 17.02 h
INSTRUM              spect
PROBHD   Z110902_0008 (
PULPROG               zg30
TD                   65536
SOLVENT              CDCl3
NS                      16
DS                       2
SWH              10000.000 Hz
FIDRES            0.305176 Hz
AQ               3.2767999 sec
RG                     203
DW                  50.000 usec
DE                   12.19 usec
TE                   291.1 K
D1              1.00000000 sec
TD0                      1
SFO1           500.1330883 MHz
NUC1                    1H
P0                    6.67 usec
P1                   20.00 usec
PLW1           17.79999924 W

F2 - Processing parameters
SI                   65536
SF             500.1300123 MHz
WDW                     EM
SSB                      0
LB                    0.30 Hz
GB                       0
PC                    1.00
```

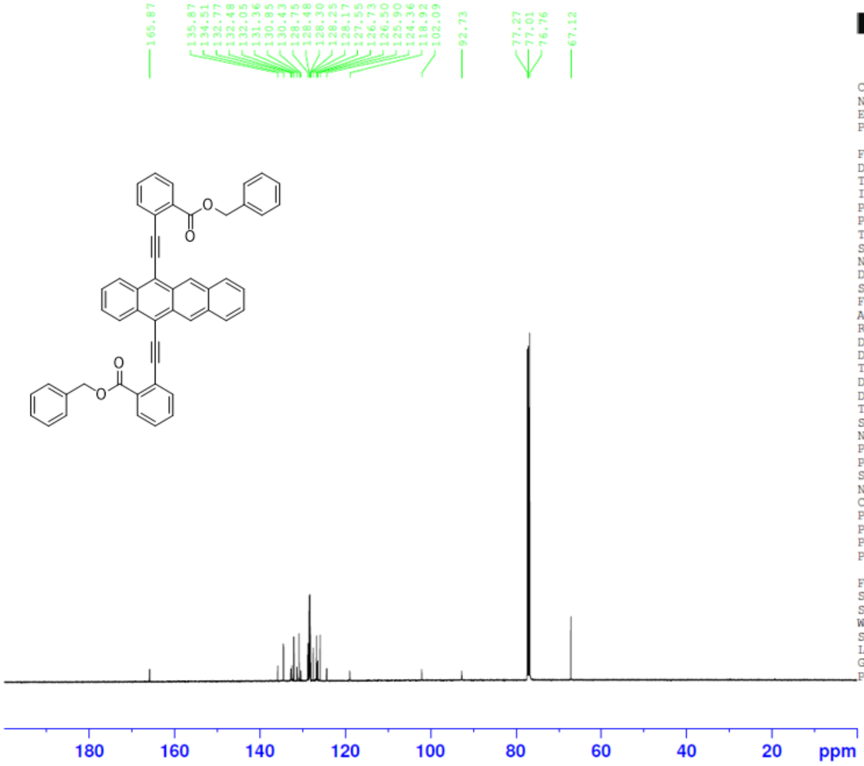

```
Current Data Parameters
NAME              2022-2-8
EXPNO                    9
PROCNO                   1

F2 - Acquisition Parameters
Date_             20220209
Time                  8.17 h
INSTRUM              spect
PROBHD   Z110902_0008 (
PULPROG               zgpg
TD                   65536
SOLVENT              CDCl3
NS                   14102
DS                       4
SWH              29761.904 Hz
FIDRES            0.908261 Hz
AQ               1.1010048 sec
RG                     203
DW                  16.800 usec
DE                    6.50 usec
TE                   292.4 K
D1              2.00000000 sec
D11             0.03000000 sec
TD0                    100
SFO1           125.7703643 MHz
NUC1                   13C
P1                    9.50 usec
PLW1           91.40000153 W
SFO2           500.1320005 MHz
NUC2                    1H
CPDPRG[2           waltz65
PCPD2                80.00 usec
PLW2           17.79999924 W
PLW12           1.11249995 W
PLW13           0.55958003 W

F2 - Processing parameters
SI                   32768
SF             125.7577890 MHz
WDW                     EM
SSB                      0
LB                    1.00 Hz
GB                       0
PC                    1.40
```

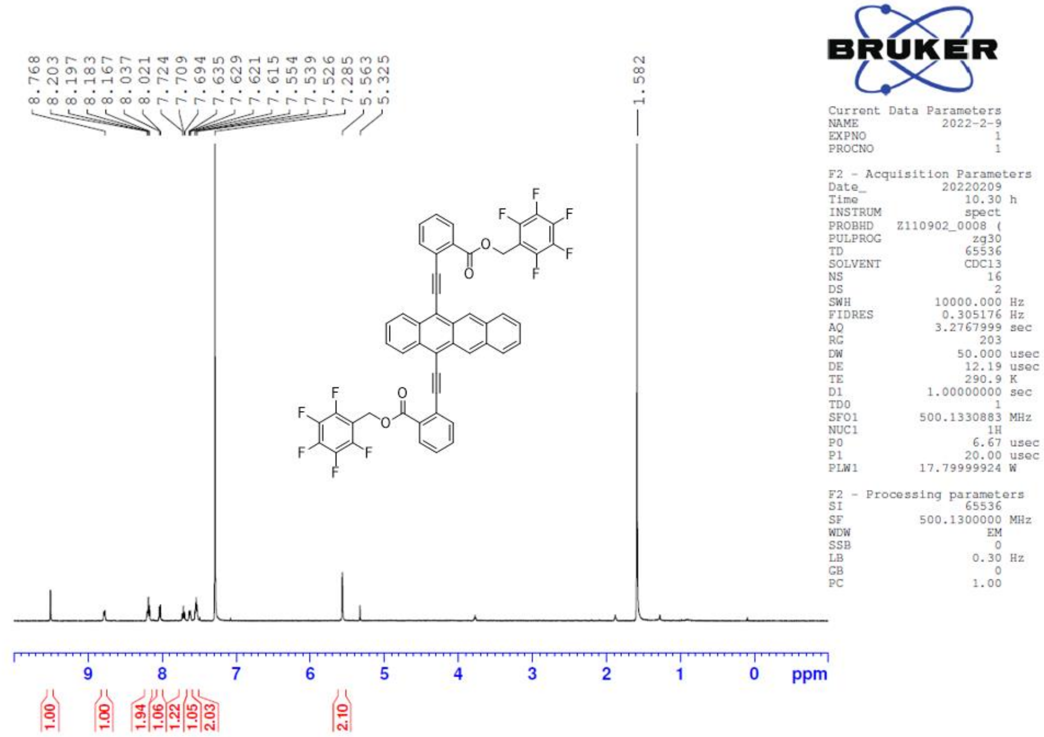
8.768
8.203
8.197
8.183
8.167
8.037
8.021
7.724
7.709
7.694
7.635
7.629
7.621
7.615
7.554
7.539
7.526
7.285
5.563
5.325
1.582
BRUKER
Current Data Parameters
NAME 2022-2-9
EXPNO 1
PROCNO 1
F2 - Acquisition Parameters
Date_ 20220209
Time 10.30 h
INSTRUM spect
PROBHD Z110902_0008 (
PULPROG zg30
TD 65536
SOLVENT CDCl3
NS 16
DS 2
SWH 10000.000 Hz
FIDRES 0.305176 Hz
AQ 3.2767999 sec
RG 203
DW 50.000 usec
DE 12.19 usec
TE 290.9 K
D1 1.00000000 sec
TD0 1
SFO1 500.1330883 MHz
NUC1 1H
P0 6.67 usec
P1 20.00 usec
PLW1 17.79999924 W
F2 - Processing parameters
SI 65536
SF 500.1300000 MHz
WDW EM
SSB 0
LB 0.30 Hz
GB 0
PC 1.00
9
8
7
6
5
4
3
2
1
0
ppm
1.00
1.00
1.94
1.06
1.22
1.05
2.03
2.10
F
O
O

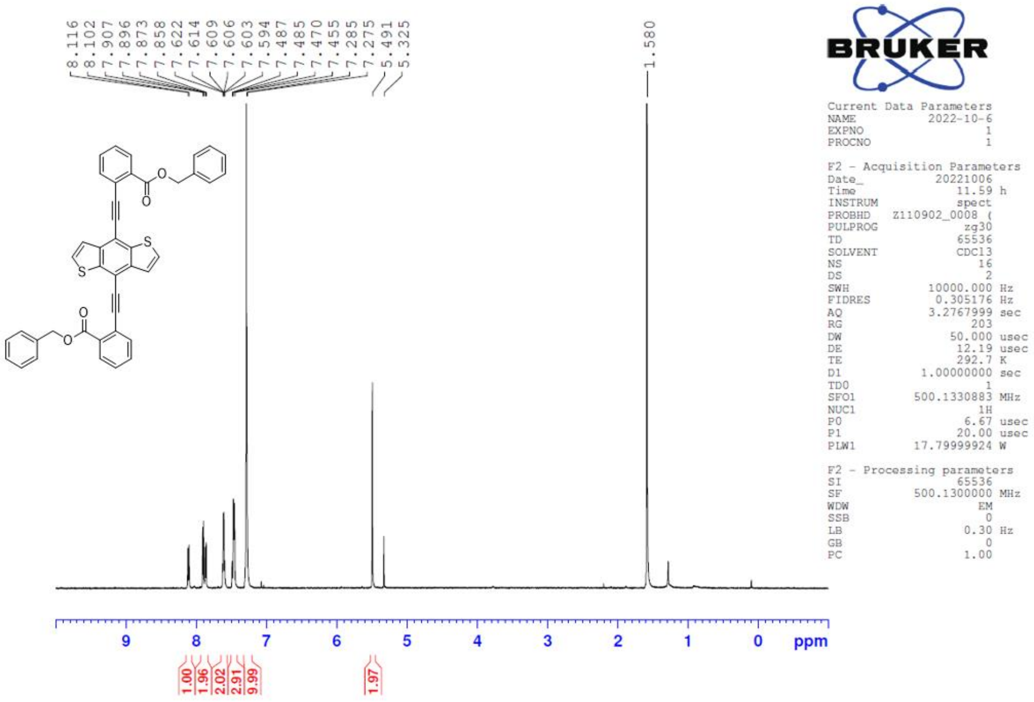
8.116
8.102
7.907
7.896
7.873
7.858
7.622
7.614
7.609
7.606
7.603
7.594
7.487
7.485
7.470
7.455
7.285
7.275
5.491
5.325
1.580
BRUKER
Current Data Parameters
NAME 2022-10-6
EXPNO 1
PROCNO 1
F2 - Acquisition Parameters
Date_ 20221006
Time 11.59 h
INSTRUM spect
PROBHD Z110902_0008 (
PULPROG zg30
TD 65536
SOLVENT CDCl3
NS 16
DS 2
SWH 10000.000 Hz
FIDRES 0.305176 Hz
AQ 3.2767999 sec
RG 203
DW 50.000 usec
DE 12.19 usec
TE 292.7 K
D1 1.00000000 sec
TD0 1
SFO1 500.1330883 MHz
NUC1 1H
P0 6.67 usec
P1 20.00 usec
PLW1 17.79999924 W
F2 - Processing parameters
SI 65536
SF 500.1300000 MHz
WDW EM
SSB 0
LB 0.30 Hz
GB 0
PC 1.00
9
8
7
6
5
4
3
2
1
0
ppm
1.00
1.96
2.02
2.91
9.99
1.97
S
O

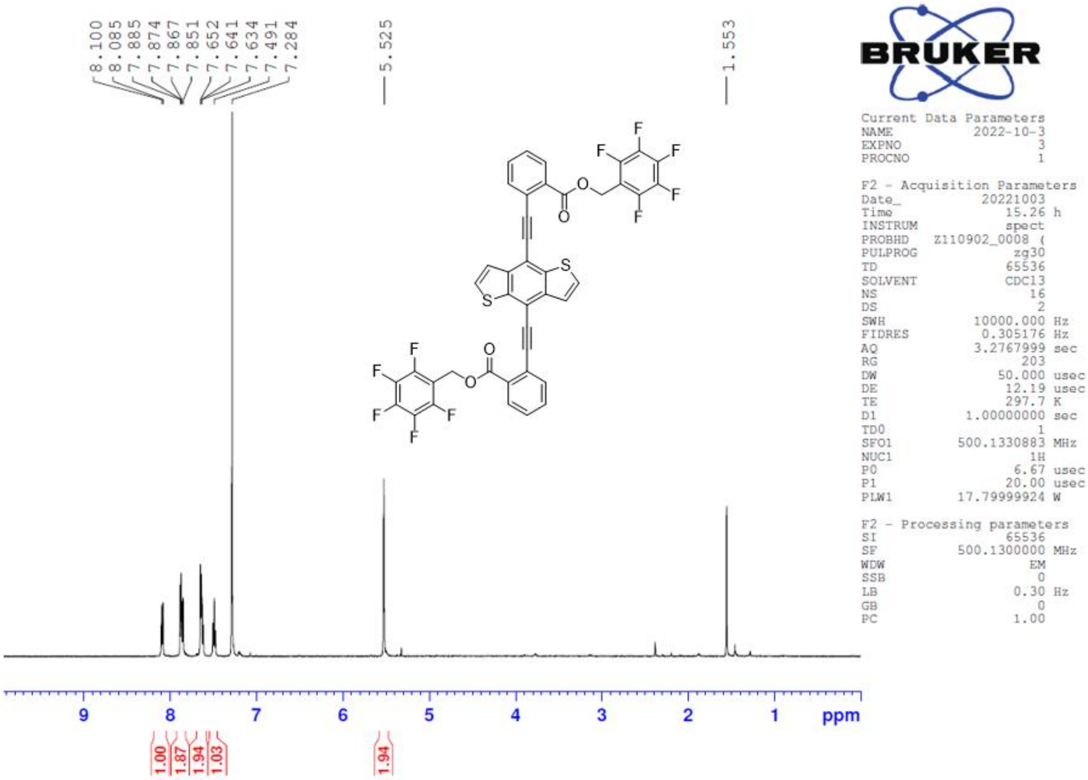

```
Current Data Parameters
NAME            2022-10-3
EXPNO                   3
PROCNO                  1

F2 - Acquisition Parameters
Date_           20221003
Time               15.26 h
INSTRUM            spect
PROBHD   Z110902_0008 (
PULPROG             zg30
TD                 65536
SOLVENT            CDCl3
NS                    16
DS                     2
SWH            10000.000 Hz
FIDRES          0.305176 Hz
AQ             3.2767999 sec
RG                   203
DW                50.000 usec
DE                 12.19 usec
TE                 297.7 K
D1            1.00000000 sec
TD0                    1
SFO1         500.1330883 MHz
NUC1                  1H
P0                  6.67 usec
P1                 20.00 usec
PLW1         17.79999924 W

F2 - Processing parameters
SI                 65536
SF           500.1300000 MHz
WDW                   EM
SSB                    0
LB                  0.30 Hz
GB                     0
PC                  1.00
```

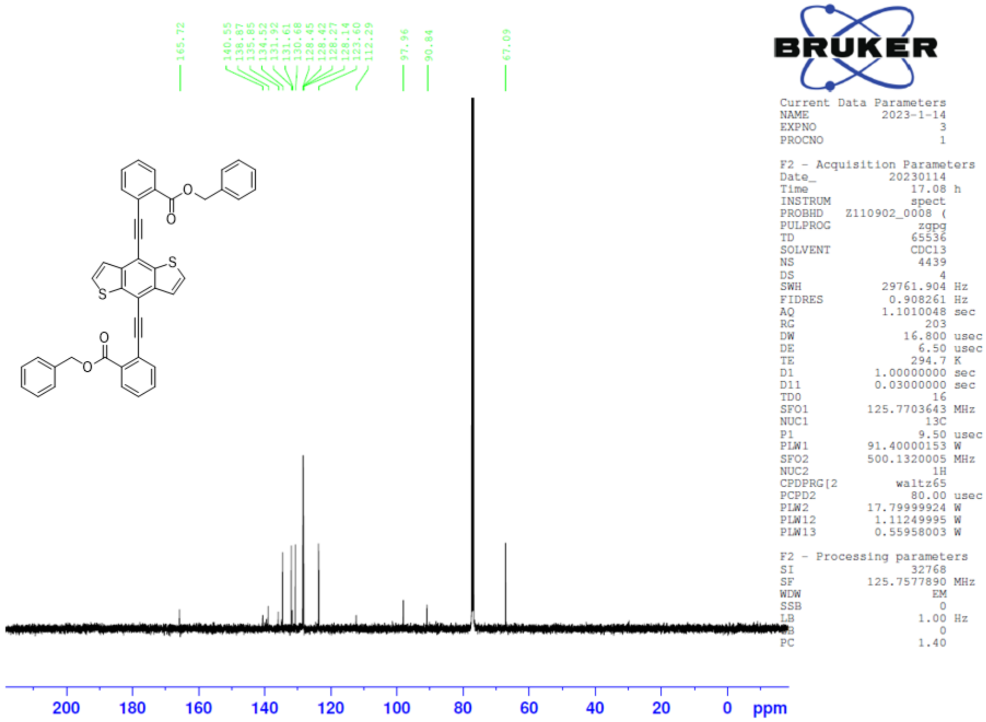

```
Current Data Parameters
NAME            2023-1-14
EXPNO                   3
PROCNO                  1

F2 - Acquisition Parameters
Date_           20230114
Time               17.08 h
INSTRUM            spect
PROBHD   Z110902_0008 (
PULPROG             zgpg
TD                 65536
SOLVENT            CDCl3
NS                  4439
DS                     4
SWH            29761.904 Hz
FIDRES          0.908261 Hz
AQ             1.1010048 sec
RG                   203
DW                16.800 usec
DE                  6.50 usec
TE                 294.7 K
D1            1.00000000 sec
D11           0.03000000 sec
TD0                   16
SFO1         125.7703643 MHz
NUC1                 13C
P1                  9.50 usec
PLW1         91.40000153 W
SFO2         500.1320005 MHz
NUC2                  1H
CPDPRG[2          waltz65
PCPD2              80.00 usec
PLW2         17.79999924 W
PLW12         1.11249995 W
PLW13         0.55958003 W

F2 - Processing parameters
SI                 32768
SF           125.7577890 MHz
WDW                   EM
SSB                    0
LB                  1.00 Hz
GB                     0
PC                  1.40
```

Chapter 5:

Tuning stiffness of free-standing hydrogen-bonded LbL films with Fe^{3+} coordination

Reproduced in part with permission from:
Yan, Y.; Feeney, M.; Davis, L. M.; Thomas, S. W. Tuning Stiffness of Free-Standing Hydrogen-Bonded LbL Films with Fe^{3+} Coordination. *ACS Applied Polymer Materials* **2022**, *4* (8), 5380-5386. DOI: 10.1021/acsapm.2c0043.[190]

5.1 Introduction

Layer-by-layer (LbL) assembly is a versatile technique for depositing thin films with two or more components.[191-194] The extensive substrate compatibility of LbL includes macroscopic planar substrates such as silicon wafers or glass slides, microparticles and nanoparticles, cells, and a variety of other possibilities.[195] Moreover, LbL is applicable to a wide diversity of materials that can comprise the deposited thin film, including biopolymers such as DNA and proteins.[196] LbL also allows control over the thickness of either free-standing thin films or coatings on the nanoscale. Chemical modification of simple, commercial materials can further enhance these advantages of LbL assembly to yield functional materials for applications that include stimuli-responsive materials,[197-199] self-healing,[200, 201] biocompatibility,[202] and drug delivery.[203]

The chemical design of such materials usually involves designing structural elements of polymers or other materials that participate in specific interactions between alternately deposited layers.[191] Although the most frequently used LbL systems rely on ion pairing between oppositely charged polyelectrolytes, other interactions such as hydrogen bonding are also broadly utilized.[204-206] Compared to ion-pairing analogs, hydrogen bonding LbL assemblies offer several advantages. For example, hydrogen bonding expands the library of polymeric building blocks beyond polyelectrolytes, which enables materials with increasingly tunable mechanical, physicochemical, optical, and even stimuli-responsive properties.[206] Also, such films can be disassembled on demand under mild conditions.[205, 207] Moreover, because these films have only weak interactions with hydrophobic substrates, such LbL assemblies can be separated from their substrates to afford free-standing films.[208]

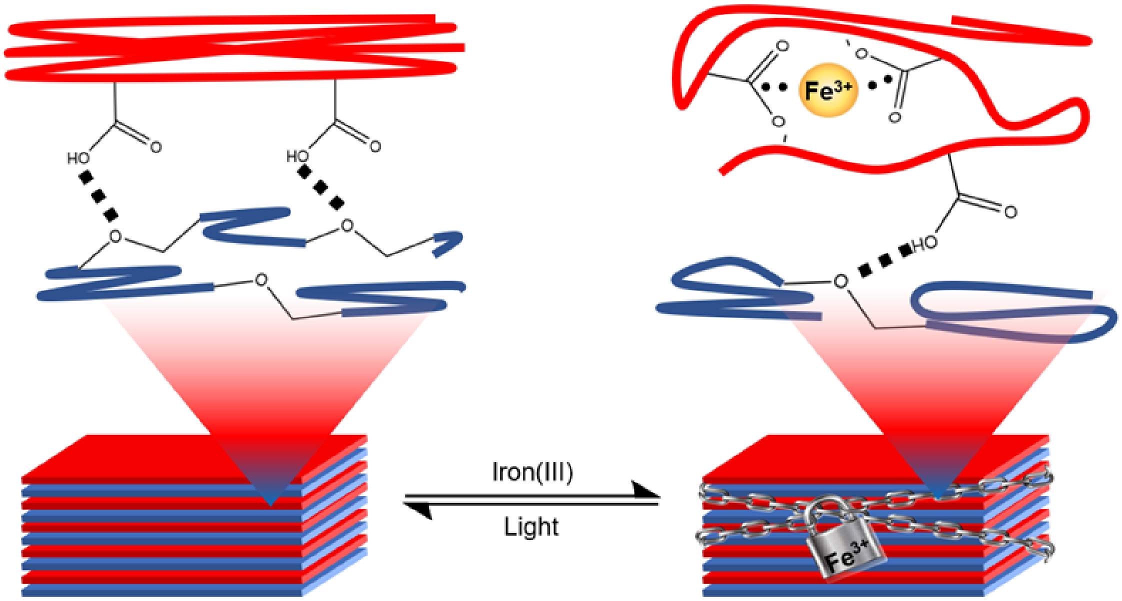

Figure 5.1: Cartoon illustration of the experimental design of this work. Reproduced from Ref.1. Copyright © 2022, American Chemical Society

5.2 Experimental Design

The layer-by-layer films described in this work comprise structurally simple, commercially available polymers—poly(ethylene oxide) (**PEO**) and poly(acrylic acid) (**PAA**). Each of these polymers is biocompatible, water-soluble, and inexpensive. Combinations of these two polymers can form stable complexes through hydrogen bonding that have found use in drug delivery[209], energy storage[210], and shape-memory materials.[211] Moreover, **PEO** substituents are frequently used as solubilizing functional groups for otherwise insoluble materials.[212] Thus, this work provides a prototype of polymeric materials compromising ether and carboxylic acid functional groups.

It has been reported that **PAA/PEO** LbL films are highly sensitive to environmental conditions, especially including elevated humidity, which can cause such materials to become too soft to handle.[208, 213, 214] Water molecules can hydrogen bond with polymers and reduce the physical crosslinking between polymer chains. To address that problem, our group crosslink the **PAA/PEO** films by iron(III) coordination, which enhances their mechanical properties as free-standing thin films and enables their handling in high humidity conditions. Also, the mechanical properties of these crosslinked films respond reversibly to UV irradiation, likely due to photo-reduction of coordinated iron(III).[215, 216]This method offers a simple, all aqueous, and synthesis free solution against the challenge in applying softened H-bonding films under high humidity.

5.3 Fabrication of LbL films and crosslinking with iron(III)

PAA/PEO films were assembled with a method adapted from Hammond and coworkers, which is driven by a combination of hydrophobic interactions and hydrogen bonding.[208] As shown in **Figure 5.2**, films were produced by a simple procedure of

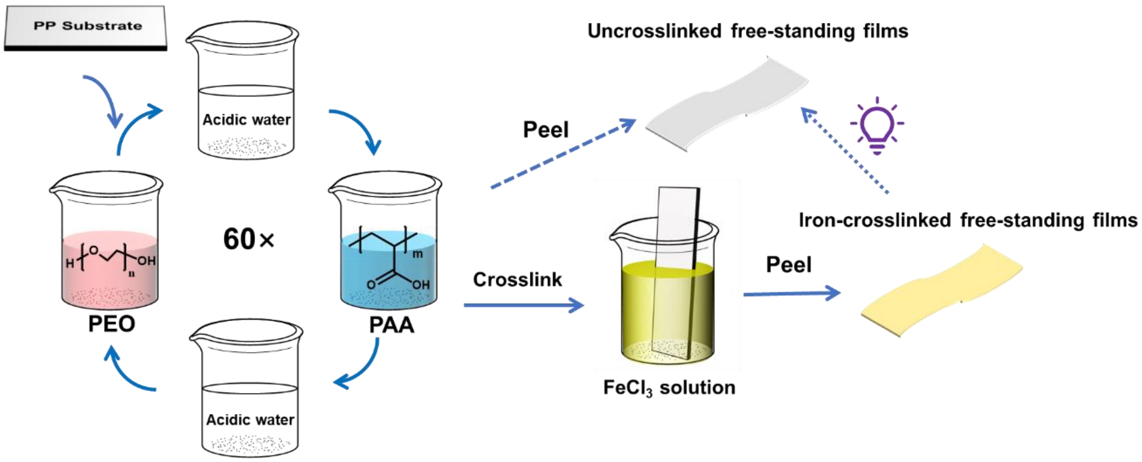

Figure 5.2: Fabrication and iron-crosslinking of **PAA/PEO** layer-by-layer films in this work. Reproduced from Ref.1. Copyright © 2022, American Chemical Society

immersing rectangular pieces of polypropylene sheet alternately in aqueous solutions of **PEO** and **PAA** (0.2% w/v), with intermediate rinsing steps to remove weakly adsorbed polymer. The polymer and rinsing solutions were held at pH 2.5 to maintain a high degree of protonation of **PAA** necessary for hydrogen bonding.[217] Peeling the film off the polypropylene substrates was routinely successful when the relative humidity (RH) was lower than 25%, yielding elastic free-standing films. These films are transparent to visible wavelengths of light and showed no obvious defects or pinholes under scanning electron microscopy (SEM), as shown in the **Figure 5.3**. The thickness of these 60-bilayer films, as determined by SEM imagine of their cross-sections, was 3-5 µm which is comparable with previously reported **PAA/PEO** films[218, 219]. Differential scanning calorimetry (DSC) revealed only one glass transition temperature (T_g) at 65 °C, indicating the polymers are fully miscible with each other, without crystalline **PEO** in the films.[208] (**Figure 5.4**)

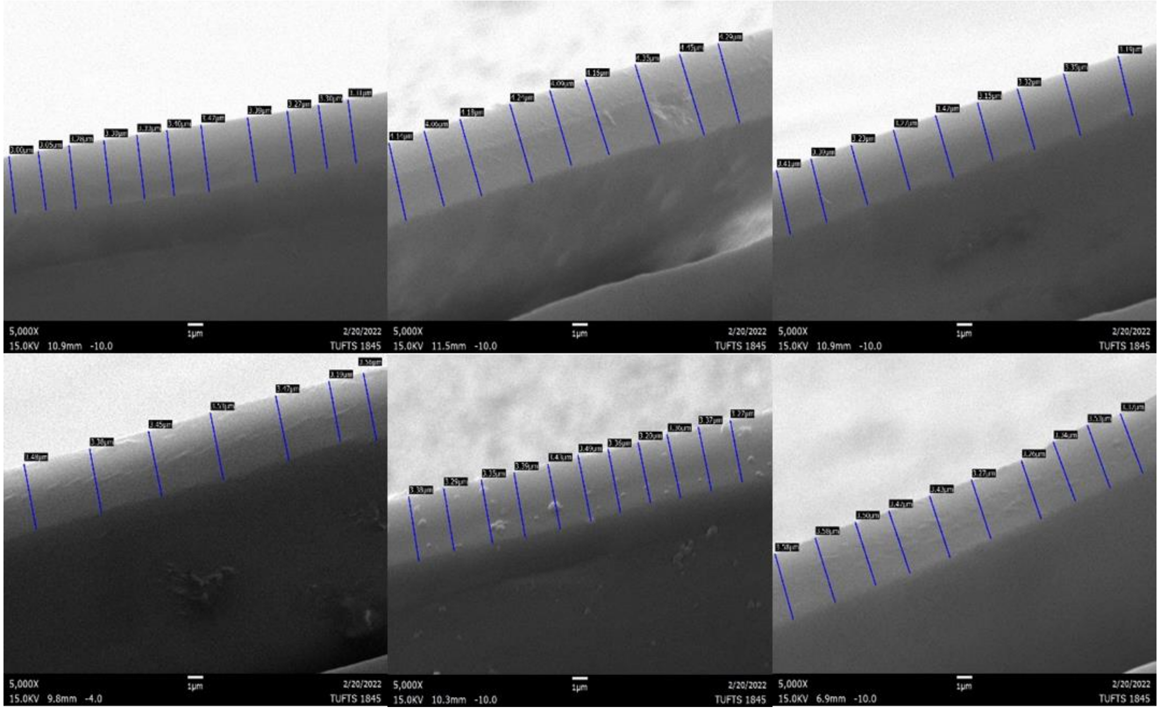

Figure 5.3: SEM cross-sections of films exposed to FeCl3 solutions: (a) 0 mM (no iron), (b) 1 mM FeCl3, (c) 5 mM FeCl3, (d) 10 mM FeCl3, (e) 15 mM FeCl3, (f) 20 mM FeCl3. All micrographs were obtained at 15 kV and 5000× magnification. Scale bars represent 1 micron. Film thicknesses are (a) 3.28±0.14, (b) 4.22±0.13, (c) 3.30±0.10, (d) 3.44±0.12, (e) 3.35±0.08, and (f) 3.43±0.12 microns. Reproduced from Ref.1. Copyright © 2022, American Chemical Society

The mechanical properties of these **PAA/PEO** films depend strongly on the environmental humidity, in that they lose mechanical integrity at higher humidity. In contrast to the easily handled films prepared at low RH, films prepared at RH higher than 40% were soft and easily deformable, making it difficult to peel them from the substrate. At even higher relative humidity (RH > 60%), the films resembled gelatinous, viscous liquids that fail to hold their own shape. To investigate this phenomenon quantitatively, we performed tensile testing on the free-standing films. The calculated Young's Moduli of these films varied from approximately 1 kPa (RH > 40%) to approximately 200 kPa (RH < 25%). We note that the range of Young's Moduli for similar films is known to be even broader: under more rigorously dried conditions the Young's Modulus of **PAA/PEO** free-standing films has been reported to be as high as 6.7 MPa.[208] Therefore, although these films maintain mechanical integrity at low humidity, water swells the polymer network at higher humidity levels, rendering these materials unusably soft as free-standing films by

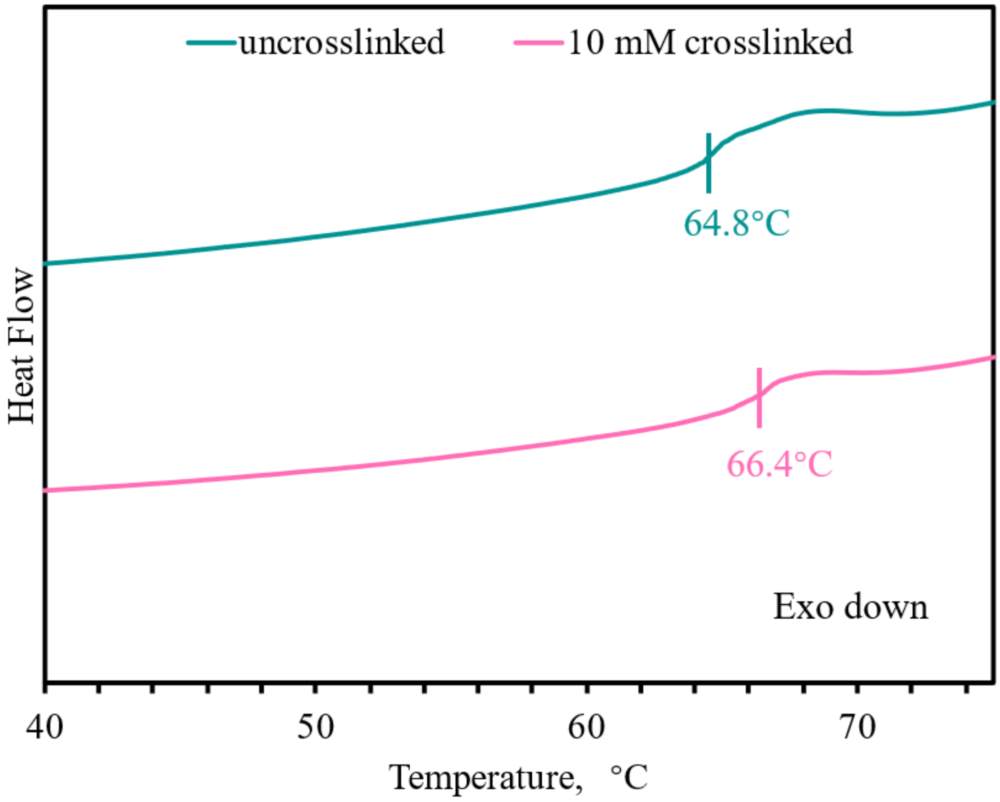

Figure 5.4: Differential scanning calorimetry results of uncrosslinked and crosslinked PAA/PEO films. Reproduced from Ref.1. Copyright © 2022, American Chemical Society

interrupting interchain hydrogen bonding.

Given the deleterious impact of humidity on these films, we expected that presence of a secondary crosslinker could maintain the mechanical properties of such films at higher humidity. Crosslinking gels by simply soaking in a multivalent ion solution is a simple, effective, and low-cost method for improving film stability,[220] and is well established for hydrogels such as those made from the polysaccharide alginate.[215] We therefore tested the impact of seven multivalent ions by immersing the films into 5 mM solutions for 10 minutes followed by 10-minute rinsing with pH 2.5 solutions. Among these metal cations investigated, iron(III) provided a significant enhancement of Young's Moduli (~100×)

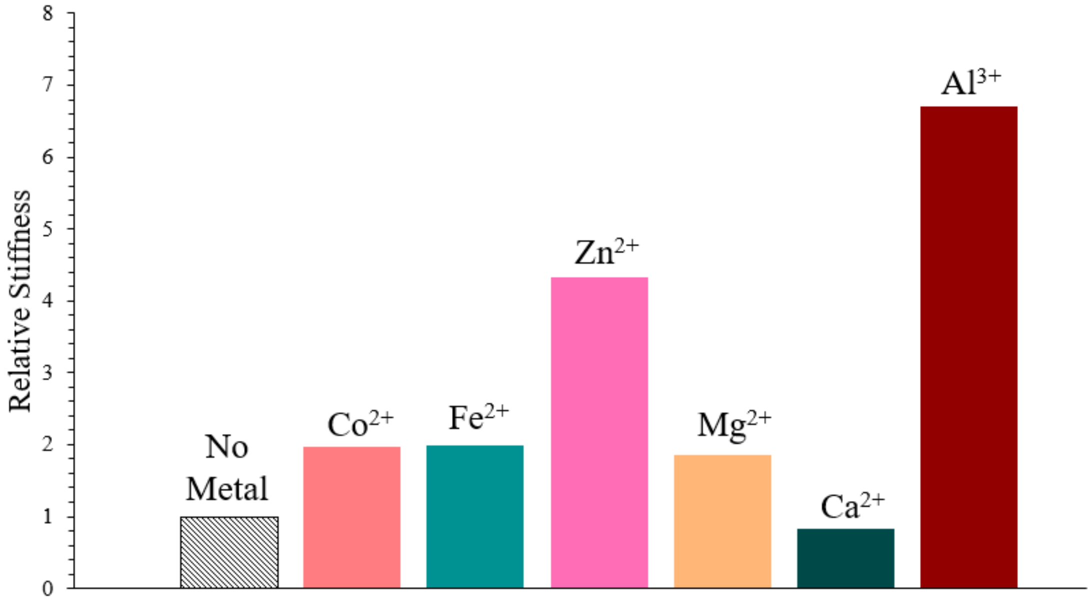

Figure 5.5: Impact of other metal ions on the Young's Modulus of develop films. Reproduced from Ref.1. Copyright © 2022, American Chemical Society

while the others—including aluminum(III) and iron(II)—did so by less than one order of magnitude as shown in **Figure 5.5**.

Therefore, in the remainder of this work, we focused on iron(III) as a crosslinker. The coordination between iron(III) and ligands on the polymer chains (likely carboxylic acid groups) was achieved by simply immersing films in an aqueous solution of $FeCl_3$ at concentrations of 1-20 mM for 10 minutes, followed by washing the films with pH 2.5 water. After drying under ambient conditions overnight, the films were a pale-yellow color, which could be recognized by eye and quantitively measured with UV-vis spectroscopy, indicating the incorporation of iron(III) ions**. (Figure 5.6)**

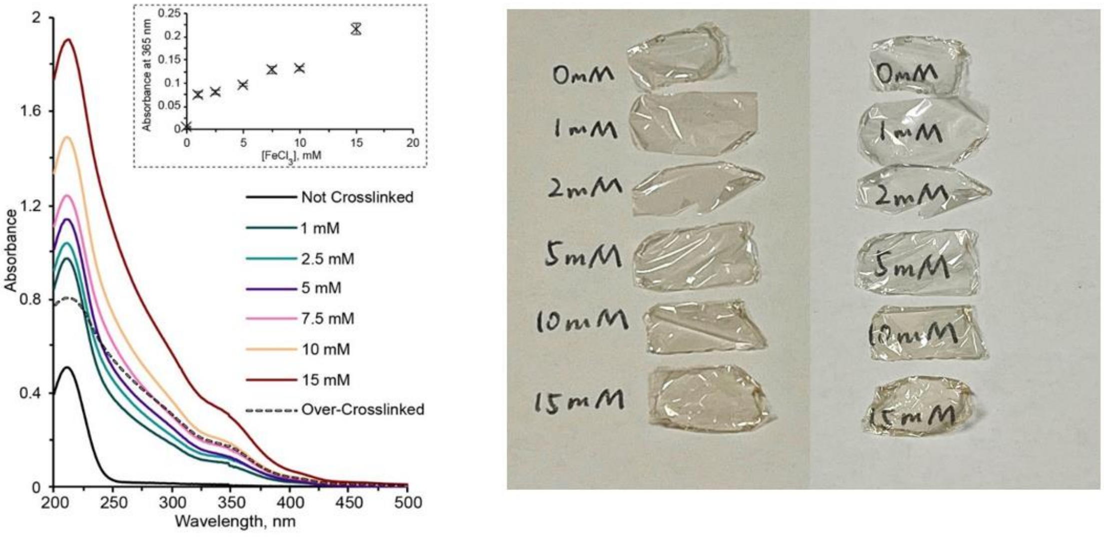

Figure 5.6: Left: The absorbance spectra of fabricated films in this work and the inset shows the relationship between iron concentration and film absorbance at 365 nm. Right: the photos of the films. Reproduced from Ref.1. Copyright © 2022, American Chemical

Analysis by SEM did not reveal any noticeable changes in the morphology of the films after crosslinking. The thickness of the films was not significantly impacted by exposure to iron solutions according to our observation under SEM. After exposure to iron(III) solutions, we could readily peel all films off the polypropylene substrates, even when RH > 40%. The glass transition temperatures of the free-standing films determined by DSC (66 °C) were unchanged from before crosslinking. This observation both demonstrates the enhancement of the mechanical properties of the films through crosslinking and addresses the practical problem of forming free-standing films of hydrogen bonding LbL films at higher levels of humidity.

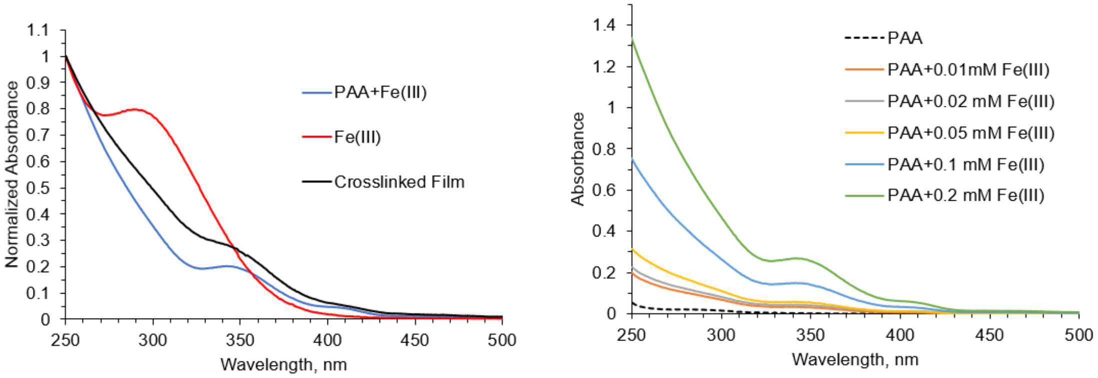

Figure 5.7: Left: Comparation of the normalized, solution-phase UV-vis spectra of $FeCl_3$ solution (Red), mixture of $FeCl_3$ solution and **PAA** solution (Blue), and solid-phase UV-vis spectrum of Fe^{3+} crosslinked **PAA/PEO** film (Black). Right: the absorbance of **PAA** solution with different amount of iron(III) ions. Reproduced from Ref.1. Copyright © 2022, American Chemical Society

5.4 Spectroscopic analysis

To better understand and optimize the crosslinking process, we varied the Fe^{3+} immersion times and concentrations. As **Figure 5.6** (left) shows, the cross-linking of these films with iron increased the absorbance significantly in the range of 200-450 nm, consistent with previous observations during the crosslinking of alginate gels[215] and

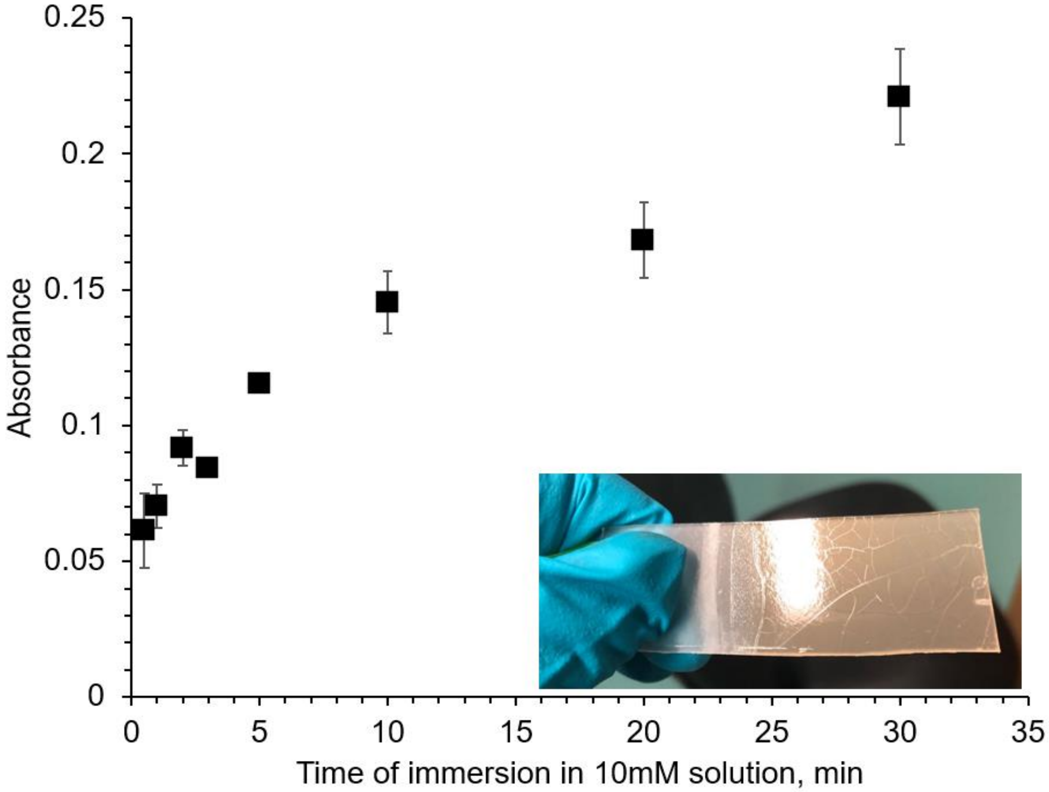

Figure 5.8: Dependence of absorbance of the freestanding LbL films at 365 nm on the immersion time in 1.0 mM $FeCl_3$ (aq) solution. Inset: Cracking of the dried films on polypropylene substrates when immersed in $FeCl_3$ longer than 20 minutes. Reproduced from Ref.1. Copyright © 2022, American Chemical Society

PAA/PEO complexes.[221] Importantly, absorbance at wavelengths longer than 250 nm is due only to the presence of iron(III) complexes, as confirmed by comparing the spectrum shape of free Fe^{3+} solution and Fe^{3+}-**PAA** complex solution. Moreover, the absorbance value of such solutions correlates with the concentration of Fe^{3+} ions when excess **PAA** was used.(**Figure 5.7**) Therefore, we could estimate the relative amount of iron(III) incorporated in these films by their absorbance values at 365 nm. We varied the immersion

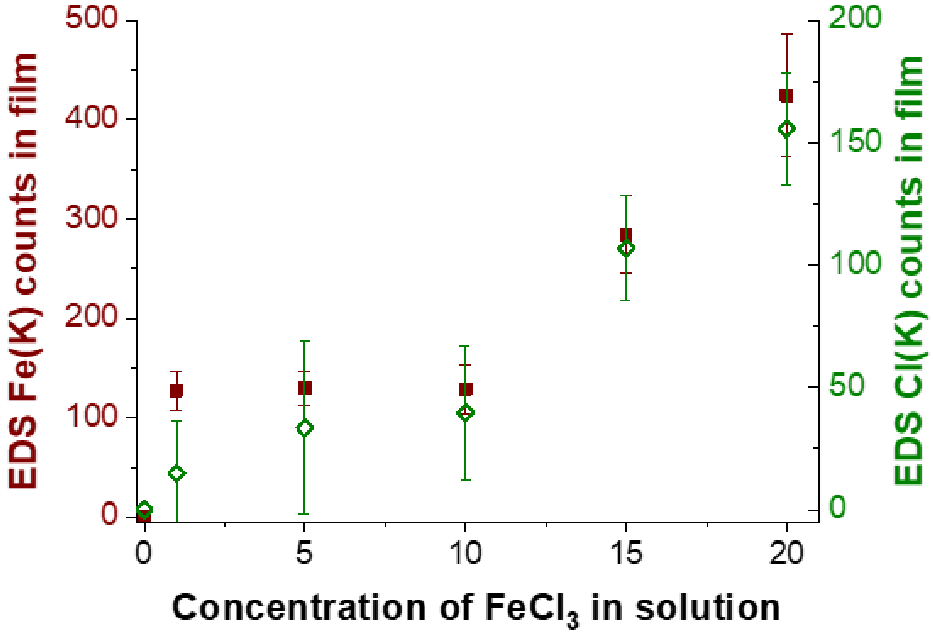

Figure 5.9: Dependence of the EDS-detected iron (red square) and chlorine (green diamond) counts of the films on the solution concentration of $FeCl_3$. Reproduced from Ref.1. Copyright © 2022, American Chemical Society

time by dipping **PAA/PEO** films in 1 mM $FeCl_3$ solutions between 1 to 30 minutes (**Figure 5.8**). As expected, films immersed in Fe^{3+} solutions for longer times showed larger absorbance values than those immersed for shorter times, increasing from 0.06 to about

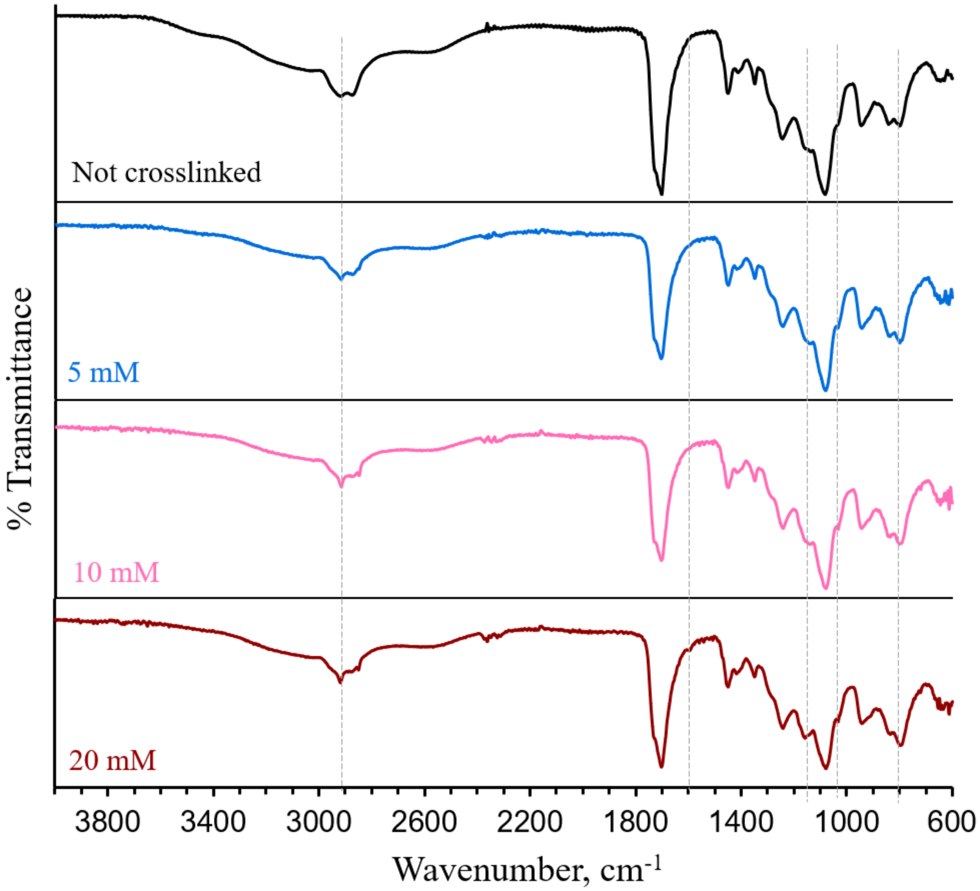

Figure 5.10: FT-IR spectra of uncrosslinked films and films crosslinked by immersion in 5 mM, 10 mM, or 20 mM $FeCl_3$ aqueous solutions. The vertical axis was scaled for better comparison. Dashed lines indicate the noticeable changes in the spectra. From left to right, the positions of the dashed line are 2920, 1590, 1140, 1050, and 790 cm^{-1}. Reproduced from Ref.1. Copyright © 2022, American Chemical Society

0.23. With immersions longer than 20 minutes, however, the shape of the absorbance spectrum changed, and the films cracked after drying. To avoid this over-exposure, we selected 10 minutes for all subsequent experiments.

With this crosslinking process, the absorbances of the films at 365 nm correlate positively with the concentration of Fe^{3+} in the immersion solutions, revealing the possibility of precise control over the extent of crosslinking through concentration. Moreover, Energy-dispersive X-ray spectroscopy (EDS) experiments are consistent with the trend we interpreted from the absorbance. Both iron and chlorine counts increased with the absorbance of the films, supporting the relationship between the absorbance and the amount of iron incorporated within the polymer films as shown in **Figure 5.9**. Finally, we estimate a 5 μm-thick film **PAA/PEO** film has on the order of 1 mmol of carboxylic acid groups in the entire film, which is more than the entirety of Fe^{3+} ions in the crosslinking solutions for even the highest concentration that we tested (30 mL of 15 mM Fe^{3+}), indicating that only a small fraction of available carboxylates in the films ligate to iron ions upon exposure to the Fe^{3+} solution.

In our crosslinked LbL films reported here, we observed only modest changes in the shapes of FT-IR spectra of these films with increasing Fe^{3+} incorporation, suggesting that even at the highest concentration of Fe^{3+}, the vast majority of carboxylate functional groups remain uncrosslinked. Both our estimate of the sub-stoichiometric amount of available Fe^{3+}

ions in the entirety of the crosslinking solution, and the acidic pH (2.5) ensuring that >90% of carboxylate functional groups are protonated further support this conclusion. As shown in **Figure 5.10** all the samples displayed characteristic peaks at 1700-1750 cm^{-1} and 1050-1100 cm^{-1}, corresponding to the stretching of carbonyl group (C=O) in **PAA** and the vibration of ether bonds (C-O-C) in **PEO**, respectively. [211] Moreover, with the concentration of incorporated iron increasing, small peaks or shoulders appeared at 1590, 1160, 1030, and 790 cm^{-1}, suggesting changes in the bonding nature within the polymeric films due to incorporation of Fe^{3+} ions.[222-224] In particular, the small peak at 1590 cm^{-1} has been observed previously in Fe^{3+}-crosslinked **PAA**-chitosan nanofibers, and has been ascribed to bidentate bridging complexes.[225] A carboxylate-iron bond is also supported by Fe^{3+} perturbing the peak at 1160 cm^{-1}, which has been ascribed previously to C-O stretching coupled to the O-H bend in **PAA**.[226]

5.5 Mechanical analysis

The free-standing nature of the films enabled characterization of their mechanical properties by standard tensile testing. The Young's Moduli of the films were calculated from the linear regime (strain < 5%) using thicknesses of 3.5 μm for all films, based on our SEM analysis. Given the sensitivity of these films to ambient humidity, we performed each set of tensile testing on films with varying levels of Fe^{3+} incorporation all on the same day, with films from the same batch of fabrication processes. To understand the influence of ambient humidity on the properties of these films, we also repeated this suite of experiments on films prepared using the same fabrication protocols on other days with different ambient relative humidity levels.

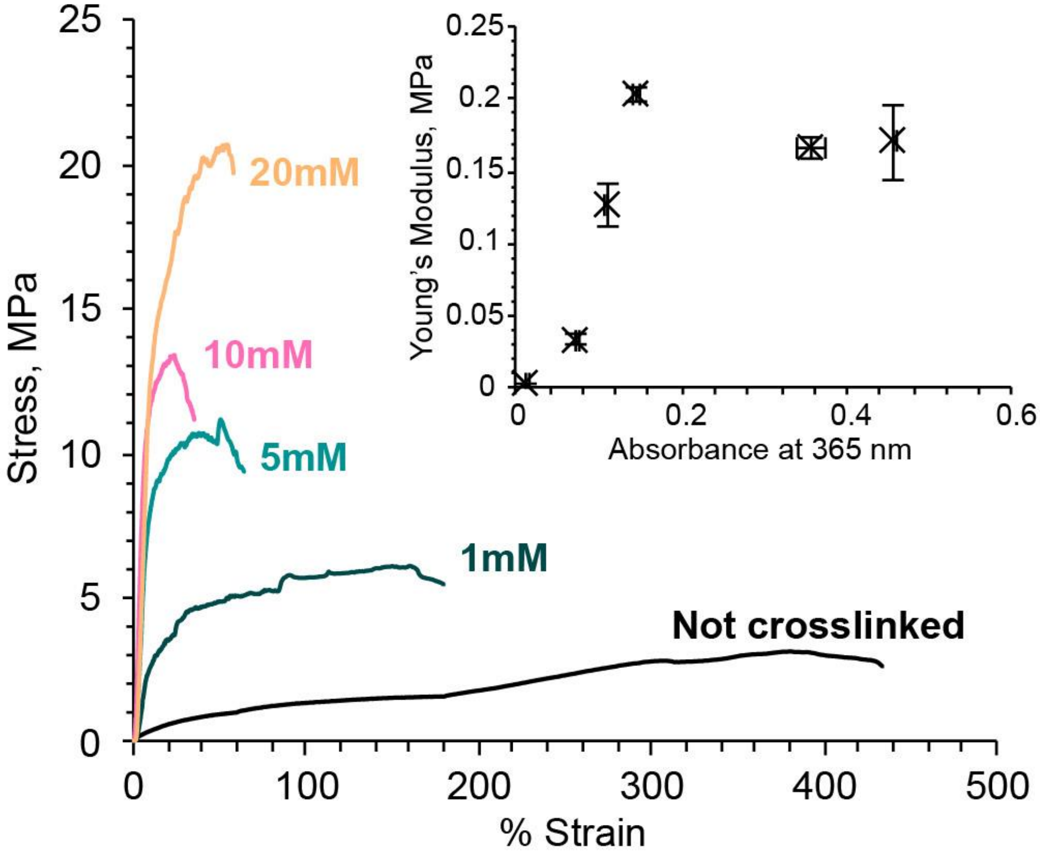

Figure 5.11: Tensile testing curves of free-standing films exposed to varying concentrations of Fe^{3+} crosslinker. The experiment was performed at RH ~ 40%. Inset: Calculated Young's moduli as a function of absorbance of films at 365 nm. The error bars represent the double standard error of the mean calculated from at least 3 successive tests on different films under the same conditions. Reproduced from Ref.1. Copyright © 2022, American Chemical Society

Figure 5.11 shows the stress-strain curves of films crosslinked with different amounts of Fe^{3+} at RH ~ 40%. In general, increasing the concentration of Fe^{3+} increased the stiffness and ultimate stress of crosslinked films, and decreased their strain at fracture. Young's

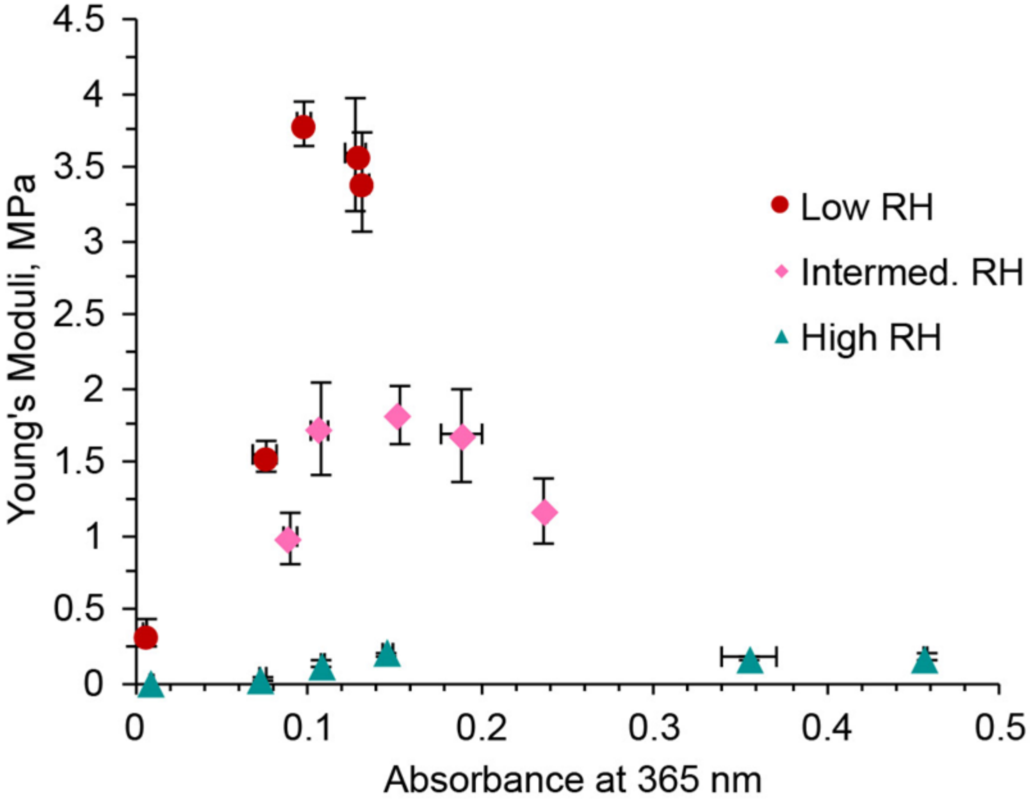

Figure 5.12: Dependence of Young's Moduli of free-standing LbL films on relative humidity and their absorbance at 365 nm. The tensile tests were performed 3 times under high relative humidity (RH ~ 40%, triangle, green), intermediate relative humidity (RH ~ 30%, diamond, pink), and low relative humidity (RH < 25%, round, brown). The error bars represent the standard error of the mean calculated from at least three successive tests under the same conditions. Reproduced from Ref.1. Copyright © 2022, American Chemical Society

moduli of these films were calculated from the slope in the elastic regime of the curves. The modulus of these films increased from 1-2 kPa for uncrosslinked films to 33 kPa for films treated with 1 mM $FeCl_3$ solution, and further to 0.20 MPa when using 10 mM solution. However, the elongation at fracture decreased from 440% to only 50% with concentrations higher than 10 mM.

We further probed the impact of moisture on the mechanical properties of crosslinked films, particularly stiffness, with additional sets of tensile tests performed under different relative humidities. The dependence of calculated Young's Moduli on both relative humidity and incorporation of Fe^{3+} is shown in Figure **5.12**. While increasing the density of crosslinking did stiffen these films regardless of humidity, these films also maintained sensitivity towards humidity after crosslinking, indicating the importance of hydrogen bonding in the structure of these films. As an example of these trends, the moduli of films with similar concentrations of Fe^{3+} (absorbance ~ 0.11) increased from 0.13 MPa at high RH (> 40%) to 1.7 MPa at intermediate RH (~33%), and was as high as 3.8 MPa at low RH (< 25%). In addition, when using an iron(III) solution with a concentration higher than 20 mM, although the absorbance could still increase, the stiffness of the films reached a plateau or even decreased slightly. The same trend has been observed by others in similar systems, who attribute this phenomenon to the decreased stability constant of the coordination resulting from the increasing acidity of the environment.[227-229]

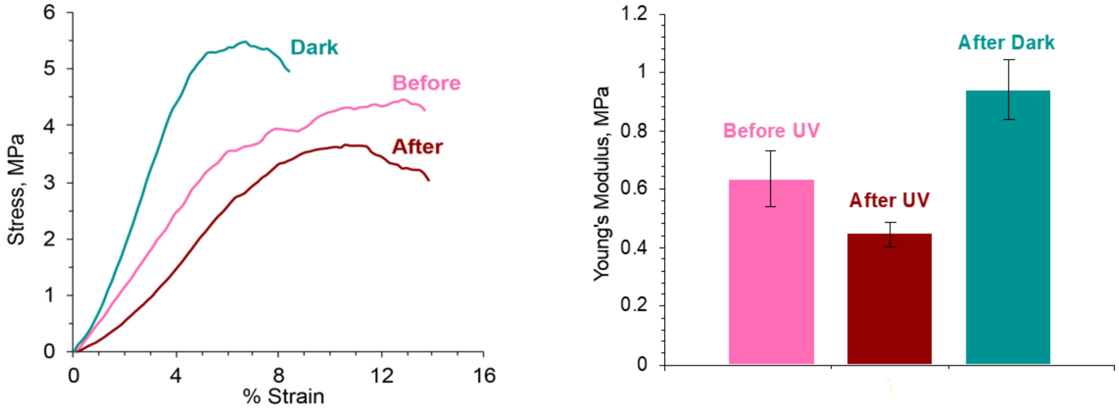

Figure 5.13: Left: Tensile curves of films before irradiation (Before, pink), after UV irradiation for 20 minutes (After, brown), and after storing in the dark for a day after irradiation (Dark, green). All the tests were performed on the same day using films from the same batch and the same crosslinking process. Right: The Young's Moduli of iron-crosslinked films without irradiation (Before UV, pink), irradiated for 20 minutes (After UV, brown), and kept in dark for one day after irradiation (After Dark, green). Reproduced from Ref.1. Copyright © 2022, American Chemical Society

5.6 Photo-responsiveness of crosslinked films

In this work, we also used UV light to control the stiffness of the iron-crosslinked **PAA/PEO** LbL films. As shown in **Figure 5.13**, irradiating (20 minutes, 2 mW/cm^2) a film crosslinked with 5 mM Fe^{3+} decreased in stiffness by 30% (0.64 MPa to 0.45 MPa). Meanwhile, the absorbance at 365 nm decreased by 17% due to the reduction of Fe^{3+} to

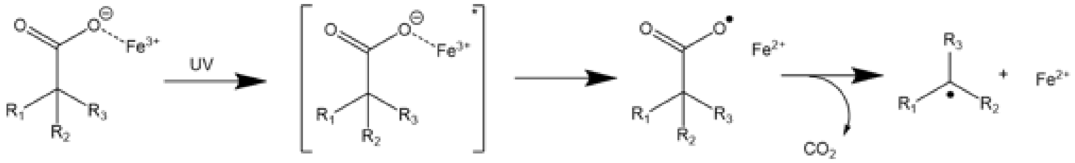

Scheme 5.1: Proposed photo-reduction of iron complex. Reproduced from Ref.1. Copyright © 2022, American Chemical Society

Fe^{2+}, which has reduced extinction efficiency in the UV.[229] The iron in these films could be re-oxidized by storing the film in the dark under otherwise ambient conditions. The stiffness recovered past the original value by approximately 30%, and the strain at break fell from 15% to 8%. We suspect that rearrangements of the cross-linking occurred during the cycle of iron reduction and oxidation, in addition to chemical changes within the films due to the irreversible nature of the overall chemical reaction. The impact of irreversible changes was further evidenced by repeating the irradiation/oxidation cycle three times **(Figure 5.13)**, in that there was some reversion of the absorbance with each step, but with noticeable fatigue. Furthermore, evidence for a cycle of photoreduction/air oxidation of the iron ions in these films arose from selective 1,10-phenanthroline complexation of Fe^{2+}, as shown in **Figure 5.14**. The signature absorbance peak of Fe^{2+}-*phen* complex (515 nm) appeared only after the film was irradiated.[230] Subsequently, the absorbance due to this complex decreased when irradiated films were stored in the dark, consistent with re-oxidation to Fe^{3+}.

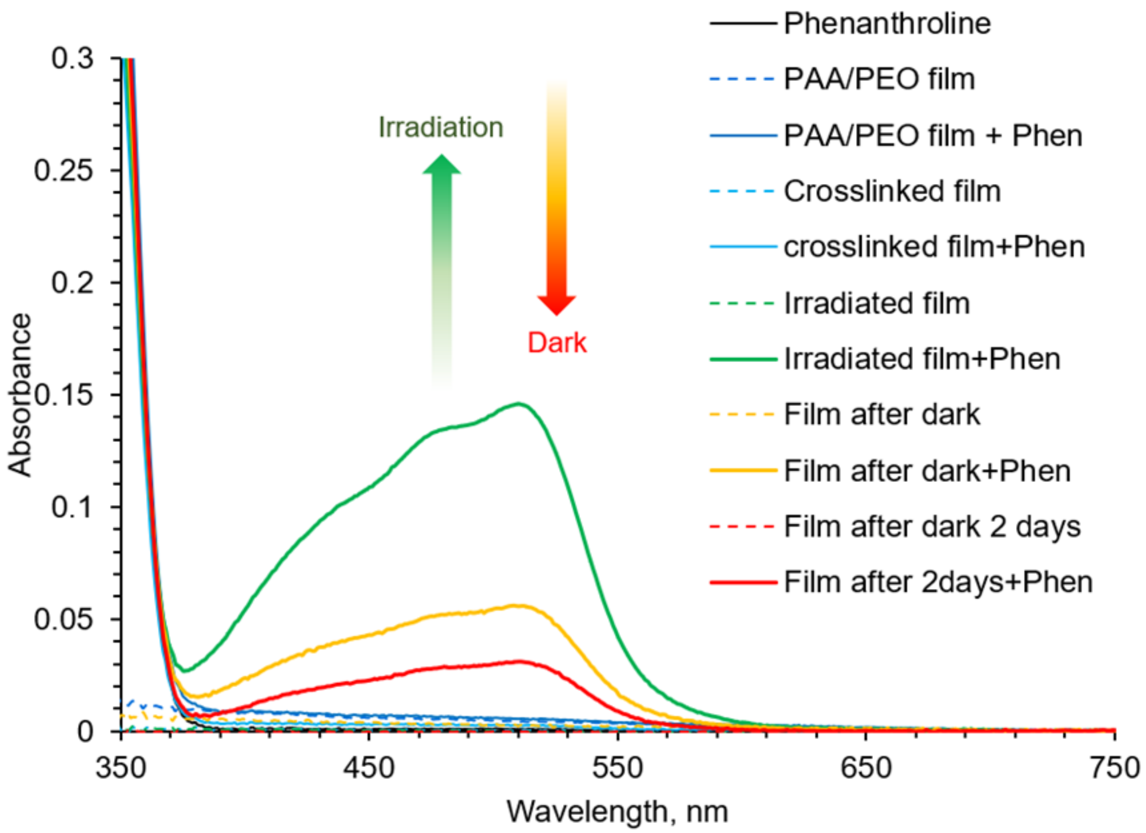

Figure 5.14: Evidence of Fe^{2+} ion formation upon irradiation of crosslinked films by complexation with 1,10-phenathroline. The absorbance spectra of supernatants without *phen* are shown with dashed lines, showing that there is no peak between 400-600 nm either before or after the irradiation. In contrast, only films irradiated with UV light did the supernatant give a signature orange color and a peak at 515 nm in the spectrum, which indicates the formation of Fe(II)-phenanthroline complex. After recovering in the dark for two days, absorbance due to the Fe^{2+} complex was 80% lower, consistent with air oxidation of Fe^{2+}. Reproduced from Ref.1. Copyright © 2022, American Chemical Society

5.7 Conclusion

We have developed an operationally simple method to overcome the poor mechanical stability of hydrogen-bonded **PAA/PEO LbL** films under high humidity environments. These films contain inexpensive polymers and readily can be assembled to a thickness of microns. The ionic crosslinking method is synthesis-free, low-cost, and readily controlled through ion concentration. The crosslinked films are also reversibly photo-responsive, which allows the use of light to modulate their mechanical properties. Disadvantages of this approach include low photo-reduction efficiency, a limitation to acidic environments, and challenges in quantitatively precise control of light-induced modulation. We anticipate that our work could provide alternative approaches for improving and tuning the mechanical stability and stiffness of various **LbL** films, which has the potential for impact in controlling cell adhesion[231] or drug delivery[232].

5.8 Experimental section

Materials

Poly(acrylic acid) (M_W ca. 240,000, 25.8% solid in water) was purchased from Scientific Polymer Products. Poly(ethylene oxide) (M_W ca. 600,000) was purchased from Polysciences. Ferric chloride hexahydrate was purchased from Fischer Scientific. All materials were used without any further purification. Deionized (DI) water was used for all film fabrication and crosslinking.

Fabrication of **PAA/PEO** Films

PAA solutions and **PEO** solutions at concentrations of 0.2% (w/v) were prepared by dissolving the polymers separately in DI water followed by stirring overnight at ambient temperature. Then, the pH of the two solutions was adjusted to 2.5 with 1 M HCl and 1 M NaOH aqueous solutions. An acidic rinsing solution was also prepared by adding 1 M HCl into DI water until the pH reached 2.5. The solutions were then filtered to remove any insoluble residues. Each filtrate was transferred into separate containers of a Midas III Automated Slide Stainer, which enables simultaneous immersion of up to 20 substrates following a user-programmed sequence. Polypropylene (**PP**) sheets (1/16-inch thickness, McMaster-Carr) were used as substrates for film deposition. **PP** substrates were cut into ~7.5 cm × 2.5 cm rectangles and washed by sequential sonication in ethanol and DI water. The slide stainer was programmed to first immerse the substrate in the **PEO** solution for 5 minutes, followed by two rinsing steps (one of 4 minutes and a second of 1 minute) in separate pH 2.5 rinsing solutions. These substrates were then immersed into the **PAA** solution, rinsed for 5 minutes as described above, to then yield a polymer bilayer deposited on each **PP** substrate. After approximately 20 hours, 60-bilayer coatings were obtained. All films were air-dried overnight in the ambient environment.

Crosslinking of **PAA/PEO** Films with Fe^{3+}

Air-dried **PAA/PEO** films on **PP** substrates were immersed into an aqueous solution of ferric chloride for 10 minutes. Different concentrations of Fe^{3+} afforded films with different degrees of crosslinking. The films were then rinsed by immersion in a pH 2.5 rinsing solution for 10 minutes to remove weakly bound iron ions. After air-drying overnight, the crosslinked films could be peeled off their PP substrates with tweezers to afford free-standing films.

Film Characterization.

Characterization experiments were performed at least three times unless described otherwise. To avoid the effect of material aging, the mechanical properties of all films were tested within three days of their preparation. The absorbances of free-standing films were measured by a UV-vis spectrophotometer in double-beam mode using a quartz glass for background subtraction spectra. The free-standing films analyzed by spectrophotometry were placed onto a quartz glass substrate before acquiring spectra.

Attenuated Total Reflection Fourier transform infrared (ATR-FTIR) spectroscopy was performed using a Jasco FTIR 6200 spectrometer equipped with PIKE Technologies Single Reflection MIRacle ATR accessory. Baseline-corrected spectra were collected in transmittance mode over a range of 600–4000 cm^{-1} at 4 cm^{-1} resolution and averaged over

32 scans to improve the signal-to-noise ratio. All the FT-IR tests were directly performed on the free-standing films over an area of ca. 1 cm^2 under ambient conditions.

Tensile testing of thin films was performed on a TA Instruments RSA3 Dynamic Mechanical Analyzer (TA Instruments, New Castle, DE). Measurements were performed under ambient conditions, with relative humidity measured and noted. Prepared films were cut into rectangular shapes, typically 10 mm × 15 mm. All samples (except those that were photo-irradiated) were equilibrated in the dark for at least 30 minutes before testing. Strain-controlled measurements were performed in transient mode, at a constant strain rate of 0.1 mm per second.

Differential scanning calorimetry was performed with a TA Discovery 250 DSC under constant nitrogen flow. Heat-cool-heat cycles were performed on the films with ramp rates for both heating and cooling of 10 ºC/min. The data were collected from the second heating process to avoid artifacts from the thermal history of samples.

Microscopy

Field-emission scanning electron microscopy (FE-SEM) was performed with an AMRAY 1845 FE-SEM with SEMView8000, refurbished by SEMTech Solutions (North Billerica, MA). Sample coupons ca. 0.5-2 cm^2 were cut for SEM imaging with scissors. Cross-sections were obtained by gently scoring the film near one edge with a razor blade and peeling back the film. Samples were then mounted on aluminum stubs using carbon adhesives. Samples were coated with 5-10 nm of sputtered gold, to limit charging during imaging, using a Polaron SC502 sputter coater.

Energy-dispersive X-ray spectroscopy (EDS) was performed using the SEM beam and a Thermo Scientific Noran System 6 detector. The EDS detector is mounted normal to the imaging beam, so the sample stage was tilted 20° towards the detector during analysis. All samples were analyzed at 2000× magnification, 15 kV imaging voltage, and a working distance of 22 mm. Preliminary experiments showed that the number of iron counts observed at a single location was sensitive to the working distance, and maximized around 22 mm. EDS maps were collected from at least four locations on all iron-containing films and averaged. For the uncrosslinked film, two locations were sampled and both showed no iron (0 counts in both locations).

Photo-responsiveness

Each film was irradiated with a 200 W Hg/Xe lamp equipped with a condensing lens, water filter, and manual shutter. Wavelengths of irradiation were selected with appropriate filters. The power density varied between 30-70 mW/cm^2 when different filters were applied. Alternatively, films were irradiated with a hand-held UV lamp (235/365 nm, 2 mW/cm^2). To measure the variation in stiffness, films were left on the PP substrates for irradiation and equilibration until subjected to tensile testing. A set of films were irradiated with the same light source a day before the tensile test and stored in the dark, which allows all the tensile tests to be performed on the same day, to minimize the impact of environmental conditions. Reversibility tests were carried out by peeling crosslinked films off the PP substrate and placing them on a piece of quartz glass, and then subjecting them to cycles of irradiating and storing in the dark. Changes in absorbance due to iron photoreduction, and subsequent air oxidation, were monitored by UV-vis spectrophotometry.

References

(1) Yan, Y.; Feeney, M.; Davis, L. M.; Thomas, S. W. Tuning Stiffness of Free-Standing Hydrogen-Bonded LbL Films with Fe³⁺ Coordination. ACS Applied Polymer Materials 2022, 4 (8), 5380-5386. DOI: 10.1021/acsapm.2c00431 (acccessed 2023-07-03T16:06:27).

(2) Borges, J.; Mano, J. F. Molecular interactions driving the layer-by-layer assembly of multilayers. Chem Rev 2014, 114 (18), 8883-8942. DOI: 10.1021/cr400531v From NLM Medline.

(3) Li, Y.; Wang, X.; Sun, J. Layer-by-layer assembly for rapid fabrication of thick polymeric films. Chem Soc Rev 2012, 41 (18), 5998-6009. DOI: 10.1039/c2cs35107b From NLM PubMed-not-MEDLINE.

(4) Zhao, S.; Caruso, F.; Dahne, L.; Decher, G.; De Geest, B. G.; Fan, J.; Feliu, N.; Gogotsi, Y.; Hammond, P. T.; Hersam, M. C.; et al. The Future of Layer-by-Layer Assembly: A Tribute to ACS Nano Associate Editor Helmuth Mohwald. ACS Nano 2019, 13 (6), 6151-6169. DOI: 10.1021/acsnano.9b03326 From NLM PubMed-not-MEDLINE.

(5) Decher, G.; Lehr, B.; Lowack, K.; Lvov, Y.; Schmitt, J. New nanocomposite films for biosensors: layer-by-layer adsorbed films of polyelectrolytes, proteins or DNA. Biosensors and Bioelectronics 1994, 9 (9-10), 677-684. DOI: 10.1016/0956-5663(94)80065-0.

(6) Ariga, K.; Lvov, Y.; Decher, G. There is still plenty of room for layer-by-layer assembly for constructing nanoarchitectonics-based materials and devices. Phys Chem Chem Phys 2022, 24 (7), 4097-4115. DOI: 10.1039/d1cp04669a From NLM PubMed-not-MEDLINE.

(7) Saurer, E. M.; Flessner, R. M.; Sullivan, S. P.; Prausnitz, M. R.; Lynn, D. M. Layer-by-layer assembly of DNA- and protein-containing films on microneedles for drug delivery to the skin. Biomacromolecules 2010, 11 (11), 3136-3143. DOI: 10.1021/bm1009443 From NLM Medline.

(8) Hu, X.; McIntosh, E.; Simon, M. G.; Staii, C.; Thomas, S. W., 3rd. Stimuli-Responsive Free-Standing Layer-By-Layer Films. Adv Mater 2016, 28 (4), 715-721. DOI: 10.1002/adma.201504219 From NLM PubMed-not-MEDLINE.

(9) Feeney, M. J.; Hu, X.; Srinivasan, R.; Van, N.; Hunter, M.; Georgakoudi, I.; Thomas, S. W., 3rd. UV and NIR-Responsive Layer-by-Layer Films Containing 6-Bromo-7-hydroxycoumarin Photolabile Groups. Langmuir 2017, 33 (41), 10877-10885. DOI: 10.1021/acs.langmuir.7b01469 From NLM Medline.

(10) Feeney, M. J.; Thomas, S. W., 3rd. Combining Top-Down and Bottom-Up with Photodegradable Layer-by-Layer Films. Langmuir 2019, 35 (43), 13791-13804. DOI: 10.1021/acs.langmuir.9b02005 From NLM PubMed-not-MEDLINE.

(11) Wang, Y.; Li, T.; Li, S.; Guo, R.; Sun, J. Healable and Optically Transparent Polymeric Films Capable of Being Erased on Demand. ACS Appl Mater Interfaces 2015, 7 (24), 13597-13603. DOI: 10.1021/acsami.5b03179 From NLM PubMed-not-MEDLINE.

(12) Skorb, E. V.; Andreeva, D. V. Layer-by-Layer approaches for formation of smart self-

healing materials. Polymer Chemistry 2013, 4 (18), 4834-4845. DOI: 10.1039/c3py00088e.

(13) Correa, S.; Boehnke, N.; Barberio, A. E.; Deiss-Yehiely, E.; Shi, A.; Oberlton, B.; Smith, S. G.; Zervantonakis, I.; Dreaden, E. C.; Hammond, P. T. Tuning Nanoparticle Interactions with Ovarian Cancer through Layer-by-Layer Modification of Surface Chemistry. ACS Nano 2020, 14 (2), 2224-2237. DOI: 10.1021/acsnano.9b09213 From NLM Medline.

(14) Alkekhia, D.; Hammond, P. T.; Shukla, A. Layer-by-Layer Biomaterials for Drug Delivery. Annu Rev Biomed Eng 2020, 22, 1-24. DOI: 10.1146/annurev-bioeng-060418-052350 From NLM Medline.

(15) Stockton, W. B.; Rubner, M. F. Molecular-Level Processing of Conjugated Polymers. 4. Layer-by-Layer Manipulation of Polyaniline via Hydrogen-Bonding Interactions. Macromolecules 1997, 30 (9), 2717-2725. DOI: 10.1021/ma9700486.

(16) Sukhishvili, S. A.; Granick, S. Layered, erasable polymer multilayers formed by hydrogen-bonded sequential self-assembly. Macromolecules 2002, 35 (1), 301-310. DOI: 10.1021/ma011346c.

(17) Kharlampieva, E.; Sukhishvili, S. A. Hydrogen-bonded layer-by-layer polymer films. Polym Rev 2006, 46 (4), 377-395. DOI: 10.1080/15583720600945386.

(18) Such, G. K.; Johnston, A. P.; Caruso, F. Engineered hydrogen-bonded polymer multilayers: from assembly to biomedical applications. Chem Soc Rev 2011, 40 (1), 19-29. DOI: 10.1039/c0cs00001a From NLM Medline.

(19) Lutkenhaus, J. L.; Hrabak, K. D.; McEnnis, K.; Hammond, P. T. Elastomeric flexible free-standing hydrogen-bonded nanoscale assemblies. J Am Chem Soc 2005, 127 (49), 17228-17234. DOI: 10.1021/ja053472s From NLM PubMed-not-MEDLINE.

(20) Kim, B. S.; Park, S. W.; Hammond, P. T. Hydrogen-bonding layer-by-layer-assembled biodegradable polymeric micelles as drug delivery vehicles from surfaces. ACS Nano 2008, 2 (2), 386-392. DOI: 10.1021/nn700408z From NLM Medline.

(21) Wang, Z.; Ouyang, L.; Li, H.; Wagberg, L.; Hamedi, M. M. Layer-by-Layer Assembly of Strong Thin Films with High Lithium Ion Conductance for Batteries and Beyond. Small 2021, 17 (32), e2100954. DOI: 10.1002/smll.202100954 From NLM PubMed-not-MEDLINE.

(22) Zou, S. F.; Lv, R. H.; Tong, Z. Z.; Na, B.; Fu, K.; Liu, H. S. In situ hydrogen-bonding complex mediated shape memory behavior of PAA/PEO blends. Polymer 2019, 183. DOI: ARTN 121878
10.1016/j.polymer.2019.121878.

(23) Feeney, M. J.; Thomas, S. W. Tuning the Negative Photochromism of Water-Soluble Spiropyran Polymers. Macromolecules 2018, 51 (20), 8027-8037. DOI: 10.1021/acs.macromol.8b01915.

(24) Nolte, A. J.; Treat, N. D.; Cohen, R. E.; Rubner, M. F. Effect of Relative Humidity on the Young’s Modulus of Polyelectrolyte Multilayer Films and Related Nonionic Polymers.

Macromolecules 2008, 41 (15), 5793-5798. DOI: 10.1021/ma800732j.
(25) Ishiyama, C.; Higo, Y. Effects of humidity on Young's modulus in poly(methyl methacrylate). J Polym Sci Pol Phys 2002, 40 (5), 460-465. DOI: DOI 10.1002/polb.10107.
(26) Narayanan, R. P.; Melman, G.; Letourneau, N. J.; Mendelson, N. L.; Melman, A. Photodegradable iron(III) cross-linked alginate gels. Biomacromolecules 2012, 13 (8), 2465-2471. DOI: 10.1021/bm300707a From NLM Medline.
(27) Chen, J.; Browne, W. R. Photochemistry of iron complexes. Coordination Chemistry Reviews 2018, 374, 15-35. DOI: 10.1016/j.ccr.2018.06.008.
(28) Swift, T.; Swanson, L.; Geoghegan, M.; Rimmer, S. The pH-responsive behaviour of poly(acrylic acid) in aqueous solution is dependent on molar mass. Soft Matter 2016, 12 (9), 2542-2549. DOI: 10.1039/c5sm02693h From NLM PubMed-not-MEDLINE.
(29) Lutkenhaus, J. L.; McEnnis, K.; Hammond, P. T. Tuning the Glass Transition of and Ion Transport within Hydrogen-Bonded Layer-by-Layer Assemblies. Macromolecules 2007, 40 (23), 8367-8373. DOI: 10.1021/ma0713557.
(30) Sung, C.; Vidyasagar, A.; Hearn, K.; Lutkenhaus, J. L. Effect of thickness on the thermal properties of hydrogen-bonded LbL assemblies. Langmuir 2012, 28 (21), 8100-8109. DOI: 10.1021/la301300h From NLM Medline.
(31) Li, H.; Yang, P.; Pageni, P.; Tang, C. Recent Advances in Metal-Containing Polymer Hydrogels. Macromol Rapid Commun 2017, 38 (14). DOI: 10.1002/marc.201700109 From NLM Medline.
(32) Calvo-Marzal, P.; Delaney, M. P.; Auletta, J. T.; Pan, T.; Perri, N. M.; Weiland, L. M.; Waldeck, D. H.; Clark, W. W.; Meyer, T. Y. Manipulating Mechanical Properties with Electricity: Electroplastic Elastomer Hydrogels. ACS Macro Lett 2012, 1 (1), 204-208. DOI: 10.1021/mz2001548 From NLM PubMed-not-MEDLINE.
(33) Yokoi, H.; Nomoto, E.; Ikoma, S. Reversible formation of iron(<scp>III</scp>) ion clusters in the poly(acrylic acid)–Fe³⁺complex gel with changes in the water content. J. Mater. Chem. 1993, 3 (4), 389-392. DOI: 10.1039/jm9930300389.
(34) Shuai, F.; Zhang, Y.; Yin, Y.; Zhao, H.; Han, X. Fabrication of an injectable iron (III) crosslinked alginate-hyaluronic acid hydrogel with shear-thinning and antimicrobial activities. Carbohydr Polym 2021, 260, 117777. DOI: 10.1016/j.carbpol.2021.117777 From NLM Medline.
(35) Kang, M.; Oderinde, O.; Liu, S.; Huang, Q.; Ma, W.; Yao, F.; Fu, G. Characterization of Xanthan gum-based hydrogel with Fe(3+) ions coordination and its reversible sol-gel conversion. Carbohydr Polym 2019, 203, 139-147. DOI: 10.1016/j.carbpol.2018.09.044 From NLM PubMed-not-MEDLINE.
(36) Malhotra, A.; Bera, T.; Zhai, L. Bioinspired Metal Ion Coordinated Polyelectrolyte Fibrous Nanoreactors. Advanced Materials Interfaces 2016, 3 (22), 1600692. DOI: 10.1002/admi.201600692 (acccessed 2023-06-06T16:09:38).
(37) Dong, J.; Ozaki, Y.; Nakashima, K. FTIR studies of conformational energies of

poly(acrylic acid) in cast films. Journal of Polymer Science Part B: Polymer Physics 1997, 35 (3), 507-515. DOI: 10.1002/(sici)1099-0488(199702)35:3<507::Aid-polb9>3.0.Co;2-o.

(38) Zheng, S. Y.; Ding, H. Y.; Qian, J.; Yin, J.; Wu, Z. L.; Song, Y. H.; Zheng, Q. Metal-Coordination Complexes Mediated Physical Hydrogels with High Toughness, Stick-Slip Tearing Behavior, and Good Processability. Macromolecules 2016, 49 (24), 9637-9646. DOI: 10.1021/acs.macromol.6b02150.

(39) Holten-Andersen, N.; Harrington, M. J.; Birkedal, H.; Lee, B. P.; Messersmith, P. B.; Lee, K. Y.; Waite, J. H. pH-induced metal-ligand cross-links inspired by mussel yield self-healing polymer networks with near-covalent elastic moduli. Proc Natl Acad Sci U S A 2011, 108 (7), 2651-2655. DOI: 10.1073/pnas.1015862108 From NLM Medline.

(40) Peng, F.; Li, G.; Liu, X.; Wu, S.; Tong, Z. Redox-responsive gel-sol/sol-gel transition in poly(acrylic acid) aqueous solution containing Fe(III) ions switched by light. J Am Chem Soc 2008, 130 (48), 16166-16167. DOI: 10.1021/ja807087z From NLM PubMed-not-MEDLINE.

(41) Harvey Jr, A. E., John A. Smart, and Edward S. Amis. Simultaneous spectrophotometric determination of iron (II) and total iron with 1, 10-phenanthroline. Analytical Chemistry 1955, 27 (1), 26-29.

(42) Kong, S. M.; Costa, D. F.; Jagielska, A.; Van Vliet, K. J.; Hammond, P. T. Stiffness of targeted layer-by-layer nanoparticles impacts elimination half-life, tumor accumulation, and tumor penetration. Proc Natl Acad Sci U S A 2021, 118 (42). DOI: 10.1073/pnas.2104826118 From NLM Medline.

(43) Esmaeilzadeh, P.; Kowitsch, A.; Liedmann, A.; Menzel, M.; Fuhrmann, B.; Schmidt, G.; Klehm, J.; Groth, T. Stimuli-Responsive Multilayers Based on Thiolated Polysaccharides That Affect Fibroblast Cell Adhesion. ACS Appl Mater Interfaces 2018, 10 (10), 8507-8518. DOI: 10.1021/acsami.7b19022 From NLM Medline.